INTEGRATED MANAGEMENT OF PFAS REMEDIATION: DEGRADATION MECHANISMS, LIFE CYCLE ASSESSMENT, AND FIRST-PRINCIPLES MODELING

by

GENGYANG LI

(Under the Direction of Ke (Luke) Li)

ABSTRACT

Per- and polyfluoroalkyl substances (PFASs) are persistent environmental contaminants that pose serious risks to human health and ecosystems due to their widespread occurrence, chemical stability, and resistance to conventional treatment processes. This dissertation investigates PFAS remediation management and degradation efficiency improvements through an integrated approach combining advanced treatment technologies, life cycle assessment (LCA), and first-principles calculations.

A comprehensive review of emerging PFAS treatment technologies—including physical concentration techniques (e.g., granular activated carbon, ion exchange, nanofiltration), chemical destruction methods (e.g., photolysis, electrochemical oxidation, plasma), and hybrid treatment trains—is conducted to evaluate their performance, limitations, and practical applicability. Special focus is placed on electrochemical oxidation (EO), and a detailed mechanistic understanding is developed through reaction pathway analysis and density functional theory (DFT) calculations. These calculations elucidate key degradation mechanisms and energetic parameters governing PFAS breakdown on different electrode materials.

Two LCA case studies are presented to assess the environmental and economic trade-offs associated with PFAS treatment technologies, particularly ion exchange combined with EO and foam fractionation. These evaluations offer insights into scalability and sustainability under varying operating conditions and energy mixes. Further, DFT-based modeling is applied to guide the development of electrode materials with enhanced catalytic activity and lower energy requirements, targeting improved PFAS degradation efficiency.

The study concludes by identifying the advantages of hybrid treatment systems that integrate concentration and destruction technologies. Recommendations are made for future research directions, including optimizing material properties, system design, and operational parameters for real-world application. Overall, this work provides a scientific foundation and practical framework for designing more efficient, cost-effective, and environmentally sustainable PFAS remediation strategies.

INDEX WORDS: PFAS, electrochemical oxidation, life cycle assessment, density functional theory, hybrid treatment, remediation, ion exchange, foam fractionation.

INTEGRATED MANAGEMENT OF PFAS REMEDIATION: DEGRADATION MECHANISMS, LIFE CYCLE ASSESSMENT, AND FIRST-PRINCIPLES MODELING

by

GENGYANG LI

BS, East China Normal University, China, 2018

MS, Arizona State University, 2021

A Dissertation Submitted to the Graduate Faculty of The University of Georgia in Partial

Fulfillment of the Requirements for the Degree

DOCTOR OF PHILOSOPHY

ATHENS, GEORGIA

2025

© 2025

GENGYANG LI

All Rights Reserved

INTEGRATED MANAGEMENT OF PFAS REMEDIATION: DEGRADATION MECHANISMS, LIFE CYCLE ASSESSMENT, AND FIRST-PRINCIPLES MODELING

by

GENGYANG LI

Major Professor: Ke Li

Committee: Henry F. Schaefer

Qingguo Huang Keshav C Das Bingqian Xu

Electronic Version Approved:

Ron Walcott Vice Provost for Graduate Education and Dean of the Graduate School The University of Georgia August 2025

DEDICATION

To my beloved husband, Hanlin, your unwavering love, patience, and belief in me carried me through the most challenging moments of this journey. You are my constant source of strength, encouragement, and laughter. I could not have done this without you.

To my sweet dogs, Domi and Marlo, your quiet companionship, gentle nudges, and joyful presence were the comfort I didn't know I needed. You reminded me to take breaks, breathe, and find joy in the little things—even during the toughest days.

To my sisters and brothers at AtCCC, Pastor Lin and Pastor's wife Jenny, and sister Huijing in Arizona, thanks for all the prayers, encouragement, and fellowship, especially when I was sick.

This work is dedicated to you all, with love and gratitude.

ACKNOWLEDGEMENTS

First and foremost, I give all glory and thanks to my Lord of Jesus Christ, whose grace, guidance, and strength have sustained me throughout this journey. In moments of doubt, fatigue, and uncertainty, my faith provided clarity, purpose, and resilience. I am deeply grateful for His presence every step of the way.

I would like to express my sincerest appreciation to my advisor, Dr. Ke Li, for his exceptional mentorship, encouragement, and unwavering support. His deep knowledge, patience, and insightful feedback have been instrumental to my academic and personal growth. I am truly grateful for the opportunity to learn under his guidance.

I also extend my heartfelt thanks to my committee members —Dr. Qingguo Huang, Dr. Keshav C. Das, and Dr. Bingqian Xu, Dr. Henry F. Schaefer, — for their time, expertise, and thoughtful input. Their diverse knowledge and critical perspectives helped shape this dissertation and broaden my understanding of environmental engineering and computational modeling.

Each of you has made a meaningful impact on my development as a scholar and individual, and I am thankful for the privilege of learning from you.

TABLE OF CONTENTS

		Page
ACKNOV	WLEDGEMENTS	v
LIST OF	TABLES	ix
LIST OF	FIGURES	xi
СНАРТЕ	I.R	
1	Introduction	1
	1.1 PFASs and the Occurrence	1
	1.2 Background and Significance	2
	1.3 Dissertation Overview	4
	1.4 References	7
2	A Review of the Emerging PFASs Treatment Technologies	8
	2.1 Emerging PFASs Treatment Technologies and Status	8
	2.2 Concentration Technologies	9
	2.3 Chemical Destruction Technologies	21
	2.4 Thermal Technologies	42
	2.5 Biological Technologies	46
	2.6 Hybrid Treatment	50
	2.7 Conclusion	53
	2.8 References	59

3	A Review on the Recent Mechanisms investigation of PFASs Electrochemical
	Oxidation Degradation: Mechanisms, DFT Calculation, and Pathways71
	3.1 Introduction
	3.2 PFASs Degradation Mechanisms by EO
	3.3 DFT Computation Applications for PFASs Degradation Mechanisms
	Investigation79
	3.4 Degradation Pathways of Some PFAS Species89
	3.5 Comparative Analysis of Electrode Materials94
	3.6 Practical Implications96
	3.7 Conclusion and Insights for Future Study97
	3.8 References 107
4	Environmental Life Cycle Assessment (LCA) of Treating PFASs with Ion Exchange
	and Electrochemical Oxidation Technology111
	4.1 Introduction
	4.2 Materials and Methods115
	4.3 Results and Discussion
	4.4 Scenario Analysis Results
	4.5 Uncertainty Analysis126
	4.6 Conclusion
	4.7 References
5	Life Cycle Assessment and Life Cycle Costing Analysis for Removing PFASs from
	Landfill Leachate with Foam Fractionation Technology
	5.1 Introduction141

	5.2 Methods	145
	5.3 Results and Discussion	148
	5.4 Conclusion	155
	5.5 References	162
6	First Principles Calculation Aided Electrode Materials Development for PFASs	
	Degradation	165
	6.1 Introduction	165
	6.2 Methodology	167
	6.3 Results and Discussion	171
	6.4 Conclusion	175
	6.5 References	180
7	Conclusion and Future Study	184
	7.1 Conclusion	184
	7.2 Future Study	186
	7.3 References	188
APPENI	DICES	
A	Supplemental material for Chapter 4	189
E	Supporting information for Chapter 5	194
C	Paper copyright permissions	206

LIST OF TABLES

Page	e
Table 2.1: The technology readiness level of the emerging PFASs treatment technologies56	6
Table 2.2: Summarized comparison across the concentration technologies for PFAS removal57	7
Table 2.3: Summarized comparison across the chemical destruction technologies for PFAS	
removal58	8
Table 3.1: C-F BDEs for C ₇ F ₁₅ COO ⁻	5
Table 3.2: Adsorption energy and activation energy reported for PFOA, PFOS, and PFBS	
degradation during EO process with DFT computation	5
Table 3.3: Overpotential η for OER calculated for anodes in EO process by DFT computation 106	6
Table 4.1: Environmental databases used for the unit emission and environmental impact factors	
133	3
Table 4.2: Impact assessment results to degrade PFASs of two log orders of magnitude in still	
bottoms 1	3
Table 4.3: Impact assessment results to degrade PFASs in still bottom 2	4
Table 5.1: Summary of Foam Fractionation Operational Parameters for PFAS Removal from	
Landfill Leachate: Laboratory, Pilot, and Full-Scale Studies	8
Table 5.2: Inventory data and environmental database used for one-stage FF system and three-	
stage FF system158	8
Table 5.3: The total environmental impact results for one-stage and three-stage FF system with	
the functional unit.	9

Table 5.4: The environmental impact normalized values for the one-stage and three-stage FF	
treatment systems (person-years per1000m³ treated)1	59
Table 6.1: ZPE corrections (T = 298 K) and entropy energy contributions for gaseous molecule	:S
and reactants1	77
Table 6.2: Adsorption energy of H ² O, PFOA, PFOS, and Eovac on the pristine Ti ₄ O ₇ and	
Nb/Ce/Pd_ Ti ₄ O ₇ surfaces electrode	77
Table 6.3: η ^{OER} of pristine Ti ₄ O ₇ and Nb/Ce/Pd_ Ti ₄ O ₇ surfaces	77

LIST OF FIGURES

Page
Figure 2.1: Technology Readiness Level
Figure 3.1: (a) Electrolytic cell schematic for electrochemical water treatment reactors101
Figure 3.2: Density of states (DOS) of (a) Ti ₄ O ₇ and (b) Ti ₄ O ₇ /MXene surface102
Figure 3.3: DFT quantification descriptors for electrodes and PFAS degradation mechanism102
Figure 3.4: The possible PFOA degradation pathways on the anode in the EO process103
Figure 3.5: The possible PFOS degradation pathways on the anode in the EO process104
Figure 4.1: Overview of the system boundary for PFASs treatment from spent IX resin135
Figure 4.2: Overview of the unit processes and inventory items considered for three different IX
and EO operation scenarios
Figure 4.3: EE/O and GWP of PFASs removal per functional unit in still bottoms 1
Figure 4.4: Relative contributions of each process to the total environmental impacts of PFOS
and PFOA in still bottoms 1136
Figure 4.5: EE/O and GWP of PFASs removal per functional unit in still bottoms 2
Figure 4.6: Relative contributions of unit processes to the total environmental impacts of PFOS,
PFOA, and PFBA in still bottoms 2
Figure 4.7: Scenario analysis results comparing total GWP for the treatment of PFOS138
Figure 4.8: Variation in GWP values from different energy mix
Figure 5.1: The system boundary of the one-stage FF system for PFASs treatment160
Figure 5.2: The system boundary of the three-stage FF system for PFASs treatment160

Figure 5.3: Relative contributions of each inventory item to the total environmental impacts in		
the one-stage (OS) and three-stage (TS) FF treatment system16	1	
Figure 5.4: The life cycle costing comparison of one-stage FF system and three-stage FF		
treatment system	1	
Figure 6.1: Free energy diagram for OER on Ti ₄ O ₇ , Nb_Ti ₄ O ₇ , Ce_Ti ₄ O ₇ , and Pd_Ti ₄ O ₇ 17	8	
Figure 6.2: DOS of the pristine Ti ₄ O ₇ and Nb/Ce/Pd_ Ti ₄ O ₇	9	

CHAPTER 1

INTRODUCTION

1.1 PFASs and the Occurrence

Per- and polyfluoroalkyl substances (PFASs) have drawn public concern recently due to their toxic properties and persistence in the environment (Rozen & Filler, 1985). PFASs substances are a broad class of emerging environmental contaminants used heavily by the industrial, commercial, and manufacturing sectors in previous decades, like surface coating, lubricants, and firefighting foams (Rahman et al., 2014). Perfluorooctane sulfonic acid (PFOS) and perfluorooctanoic acid (PFOA) are two of the most well-known and broadly researched since they came into production in 1940s and related health concerns were raised as early as the 1960s (Crone et al., 2019). There are various potential health effects that have been attributed to PFASs exposure, particularly PFOS and PFOA which are highly toxic and suspected carcinogens (Wanninayake, 2021). In the environment, PFASs are highly persistent and bioaccumulate within biota and humans. Because of this, PFASs species have been consistently detected within the environment, in food products, and humans (Hori et al., 2004).

Through the Unregulated Contaminant Monitoring Rule (UCMR), the USEPA gathers data on the occurrence of PFASs in drinking water that is nationally representative from all utilities and statistical samples. The preliminary drinking water health advisory levels for PFOS and PFOA were set at 200 ng/L and 400 ng/L, respectively, by the USEPA in 2009. The USEPA standards were then tightened in 2016 to 70 ng/L for either PFOS, PFOA, or their combined

amount. Additionally, several states have set lower PFAS regulatory or recommendation thresholds.

Nearly 37,000 PFAS sample data from 4,920 US drinking water utilities were submitted by the UCMR3 to report on the presence of PFAS in the environment between 2013 and 2015. (USEPA, 2017). Approximately 79% of the US population was served by the public water systems (PWS) chosen for inclusion in UCMR3 (USEPA, 2017). The UCMR3 data thus represents the information on PFAS presence in US drinking water that is the most directly pertinent. According to these data, PFBS was only discovered in big systems (those that served more than 1000 people), with low detection rates (0.05%) but high average values (212 ng/L in surface water and 136 ng/L in groundwater). The most common substance to be found in every system was PFOA, at 1.03%. The greatest maximum concentration, PFOS, had a detection frequency of 0.79 percent and a maximum value of 7,000 ng/L. The typical PFHxS concentration in small groundwater systems (feeding 1000 people) was 409 ng/L. The mean PFHpA system concentrations in groundwater and large surface waters, respectively, were only 19 ng/L and 28 ng/L, respectively. The mean PFNA values in big surface systems were 54 ng/L and in groundwater systems they were 35 ng/L. According to the UCMR3 data, groundwater was the site of 72% of all PFAS detections, and average total PFAS concentrations in groundwater were greater than in surface water across all system sizes (210 ng/L vs. 90 ng/L) (Crone et al., 2019).

1.2 Background and Significance

Per- and polyfluoroalkyl substances (PFAS) have been used extensively in industrial and consumer applications due to their thermal stability, chemical inertness, and surfactant properties. However, these same attributes also make PFAS highly resistant to environmental

degradation, leading to their persistent accumulation in natural waters, soils, biota, and human populations. Mounting evidence links PFAS exposure to adverse health outcomes, including cancer, endocrine disruption, and developmental toxicity, prompting regulatory agencies and the public to demand effective strategies for their detection, removal, and destruction.

Traditional water treatment technologies such as granular activated carbon (GAC) and ion exchange (IX) have demonstrated success in concentrating PFAS but do not mineralize these compounds, necessitating secondary treatment or disposal methods that can create additional environmental burdens. Emerging destruction technologies—such as electrochemical oxidation (EO), photolysis, plasma, and thermal processes—offer the potential for complete PFAS degradation. Among these, EO has gained significant attention due to its operability under ambient conditions, modularity, and ability to achieve high removal efficiencies for long-chain PFAS.

Despite these advantages, EO technologies face several limitations, including high energy consumption, limited effectiveness for short-chain PFAS, and the need for durable, cost-effective electrode materials. Addressing these challenges requires a deeper mechanistic understanding of PFAS degradation pathways and the electrochemical behaviors of various anode materials. First-principles modeling, particularly density functional theory (DFT), provides a powerful framework to investigate these fundamental interactions at the atomic level. DFT calculations enable researchers to quantify bond dissociation energies, activation barriers, adsorption energies, and overpotentials—parameters that directly inform electrode performance and guide rational material design.

Beyond treatment performance, the environmental and economic sustainability of PFAS remediation strategies must also be assessed. Life cycle assessment (LCA) offers a systems-level

perspective that evaluates the trade-offs associated with different treatment pathways, including greenhouse gas emissions, resource consumption, and operational costs. Integrating LCA with experimental and computational research ensures that proposed solutions are not only technically effective but also viable and scalable for real-world implementation.

This dissertation addresses these multifaceted challenges by combining laboratory-scale EO studies, DFT-based material modeling, and LCA analyses to develop a comprehensive and integrated approach for PFAS remediation. The work is significant in its ability to bridge molecular-level insights with practical engineering considerations, ultimately contributing to the development of efficient, cost-effective, and environmentally sustainable treatment systems for one of the most persistent environmental contaminants of our time.

1.3 Dissertation Overview

This dissertation is structured into seven chapters, presenting an integrated framework for advancing PFAS remediation technologies through a combined approach of mechanistic investigation, environmental life cycle assessment (LCA), and first-principles computational modeling. The goal is to evaluate, optimize, and guide the development of treatment strategies that are both technically effective and environmentally sustainable.

Chapter 1 introduces the occurrence, risks, and regulatory challenges associated with PFAS contamination. It outlines the motivation for this research and provides an overview of the dissertation's scope, objectives, and methodology.

Chapter 2 presents a comprehensive review of emerging PFAS treatment technologies, including physical concentration methods (e.g., GAC, IX, NF), chemical destruction techniques (e.g., EO, UV, plasma), and hybrid treatment systems. The performance, readiness levels,

advantages, and limitations of each method are critically compared to establish the current technological landscape.

Chapter 3 delves into the mechanistic understanding of PFAS degradation via electrochemical oxidation (EO). This chapter synthesizes experimental findings and density functional theory (DFT) studies to elucidate key reaction pathways, including direct electron transfer, decarboxylation, hydroxylation, and hydrolysis. The role of electrode materials and operational parameters is also examined.

Chapter 4 conducts a life cycle assessment of a combined ion exchange (IX) and EO system for PFAS removal from wastewater. Environmental impacts such as energy use and greenhouse gas emissions are quantified under different operational scenarios to identify sustainability trade-offs and optimization opportunities.

Chapter 5 extends the LCA methodology to evaluate foam fractionation (FF) technology for PFAS removal from landfill leachate. A comparative analysis is performed between one-stage and three-stage FF systems, incorporating life cycle costing (LCC) to assess economic feasibility alongside environmental performance.

Chapter 6 focuses on the use of first-principles DFT modeling to support the development of high-performance electrode materials for EO-based PFAS degradation.

Calculations of adsorption energies, overpotential for oxygen evolution reactions, oxygen vacancy formation energies (Eovac), and density of states provide molecular-level insights into electrode-PFAS interactions, guiding material selection and design.

Chapter 7 concludes the dissertation by summarizing key findings across the experimental, modeling, and sustainability domains. It offers recommendations for future

research, including system integration, real-world deployment, and the need for cross-disciplinary efforts to tackle PFAS contamination holistically.

Together, the chapters form a cohesive body of work that bridges molecular theory, engineering practice, and environmental sustainability. This dissertation contributes to the growing body of knowledge needed to design scalable, effective, and responsible solutions for PFAS remediation in complex water matrices.

1.4 References

- Rozen, S., & Filler, R. (1985). Alpha-Fluorocarbonyl Compounds and Related Chemistry. *Tetrahedron*, 41(7), 1111-1153. https://doi.org/Doi 10.1016/S0040-4020(01)96514-7
- Rahman, M. F., Peldszus, S., & Anderson, W. B. (2014). Behaviour and fate of perfluoroalkyl and polyfluoroalkyl substances (PFASs) in drinking water treatment: A review. *Water Research*, *50*, 318-340. https://doi.org/10.1016/j.watres.2013.10.045
- Crone, B. C., Speth, T. F., Wahman, D. G., Smith, S. J., Abulikemu, G., Kleiner, E. J., & Pressman, J. G. (2019). Occurrence of Per- and Polyfluoroalkyl Substances (PFAS) in Source Water and Their Treatment in Drinking Water. *Crit Rev Environ Sci Technol*, 49(24), 2359-2396. https://doi.org/10.1080/10643389.2019.1614848
- Wanninayake, D. M. (2021). Comparison of currently available PFAS remediation technologies in water: A review. *J Environ Manage*, 283, 111977. https://doi.org/10.1016/j.jenvman.2021.111977
- Hori, H., Hayakawa, E., Einaga, H., Kutsuna, S., Koike, K., Ibusuki, T., Kiatagawa, H., & Arakawa, R. (2004). Decomposition of environmentally persistent perfluorooctanoic acid in water by photochemical approaches. *Environmental Science & Technology*, *38*(22), 6118-6124. https://doi.org/10.1021/es049719n

CHAPTER 2

A REVIEW OF THE EMERGING PFAS TREATMENT TECHNOLOGIES

2.1 Emerging PFASs Treatment Technologies and Status

Numerous remediation technologies for per- and polyfluoroalkyl substances (PFASs) have been evaluated and documented in the literature. These technologies can be broadly categorized into two main types: concentration/separation methods and destruction techniques. Concentration-based processes reviewed in this paper include granular activated carbon (GAC) adsorption, ion exchange resin (IXR) adsorption, reverse osmosis (RO), nanofiltration (NF), foam fractionation (FF), and ozofractionation (OF). On the other hand, advanced oxidation processes such as photochemical oxidation, electrochemical oxidation (EO), and supercritical water oxidation (SCWO) represent key destruction approaches. Additionally, emerging technologies such as plasma treatment, sonolysis, and advanced reduction processes (ARPs) have garnered increasing attention. Among thermal destruction technologies, incineration is the most developed and has already been implemented in commercial treatment facilities. In contrast, pyrolysis, gasification, and hydrothermal liquefaction are relatively novel techniques still in early stages of development for PFAS removal.

This review focuses on the removal efficiency and energy requirements of these emerging PFAS treatment technologies. It synthesizes findings from peer-reviewed literature published in the last decade, emphasizing the state of development for each method. Based on

this literature review, the Technology Readiness Level (TRL) of these technologies is presented in Table 2.1 and illustrated in Figure 2.1.

Among the concentration/separation methods, only GAC adsorption has reached the level of actual system deployment in operational environmental settings. IXR adsorption and RO/NF systems are considered well-developed and technically qualified. In contrast, OF and FF technologies have only been demonstrated in relevant environmental settings, while EO for PFAS removal remains at the laboratory validation stage.

Regarding destruction technologies—including chemical, thermal, and biological approaches—only incineration has been developed to the point of full-scale operational deployment. EO has reached the stage of demonstration in relevant environments. Meanwhile, photochemical oxidation, plasma treatment, sonolysis, ARPs, SCWO, and biodegradation have only been validated in laboratory-scale experiments. Pyrolysis, gasification, hydrothermal liquefaction, and phytoremediation are in the conceptual or experimental phase, with proof-of-concept demonstrated through preliminary studies. These technologies are considered nascent, and substantial research is still required to assess their viability for large-scale PFAS remediation.

2.2 Concentration Technologies

The summarized comparison Table 2.2 highlights the performance, advantages, and limitations of various concentration-based technologies for PFAS removal, including Reverse Osmosis (RO), Nanofiltration (NF), Foam Fractionation (FF), Ozofractionation (OF), Electrocoagulation (EC), Granular Activated Carbon (GAC), and Ion Exchange (IX). RO and NF demonstrate the highest removal efficiencies (>99% and 90–99%, respectively), especially for

both long- and short-chain PFAS, but come with high energy demands and fouling concerns. FF and OF offer cost-effective and energy-efficient options with good removal rates for long-chain PFAS, although they struggle with short-chain compounds and require post-treatment for residuals. EC, particularly with optimized anode materials like Al-Zn, shows promise in treating a wide range of PFASs with low sludge generation and operational simplicity, yet its effectiveness depends on water chemistry and system design. GAC and IX remain widely used due to their simplicity and moderate cost; however, they are less effective for short-chain PFAS and require frequent regeneration or replacement. Overall, each method presents trade-offs in terms of cost, energy, selectivity, and scalability, suggesting that integrated or hybrid treatment trains may be necessary for comprehensive PFAS remediation.

2.2.1 Granular Activated Carbon

Granular activated carbon (GAC) is widely used for the removal of PFAS in water treatment due to its relatively low cost and broad applicability (Du et al., 2015). In 2005, 3M successfully utilized GAC to remove PFOS from wastewater, which spurred extensive research and commercial application of activated carbon for PFAS removal. Today, GAC is considered a mature technology that can be implemented at both municipal water treatment facilities and point-of-entry domestic systems, either as a standalone solution or integrated into a multi-barrier treatment train (Crone et al., 2019). GAC has demonstrated high efficiency—often exceeding 90%—in removing PFOS at concentrations in the parts-per-billion (ppb) or micrograms per liter (µg/L) range. However, its performance is less effective against short-chain perfluoroalkyl carboxylic acids (PFCAs) such as PFHxA, PFPeA, PFBS, and PFBA (Inyang & Dickenson, 2017; Ross et al., 2018).

PFAS removal by GAC is influenced by several factors, including operational time, GAC type, and surface loading rate. Commonly studied GAC types include Filtrasorb® 400 and Filtrasorb 600 (F600). Reported operational times range from as little as 6 minutes to over 9020 minutes. Surface loading rates can vary significantly, from 618 gallons per minute (GPM) in full-scale drinking water treatment plants to 1.77 GPM in laboratory-scale systems.

A full-scale study by Belkouteb et al. (2020) monitored the removal of five PFAS compounds from 2015 to 2017. Initial concentrations of PFHxA, PFOA, PFBS, PFHxS, and PFOS were 11 ng/L, 16 ng/L, 12 ng/L, 85 ng/L, and 35 ng/L, respectively. Using Filtrasorb® 400, the researchers evaluated the long-term performance of GAC and the influence of flow rate. For a "young" GAC filter that treated 5725 bed volumes (BV) over 63 days, PFAS removal ranged from 92% to 100%. In contrast, an "aged" filter that had processed 29,300 BV over 357 days saw removal efficiencies as low as 7.0%. Notably, reducing the flow rate from 39 to 29 L/s resulted in an average increase in PFAS removal efficiency of 14% for old filters and 6.5% for new ones. The study also confirmed that PFSA removal generally outperforms PFCA removal, and GAC exhibits greater affinity for long-chain PFAS than short-chain variants. The estimated cost of GAC treatment ranged from \$0.02 to \$0.10 per cubic meter of treated water.

Additionally, lowering flow rates after meeting treatment goals could extend GAC lifespan and reduce costs by up to 26%.

A similar full-scale study conducted at a municipal water treatment plant by Appleman et al. (2014) evaluated PFAS removal using Calgon Filtrasorb 600 (F600) in a lead-lag configuration processing 1.4–1.5 m³/min, with an empty bed contact time (EBCT) of 13 minutes. Initial PFAS concentrations were 1.83 µg/L for PFBA, 22% for PFPeA, 68% for PFHxA, 92%

for PFOA, 41% for PFHxS, and 95% for PFOS. Post-treatment concentrations were significantly lower, indicating substantial removal—especially for long-chain PFAS.

Rodowa et al. (2020) conducted a pilot study using DSR-A 8x40 GAC to treat PFAS-contaminated groundwater from aqueous film-forming foam (AFFF) sources. Operating at 1.87 m³/h with a 13-minute EBCT, the study observed earlier breakthrough of short-chain PFCAs compared to their sulfonate counterparts with the same chain length (e.g., PFHxA before PFPeS, PFHpA before PFHxS, and PFOA before PFHpS).

Woodard et al. (2017) also conducted a pilot study using Filtrasorb® 400 at a groundwater treatment facility. With an EBCT of 5 minutes per vessel and a flow rate of approximately 1.8 GPM, the system treated 100,486 gallons of water (11,165 BV). The removal efficiencies were 71% for PFOA and 50% for PFOS.

In another 18-month study, Inyang and Dickenson compared the PFAS removal performance of biochar and anthracite to Norit GAC 830. Operating at a constant flow rate of 1.77 GPM and an EBCT of 8 minutes, the average influent concentrations of PFPnA, PFHxA, PFOA, and PFOS were approximately 17.6 ng/L, 9.5 ng/L, 7.3 ng/L, and 4.1 ng/L, respectively. Among the tested materials, GAC showed the highest removal performance, with 61% effectiveness for PFOS.

To enhance GAC performance, Xu et al. (2020) synthesized a novel composite material—Fe₃O₄@GAC (2:1)—by hydrothermally loading Fe₃O₄ nanoparticles onto GAC. Compared to conventional GAC, which achieved 58.9% PFOA removal at an initial concentration of 0.241 mmol/L, Fe₃O₄@GAC reached 79.1% removal at pH 4.0 after 24 hours. The composite exhibited a second-order rate constant 6.3 times higher and a 13.4% greater

equilibrium adsorption capacity, suggesting enhanced performance in high-concentration and hard water environments.

McCleaf et al. (2017) investigated the effect of perfluorocarbon chain length and functional group on PFAS removal using Filtrasorb® 400 in column tests operated at 36 mL/min with a 6-minute EBCT. Over 217 days, 14 PFAS compounds with a total initial concentration of 484.1 μg/L were monitored. The average removal efficiency was 62%, but PFBA and PFPeA showed the lowest removal rates at 14% and 32%, respectively. PFAS with longer chain lengths and sulfonate functional groups exhibited higher removal efficiencies, underscoring the importance of PFAS structure in treatment design and system performance.

Overall, GAC is a well-established and effective treatment method for many long-chain PFAS, and full-scale applications have been successfully implemented in drinking water treatment plants (DWTPs). However, its performance for short-chain PFAS is significantly less robust. Additionally, co-contaminants and natural organic matter can interfere with PFAS adsorption, further reducing removal efficiency. Continued research and innovation—such as material enhancements and operational optimization—are necessary to improve GAC's applicability for a broader range of PFAS compounds.

2.2.2 Anion Exchange Resin (IXR)

Anion exchange (IX) involves the reversible exchange of negatively charged ions between a polymeric resin surface and an aqueous solution (Levchuk et al., 2018). This well-established technology is widely used for removing various contaminants in municipal and groundwater treatment (Ross et al., 2018). In recent years, extensive studies have shown that IX effectively removes PFAS from surface water, groundwater, and wastewater. Notably, IX has

demonstrated higher efficacy in eliminating short-chain PFAS, which are typically not well removed by granular activated carbon (GAC) (Dixit et al., 2021).

Commonly used resins include strong-base anion exchange resins (SB-AERs) such as Purolite A860, Purofine PFA694E, Purolite A-600, Sorbix A3F, and Purolite FerrIX A33E (Dixit et al., 2020). Reported adsorption capacities vary from 100 to 2000 mg PFAS/g of resin (Vo et al., 2020), with isotherm uptake capacities for PFOA and PFOS reaching up to 5 mmol/g on commercial resins like IRA 958 and IRA 67 (Dixit et al., 2021). Further details on PFAS removal mechanisms and adsorption kinetics are comprehensively discussed in reviews by Dixit et al. (2021) and Vo et al. (2020).

The PFAS removal efficiency of IX depends on several factors, including resin type, PFAS molecular structure, water chemistry, and co-occurring contaminants. Polystyrenic resins typically exhibit a higher affinity for PFAS, while polyacrylic resins are more effective at removing natural organic matter (NOM), which can interfere with PFAS adsorption when present (Dixit et al., 2021).

Boyer et al. (2021) investigated the effects of PFAS structure, resin characteristics, and ion exchange stoichiometry under batch and continuous-flow conditions. They found that water chemistry—specifically pH, inorganic ions, NOM, and co-contaminants—significantly influences IX performance. The Langmuir isotherm best described adsorption behavior at high PFAS concentrations. Their results supported resin selectivity trends, with the following order of increasing selectivity: PFBA < PFHxA < GenX < PFBS < PFOA < PFHxS < FOSA < PFOS. Chain length also influences PFAS removal efficiency. Long-chain PFAS are generally more effectively removed than short-chain compounds. In McCleaf et al.'s (2017) column experiments using Purolite® A600 (EBCT: 4.9 min; flow rate: 36 mL/min), 14 PFAS were monitored,

revealing an average removal efficiency of 62%. PFOS (C8) showed the highest removal (96%), while PFBA (C4) had the lowest (10%).

Zeng et al. (2020) further examined the impact of PFAS chain length across six groundwater samples treated with Purofine PFA694E. Despite variability in PFAS concentrations (156–7044 ng/L), long-chain PFAS were consistently more effectively removed. Similarly, Park et al. (2020) evaluated magnetic IXR for removing nine PFAS (total 300 ng/L) from low-NOM groundwater. At a resin dose of 15 mL/L, long-chain carboxylic PFAS (e.g., PFOA, PFDA) and sulfonic PFAS (e.g., PFBS, PFOS) were removed with an average efficiency of 80%, with PFOS at 82% and PFBA at 38%.

Full-scale IX applications have also shown promise. Appleman et al. (2014) demonstrated PFAS removal using Purolite FerrIX A33E, achieving removal rates of 97% for PFHxS and 92% for PFOS. Partial removal was also observed for PFHpA (46%), PFOA (75%), and PFBS (81%).

In summary, IX offers significant advantages over GAC, particularly for capturing short-chain PFAS and enabling resin regeneration. However, challenges remain. A key issue is the management of PFAS-laden brines from resin regeneration using methanol and salt solutions, which produce concentrated waste streams that are difficult and potentially hazardous to handle. Consequently, the current practice often involves single-use IXR followed by off-site incineration. There is an urgent need to develop cost-effective and environmentally sound destruction technologies that can be integrated with IX systems to reduce reliance on incineration.

2.2.3 Reverse Osmosis (RO) and Nanofiltration (NF)

Reverse osmosis (RO) and nanofiltration (NF) have proven to be highly effective and durable technologies for the removal of PFAS, regardless of chain length. These membrane separation technologies offer significant advantages over other concentration methods, particularly in terms of removal efficiency and operational flexibility. Reported PFAS removal efficiencies exceed 99% for RO membranes and range between 90% and 99% for NF membranes.

RO processes typically operate under high pressures (10–100 bar) and utilize membranes with extremely small pore sizes (0.1–1 nm), resulting in significant energy costs (Ahmed et al., 2020). NF systems, in comparison, operate at lower pressures (5–40 bar) with slightly larger pore sizes (0.5–2 nm). The most commonly used commercial membranes for PFAS removal in both RO and NF applications are thin-film composite polyamide membranes (Misdan et al., 2014). Mastropietro et al. (2021) reviewed recent advances in membrane technologies for PFAS removal, confirming the high performance of RO (>99% removal) and NF (90–99% removal) systems. The rejection of PFOS using thin-film composite RO membranes was first demonstrated by Tang et al. (2006), who tested a wide range of PFOS concentrations (0.5–1600 ppm) at pH 4. Their results showed greater than 99% rejection for feed concentrations above 1 ppm. Similarly, Baudequin et al. (2014) reported PFOS rejection efficiencies between 99.4% and 99.9% at both laboratory and industrial scales using PA composite membranes at a permeability of 0.5 L h⁻¹ m⁻² bar⁻¹.

The performance of NF membranes under high PFOA concentrations was examined by Hang et al. (2015), who tested NF270 and NF90 membranes at PFOA concentrations of 100, 1000, and 10,000 mg/L. Their findings indicated superior rejection performance for the NF90

membrane, achieving nearly 100% rejection at concentrations below 800 mg/L. In contrast, NF270 showed lower rejection rates, which improved at higher PFOA concentrations due to surface accumulation of the compound.

Despite these high removal efficiencies, RO and NF cannot completely resolve PFAS contamination as the retained concentrate stream still contains high levels of PFAS. Managing this waste stream remains a major technical and economic challenge due to the lack of viable and cost-effective treatment options (Mastropietro et al., 2021). Therefore, hybrid treatment approaches are being explored to integrate RO/NF with complementary technologies.

In conclusion, RO and NF are proven, effective technologies for removing both long- and short-chain PFAS in a single treatment step. However, their application is constrained by high energy demands, membrane fouling, and concentrate management challenges. For groundwater treatment, it is critical to monitor and control factors such as suspended solids and water chemistry to mitigate membrane fouling. Ultimately, to address the diverse PFAS mixtures and co-contaminants present in real water matrices, a combination of treatment methods is necessary.

2.2.4 Ozofractionation (OF) and Foam Fractionation (FF)

Foam fractionation (FF) is a process that separates surface-active compounds from aqueous solutions through their enrichment in rising foam (Buckley et al., 2021). Building on this concept, Dickson (2014) proposed *ozofractionation* (OF) as a combined treatment approach that integrates FF with ozone application. OF and FF have recently gained attention for PFAS remediation in groundwater due to their low capital and energy requirements, as well as their minimal interference from co-contaminants (John Horst et al., 2018).

Multiple studies have indicated that gas flow rate and bubble surface area are the most critical factors influencing PFAS removal efficiency in FF and OF processes. Typically, PFAS recovery improves with increased gas flow or greater bubble surface area.

Meng et al. (2018) investigated PFAS removal via foam collection and aeration. Their results demonstrated that PFOS removal reached 96% after two hours at an aeration rate of 75 mL/min, with PFOS concentrations in the collected foam reaching up to 6.5 mmol/L, favoring potential recovery and reuse. Kinetic analyses further confirmed that PFOS removal increased with higher aeration flow rates. However, the method showed diminished performance with higher initial PFOS concentrations and was less effective for short-chain PFAS, achieving only about 50% removal for PFHxS and 30% for PFBS after two hours of treatment.

McCleaf et al. (2021) reported that foam fractionation successfully removed more than 90% of several PFAS, including PFOA (C7), PFOS (C8), PFHxS (C6), PFHpA (C6), and 6:2 FTSA, from landfill leachate in both batch and continuous systems. Moderately effective removal (50–80%) was observed for PFNA (C8), PFPeS (C4), PFHxA (C5), PFHpS (C7), and PFBS (C4), while removal rates dropped to 20–50% for compounds such as EtFOSAA (C8), PFBA (C3), PFDA (C9), FOSA (C8), PFPeA (C4), and MeFOSAA (C8). Improved removal efficiencies were associated with increased air flow rates, the presence of iron(III) oxide (Fe³+) as a coagulant, higher conductivity, and greater initial PFAS concentrations in untreated leachate.

OF has also been implemented at full scale for treating fluorotelomer foam-contaminated surface and wastewater. Ross et al. (2017) described a modular OF system located in Brisbane, Australia, consisting of a feed tank, reaction vessels, an ozone generator, and a sand filter. This system achieved over 97% removal of 28 PFAS compounds across a wide range of influent concentrations (100–5,400 μg/L).

Despite its many advantages, the OF/FF process generates a concentrated PFAS waste stream that requires careful management. Moreover, due to the difficulty in achieving ultra-low (ng/L) regulatory limits, FF and OF are more suited as preliminary treatment steps within a broader treatment train that integrates additional polishing technologies to meet stringent discharge or reuse standards.

2.2.5 Electrocoagulation (EC)

Electrocoagulation (EC) has emerged as an effective alternative to conventional coagulation processes for wastewater treatment. EC offers several advantages, including reduced sludge generation, the elimination of chemical coagulants and flocculants, simple equipment design, ease of operation, and high pollutant removal efficiency. It has been successfully used to remove various contaminants—such as heavy metals, surfactants, phenol, and boron—through the in-situ generation of metal hydroxides from anodic electrooxidation. Recent studies have also demonstrated the potential of EC for the removal of per- and polyfluoroalkyl substances (PFASs) from water (Garg et al., 2021).

The performance of EC is influenced by several operational parameters, including anode material, current density, pH, and mixing speed. Commonly studied anode materials include zinc, iron, and aluminum.

Lin et al. (2015) investigated the sorption of perfluoroalkyl acids (PFAAs) using metal hydroxide flocs generated in situ via EC in deionized water with 10 mM NaCl as a supporting electrolyte. Among four tested metal hydroxide flocs, zinc hydroxide exhibited the highest removal efficiency for a broad range of PFOA and PFOS concentrations at a zinc dosage of 150 mg/L and energy consumption of just 0.18 Wh/L. Hydrophobic interactions were identified as

the primary mechanism for PFAA sorption onto the flocs, suggesting the applicability of zincbased EC for treating industrial and contaminated water sources.

Wang et al. (2016) further explored the impact of cathode materials and background anions on PFOA removal using EC with zinc anodes. Batch tests showed that hydroxide flocs formed with stainless steel cathodes were more effective than those formed with aluminum. The presence of Cl⁻ or NO₃⁻ significantly enhanced removal efficiency (>97%), while carbonate and bicarbonate (CO₃²/HCO₃⁻) severely inhibited performance, reducing PFOA removal to below 10%. These differences were attributed to the distinct physicochemical characteristics of flocs formed under varying electrolyte and electrode conditions.

Yang et al. (2016) evaluated EC performance using iron electrodes for treating wastewater from the organic fluorine industry with moderate PFAA concentrations. Optimal conditions included a current density of 25 mA/cm², stirring speed of 180 rpm, and 2 g/L NaCl as a supporting electrolyte. Under these conditions, over 99% of PFOS (initial concentration: 0.25 mM) was removed within 50 minutes. The primary removal mechanism was electrostatic adsorption of PFAAs onto iron hydroxide flocs, with zeta potential analysis confirming chain-length-dependent removal efficiencies.

Liu et al. (2018) applied periodically reversed electrocoagulation (PREC) using various anode combinations—Fe-Fe, Fe-Zn, Fe-Al, Al-Al, Zn-Zn, and Al-Zn—to treat groundwater contaminated with PFOA (1 mg/L). The Al-Zn electrode pair achieved the highest removal efficiency (up to 99.6%) under optimal conditions (9 V, 500 rpm), with an energy consumption of 43.93 kWh/kg PFOA removed. In real groundwater samples, the method achieved a conversion efficiency of 79.4% after 60 minutes, with removal efficiencies ranked as: PFOA

(79%) > PFHpA (48%) > PFHxA (34%). These results highlight a preferential adsorption of longer-chain PFASs due to their higher hydrophobicity.

In a related study, Bao et al. (2020) optimized PREC conditions using Al-Zn electrodes to treat 1 mg/L of perfluoroalkyl sulfonic acids (PFSAs) in synthetic groundwater. The optimal removal was achieved at 12 V, pH 7.0, and a stirring speed of 400 rpm. Within the first 10 minutes, removal efficiencies reached 87.4% for PFBS, 95.6% for PFHxS, and 100% for PFOS. In natural groundwater, the improved PREC approach achieved removal efficiencies ranging from 59.0% to 100% for the three target PFSA analytes after 60 minutes. Long-chain PFASs such as PFHxS and PFOS were more effectively removed due to their stronger hydrophobic interactions with Al-Zn hydroxide flocs compared to the short-chain PFBS.

EC, especially with optimized electrode combinations and process parameters, is a promising technology for PFAS removal in both synthetic and real water matrices. However, integration with other treatment technologies may be needed to meet stringent regulatory limits for short-chain PFAS.

2.3 Chemical Destruction Technologies

2.3.1 Photocatalysis

Photocatalysis is a widely used advanced water treatment process that involves the transfer of electrons from an electron donor to an acceptor, leading to the chemical transformation of contaminants either directly or through the formation of reactive species (Nzeribe et al., 2019). However, incomplete mineralization can occur during chemical oxidation, producing intermediates and byproducts that may be more toxic and persistent than the original contaminants, which increases operational costs due to longer processing times and byproduct

disposal. The use of ultraviolet (UV) irradiation—via UV lamps or natural sunlight—can enhance oxidation by accelerating reactions and generating free radicals, often resulting in more complete mineralization (Xu et al., 2017).

PFAS compounds are highly stable and resistant to direct electron transfer oxidation, prompting researchers to focus on free radical oxidation processes for their degradation (Umar, 2021). Photodegradation without external chemical additives also shows promise (Lyu et al., 2015). The most commonly studied UV-based advanced oxidation processes for PFAS degradation include UV/H₂O₂, UV/sulfite, and UV/Fe³⁺ systems (Umar, 2021). Factors such as pH, initial PFAS concentration, and reaction time significantly influence decomposition and defluorination efficiency.

Interestingly, the addition of H₂O₂ can sometimes inhibit PFOA degradation due to competitive photon absorption. For example, Thi et al. (2013) found that direct UV photolysis achieved about 52% PFOA degradation after 12 hours, whereas UV/ H₂O₂ achieved only ~32%. This reduction is attributed to the reaction of photogenerated electrons with H₂O₂ and hydroxyl radicals, which lowers degradation efficiency (Hori et al., 2004). However, adding carbonate radicals (CO₃• to the UV/H₂O₂ system led to complete PFOA decomposition and the highest defluorination efficiency (~82%), demonstrating carbonate radicals' potential as effective oxidants in such systems. Despite UV/ H₂O₂'s limited effectiveness for PFAS alone, it may work well in real water matrices containing carbonate species.

Sulfate (SO₄•¯) and persulfate (S₂O₈•²¯) radicals generated by UV irradiation have also been studied for PFAS degradation. Gu et al. (2016) showed that 98% of PFOS was decomposed within 30 minutes at pH 9.2 under a UV/sulfite system with an energy cost of 220 KJ/μM. Similarly, Qian et al. (2016) reported 85.6% PFOA degradation after 8 hours under UV-

persulfate irradiation, though degradation was slower in wastewater matrices compared to pure water. The presence of chloride and carbonate ions suppressed PFOA degradation until chloride was converted to chlorite, highlighting water matrix impacts on treatment performance.

The use of ferric ions (Fe³⁺) as catalysts in photodegradation has gained attention. Liang et al. (2016) demonstrated that vacuum UV light alone could fully decompose PFOA over 144 hours, but in the presence of Fe³⁺ (20 μM), total defluorination occurred in half the time (72 hours), with hydroxyl radicals playing a key role. Jin et al. (2014) observed a significant decrease in PFOS concentration under UV irradiation with ferric ions, with a rate constant of 1.67 d⁻¹. Lyu et al. (2015) showed that PFOS can be rapidly degraded through direct photolysis at high pH (11.8) and elevated temperature (100°C), with reductive species such as hydrated electrons from water photolysis playing crucial roles. Lower pH values strongly inhibited degradation.

Additionally, Duan et al. (2020) investigated boron nitride (BN) as a photocatalyst and found it to be more active than TiO₂ for PFOA degradation under UV light. After 4 hours, PFOA concentrations dropped significantly, though short-chain PFAS byproducts accounted for 16% of the residual contamination. BN also showed some activity against GenX, a newer PFAS compound.

While potocatalysis effectively degrades low-concentration PFAS, several challenges remain before wide-scale adoption. These include understanding how organic matter and co-contaminants affect degradation, reducing energy consumption through process optimization or combined treatment trains, and assessing the toxicity of treated water to ensure safety. Future research should focus on these areas to improve the viability and safety of UV-based PFAS treatments.

2.3.2 Electrochemical Oxidation

In recent years, electrochemical oxidation (EO) has garnered significant attention for PFAS treatment due to its ability to completely mineralize PFOA, PFOS, and other representative PFAS compounds (Sharma et al., 2022). EO has demonstrated high efficiency in degrading PFAS in water, and it typically consumes less energy compared to other destruction technologies such as photolysis and sonolysis (Sukeesan et al., 2021). However, EO is less effective at degrading short-chain PFASs, and challenges remain including potential metal electrode corrosion and the formation of undesirable toxic by-products, such as chlorinated compounds (Wanninayake, 2021). Therefore, careful selection of the electrode material is critical, as the anode plays a key role in the EO process. Various electrode materials have been investigated, including titanium dioxide (TiO₂), titanium suboxide (Ti₄O₇), lead dioxide (PbO₂), stannous dioxide (SnO₂), boron-doped diamond (BDD), platinum (Pt), and carbon-based electrodes (Wanninayake, 2021; Ibrahim Abouelamaiem et al., 2018).

Several studies have explored factors influencing EO degradation of PFASs, including anode materials, reactor configuration, current density, electrolytes, pH, initial PFAS concentration, and the oxidative species involved. This review discusses the effects of these parameters on EO performance, PFAS removal efficiency, and energy consumption.

2.3.2.1 Effect of Anode Materials

The efficiency of EO strongly depends on the anode's electron transfer capacity, hydroxyl radical (•OH) generation ability, and oxygen evolution potential (OEP). Over the past decade, three main types of anodes have been extensively studied: mixed metal oxide (MMO) anodes, boron-doped diamond (BDD), and Magnéli phase Ti₄O₇.

BDD, PbO₂, and SnO₂ are considered "non-active" anodes, meaning they act as inert substrates where minimal interaction occurs between the electrode and the reactants or products. However, BDD's high cost (~\$7000/m²) limits its widespread use (Veciana et al., 2022). Alternatives such as SnO₂ and PbO₂ are more affordable but suffer from short lifespans and potential metal leaching, hindering commercial deployment (Wu et al., 2014). Recently, titanium oxides, especially Magnéli phase Ti₄O₇, have gained attention as promising materials due to their excellent conductivity, stability, and cost-effectiveness.

A summary of recent studies shows that PFOA removal efficiencies on BDD range from 41% (Pierpaoli et al., 2021) to 99% (Schaefer et al., 2017), while Ti4O7 achieves between 77.2% (Liang et al., 2018) and 99.9% (Le et al., 2019).

2.3.2.1.1 BDD Anode

BDD was the first widely studied anode for PFAS EO starting in 2008, favored for its high OEP (2.7 V vs. SHE), wide potential window, durability, chemical stability, and mechanical strength (Niu et al., 2016; Schaefer et al., 2015). BDD is synthesized by doping diamond with boron, though variations in boron concentration (e.g., 0.5k to 10k ppm) appear to have minimal impact on PFOA and PFOS removal (Pierpaoli et al., 2021). Lab and full-scale studies have confirmed effective PFAS degradation with BDD (Gomez-Ruiz et al., 2017; Zhuo et al., 2012). For instance, Gomez-Ruiz et al. (2017) reported 99.74% PFAS removal and 91.10% TOC reduction after 10 hours of treatment of industrial wastewater, albeit with a high energy consumption of 256 kWh/m³.

2.3.2.1.2 MMO Anodes

Common MMO anodes include PbO₂ and SnO₂, which are semiconductors with a band gap of about 3.5 eV and require doping (typically Sb for SnO₂ and Ce for PbO₂) to improve

conductivity (Lin et al., 2012; Duan et al., 2014). Ti substrates are widely used for these anodes (Lin et al., 2012; Santos et al., 2014). Ce-doped PbO₂ effectively degrades high concentrations of PFOA, achieving 99.5% removal at 23 mg/L in 3 hours at 5 mA/cm² with NaClO₄ electrolyte (Lin et al., 2018). However, short-chain PFASs like PFBA are less efficiently degraded (31.8% removal at 100 mg/L after 1.5 hours at 20 mA/cm²) (Ibrahim Abouelamaiem et al., 2018). Ti/SnO₂–F electrodes have demonstrated rapid PFOA decomposition (99% within 30 minutes at 20 mA/cm²) (Yang et al., 2015). Modified Ti/SnO₂-Sb/PbO₂-PTFE anodes achieved 92.1% PFOS degradation at pH 3 in 3 hours, although their service life is limited to under 50 hours (Zhuo et al., 2020).

2.3.2.1.3 Ti₄O₇ Anodes

Magnéli phase Ti₄O₇ electrodes are emerging as highly promising due to their high conductivity (\$0.36/m²) (Walsh & Wills, 2010). Ti₄O₇ has demonstrated efficient degradation of PFOA, PFOS, and other PFASs under ambient conditions (20–25 °C, neutral pH). Lin et al. (2018) showed that Ti₄O₇ outperforms PbO2 and BDD in oxidizing PFOA and PFOS, achieving 99.9% and 93.1% degradation respectively in 3 hours at 5 mA/cm². Energy consumption was relatively low at 14.2 kWh/m³ for PFOA and 36.9 kWh/m³ for PFOS. Huang et al. (2020) developed a Ti₄O₇-based electrode that removed 87% of PFOA in 1 hour at 10 mA/cm² with concurrent fluoride release of 77.9%. The electrical energy per order (EE/O) was 57.1 kWh/m³. Doping Ti₄O₇ with Ce³+ enhances electrochemical reactivity by accelerating charge transfer and boosting hydroxyl radical production by 37–129% (Lin et al., 2021). At 3% doping, PFOS oxidation rates were 2.4 times higher than undoped Ti₄O₇, achieving 98.9% removal in 2 hours with an energy cost of 3.8–4.5 kWh/m³.

2.3.2.1.4 Comparison of Anodes

While all these anodes effectively degrade PFASs, they differ in lifespan, energy consumption, by-product generation, and commercial viability. MMO anodes typically last only tens of hours, whereas BDD offers longer service life, and Ti₄O₇ can last up to three years (Yaye Wang et al., 2022). Under identical conditions (10 mA/cm², 20 min), Ti₄O₇ outperforms BDD for PFOS degradation (98.6% vs. 85.7%) (L. Wang et al., 2020). Ti₄O₇ also consumes less energy (3.6 kWh/m³ vs. 19.9 kWh/m³ for BDD) for 90% PFOS removal. Both anodes generate chlorate and perchlorate from chloride ions, but these by-products form much more slowly on Ti₄O₇, making it preferable for PFAS treatment in chloride-rich matrices such as groundwater (Yaye Wang et al., 2022).

Overall, Ti₄O₇ stands out as a promising anode material due to its high porosity, large electroactive surface area, chemical stability in harsh environments, low energy requirements, and cost-effectiveness.

2.3.2.2 Effect of Reactor Configuration

Several recent studies have explored the impact of reactor design on improving electrochemical oxidation (EO) performance for PFAS degradation. Reactor configuration—specifically, operating in flow-by or flow-through mode—has a significant effect on PFAS mass transfer rates. To overcome mass transfer limitations, reactive electrochemical membrane (REM) systems have been proposed. These systems use porous materials that simultaneously function as both membrane and anode, allowing filtration of contaminated water while enhancing interfacial mass transfer.

Wang et al. reported that REM systems generally outperform conventional batch reactors.

This improvement is attributed to an increased effective electroactive surface area (EESA),

enhanced interfacial mass transfer, and amplified electric fields within the microporous structures of the membrane (Wang et al., 2022).

Liang et al. were the first to demonstrate effective decomposition of PFOA and PFOS in concentrated ion exchange resin (IXR) waste using a 3D ceramic electrode made of Magnéli phase Ti₄O₇. They also compared EO performance using different batch reactor setups: one-sided (one anode and one cathode) and two-sided (one anode and two cathodes). The two-sided configuration significantly enhanced degradation efficiency, likely due to the increased reactive surface area provided by the additional cathode (Liang et al., 2018).

L. Wang et al. showed that flow-through Ti₄O₇ reactors achieved surface-normalized electrooxidation rate constants 1–2 orders of magnitude higher than those in flow-by mode. Specifically, the rate constants for PFOA and PFOS were 4.4×10^{-5} m/s and 1.3×10^{-4} m/s in flow-through mode, compared to 5.74×10^{-6} m/s and 8.81×10^{-6} m/s, respectively, in flow-by operation (L. Wang et al., 2020).

Shi et al. investigated PFOS degradation in a REM system using a porous Magnéli phase titanium suboxide ceramic membrane. Under cross-flow filtration and an anodic potential of 3.15 V vs. the standard hydrogen electrode (SHE), they achieved near-complete PFOS removal (98.30 \pm 0.51%). The PFOS removal efficiency in REM operation was significantly higher than in batch mode under the same anodic potential (Shi et al., 2019).

Similarly, Le et al. studied a Magnéli phase Ti₄O₇ REM system for treating PFOA and PFOS. They achieved approximately 5-log removal of both compounds in a single pass, with residence times of ~11 seconds at 3.3 V/SHE for PFOA and 3.6 V/SHE for PFOS. Initial concentrations of 4.14 mg/L (PFOA) and 5 mg/L (PFOS) were reduced to <86 ng/L and 35 ng/L,

respectively. Energy consumption per log removal was 5.1 kWh/m³ for PFOA and 6.7 kWh/m³ for PFOS, demonstrating high treatment efficiency (Le et al., 2019).

Fenti et al. tested a bench-scale flow-through EO reactor using a mesh anode made of Magnéli-phase titanium suboxides (TinO_{2n-1}) to treat PFAS-impacted groundwater in situ. At a flow rate of 3 L/min and an initial PFOS concentration of 200 μg/L, the system achieved >99% removal. Furthermore, the Ti_nO_{2n-1} anodes demonstrated higher PFOS oxidation rates and lower energy consumption compared to boron-doped diamond (BDD) and IrO₂–Ta₂O₅ mixed metal oxide (MMO) anodes (Fenti et al., 2022).

2.3.2.3 Effect of Current Density

Current density—defined as the amount of electric current per unit surface area of the electrode—is a critical operational parameter in EO processes. It directly influences the generation rate of reactive oxidative species, particularly hydroxyl radicals (·OH), which are primarily responsible for PFAS degradation (Chen, 2004).

At low current densities, PFAS degradation is often insufficient. This is typically due to the applied potential being lower than the threshold required for direct oxidation of PFAS, or because the anode generates an inadequate concentration of ·OH. Several studies have shown that increasing the current density enhances the generation of ·OH, thereby improving degradation efficiency (Niu et al., 2016). However, this improvement comes at the cost of higher energy consumption, which is a key consideration in the overall feasibility and sustainability of EO systems.

For instance, Pierpaoli et al. (2021) demonstrated that higher current densities significantly increased the degradation of PFOA and PFOS in landfill leachate using a boron-doped diamond (BDD) anode. At a current density of 75 mA/cm², average removal efficiencies

of 80% for PFOA and 78% for PFOS were achieved after 8 hours of treatment. In contrast, lowering the current density to 25 mA/cm² reduced the removal efficiencies by approximately half, likely due to the prevalence of competing side reactions in the complex leachate matrix. The energy consumption associated with these removal efficiencies was substantial. Achieving 80% PFOA and 75% PFOS removal at 75 mA/cm² required 114 kWh/m³ and 106 kWh/m³, respectively. These findings underscore the trade-off between treatment performance and energy cost when optimizing current density for PFAS degradation via EO.

2.3.2.4 Effect of Electrolytes

Supporting electrolytes are essential in electrochemical oxidation (EO) processes, as they provide an electroconductive medium, reduce solution resistance, and minimize voltage drop across the electrochemical reactor. Commonly used electrolytes include sodium sulfate (Na₂SO₄), sodium chloride (NaCl), sodium perchlorate (NaClO₄), and sodium nitrate (NaNO₃). Beyond their role in conductivity, certain electrolytes can influence the generation of reactive oxidative species and thereby enhance PFAS degradation efficiency.

Among these, sodium sulfate (Na₂SO₄) has emerged as a particularly effective electrolyte. Studies have shown that Na₂SO₄ not only improves electroconductivity but also promotes the formation of sulfate radicals (SO₄•¬), which contribute significantly to PFAS degradation (Liu et al., 2019). For example, Liu et al. (2019) found that the PFOA oxidation rate in a sulfate-based electrolyte was 2.3 to 3.4 times higher than those observed with nitrate or perchlorate electrolytes. Similarly, Barisci and Suri (2020) reported superior degradation performance with sodium sulfate compared to sodium chloride, attributing this to the enhanced generation of sulfate radicals, which provide a more effective oxidative pathway for PFOA.

However, the concentration of the electrolyte also plays a crucial role, especially in terms of energy efficiency. At low concentrations (<20 mM), the solution resistance increases, leading to higher energy consumption during treatment. Conversely, excessively high concentrations (>100 mM) can negatively affect the generation of fluoride ions (F⁻) from PFAS degradation when using boron-doped diamond (BDD) anodes. Sukeesan et al. (2021) observed a decline in F⁻ formation at higher Na₂SO₄ concentrations, suggesting that optimal electrolyte dosing is necessary to balance performance and energy consumption.

Overall, the choice and concentration of the supporting electrolyte can significantly impact the efficiency, mechanisms, and energy demands of PFAS degradation in EO systems.

2.3.2.5 *Effect of pH*

The pH of the solution during electrochemical treatment can fluctuate due to the generation of H⁺ and OH⁻ ions during water oxidation. This shift in pH can significantly influence electrochemical oxidation (EO) efficiency by affecting hydroxyl radical (•OH) generation, the oxygen evolution reaction (OER), and the longevity of the anode. Additionally, pH influences PFAS sorption behavior and interactions with the electrode surface.

Previous studies have consistently shown that acidic conditions are generally more favorable for PFAS degradation during EO. Under low pH, enhanced •OH generation and a higher oxygen overpotential promote more efficient oxidation of PFAS compounds (Niu et al., 2016). Moreover, PFAS sorption onto anode surfaces tends to increase at lower pH, which can facilitate closer contact between PFAS molecules and reactive sites, thereby improving degradation efficiency (Schaefer et al., 2015).

Acidic conditions also inhibit the oxygen evolution reaction, which competes with PFAS oxidation for available charge, thereby further enhancing treatment efficiency (Lin et al., 2012;

Zhuo et al., 2012). For instance, Lin et al. (2012) reported that the rate constant for PFOA degradation over a Ti/SnO₂–Sb anode at an initial pH of 5 was approximately twice as high as that at pH 11. The corresponding half-life ($t_1/2$) increased from 27.7 minutes at pH 5 to 57.8 minutes at pH 11. Similarly, Zhuo et al. (2012) demonstrated that the degradation rate of PFOA on a Si/BDD anode followed the trend pH 3 > pH 9 > pH 12, indicating superior performance under acidic conditions.

These findings underscore the importance of optimizing pH conditions to maximize PFAS removal efficiency during electrochemical treatment.

2.3.3 Sonolysis

Sonolysis refers to the degradation of compounds through acoustic cavitation, which occurs when ultrasonic irradiation induces the rapid formation, growth, and collapse of microbubbles in aqueous solutions. These implosions create extreme local conditions, with temperatures inside the collapsing bubbles reaching 4,000–10,000 K, and temperatures near the bubble interface ranging from 1,000–1,500 K. These high-energy environments facilitate both pyrolytic and radical-driven reactions capable of decomposing persistent contaminants like PFAS. Volatile compounds tend to degrade inside the cavitation bubbles, while hydroxyl radicals (*OH) generated in the surrounding liquid phase oxidize other substances in the bulk solution (Rodriguez-Freire et al., 2015). As a result, sonolysis is considered an effective advanced oxidation process (AOP).

The degradation efficiency of PFAS via sonolysis is influenced by the physicochemical properties of the target compound, including hydrophobicity, surface tension, surface activity, and volatility. Additionally, operational factors such as ultrasonic frequency, power density,

reactor geometry, temperature, and pH significantly impact treatment performance (Vecitis et al., 2008).

Due to its operational simplicity, low risk of secondary pollutant formation, and safety, sonolysis has been widely applied in environmental remediation research. Numerous studies have reported promising degradation of various PFAS under laboratory conditions. Cao et al. (2020) comprehensively reviewed the influence of parameters such as frequency, temperature, additives, initial PFAS concentrations, and chemical structure on sonolytic performance. According to a meta-analysis by Sidnell et al. (2022), optimal degradation conditions for perfluoroalkyl oxoacids (PFOX) included frequencies of 300–500 kHz, temperatures between 20–30 °C, and solution pH values ranging from 3.2–4.0. However, these conditions may vary based on PFAS chain length and structure, with short-chain PFAS showing improved degradation at frequencies above 600 kHz.

Gole et al. (2018) investigated the sonolytic treatment of PFAS mixtures in two commercially available aqueous film-forming foams (AFFFs), using a 12-transducer reactor operating at either 500 kHz or 1 MHz with 12 kW input power. PFAS degradation efficiency was found to inversely correlate with initial pH up to pH 4. In a 13-hour treatment, they achieved reductions of ~90.5% for perfluoroalkyl sulfonates (PFSAs), ~38.4% for perfluoroalkyl carboxylates (PFCAs), and ~26.6% for fluorotelomer sulfonates (FTSs). The estimated energy consumption was 6.9 kJ/L for 3M-AFFF and 7.3 kJ/L for ANSUL-AFFF at a 500x dilution.

Lee et al. (2016) studied the enhancement of PFOA sonodegradation using periodate (PI) at 40 kHz. The addition of 45 mM PI accelerated PFOA degradation rates by over ninefold compared to ultrasound alone, with 96.5% removal and 95.7% defluorination achieved in 120 minutes at pH 3.9. The enhancement was attributed to the generation of IO₄• radicals under

acidic conditions. Notably, sparging with nitrogen improved degradation compared to air and oxygen, due to reduced competition from radical scavenging species (IO₃•). The optimal degradation was achieved under acidic conditions (pH 3.9), with high PI dosage (45 mM) and nitrogen sparging.

In conclusion, while sonolysis is generally less effective than other PFAS-destructive technologies in terms of energy efficiency and scalability, it offers advantages such as low production of toxic or short-chain by-products. However, significant barriers—such as high energy demands for complete mineralization and limited scalability—must be addressed before full-scale practical applications are feasible (Cao et al., 2020).

2.3.4 Plasma-based Treatment

Plasma, often referred to as the fourth state of matter, is defined as an overall electrically neutral ionized gas composed of free electrons, ions, and photons, typically generated by an intense electric field (Palma et al., 2022). In water treatment, plasma discharges are produced within a channel where high-energy electrons interact with water molecules via inelastic collisions, initiating a cascade of reactive processes (Palma et al., 2022). Plasma can be classified into thermal and non-thermal categories based on electron temperature. Most plasma-based water treatments employ non-thermal plasma (NTP) due to its suitability for operation at atmospheric pressure and ambient temperatures (Nzeribe et al., 2019).

Over the past two decades, NTP has garnered increasing attention for its efficiency in PFAS degradation and operational versatility. It can be generated using ambient air or with the support of gases such as He, Ne, Ar, O₂, and N₂. The high-energy electrical discharges create a complex mixture of reactive oxygen and nitrogen species (RONS), including hydroxyl radicals

(•OH), atomic hydrogen (H•), superoxide (O2•–), hydrogen peroxide (H2O2), ozone (O3), singlet oxygen (¹O2), and free electrons. Additionally, plasma discharges produce localized heat, shockwaves, and UV radiation, which collectively contribute to contaminant degradation (Saleem et al., 2020). Importantly, this multi-modal oxidative process does not require external chemical additives, making plasma a relatively green technology (Palma et al., 2022). However, one drawback is that long-chain PFAS often degrade into short-chain PFAS intermediates, which may retain environmental persistence and toxicity (Singh, Fernando, et al., 2019).

Three general plasma application strategies are employed in water treatment, direct discharge, indirect discharge, and bubbling method. In direct discharge mode, electrodes are submerged in water, producing streamers and sparks directly in the bulk solution (Palma et al., 2022). Electrodes are positioned above the water surface; reactive species generated in the gas phase diffuse into the liquid in the indirect discharge process (Palma et al., 2022). With the application of bubbling method, Plasma is generated inside gas bubbles that are then introduced into the water, facilitating effective dispersion of reactive species (Palma et al., 2022).

Among the various reactor designs, Dielectric Barrier Discharge (DBD) and Corona Discharge (CD) reactors are the most widely studied for PFAS degradation (Mahyar et al., 2019).

Plasma performance depends heavily on reactor design, gas composition, and water matrix characteristics, such as: pH, Nitrate (NO₃⁻), and Dissolved Organic Matter (DOM). NTP treatments often result in solution acidification, particularly under air or nitrogen atmospheres (Stratton et al., 2017). However, acidic conditions have been shown to inhibit PFAS degradation (Bolouki et al., 2021), making pH monitoring essential throughout treatment (Palma et al., 2022).

Nitrate (NO₃⁻) acts as a strong scavenger of aqueous electrons, which are critical for PFAS transformation. Fan et al. (2021) and Stratton et al. (2017) found that 10 mM NaNO₃ could nearly halt the degradation of 20 mM PFOA, highlighting the inhibitory effects of nitrate on NTP performance. DOM competes for reactive species, particularly •OH radicals, thus reducing PFAS degradation efficiency. Pretreatment to remove DOM may be necessary when treating natural waters (Cui et al., 2019).

2.3.5 Advanced Reductive Processes (ARPs)

Studies related to advanced reduction processes (ARPs) for water treatment have grown exponentially since the term was first introduced in 2013 (Vellanki et al., 2013). ARPs are a class of treatment processes that combine activation methods with reducing agents to generate highly reductive radicals capable of destroying contaminants in water. Activation methods include ultraviolet (UV) light, ultrasound, electron beam irradiation, and microwaves, while common reducing solutes include dithionite, sulfite, ferrous iron, nitrilotriacetic acid, and sulfide. Among these, sulfite (SO₃²⁻) and iodide (I⁻) are the most frequently used (Waclawek et al., 2022).

ARPs have been shown to effectively remove various contaminants such as vinyl chloride, perchlorate, bromate, nitrate, chromium, and 2,4,6-trichlorophenol (Liu et al., 2013). Recently, ARPs have received increasing attention due to their demonstrated ability to degrade various per- and polyfluoroalkyl substances (PFAS) in water. The destruction of PFAS during ARP treatment is primarily attributed to the generation of reductive radicals, including hydrated electrons (eaq⁻), hydrogen radicals (H•), sulfite radical anions (SO₂•⁻), and sulfur dioxide radical anions (SO₂•⁻), depending on the activation method and chemical solute used (Cui et al., 2020). The degradation of perfluorocarboxylic acids (PFCAs) primarily occurs through nucleophilic

attack by hydrated electrons, initiating with C–F bond cleavage rather than C–C bond cleavage (Park et al., 2009).

UV/sulfite reduction has been shown to be effective in the defluorination of PFOS, PFOA, and their substitutes such as F-53B. For instance, Sun et al. (2018) demonstrated that under UV irradiation at 365 nm, PFOS and PFOA (20 mg/L each) could be nearly completely degraded within 60 minutes in the presence of 2.4 g/L sulfite and buffer. Bao et al. (2019) showed that F-53B, a PFOS substitute, degraded more rapidly than PFOS under the same conditions (pH 10, 30 °C), with 90% degradation (from 55.2 mg/L) within 60 minutes. These findings suggest that ARPs represent a promising approach for controlling PFAS emissions and mitigating ecological risks.

Generally, PFAS degradation behaviors depend heavily on their functional head groups, and for specific PFAS types, the degradation kinetics may also be influenced by the length of the fluoroalkyl chain (Park et al., 2009). For example, Gu, Liu, Zhang et al. (2017) reported that the observed degradation rate constant (k_obs) of PFOA (0.455 min⁻¹) was nearly four times higher than that of PFOS (0.118 min⁻¹) in a high-photon flux UV/sulfite system at pH 9.2 and 25 °C, with ~5 mg/L of initial dissolved oxygen (DO).

Hydrated electron-driven reductive degradation has been proven highly effective for the chemical destruction of PFAS in water. Near-complete degradation of various PFAS compounds has been achieved under appropriate operational conditions (Z. Y. Sun et al., 2018). Key factors influencing PFAS degradation include pH, DO, humic acid (HA), water matrix composition, and temperature. Among these, pH plays a particularly crucial role. Literature reports pH ranges from 6 to 11, with higher degradation efficiencies observed at pH > 9.2 (Gu et al., 2016; Liu et al., 2013).

The presence of dissolved oxygen has been shown to significantly reduce the rate and efficiency of PFAS degradation in most ARP systems, primarily due to O₂ acting as a scavenger of hydrated electrons. Therefore, deoxygenation prior to treatment is essential—commonly achieved using inert gases such as nitrogen. In addition to scavenging eaq⁻, DO can also absorb UV photons, further decreasing the yield of reactive species.

Humic acid, a major component of dissolved organic matter, can also influence ARP efficiency. For example, Sun et al. (2017) reported that the presence of 1.0 mg/L HA enhanced the photolysis rate of PFOA in a UV/iodide system during the initial phase of treatment. Under similar conditions, PFOS removal was 86% with HA compared to 51.7% without. Moreover, Guo et al. (2019) found that the energy required to reduce PFOA by half was 4.02 kJ/μmol in the presence of HA, lower than 4.54 kJ/μmol without HA. These results suggest that HA can reduce the energy demand for PFAS decomposition in photo-reductive systems.

Future research should focus on minimizing the scavenging effects of coexisting species—particularly H+, DO, and natural organic matter—to improve the overall efficiency of ARPs. Reducing the inhibition caused by H+ would decrease reliance on alkaline conditions and reduce the need for costly pH adjustment. Additionally, developing new and more efficient methods for generating hydrated electrons could significantly enhance ARP performance. Further investigation is also needed into the identity and toxicity of transformation products and byproducts formed during ARP treatment. Lastly, integrating ARPs with concentration technologies such as electrocoagulation (EC) may lead to the development of more robust and energy-efficient treatment systems.

2.3.6 Supercritical Water Oxidation (SCWO)

Water becomes supercritical above 374 °C and 22.1 MPa, entering a unique state characterized by enhanced solubility of organic compounds and accelerated oxidation reactions. Supercritical water (SCW) exists as a single fluid phase with significantly reduced density, allowing it to dissolve gases and organic materials effectively, while simultaneously precipitating inorganic species. Supercritical water oxidation (SCWO) takes advantage of this environment, using oxidative free-radical mechanisms—primarily driven by hydroxyl radicals (•OH)—to convert organic contaminants into carbon dioxide (CO₂) and water (J. Li et al., 2022). SCWO has been successfully applied for the destruction of hazardous and recalcitrant wet wastes that are unsuitable for landfilling or incineration. However, the process faces significant challenges, including severe equipment corrosion and high energy demands due to the extreme temperatures and pressures required.

To date, only a limited number of studies have investigated the degradation of PFASs via SCWO. Two primary reactor configurations are employed: continuous flow and batch reactors. Continuous SCWO systems typically operate at temperatures between 500–650 °C with residence times ranging from 5 to 60 seconds. Batch reactors, by contrast, function at lower temperatures (400–500 °C) but require longer residence times due to material limitations. In both systems, temperature and residence time play critical roles in determining PFAS destruction efficiency.

Pinkard et al. (2021) examined the effects of temperature and residence time on PFAS degradation using a batch SCWO reactor operating between 425 and 500 °C, with residence times from 0 to 60 minutes. Their findings revealed that PFOS could be oxidized to hydrogen fluoride (HF) and CO₂. The study concluded that temperature had a more pronounced effect on

PFOS degradation than residence time. A maximum PFOS destruction efficiency of 70.0% and defluorination efficiency of 78.2% were achieved after 60 minutes at 500 °C, using an initial PFOS concentration of 28.63 mg/L and an excess of H₂O₂. However, this level of degradation was insufficient to reduce PFOS concentrations below the U.S. EPA health advisory limit of 70 ng/L. Additionally, extending residence time beyond 60 minutes provided minimal additional benefit at this temperature.

Krause et al. (2022) evaluated the performance of SCWO continuous flow systems in treating dilute aqueous film-forming foam (AFFF) solutions at 590 °C with a 60-second residence time. Three independent demonstrations conducted by different SCWO technology providers reported PFAS removal efficiencies exceeding 99%, including significant reductions in PFOS and PFOA concentrations. For instance, PFOS concentrations decreased from 26.2 mg/L to 240 μ g/L, 30.4 mg/L to 310 μ g/L, and 190 mg/L to 8.57 μ g/L across the three systems. Similar reductions were observed for PFOA, with concentrations dropping from 930 to 0.14 μ g/L, 883 to 0.102 μ g/L, and from 3,100 μ g/L to non-detectable levels.

McDonough et al. (2022) conducted a field validation study of SCWO to treat concentrated waste streams containing 12 perfluoroalkyl acids (PFAAs), including PFBA, PFPeA, PFHxA, PFHpA, PFOA, PFBS, PFPeS, PFHxS, PFHpS, PFOS, PFNS, and PFDS. Their results demonstrated greater than 99.9% destruction and removal efficiency after approximately 120 minutes of continuous flow treatment at 650 °C, with an overall defluorination efficiency of approximately 62.6%.

Similarly, Espanani et al. (2022) developed a pilot-scale SCWO system capable of operating continuously at a flow rate of 3.8 L/h for AFFF remediation. Their results showed that

total PFAS conversion efficiency exceeded 99% when temperatures surpassed ~615 °C, with degradation efficiency strongly correlated with increasing temperature.

As a destructive treatment technology, SCWO offers a potential alternative to incineration and a long-term solution for PFAS-containing wastewater, particularly in contrast to deep well injection or landfilling. However, the process is energy-intensive. It requires approximately 3,060 kJ/kg to pressurize and heat water from 20 °C to supercritical conditions at 25 MPa and 500 °C. The average energy input per mass of PFAS was estimated at 1.1 × 10⁵ kWh/kg, which is 5–20 times higher than the energy requirements for electrochemical oxidation or plasma-based methods. The specific energy consumption (EE/O) for SCWO was reported as approximately 1,398 kWh/m³ (Krause et al., 2022). Therefore, a comprehensive assessment of the process—including its energy demand, equipment durability, and the toxicity and composition of byproducts—is essential for evaluating SCWO's feasibility as a reliable and safe PFAS treatment method.

2.3.7 Comparison of the Chemistry Destruction Technologies

The comparison of chemical destruction technologies for PFAS removal—namely Electrochemical Oxidation (EO), Non-Thermal Plasma (ch), and Supercritical Water Oxidation (SCWO)—highlights distinct advantages and limitations associated with each method in the Table 2.3. EO stands out for its relatively high degradation efficiency and low energy consumption, particularly in field-scale applications, though it is less effective on short-chain PFAS and may produce toxic by-products. NTP offers a promising, emerging approach with comparable energy use to EO, but is largely at the laboratory development stage and still faces challenges in achieving high energy efficiency and minimizing toxic intermediates. SCWO

demonstrates the highest PFAS destruction and defluorination efficiency, including for both short- and long-chain PFAS, making it a viable long-term solution. However, its implementation is hindered by extremely high energy demands, potential equipment corrosion, and the need for careful monitoring of reaction by-products. Overall, while no single method is universally optimal, EO and NTP may be suited for smaller-scale or lower-strength applications, whereas SCWO holds promise for large-scale treatment if energy and material limitations can be addressed.

2.4 Thermal Technologies

2.4.1 Incineration

While wastewater solids are often used as an energy source, their combustion is typically classified as incineration due to the traditional definition involving the burning of waste materials (Winchell et al., 2021). During incineration at sufficiently high temperatures and adequate residence times, carbon-halogen bonds in halogenated organic compounds—such as polychlorinated biphenyls (PCBs) and ozone-depleting substances (ODSs)—can be broken. This allows the resulting halogens to be captured in the flue gas, commonly as alkali-halogen salts via scrubbing systems. The destruction of halogenated organics generally proceeds via radical reactions and unimolecular decomposition. However, fluorinated organics, like PFAS, typically require higher temperatures than chlorinated compounds to achieve 99.99% destruction efficiency within a 1-second residence time.

Current incineration systems must meet stringent air pollution control requirements to comply with emissions standards. Winchell et al. (2021) examined thermal degradation and incineration practices at municipal water resource recovery facilities (WRRFs), which primarily

utilize two furnace technologies: multiple hearth furnaces (MHFs) and fluidized bed furnaces (FBFs) for treating solids from liquid processes. These systems provide long residence times and high turbulence, promoting more complete combustion. Most studies and industry guidelines recommend operating at temperatures above 1,000°C to ensure effective PFAS destruction. Indeed, incineration is currently the only commercially available method for PFAS destruction (Loganathan et al., 2007).

A full-scale study of a facility using an FBF incinerator reported operating temperatures of 830°C and gas residence times of 8 seconds (MacGregor, 2020). Comprehensive sampling of the system's inputs and outputs revealed a reduction in the mass flow of 28 PFAS compounds across the sewage sludge incinerator (SSI), with the exception of 6:2 fluorotelomer sulfonate. Combustion completeness—and thus PFAS destruction efficiency—is influenced by temperature, residence time, turbulence, and stoichiometry (the balance of waste, oxygen, and fuel gases in the flame zone). While 1,000°C is considered optimal for PFAS destruction, standard sewage sludge incinerators are limited to maximum combustion temperatures of 950°C, with a regulatory minimum of 850°C for flue gas (Schnell et al., 2020). Treating PFAS-containing sludge at these elevated conditions increases energy demand by approximately 15% compared to standard sludge treatment.

Laboratory-scale incineration studies have also provided insight. Taylor et al. (2014) investigated fluorotelomer-based polymer (FTBP) incineration in a two-phase system. They found that while FTBPs can be a precursor to perfluorooctanoic acid (PFOA), incineration at 1,000°C with a 2-second residence time eliminated detectable PFOA formation. Hydrogen fluoride (HF) was detected in concentrations of 3.2–6.6 mg/dscm at 13% oxygen in the exhaust stream, indicating successful degradation of fluorinated compounds.

Altarawneh et al. (2022) conducted theoretical modeling of the thermal decomposition of perfluoropentanoic acid (PFPA, C₄F₉C(O)OH) under incinerator-like conditions. Their model predicted decomposition pathways at 800–1500 K and residence times of 2–25 seconds. At 1020 K and 2 seconds, PFPA was completely decomposed, primarily via HF elimination and formation of a reactive α-lactone intermediate, which further degraded into smaller fluorinated products like C₃F₇COF.

Finally, increasing landfilling or incineration of biosolids rejected due to PFAS contamination may impose financial and environmental burdens on municipalities. As of 2019, approximately 16% of wastewater solids in the U.S. were incinerated (EPA, 2019). Expanding this practice to manage PFAS could significantly increase treatment costs and raise additional environmental concerns.

2.4.2 Pyrolysis and Gasification

Non-incineration thermal processes—specifically pyrolysis and gasification—are emerging as promising alternatives for the treatment of wastewater treatment plant (WWTP) solids contaminated with PFAS (Berg et al., 2022).

Pyrolysis involves the thermal decomposition of solid or semi-solid materials in the absence of oxygen, typically operating between 300°C and 1,000°C. In contrast, gasification utilizes limited oxygen or steam to achieve partial combustion at higher temperatures, generally between 800°C and 1,650°C (Patel et al., 2020). While gasification primarily yields low-carbon ash, pyrolysis produces a char byproduct that may have beneficial reuse potential. Both processes can also generate a hydrogen-rich synthetic gas (syngas) depending on operational conditions.

The combination of high temperature, extended residence time, and subsequent combustion of the syngas in a thermal oxidizer could, in theory, break down PFAS compounds into inert or less persistent constituents. Importantly, both pyrolysis and gasification operate with significantly lower air flow requirements than traditional incineration, potentially reducing the size and capital cost of associated air pollution control equipment. More details on these technologies are provided in the U.S. EPA's research brief on biosolids pyrolysis and gasification (Acheson et al., 2021).

However, limited experimental data exist on the effectiveness of pyrolysis and gasification for PFAS destruction. For example, Kim et al. (2015) conducted laboratory-scale pyrolysis of sewage sludge at 300°C and 700°C. Their findings indicated that residual concentrations of PFOA and PFOS (15.8–16.9 ng/g) in the resulting biochar remained largely unchanged post-treatment. This outcome was unexpected, given the prevailing assumption in the literature that PFAS compounds volatilize below 700°C. The underlying reasons for the persistence of PFAS in these trials remain unclear.

While these technologies hold promise, commercial implementation faces several challenges, including high initial investment costs and substantial knowledge gaps regarding PFAS destruction mechanisms. Further research is essential to validate the complete thermal breakdown of PFAS during pyrolysis and gasification and to evaluate the formation of any toxic or persistent byproducts resulting from incomplete combustion.

2.5 Biological Technologies

2.5.1 Phytoremediation

Phytoremediation refers to the use of plants to absorb, accumulate, and sometimes transform harmful environmental pollutants. Due to its cost-effectiveness, environmental sustainability, and operational simplicity, phytoremediation has gained growing attention as a potential method for remediating PFAS-contaminated environments (T. T. Wang et al., 2020). This approach requires minimal infrastructure and technical expertise, making it especially attractive for large-scale or remote applications with limited resources.

Wetland plants play a particularly important role in PFAS phytoremediation. Several studies have investigated the potential of aquatic plants in constructed wetlands and natural water bodies, showing some promise for PFAS uptake. However, the overall removal efficiency of PFASs via wetland phytoremediation remains limited (Dalahmeh et al., 2018). A comprehensive review by Mayakaduwage et al. (2022) outlined the key mechanisms governing PFAS uptake in both soil-plant and water-plant systems. Factors such as PFAS molecular structure and the physiological traits of plant species (e.g., root morphology, transpiration rate) were shown to influence both bioaccumulation and translocation within plant tissues.

Hydroponic studies on *Alisma orientale*, a wetland plant, have explored the mechanisms of PFOA and PFOS uptake and subcellular distribution. These studies found that water transporters and anion channels facilitate active uptake of PFAS compounds through the roots. Once absorbed, PFASs were predominantly localized in the cell wall (45.6–58.4%) and water-soluble fractions (46.2–70.8%) of the plant cells (T. T. Wang et al., 2020).

Field research near a fire training site at Stockholm Arlanda Airport (Sweden) by Gobelius et al. (2017) analyzed PFAS uptake in native vegetation exposed to contaminated soil and groundwater. Concentrations of Σ26PFAS ranged from 16 to 160 ng/g (dry weight) in soil and 1,200 to 34,000 ng/L in groundwater. Various plant species were collected, including wild strawberries, silver birch, Norway spruce, and beechfern. The highest bioconcentration factors (BCFs) for PFOS were observed in beechfern (906) and spruce (41). Despite this, the total PFAS burden per tree was relatively low (up to 11 mg), suggesting that PFAS bioconcentration in trees may be significantly lower than for heavy metals.

In a controlled greenhouse study, Huff et al. (2020) evaluated PFAS uptake in seven woody and eight herbaceous plant species exposed to six PFAS compounds (including PFPeA, PFHxA, PFOA, PFBS, and PFHxS). *Festuca rubra* emerged as the most efficient accumulator, with BCFs ranging from 11.0 (PFOS) to 111.2 (PFPeA). This species also demonstrated the highest uptake of PFOA, PFHxS, and PFOS (11%, 13%, and 4% respectively). Notably, over 25% of PFPeA, PFHxA, and PFBS added during a 12-week exposure were recovered in its aboveground biomass. These findings support the potential of integrated phytoremediation systems combining short-lived herbaceous plants with longer-lived woody species for enhanced PFAS remediation performance.

Although several studies confirm the ability of plants to accumulate PFAS, phytoremediation remains less effective compared to destructive technologies. Most current research focuses on comparing plant species' translocation and bioaccumulation capacities, with limited data on actual field-scale remediation efficacy or long-term outcomes (Mayakaduwage et al., 2022). Further research is needed to optimize plant selection, understand PFAS behavior within plant systems, and assess the feasibility of scaling up this method for practical applications.

2.5.2 Biodegradation

Compared to physical and chemical remediation approaches, biological treatment offers several advantages, including lower capital investment, reduced environmental disruption, and greater sustainability. Biodegradation, in particular, has been widely recognized for its effectiveness in treating persistent organic pollutants. However, limited success has been achieved in the biodegradation of PFAS, especially for highly stable compounds like PFOA and PFOS. While some studies have reported the release of fluoride ions during microbial treatment—indicating cleavage of the strong C–F bond—overall degradation rates have generally been low.

Zhang et al. (2022) reviewed the state of PFAS microbial degradation and emphasized that microbial species selection plays a critical role in determining degradation efficiency. External factors, such as co-substrates (e.g., carbon sources like lactate), pH, and temperature, also significantly influence biodegradation performance. Given the diverse environmental matrices (wastewater, sediment, soil), tailoring biological treatment strategies to site-specific conditions is essential for optimizing PFAS removal.

Among microbial candidates, the genus *Pseudomonas* has shown notable potential for PFAS degradation. Several studies have investigated *Pseudomonas* strains for this purpose. For instance, Kwon et al. (2014) were the first to report PFOS biodegradation by *Pseudomonas aeruginosa* strain HJ4, achieving a 67% removal of PFOS (1400–1800 μg/L) in activated sludge after 48 hours of incubation under optimal growth conditions (pH 7–9).

Kim et al. (2014) examined the degradation of 6:2 fluorotelomer alcohol (6:2 FTOH) using four fluoroacetate- and three alkane-degrading microorganisms, including *Pseudomonas fluorescens DSM 8341*, *Mycobacterium vaccae JOB5*, *Pseudomonas oleovorans*, and

Pseudomonas butanovora. Their results demonstrated nearly complete 6:2 FTOH degradation by *P. fluorescens* DSM 8341 and *P. butanovora*, although *P. fluorescens* also produced PFBA as a terminal byproduct. *P. oleovorans* and *M. vaccae JOB5* achieved degradation efficiencies of 58–81% and 71–76%, respectively.

Pseudomonas parafulva strain YAB1, isolated from PFAS-contaminated soil, was shown by Yi et al. (2016) to degrade PFOA with removal efficiencies ranging from 32.4% to 48.1%. Optimal conditions for degradation included a temperature of 30°C, pH 7, and an inoculum concentration of 2%. The addition of 1 g/L glucose significantly enhanced degradation, confirming glucose as an effective co-substrate to support bacterial activity.

Biodegradation's key advantages include cost-effectiveness, reduced need for chemicals, and energy efficiency. However, it also faces several major limitations. Biodegradation is relatively slow, often requiring days to weeks for meaningful PFAS reduction. Furthermore, complete mineralization of PFAS is rarely achieved, and partial degradation may lead to the formation of toxic intermediates such as FTOHs without C–F bond cleavage (Shaw et al., 2019). For practical implementation, several factors—such as salinity, redox potential, ionic strength, and reactor design—must be optimized based on the specific environmental matrix.

Overall, while microbial treatment shows promise, its application to PFAS-contaminated sites remains constrained by slow kinetics, incomplete degradation, and insufficient understanding of degradation pathways. Continued research is needed to enhance microbial efficacy, optimize operational parameters, and minimize the formation of potentially harmful byproducts.

2.6 Hybrid Treatment

Since 2015, a growing trend in PFAS remediation has involved the development of *treatment train* processes to effectively achieve in-situ PFAS removal (Lu et al., 2020). These hybrid approaches integrate concentration and destruction technologies, increasing overall efficiency and enabling site-specific flexibility. This section reviews recent studies and practical implementations of such treatment trains.

The most commonly employed concentration methods include granular activated carbon (GAC), ion exchange resins (IXR), electrocoagulation (EC), and ozone/foam fractionation (OF/FF), while destruction approaches often utilize nanofiltration (NF), electrooxidation (EO), ultraviolet (UV) irradiation, and incineration.

2.6.1 GAC/IXR + NF

Franke et al. (2019) reported a practical full-scale drinking water treatment strategy that combined GAC or IXR with a nanofiltration (NF) pilot plant. NF achieved over 98% removal of PFAS while simultaneously meeting other water quality goals, such as reductions in dissolved organic carbon (DOC) and mineral hardness. IXR demonstrated up to three times longer saturation half-times than GAC but showed a faster decline in efficiency. After treating 15,000 bed volumes (BVs), GAC maintained 20% PFAS removal. Franke et al. (2021) further showed that GAC and IXR removed 2.6 and 4.1 times more PFAS mass, respectively, from NF concentrate than from raw water.

2.6.2 GAC/IXR + Incineration

Watanabe et al. (2018) investigated the thermal mineralization of PFOA, PFHxA, and PFOS pre-adsorbed onto GAC at 700 °C under a nitrogen atmosphere. Under alkaline conditions, fluorine recovery increased significantly—to 74%, 91%, and 90% for PFOA, PFHxA, and

PFOS, respectively—compared to <30%, 46%, and 72% without pre-adsorption. However, high energy demand and the risk of PFAS volatilization limit large-scale application of thermal treatment.

2.6.3 IXR + EO

Wang et al. (2021) studied EO treatment of ion exchange regeneration brine using Ti₄O₇ as the anode. Ten monitored PFAAs were degraded by 98.1% over 200 hours, with over 79% total organic carbon (TOC) removal. However, byproducts such as chlorate and perchlorate were detected after 8 hours.

In a pilot-scale study, Liang et al. (2022) coupled regenerable IXR with EO to treat groundwater impacted by aqueous film-forming foam. EO treatment of IXR-concentrated waste achieved 80–98% destruction of PFOS and PFOA, with electric energy per order (EE/O) ranging from 0.13 to 0.16 kWh/m³—significantly more cost-effective than standalone EO (Lin et al., 2018).

2.6.4 NF + EO

Soriano et al. (2017) developed a treatment train for PFHxA-contaminated industrial water using NF separation followed by EO. The NF270 membrane achieved 99.6% PFHxA rejection without fouling, increasing PFHxA concentration in the retentate to 870 mg/L. Using a boron-doped diamond (BDD) anode, EO at 50 A/m² removed 98% PFHxA and over 95% TOC in 2 hours, consuming 15.2 kWh/m³.

2.6.5 EC + EO

Shi et al. (2021) evaluated a novel train integrating EC (with a zinc anode) and EO (with Ti₄O₇) for removing ten PFASs (0.5 μM each). EC efficiently removed long-chain PFASs and promoted foam separation. EO treatment following EC achieved >90% removal of most PFASs,

except PFHxA (55%) and PFHpA (82%). Removal efficiency strongly correlated with PFAS chain length.

2.6.6 IXR + Plasma

Onvector's pilot system demonstrated the destruction of 97% of PFASs in IXR regeneration brine using Plasma Vortex technology. The system achieved single-digit ng/L concentrations with energy consumption around 10,000 kWh/kg PFAS mineralized and mineralization rates of 3–5 g/h. The system is scalable by adding more reactors and met federal and state drinking water standards without excessive operational cost (Onvector Case Study).

2.6.7 OF/FF + UV

Although OF/FF has not been widely integrated into full-scale treatment trains, it holds promise for early-stage treatment of sludge or residuals from downstream processes. Dai et al. (2019) found that UV alone removed only 16.8% PFAS, but ozonated air fractionation enhanced removal to >95% due to increased hydroxyl radicals. Maximum efficiency (87%) was achieved at 30 L/min air flow and 1.4 L/min feed flow (10 min residence time). PFSA compounds were more efficiently removed than PFCA, reflecting their greater hydrophobicity and gas bubble affinity.

Lyu et al. (2020) applied foam fractionation to enhance PFOS photodegradation. At pH 11 and gas flow rate of 1.0 L/min, removal reached 95.5%, with the degradation rate 8.76 times higher than without foam fractionation.

2.6.8 EO + UV

C. Li et al. (2022) explored PFOS removal via EO with UV enhancement using a Magnéli-phase Ti₄O₇ anode. UV radiation (<400 nm) significantly accelerated degradation. At pH 5.6 and current density of 15 mA/cm², 99.1% PFOS removal was achieved in 2 hours.

EO + UV showed improved kinetics and higher TOC removal (56.3%) compared to EO alone (39.4%), though with a slightly higher EE/O (28.0 kWh/m³ vs. 17.3 kWh/m³).

While single techniques can be limited by energy demands, incomplete degradation, or specificity to PFAS chain lengths, hybrid treatments—especially those integrating electrochemical methods with GAC, IXR, or NF—offer a more comprehensive and cost-effective solution. These strategies address multiple challenges associated with PFAS remediation and hold significant promise for real-world application.

2.7 Conclusion

This study evaluates the viability, effectiveness, and cost-efficiency of various PFAS treatment technologies based on a comprehensive review of recent literature. Granular Activated Carbon (GAC) is a well-established technology, particularly effective for long-chain PFASs. It has been widely implemented in full-scale drinking water treatment plants. However, GAC shows limited removal efficiency for short-chain PFASs, and its performance can be compromised by the presence of co-contaminants and natural organic matter that compete for adsorption sites.

Ion Exchange (IX) offers several advantages over GAC, including higher removal efficiency for short-chain PFAS and the potential for resin regeneration and reuse. However, there are still knowledge gaps regarding the performance and cost trade-offs between single-use and regenerable IX systems. Currently, methanol and brine rinsing are used for regeneration, which generates highly concentrated PFAS waste streams that are challenging to manage. Due to these concerns, single-use IX with off-site incineration remains the primary approach. To

improve sustainability, cost-effective destruction methods that can be integrated with IX are urgently needed.

Reverse Osmosis (RO) and Nanofiltration (NF) are highly effective for both long- and short-chain PFASs, offering single-step treatment with high rejection rates. However, their application is limited by high energy consumption, capital costs, and membrane fouling.

Pretreatment of source water to control suspended solids and chemical composition is critical for effective operation. Due to the complex composition of PFAS-contaminated water, multi-barrier approaches are recommended.

Ozofractionation (OF) and Foam Fractionation (FF) show promise, particularly for preconcentrating PFAS from complex matrices like landfill leachate. However, these methods require further development to effectively manage concentrated residuals and consistently achieve regulatory thresholds (e.g., ng/L levels). Integration with downstream polishing steps is necessary for full-scale application.

Photocatalyst (e.g., UV-based methods) is effective at degrading PFAS at low concentrations, but challenges remain in terms of energy costs, treatment duration, and the presence of co-contaminants. Future work should focus on optimizing treatment efficiency, reducing toxicity of by-products, and understanding the fate of transformation products to ensure treated water safety.

Electrochemical Oxidation (EO) shows strong potential for PFAS destruction, though its scalability is limited by the cost of advanced anode materials, reactor design complexity, and low PFAS concentrations in real-world applications. Integrating EO with IXR or NF to preconcentrate PFAS and increase conductivity could improve efficiency. Further development in electrode materials and scalable reactor configurations is essential for field application.

Sonolysis is less efficient than other destructive technologies but has the advantage of producing fewer harmful by-products. Before practical implementation, its scalability and energy efficiency must be addressed.

Advanced Reduction Processes (ARPs) require further research to minimize scavenging effects from coexisting species (e.g., H⁺, dissolved oxygen, NOM) that limit the generation of hydrated electrons (e⁻_aq). Developing more efficient e⁻_aq production methods and mitigating pH dependency could significantly reduce operational costs. Additionally, the formation and toxicity of transformation by-products need to be better understood. Coupling ARPs with preconcentration methods such as EC may offer a promising direction for future systems.

Overall, no single technique is universally effective for PFAS remediation. Hybrid treatment trains combining separation (e.g., GAC, IXR, NF) with destructive technologies (e.g., EO, UV, plasma) offer a more sustainable, energy-efficient, and cost-effective approach. Among the technologies reviewed, hybrid systems involving electrochemical methods paired with GAC, IXR, or NF show the most promise for advancing the remediation of PFAS-contaminated water and overcoming the limitations of standalone techniques.

Table 2.1:The technology readiness level of the emerging PFASs treatment technologies

TRL Factor	Concentration technologies					
9	Granular Activated Carbon (GAC)					
7	Ion-Exchange Resin (IXR)					
7	Reverse Osmosis (RO) and Nanofiltration (NF)					
5	Ozofractionation (OF) and Foam Fractionation (FF)					
4	Electrocoagulation (EC)					
Chemical Destruction Technologies						
4	Photocatalysis					
6	Electrochemical oxidation (EO)					
4	Plasma					
4	Sonolysis					
4	Advanced reductive processes (APRs)					
4	Supercritical Water Oxidation (SCWO)					
	Thermal technologies					
9	Incineration					
3	Pyrolysis and gasification					
3	Hydrothermal liquefaction					
Biological technologies						
3	Phytoremediation					
3	Biodegradation					

TECHNOLOGY READINESS LEVEL (TRL)



Figure 2.1: Technology Readiness Level

Table 2.2: Summarized Comparison Across the Concentration Technologies for PFAS Removal

Technology	PFAS Removal Efficiency	Best for	Short- Chain PFAS	Energy Demand	Advantages	Limitations
Granular Activated Carbon (GAC)	80–99% (better for long-chain)	Drinking water, municipal systems	Low (<50%)	Low	Cost-effective, widely used, easy to operate and regenerate	Poor performance for short- chain PFAS, frequent replacement, breakthrough risk
Ion Exchange (IX)	>90% for many PFAS, incl. short-chain	Drinking water, polishing step	Moderate (50–90%)	Low	High affinity resins available, good for wide PFAS spectrum	Resin fouling, regeneration complexity, disposal of spent resin
Reverse Osmosis (RO)	>99% for both long- and short- chain PFAS	Drinking water treatment	High (>99%)	High (10–100 bar)	Excellent removal efficiency, commercial availability	High energy cost, membrane fouling, requires pre-treatment, concentrate disposal challenge
Nanofiltration (NF)	90–99% (higher for long-chain)	Municipal/indu strial water treatment	Moderate	Moderate (5–40 bar)	Lower energy than RO, good for long-chain PFAS	Less effective for short- chain PFAS, potential fouling, brine management
Foam Fractionation (FF)	80–>90% for long-chain PFAS	Surface/ground water, landfill leachate	Low to moderate	Low	Low capital and operational cost, selective for long-chain PFAS	Ineffective for short-chain PFAS, foam management, not effective as standalone for ng/L targets
Ozofractionatio n (OF)	>97% total PFAS in pilot studies	Firefighting foam-impacted sites	Moderate (varies)	Moderate	Combines degradation (ozone) with separation (foam), mobile systems possible	Waste stream requires post- treatment, ozone system complexity
Electrocoagulati on (EC)	Up to 99.6% for long-chain PFAS	Industrial wastewater, groundwater	Low to moderate	Low to Moderate	No chemical coagulants needed, low sludge, effective for long-chain PFAS	Lower efficiency for short- chain PFAS, dependent on water chemistry, electrode fouling possible

Table 2.3: Summarized Comparison Across the Chemical Destruction Technologies for PFAS Removal

Technology	Mechanism	PFAS Types Treated	Destruction Efficiency	Typical Conditions	Key Advantages	Major Challenges
Photocatalysis	UV or visible light activates catalysts	PFOA, PFOS	30–90% in lab studies	UV/visible light, catalysts, ambient T	Low energy input, sustainable	Low quantum efficiency; catalyst deactivation
Electrochemic al Oxidation (EO)	Direct and indirect oxidation at electrodes (e.g., BDD anodes)	PFOS, PFOA, GenX, others	70–99.9% depending on system	Ambient–60 °C, applied voltage/current	Modular, no chemical addition, scalable	Electrode fouling, high energy cost for dilute streams
Sonolysis	Ultrasonic cavitation generates reactive radicals	PFOA, PFOS	~60–90% (in lab)	High-frequency ultrasound	No chemical addition, mild conditions	Limited scalability, low energy efficiency
Plasma-Based Technologies	Plasma discharge generates reactive species (e.g., •OH, e ⁻ aq, O ₃)	PFOS, PFOA, GenX	>90% in lab conditions	Atmospheric pressure, room temperature	Chemical-free, rapid degradation	Energy intensive, incomplete defluorination, scalability concerns
Advanced Reduction Processes	Reductive degradation using hydrated	PFOS, PFOA, F- 53B, other	Up to ~100% under optimized	UV (254–365 nm), alkaline pH (>9), reducing	Effective for short-chain and long-chain PFAS;	Requires deaeration; high pH needed; radical scavenging by
(ARPs)	electrons (e ⁻ aq), SO ₃ • ⁻ , SO ₂ • ⁻	PFASs	conditions	agent (e.g., SO ₃ ²⁻)	potential for defluorination	co-solutes (O ₂ , H ⁺ , NOM)
Supercritical Water Oxidation (SCWO)	Oxidation via •OH radicals in supercritical water	AFFF, PFOS, PFOA, multiple PFAAs	>99.9% (in continuous systems); ~70% in batch	T > 500–650 °C, P > 22.1 MPa, residence time 5– 120 min	High efficiency; effective mineralization	High energy demand; corrosion; byproduct management; high capital cost

2.8 References

- Acheson, C., Mills, M., Krause, M., & Thoma, E. (2021). Potential PFAS destruction technology: pyrolysis and gasification.
- Ahmed, F. E., Hashaikeh, R., & Hilal, N. (2020). Hybrid technologies: The future of energy efficient desalination A review. *Desalination*, 495. https://doi.org/ARTN 11465910.1016/j.desal.2020.114659
- Almassi, S., Li, Z., Xu, W., Pu, C., Zeng, T., & Chaplin, B. P. (2019). Simultaneous Adsorption and Electrochemical Reduction of N-Nitrosodimethylamine Using Carbon-Ti4O7 Composite Reactive Electrochemical Membranes. *Environ Sci Technol*, *53*(2), 928-937. https://doi.org/10.1021/acs.est.8b05933
- Altarawneh, M., Almatarneh, M. H., & Dlugogorski, B. Z. (2022). Thermal decomposition of perfluorinated carboxylic acids: Kinetic model and theoretical requirements for PFAS incineration. *Chemosphere*, 286. https://doi.org/ARTN 13168510.1016/j.chemosphere.2021.131685
- Appleman, T. D., Higgins, C. P., Quinones, O., Vanderford, B. J., Kolstad, C., Zeigler-Holady, J. C., & Dickenson, E. R. (2014). Treatment of poly- and perfluoroalkyl substances in U.S. full-scale water treatment systems. *Water Res*, *51*, 246-255. https://doi.org/10.1016/j.watres.2013.10.067
- Bao, J., Yu, W. J., Liu, Y., Wang, X., Liu, Z. Q., & Duan, Y. F. (2020). Removal of perfluoroalkanesulfonic acids (PFSAs) from synthetic and natural groundwater by electrocoagulation. *Chemosphere*, 248, 125951. https://doi.org/10.1016/j.chemosphere.2020.125951
- Bao, Y. X., Huang, J., Cagnetta, G., & Yu, G. (2019). Removal of F-538 as PFOS alternative in chrome plating wastewater by UV/Sulfite reduction. *Water Research*, *163*. https://doi.org/ARTN 11490710.1016/j.watres.2019.114907
- Barisci, S., & Suri, R. (2020). Electrooxidation of short and long chain perfluorocarboxylic acids using boron doped diamond electrodes. *Chemosphere*, 243, 125349. https://doi.org/10.1016/j.chemosphere.2019.125349
- Baudequin, C., Mai, Z. H., Rakib, M., Deguerry, I., Severac, R., Pabon, M., & Couallier, E. (2014). Removal of fluorinated surfactants by reverse osmosis Role of surfactants in membrane fouling. *Journal of Membrane Science*, 458, 111-119. https://doi.org/10.1016/j.memsci.2014.01.063
- Belkouteb, N., Franke, V., McCleaf, P., Kohler, S., & Ahrens, L. (2020). Removal of per- and polyfluoroalkyl substances (PFASs) in a full-scale drinking water treatment plant: Long-term performance of granular activated carbon (GAC) and influence of flow-rate. *Water Res*, 182, 115913. https://doi.org/10.1016/j.watres.2020.115913
- Berg, C., Crone, B., Gullett, B., Higuchi, M., Krause, M. J., Lemieux, P. M., Martin, T., Shields, E. P., Struble, E., Thoma, E., & Whitehill, A. (2022). Developing innovative treatment technologies for PFAS-containing wastes. *Journal of the Air & Waste Management Association*, 72(6), 540-555. https://doi.org/10.1080/10962247.2021.2000903
- Bolouki, N., Kuan, W. H., Huang, Y. Y., & Hsieh, J. H. (2021). Characterizations of a Plasma-Water System Generated by Repetitive Microsecond Pulsed Discharge with Air, Nitrogen, Oxygen, and Argon Gases Species. *Applied Sciences-Basel*, 11(13). https://doi.org/ARTN 615810.3390/app11136158
- Boyer, T. H., Fang, Y., Ellis, A., Dietz, R., Choi, Y. J., Schaefer, C. E., Higgins, C. P., & Strathmann, T. J. (2021). Anion exchange resin removal of per- and polyfluoroalkyl

- substances (PFAS) from impacted water: A critical review. *Water Res*, 200, 117244. https://doi.org/10.1016/j.watres.2021.117244
- Buckley, T., Xu, X. Y., Rudolph, V., Firouzi, M., & Shukla, P. (2021). Review of foam fractionation as a water treatment technology. *Separation Science and Technology*. https://doi.org/10.1080/01496395.2021.1946698
- Chetverikov, S. P., Sharipov, D. A., Korshunova, T. Y., & Loginov, O. N. (2017). Degradation of Perfluorooctanyl Sulfonate by Strain Pseudomonas plecoglossicida 2.4-D. *Applied Biochemistry and Microbiology*, *53*(5), 533-538. https://doi.org/10.1134/S0003683817050027
- Crone, B. C., Speth, T. F., Wahman, D. G., Smith, S. J., Abulikemu, G., Kleiner, E. J., & Pressman, J. G. (2019). Occurrence of Per- and Polyfluoroalkyl Substances (PFAS) in Source Water and Their Treatment in Drinking Water. *Crit Rev Environ Sci Technol*, 49(24), 2359-2396. https://doi.org/10.1080/10643389.2019.1614848
- Cui, J., Gao, P., & Deng, Y. (2020). Destruction of Per- and Polyfluoroalkyl Substances (PFAS) with Advanced Reduction Processes (ARPs): A Critical Review. *Environ Sci Technol*, 54(7), 3752-3766. https://doi.org/10.1021/acs.est.9b05565
- Cui, Y. Y., Yu, J. W., Su, M., Jia, Z. Y., Liu, T. T., Oinuma, G., & Yamauchi, T. (2019). Humic acid removal by gas-liquid interface discharge plasma: performance, mechanism and comparison to ozonation. *Environmental Science-Water Research & Technology*, *5*(1), 152-160. https://doi.org/10.1039/c8ew00520f
- Dai, X., Xie, Z., Dorian, B., Gray, S., & Zhang, J. (2019). Comparative study of PFAS treatment by UV, UV/ozone, and fractionations with air and ozonated air. *Environmental Science:* Water Research & Technology, 5(11), 1897-1907. https://doi.org/10.1039/c9ew00701f
- Dalahmeh, S., Tirgani, S., Komakech, A. J., Niwagaba, C. B., & Ahrens, L. (2018). Per- and polyfluoroalkyl substances (PFASs) in water, soil and plants in wetlands and agricultural areas in Kampala, Uganda. *Sci Total Environ*, 631-632, 660-667. https://doi.org/10.1016/j.scitotenv.2018.03.024
- Dixit, F., Barbeau, B., Mostafavi, S. G., & Mohseni, M. (2020). Efficient removal of GenX (HFPO-DA) and other perfluorinated ether acids from drinking and recycled waters using anion exchange resins. *J Hazard Mater*, *384*, 121261. https://doi.org/10.1016/j.jhazmat.2019.121261
- Dixit, F., Dutta, R., Barbeau, B., Berube, P., & Mohseni, M. (2021). PFAS removal by ion exchange resins: A review. *Chemosphere*, 272. https://doi.org/ARTN12977710.1016/j.chemosphere.2021.129777
- Du, Z., Deng, S., Chen, Y., Wang, B., Huang, J., Wang, Y., & Yu, G. (2015). Removal of perfluorinated carboxylates from washing wastewater of perfluorooctanesulfonyl fluoride using activated carbons and resins. *J Hazard Mater*, 286, 136-143. https://doi.org/10.1016/j.jhazmat.2014.12.037
- Duan, L., Wang, B., Heck, K., Guo, S., Clark, C. A., Arredondo, J., Wang, M., Senftle, T. P., Westerhoff, P., Wen, X., Song, Y., & Wong, M. S. (2020). Efficient Photocatalytic PFOA Degradation over Boron Nitride. *Environmental Science & Technology Letters*, 7(8), 613-619. https://doi.org/10.1021/acs.estlett.0c00434
- Espanani, R., Barizuddin, S., & Jacoby, W. (2022). Treatment of aqueous fire-fighting foam using supercritical water oxidation.

- Fan, J., Wu, H., Liu, R., Meng, L., Fang, Z., Liu, F., & Xu, Y. (2021). Non-thermal plasma combined with zeolites to remove ammonia nitrogen from wastewater. *J Hazard Mater*, 401, 123627. https://doi.org/10.1016/j.jhazmat.2020.123627
- Fenti, A., Jin, Y., Rhoades, A. J. H., Dooley, G. P., Iovino, P., Salvestrini, S., Musmarra, D., Mahendra, S., Peaslee, G. F., & Blotevogel, J. (2022). Performance testing of mesh anodes for in situ electrochemical oxidation of PFAS. *Chemical Engineering Journal Advances*, 9. https://doi.org/10.1016/j.ceja.2021.100205
- Franke, V., McCleaf, P., Lindegren, K., & Ahrens, L. (2019). Efficient removal of per- and polyfluoroalkyl substances (PFASs) in drinking water treatment: nanofiltration combined with active carbon or anion exchange. *Environmental Science: Water Research & Technology*, 5(11), 1836-1843. https://doi.org/10.1039/c9ew00286c
- Franke, V., Ullberg, M., McCleaf, P., Wålinder, M., Köhler, S. J., & Ahrens, L. (2021). The Price of Really Clean Water: Combining Nanofiltration with Granular Activated Carbon and Anion Exchange Resins for the Removal of Per- And Polyfluoralkyl Substances (PFASs) in Drinking Water Production. *ACS ES&T Water*, 1(4), 782-795. https://doi.org/10.1021/acsestwater.0c00141
- Garg, S., Wang, J. S., Kumar, P., Mishra, V., Arafat, H., Sharma, R. S., & Dumee, L. F. (2021). Remediation of water from per-/poly-fluoroalkyl substances (PFAS) Challenges and perspectives. *Journal of Environmental Chemical Engineering*, *9*(4). https://doi.org/ARTN 10578410.1016/j.jece.2021.105784
- Gobelius, L., Lewis, J., & Ahrens, L. (2017). Plant Uptake of Per- and Polyfluoroalkyl Substances at a Contaminated Fire Training Facility to Evaluate the Phytoremediation Potential of Various Plant Species. *Environ Sci Technol*, *51*(21), 12602-12610. https://doi.org/10.1021/acs.est.7b02926
- Gole, V. L., Sierra-Alvarez, R., Peng, H., Giesy, J. P., Deymier, P., & Keswani, M. (2018). Sono-chemical treatment of per- and poly-fluoroalkyl compounds in aqueous film-forming foams by use of a large-scale multi-transducer dual-frequency based acoustic reactor. *Ultrason Sonochem*, 45, 213-222. https://doi.org/10.1016/j.ultsonch.2018.02.014
- Gomez-Ruiz, B., Diban, N., & Urtiaga, A. (2019). Comparison of microcrystalline and ultrananocrystalline boron doped diamond anodes: Influence on perfluorooctanoic acid electrolysis. *Separation and Purification Technology*, 208, 169-177. https://doi.org/10.1016/j.seppur.2018.03.044
- Gomez-Ruiz, B., Gómez-Lavín, S., Diban, N., Boiteux, V., Colin, A., Dauchy, X., & Urtiaga, A. (2017). Efficient electrochemical degradation of poly- and perfluoroalkyl substances (PFASs) from the effluents of an industrial wastewater treatment plant. *Chemical Engineering Journal*, 322, 196-204. https://doi.org/10.1016/j.cej.2017.04.040
- Gu, Y., Dong, W., Luo, C., & Liu, T. (2016). Efficient Reductive Decomposition of Perfluorooctanesulfonate in a High Photon Flux UV/Sulfite System. *Environ Sci Technol*, 50(19), 10554-10561. https://doi.org/10.1021/acs.est.6b03261
- Gu, Y. R., Liu, T. Z., Wang, H. J., Han, H. L., & Dong, W. Y. (2017). Hydrated electron based decomposition of perfluorooctane sulfonate (PFOS) in the VUV/sulfite system. *Science of the Total Environment*, 607, 541-548. https://doi.org/10.1016/j.scitotenv.2017.06.197
- Gu, Y. R., Liu, T. Z., Zhang, Q., & Dong, W. Y. (2017). Efficient decomposition of perfluorooctanoic acid by a high photon flux UV/sulfite process: Kinetics and associated toxicity. *Chemical Engineering Journal*, *326*, 1125-1133. https://doi.org/10.1016/j.cej.2017.05.156

- Guo, C. X., Zhang, C. J., Sun, Z. Y., Zhao, X. Y., Zhou, Q., & Hoffmann, M. R. (2019). Synergistic impact of humic acid on the photo-reductive decomposition of perfluorocctanoic acid. *Chemical Engineering Journal*, *360*, 1101-1110. https://doi.org/10.1016/j.cej.2018.10.204
- Hang, X., Chen, X., Luo, J., Cao, W., & Wan, Y. (2015). Removal and recovery of perfluorooctanoate from wastewater by nanofiltration. *Separation and Purification Technology*, 145, 120-129. https://doi.org/10.1016/j.seppur.2015.03.013
- Hori, H., Hayakawa, E., Einaga, H., Kutsuna, S., Koike, K., Ibusuki, T., Kiatagawa, H., & Arakawa, R. (2004). Decomposition of environmentally persistent perfluorooctanoic acid in water by photochemical approaches. *Environmental Science & Technology*, *38*(22), 6118-6124. https://doi.org/10.1021/es049719n
- Huang, D., Wang, K., Niu, J., Chu, C., Weon, S., Zhu, Q., Lu, J., Stavitski, E., & Kim, J. H. (2020). Amorphous Pd-Loaded Ti4O7 Electrode for Direct Anodic Destruction of Perfluorooctanoic Acid. *Environ Sci Technol*, 54(17), 10954-10963. https://doi.org/10.1021/acs.est.0c03800
- Huff, D. K., Morris, L. A., Sutter, L., Costanza, J., & Pennell, K. D. (2020). Accumulation of six PFAS compounds by woody and herbaceous plants: potential for phytoextraction. *Int J Phytoremediation*, 22(14), 1538-1550. https://doi.org/10.1080/15226514.2020.1786004
- Ibrahim Abouelamaiem, D., Mostazo-López, M. J., He, G., Patel, D., Neville, T. P., Parkin, I. P., Lozano-Castelló, D., Morallón, E., Cazorla-Amorós, D., Jorge, A. B., Wang, R., Ji, S., Titirici, M.-M., Shearing, P. R., & Brett, D. J. L. (2018). New insights into the electrochemical behaviour of porous carbon electrodes for supercapacitors. *Journal of Energy Storage*, 19, 337-347. https://doi.org/10.1016/j.est.2018.08.014
- Inyang, M., & Dickenson, E. R. V. (2017). The use of carbon adsorbents for the removal of perfluoroalkyl acids from potable reuse systems. *Chemosphere*, *184*, 168-175. https://doi.org/10.1016/j.chemosphere.2017.05.161
- Jin, L., Zhang, P., Shao, T., & Zhao, S. (2014). Ferric ion mediated photodecomposition of aqueous perfluorooctane sulfonate (PFOS) under UV irradiation and its mechanism. *J Hazard Mater*, 271, 9-15. https://doi.org/10.1016/j.jhazmat.2014.01.061
- John Horst, Jeff McDonough, Ian Ross, & Dickson, M. (2018). Water Treatment Technologies for PFAS The Next Generation. *Groundwater Monitoring&Remediation*.
- Kim, J. H., Ok, Y. S., Choi, G. H., & Park, B. J. (2015). Residual perfluorochemicals in the biochar from sewage sludge. *Chemosphere*, *134*, 435-437. https://doi.org/10.1016/j.chemosphere.2015.05.012
- Kim, M. H., Wang, N., & Chu, K. H. (2014). 6:2 Fluorotelomer alcohol (6:2 FTOH) biodegradation by multiple microbial species under different physiological conditions. *Applied Microbiology and Biotechnology*, *98*(4), 1831-1840. https://doi.org/10.1007/s00253-013-5131-3
- Krause, M. J., Thoma, E., Sahle-Damesessie, E., Crone, B., Whitehill, A., Shields, E., & Gullett, B. (2022). Supercritical Water Oxidation as an Innovative Technology for PFAS Destruction. *Journal of Environmental Engineering*, *148*(2). https://doi.org/10.1061/(asce)ee.1943-7870.0001957
- Kwon, B. G., Lim, H. J., Na, S. H., Choi, B. I., Shin, D. S., & Chung, S. Y. (2014). Biodegradation of perfluorooctanesulfonate (PFOS) as an emerging contaminant. *Chemosphere*, 109, 221-225. https://doi.org/10.1016/j.chemosphere.2014.01.072

- Le, T. X. H., Haflich, H., Shah, A. D., & Chaplin, B. P. (2019). Energy-Efficient Electrochemical Oxidation of Perfluoroalkyl Substances Using a Ti4O7 Reactive Electrochemical Membrane Anode. *Environmental Science & Technology Letters*, 6(8), 504-510. https://doi.org/10.1021/acs.estlett.9b00397
- Lee, Y. C., Chen, M. J., Huang, C. P., Kuo, J., & Lo, S. L. (2016). Efficient sonochemical degradation of perfluorooctanoic acid using periodate. *Ultrasonics Sonochemistry*, *31*, 499-505. https://doi.org/10.1016/j.ultsonch.2016.01.030
- Levchuk, I., Marquez, J. J. R., & Sillanpaa, M. (2018). Removal of natural organic matter (NOM) from water by ion exchange A review. *Chemosphere*, 192, 90-104. https://doi.org/10.1016/j.chemosphere.2017.10.101
- Lewis, A. J., Joyce, T., Hadaya, M., Ebrahimi, F., Dragiev, I., Giardetti, N., Yang, J., Fridman, G., Rabinovich, A., Fridman, A. A., McKenzie, E. R., & Sales, C. M. (2020). Rapid degradation of PFAS in aqueous solutions by reverse vortex flow gliding arc plasma. *Environmental Science: Water Research & Technology*, *6*(4), 1044-1057. https://doi.org/10.1039/c9ew01050e
- Li, C., Wang, Y., Wang, Y., Wang, Z., & Huang, Q. (2022). Electrochemical oxidation combined with UV irradiation for synergistic removal of perfluorooctane sulfonate (PFOS) in water. *J Hazard Mater*, 436, 129091. https://doi.org/10.1016/j.jhazmat.2022.129091
- Li, J., Austin, C., & Austin, C. (2022). PFOS Destruction in a Continuous Supercritical Water Oxidation Reactor.
- Liang, S., Mora, R., Huang, Q., Casson, R., Wang, Y., Woodard, S., & Anderson, H. (2022). Field demonstration of coupling ion-exchange resin with electrochemical oxidation for enhanced treatment of per- and polyfluoroalkyl substances (PFAS) in groundwater. *Chemical Engineering Journal Advances*, 9. https://doi.org/10.1016/j.ceja.2021.100216
- Liang, S., Pierce, R. D., Lin, H., Chiang, S.-Y. D., & Huang, Q. J. (2018). Electrochemical oxidation of PFOA and PFOS in concentrated waste streams. *Remediation Journal*, 28(2), 127-134. https://doi.org/10.1002/rem.21554
- Liang, X. Y., Cheng, J. H., Yang, C., & Yang, S. W. (2016). Factors influencing aqueous perfluorooctanoic acid (PFOA) photodecomposition by VUV irradiation in the presence of ferric ions. *Chemical Engineering Journal*, 298, 291-299. https://doi.org/10.1016/j.cej.2016.03.150
- Lin, H., Niu, J., Ding, S., & Zhang, L. (2012). Electrochemical degradation of perfluorooctanoic acid (PFOA) by Ti/SnO2-Sb, Ti/SnO2-Sb/PbO2 and Ti/SnO2-Sb/MnO2 anodes. *Water Res*, 46(7), 2281-2289. https://doi.org/10.1016/j.watres.2012.01.053
- Lin, H., Niu, J., Liang, S., Wang, C., Wang, Y., Jin, F., Luo, Q., & Huang, Q. (2018).

 Development of macroporous Magnéli phase Ti4O7 ceramic materials: As an efficient anode for mineralization of poly- and perfluoroalkyl substances. *Chemical Engineering Journal*, 354, 1058-1067. https://doi.org/10.1016/j.cej.2018.07.210
- Lin, H., Wang, Y., Niu, J., Yue, Z., & Huang, Q. (2015). Efficient Sorption and Removal of Perfluoroalkyl Acids (PFAAs) from Aqueous Solution by Metal Hydroxides Generated in Situ by Electrocoagulation. *Environ Sci Technol*, 49(17), 10562-10569. https://doi.org/10.1021/acs.est.5b02092
- Lin, H., Xiao, R., Xie, R., Yang, L., Tang, C., Wang, R., Chen, J., Lv, S., & Huang, Q. (2021). Defect Engineering on a Ti4O7 Electrode by Ce(3+) Doping for the Efficient

- Electrooxidation of Perfluorooctanesulfonate. *Environ Sci Technol*, *55*(4), 2597-2607. https://doi.org/10.1021/acs.est.0c06881
- Liu, X., Yoon, S., Batchelor, B., & Abdel-Wahab, A. (2013). Photochemical degradation of vinyl chloride with an Advanced Reduction Process (ARP) Effects of reagents and pH. *Chemical Engineering Journal*, 215, 868-875. https://doi.org/10.1016/j.cej.2012.11.086
- Liu, Y., Fan, X., Quan, X., Fan, Y., Chen, S., & Zhao, X. (2019). Enhanced Perfluorooctanoic Acid Degradation by Electrochemical Activation of Sulfate Solution on B/N Codoped Diamond. *Environ Sci Technol*, *53*(9), 5195-5201. https://doi.org/10.1021/acs.est.8b06130
- Liu, Y., Hu, X. M., Zhao, Y., Wang, J., Lu, M. X., Peng, F. H., & Bao, J. (2018). Removal of perfluorooctanoic acid in simulated and natural waters with different electrode materials by electrocoagulation. *Chemosphere*, 201, 303-309. https://doi.org/10.1016/j.chemosphere.2018.02.129
- Loganathan, B. G., Sajwan, K. S., Sinclair, E., Senthil Kumar, K., & Kannan, K. (2007). Perfluoroalkyl sulfonates and perfluorocarboxylates in two wastewater treatment facilities in Kentucky and Georgia. *Water Res*, *41*(20), 4611-4620. https://doi.org/10.1016/j.watres.2007.06.045
- Lu, D., Sha, S., Luo, J., Huang, Z., & Zhang Jackie, X. (2020). Treatment train approaches for the remediation of per- and polyfluoroalkyl substances (PFAS): A critical review. *J Hazard Mater*, 386, 121963. https://doi.org/10.1016/j.jhazmat.2019.121963
- Lyu, X.-J., Liu, Y., Chen, C., Sima, M., Lyu, J.-F., Ma, Z.-Y., & Huang, S. (2020). Enhanced use of foam fractionation in the photodegradation of perfluorooctane sulfonate (PFOS). *Separation and Purification Technology*, 253. https://doi.org/10.1016/j.seppur.2020.117488
- Lyu, X. J., Li, W. W., Lam, P. K., & Yu, H. Q. (2015). Insights into perfluorooctane sulfonate photodegradation in a catalyst-free aqueous solution. *Sci Rep*, *5*, 9353. https://doi.org/10.1038/srep09353
- Mahyar, A., Miessner, H., Mueller, S., Hama Aziz, K. H., Kalass, D., Moeller, D., Kretschmer, K., Robles Manuel, S., & Noack, J. (2019). Development and Application of Different Non-thermal Plasma Reactors for the Removal of Perfluorosurfactants in Water: A Comparative Study. *Plasma Chemistry and Plasma Processing*, *39*(3), 531-544. https://doi.org/10.1007/s11090-019-09977-6
- Mastropietro, T. F., Bruno, R., Pardo, E., & Armentano, D. (2021). Reverse osmosis and nanofiltration membranes for highly efficient PFASs removal: overview, challenges and future perspectives. *Dalton Trans*, *50*(16), 5398-5410. https://doi.org/10.1039/d1dt00360g
- Mayakaduwage, S., Ekanayake, A., Kurwadkar, S., Rajapaksha, A. U., & Vithanage, M. (2022). Phytoremediation prospects of per- and polyfluoroalkyl substances: A review. *Environ Res*, 212(Pt B), 113311. https://doi.org/10.1016/j.envres.2022.113311
- McCleaf, P., Englund, S., Ostlund, A., Lindegren, K., Wiberg, K., & Ahrens, L. (2017). Removal efficiency of multiple poly- and perfluoroalkyl substances (PFASs) in drinking water using granular activated carbon (GAC) and anion exchange (AE) column tests. *Water Res*, 120, 77-87. https://doi.org/10.1016/j.watres.2017.04.057
- McCleaf, P., Kjellgren, Y., & Ahrens, L. (2021). Foam fractionation removal of multiple perand polyfluoroalkyl substances from landfill leachate. *AWWA Water Science*, *3*(5). https://doi.org/10.1002/aws2.1238

- McDonough, J. T., Kirby, J., Bellona, C., Quinnan, J. A., Welty, N., Follin, J., & Liberty, K. (2022). Validation of supercritical water oxidation to destroy perfluoroalkyl acids. *Remediation-the Journal of Environmental Cleanup Costs Technologies & Techniques*, 32(1-2), 75-90. https://doi.org/ARTN 2171110.1002/rem.21711
- Meng, P., Deng, S., Maimaiti, A., Wang, B., Huang, J., Wang, Y., Cousins, I. T., & Yu, G. (2018). Efficient removal of perfluorooctane sulfonate from aqueous film-forming foam solution by aeration-foam collection. *Chemosphere*, 203, 263-270. https://doi.org/10.1016/j.chemosphere.2018.03.183
- Misdan, N., Lau, W. J., Ismail, A. F., Matsuura, T., & Rana, D. (2014). Study on the thin film composite poly(piperazine-amide) nanofiltration membrane: Impacts of physicochemical properties of substrate on interfacial polymerization formation. *Desalination*, *344*, 198-205. https://doi.org/10.1016/j.desal.2014.03.036
- Muzyka, K., Sun, J., Fereja, T. H., Lan, Y., Zhang, W., & Xu, G. (2019). Boron-doped diamond: current progress and challenges in view of electroanalytical applications. *Analytical Methods*, 11(4), 397-414. https://doi.org/10.1039/c8ay02197j
- Nau-Hix, C., Multari, N., Singh, R. K., Richardson, S., Kulkarni, P., Anderson, R. H., Holsen, T. M., & Mededovic Thagard, S. (2021). Field Demonstration of a Pilot-Scale Plasma Reactor for the Rapid Removal of Poly- and Perfluoroalkyl Substances in Groundwater. *ACS ES&T Water*, *I*(3), 680-687. https://doi.org/10.1021/acsestwater.0c00170
- Niu, J., Li, Y., Shang, E., Xu, Z., & Liu, J. (2016). Electrochemical oxidation of perfluorinated compounds in water. *Chemosphere*, *146*, 526-538. https://doi.org/10.1016/j.chemosphere.2015.11.115
- Nzeribe, B. N., Crimi, M., Mededovic Thagard, S., & Holsen, T. M. (2019). Physico-Chemical Processes for the Treatment of Per- And Polyfluoroalkyl Substances (PFAS): A review. *Critical Reviews in Environmental Science and Technology*, 49(10), 866-915. https://doi.org/10.1080/10643389.2018.1542916
- Palma, D., Richard, C., & Minella, M. (2022). State of the art and perspectives about non-thermal plasma applications for the removal of PFAS in water. *Chemical Engineering Journal Advances*, 10. https://doi.org/10.1016/j.ceja.2022.100253
- Park, H., Vecitis, C. D., Cheng, J., Choi, W., Mader, B. T., & Hoffmann, M. R. (2009). Reductive Defluorination of Aqueous Perfluorinated Alkyl Surfactants: Effects of Ionic Headgroup and Chain Length. *Journal of Physical Chemistry A*, 113(4), 690-696. https://doi.org/10.1021/jp807116q
- Park, M., Daniels, K. D., Wu, S., Ziska, A. D., & Snyder, S. A. (2020). Magnetic ion-exchange (MIEX) resin for perfluorinated alkylsubstance (PFAS) removal in groundwater: Roles of atomic charges for adsorption. *Water Res*, *181*, 115897. https://doi.org/10.1016/j.watres.2020.115897
- Patel, S., Kundu, S., Halder, P., Ratnnayake, N., Marzbali, M. H., Aktar, S., Selezneva, E., Paz-Ferreiro, J., Surapaneni, A., de Figueiredo, C. C., Sharma, A., Megharaj, M., & Shah, K. (2020). A critical literature review on biosolids to biochar: an alternative biosolids management option. *Reviews in Environmental Science and Bio-Technology*, *19*(4), 807-841. https://doi.org/10.1007/s11157-020-09553-x
- Pierpaoli, M., Szopinska, M., Wilk, B. K., Sobaszek, M., Luczkiewicz, A., Bogdanowicz, R., & Fudala-Ksiazek, S. (2021). Electrochemical oxidation of PFOA and PFOS in landfill leachates at low and highly boron-doped diamond electrodes. *J Hazard Mater*, 403, 123606. https://doi.org/10.1016/j.jhazmat.2020.123606

- Pinkard, B. R., Shetty, S., Stritzinger, D., Bellona, C., & Novosselov, I. V. (2021). Destruction of perfluorooctanesulfonate (PFOS) in a batch supercritical water oxidation reactor. *Chemosphere*, 279, 130834. https://doi.org/10.1016/j.chemosphere.2021.130834
- Qian, Y. J., Guo, X., Zhang, Y. L., Peng, Y., Sun, P. Z., Huang, C. H., Niu, J. F., Zhou, X. F., & Crittenden, J. C. (2016). Perfluorooctanoic Acid Degradation Using UV-Persulfate Process: Modeling of the Degradation and Chlorate Formation. *Environmental Science & Technology*, 50(2), 772-781. https://doi.org/10.1021/acs.est.5b03715
- Rahman, M. F., Peldszus, S., & Anderson, W. B. (2014). Behaviour and fate of perfluoroalkyl and polyfluoroalkyl substances (PFASs) in drinking water treatment: A review. *Water Research*, *50*, 318-340. https://doi.org/10.1016/j.watres.2013.10.045
- Rodowa, A. E., Knappe, D. R. U., Chiang, S.-Y. D., Pohlmann, D., Varley, C., Bodour, A., & Field, J. A. (2020). Pilot scale removal of per- and polyfluoroalkyl substances and precursors from AFFF-impacted groundwater by granular activated carbon. *Environmental Science: Water Research & Technology*, *6*(4), 1083-1094. https://doi.org/10.1039/c9ew00936a
- Rodriguez-Freire, L., Balachandran, R., Sierra-Alvarez, R., & Keswani, M. (2015). Effect of sound frequency and initial concentration on the sonochemical degradation of perfluorooctane sulfonate (PFOS). *Journal of Hazardous Materials*, 300, 662-669. https://doi.org/10.1016/j.jhazmat.2015.07.077
- Ross, I., Hurst, J., Miles, J., Houtz, E., McDonough, J., & Burdick, J. (2017). Remediation of poly-and perfluoro alkyl substances: developing remediation technologies for emerging challenges.
- Ross, I., McDonough, J., Miles, J., Storch, P., Thelakkat Kochunarayanan, P., Kalve, E., Hurst, J., S. Dasgupta, S., & Burdick, J. (2018). A review of emerging technologies for remediation of PFASs. *Remediation Journal*, 28(2), 101-126. https://doi.org/10.1002/rem.21553
- Rozen, S., & Filler, R. (1985). Alpha-Fluorocarbonyl Compounds and Related Chemistry. *Tetrahedron*, *41*(7), 1111-1153. https://doi.org/Doi 10.1016/S0040-4020(01)96514-7
- Saleem, M., Biondo, O., Sretenović, G., Tomei, G., Magarotto, M., Pavarin, D., Marotta, E., & Paradisi, C. (2020). Comparative performance assessment of plasma reactors for the treatment of PFOA; reactor design, kinetics, mineralization and energy yield. *Chemical Engineering Journal*, 382. https://doi.org/10.1016/j.cej.2019.123031
- Schaefer, C. E., Andaya, C., Maizel, A., & Higgins, C. P. (2019). Assessing Continued Electrochemical Treatment of Groundwater Impacted by Aqueous Film-Forming Foams. *Journal of Environmental Engineering*, 145(12). https://doi.org/10.1061/(asce)ee.1943-7870.0001605
- Schaefer, C. E., Andaya, C., Urtiaga, A., McKenzie, E. R., & Higgins, C. P. (2015). Electrochemical treatment of perfluorooctanoic acid (PFOA) and perfluorooctane sulfonic acid (PFOS) in groundwater impacted by aqueous film forming foams (AFFFs). *J Hazard Mater*, 295, 170-175. https://doi.org/10.1016/j.jhazmat.2015.04.024
- Schnell, M., Horst, T., & Quicker, P. (2020). Thermal treatment of sewage sludge in Germany: A review. *Journal of Environmental Management*, 263. https://doi.org/ARTN 110367 10.1016/j.jenvman.2020.110367
- Sharma, S., Shetti, N. P., Basu, S., Nadagouda, M. N., & Aminabhavi, T. M. (2022). Remediation of per- and polyfluoroalkyls (PFAS) via electrochemical methods. *Chemical Engineering Journal*, 430. https://doi.org/10.1016/j.cej.2021.132895

- Shaw, D. M. J., Munoz, G., Bottos, E. M., Duy, S. V., Sauve, S., Liu, J. X., & Van Hamme, J. D. (2019). Degradation and defluorination of 6:2 fluorotelomer sulfonamidoalkyl betaine and 6:2 fluorotelomer sulfonate by Gordonia sp. strain NB4-1Y under sulfur-limiting conditions. *Science of the Total Environment*, 647, 690-698. https://doi.org/10.1016/j.scitotenv.2018.08.012
- Shi, H., Chiang, S. D., Wang, Y., Wang, Y., Liang, S., Zhou, J., Fontanez, R., Gao, S., & Huang, Q. (2021). An electrocoagulation and electrooxidation treatment train to remove and degrade per- and polyfluoroalkyl substances in aqueous solution. *Sci Total Environ*, 788, 147723. https://doi.org/10.1016/j.scitotenv.2021.147723
- Shi, H., Wang, Y., Li, C., Pierce, R., Gao, S., & Huang, Q. (2019). Degradation of Perfluorooctanesulfonate by Reactive Electrochemical Membrane Composed of Magneli Phase Titanium Suboxide. *Environ Sci Technol*, *53*(24), 14528-14537. https://doi.org/10.1021/acs.est.9b04148
- Singh, R. K., Fernando, S., Baygi, S. F., Multari, N., Thagard, S. M., & Holsen, T. M. (2019). Breakdown Products from Perfluorinated Alkyl Substances (PFAS) Degradation in a Plasma-Based Water Treatment Process. *Environ Sci Technol*, *53*(5), 2731-2738. https://doi.org/10.1021/acs.est.8b07031
- Singh, R. K., Multari, N., Nau-Hix, C., Anderson, R. H., Richardson, S. D., Holsen, T. M., & Mededovic Thagard, S. (2019). Rapid Removal of Poly- and Perfluorinated Compounds from Investigation-Derived Waste (IDW) in a Pilot-Scale Plasma Reactor. *Environ Sci Technol*, *53*(19), 11375-11382. https://doi.org/10.1021/acs.est.9b02964
- Singh, R. K., Multari, N., Nau-Hix, C., Woodard, S., Nickelsen, M., Mededovic Thagard, S., & Holsen, T. M. (2020). Removal of Poly- and Per-Fluorinated Compounds from Ion Exchange Regenerant Still Bottom Samples in a Plasma Reactor. *Environ Sci Technol*, 54(21), 13973-13980. https://doi.org/10.1021/acs.est.0c02158
- Song, Z., Tang, H. Q., Wang, N., Wang, X. B., & Zhu, L. H. (2014). Activation of persulfate by UV and Fe2+ for the defluorination of perfluorooctanoic acid. *Advances in Environmental Research-an International Journal*, *3*(3), 185-197. https://doi.org/10.12989/aer.2014.3.3.185
- Soriano, A., Gorri, D., & Urtiaga, A. (2017). Efficient treatment of perfluorohexanoic acid by nanofiltration followed by electrochemical degradation of the NF concentrate. *Water Res*, 112, 147-156. https://doi.org/10.1016/j.watres.2017.01.043
- Stratton, G. R., Dai, F., Bellona, C. L., Holsen, T. M., Dickenson, E. R., & Mededovic Thagard, S. (2017). Plasma-Based Water Treatment: Efficient Transformation of Perfluoroalkyl Substances in Prepared Solutions and Contaminated Groundwater. *Environ Sci Technol*, 51(3), 1643-1648. https://doi.org/10.1021/acs.est.6b04215
- Sukeesan, S., Boontanon, N., & Boontanon, S. K. (2021). Improved electrical driving current of electrochemical treatment of Per- and Polyfluoroalkyl Substances (PFAS) in water using Boron-Doped Diamond anode. *Environmental Technology & Innovation*, 23. https://doi.org/10.1016/j.eti.2021.101655
- Sun, M., Zhou, H., Xu, B., & Bao, J. X. (2018). Distribution of perfluorinated compounds in drinking water treatment plant and reductive degradation by UV/SO32- process. *Environmental Science and Pollution Research*, 25(8), 7443-7453. https://doi.org/10.1007/s11356-017-1024-9

- Sun, Z. Y., Zhang, C. J., Chen, P., Zhou, Q., & Hoffmann, M. R. (2017). Impact of humic acid on the photoreductive degradation of perfluorooctane sulfonate (PFOS) by UV/Iodide process. *Water Research*, *127*, 50-58. https://doi.org/10.1016/j.watres.2017.10.010
- Sun, Z. Y., Zhang, C. J., Xing, L., Zhou, Q., Dong, W. B., & Hoffmann, M. R. (2018). UV/Nitrilotriacetic Acid Process as a Novel Strategy for Efficient Photoreductive Degradation of Perfluorooctanesulfonate. *Environmental Science & Technology*, 52(5), 2953-2962. https://doi.org/10.1021/acs.est.7b05912
- Tang, C. Y. Y., Fu, Q. S., Robertson, A. P., Criddle, C. S., & Leckie, J. O. (2006). Use of reverse osmosis membranes to remove perfluorooctane sulfonate (PFOS) from semiconductor wastewater. *Environmental Science & Technology*, 40(23), 7343-7349. https://doi.org/10.1021/es060831q
- Taylor, P. H., Yamada, T., Striebich, R. C., Graham, J. L., & Giraud, R. J. (2014). Investigation of waste incineration of fluorotelomer-based polymers as a potential source of PFOA in the environment. *Chemosphere*, *110*, 17-22. https://doi.org/10.1016/j.chemosphere.2014.02.037
- Thi, L. A. P., Do, H. T., Lee, Y. C., & Lo, S. L. (2013). Photochemical decomposition of perfluorooctanoic acids in aqueous carbonate solution with UV irradiation. *Chemical Engineering Journal*, 221, 258-263. https://doi.org/10.1016/j.cej.2013.01.084
- Trojanowicz, M., Bojanowska-Czajka, A., Bartosiewicz, I., & Kulisa, K. (2018). Advanced Oxidation/Reduction Processes treatment for aqueous perfluorooctanoate (PFOA) and perfluorooctanesulfonate (PFOS) A review of recent advances. *Chemical Engineering Journal*, 336, 170-199. https://doi.org/10.1016/j.cej.2017.10.153
- Umar, M. (2021). Reductive and Oxidative UV Degradation of PFAS-Status, Needs and Future Perspectives. *Water*, *13*(22). https://doi.org/ARTN 318510.3390/w13223185
- Uwayezu, J. N., Carabante, I., Lejon, T., van Hees, P., Karlsson, P., Hollman, P., & Kumpiene, J. (2021). Electrochemical degradation of per- and poly-fluoroalkyl substances using boron-doped diamond electrodes. *J Environ Manage*, 290, 112573. https://doi.org/10.1016/j.jenvman.2021.112573
- Veciana, M., Braunig, J., Farhat, A., Pype, M. L., Freguia, S., Carvalho, G., Keller, J., & Ledezma, P. (2022). Electrochemical oxidation processes for PFAS removal from contaminated water and wastewater: fundamentals, gaps and opportunities towards practical implementation. *J Hazard Mater*, 434, 128886. https://doi.org/10.1016/j.jhazmat.2022.128886
- Vecitis, C. D., Park, H., Cheng, J., Mader, B. T., & Hoffmann, M. R. (2008). Kinetics and mechanism of the sonolytic conversion of the aqueous perfluorinated surfactants, perfluorooctanoate (PFOA), and perfluorooctane sulfonate (PFOS) into inorganic products. *Journal of Physical Chemistry A*, 112(18), 4261-4270. https://doi.org/10.1021/jp801081y
- Vellanki, B. P., Batchelor, B., & Abdel-Wahab, A. (2013). Advanced Reduction Processes: A New Class of Treatment Processes. *Environmental Engineering Science*, *30*(5), 264-271. https://doi.org/10.1089/ees.2012.0273
- Vo, H. N. P., Ngo, H. H., Guo, W. S., Nguyen, T. M. H., Li, J. X., Liang, H., Deng, L. J., Chen, Z., & Nguyen, T. A. H. (2020). Poly?and perfluoroalkyl substances in water and wastewater: A comprehensive review from sources to remediation. *Journal of Water Process Engineering*, 36. https://doi.org/ARTN 10139310.1016/j.jwpe.2020.101393

- Waclawek, S., Ma, X., Sharma, V. K., Xiao, R., O'Shea, K. E., & Dionysiou, D. D. (2022). Making waves: Defining advanced reduction technologies from the perspective of water treatment. *Water Res*, 212, 118101. https://doi.org/10.1016/j.watres.2022.118101
- Walsh, F. C., & Wills, R. G. A. (2010). The continuing development of Magnéli phase titanium sub-oxides and Ebonex® electrodes. *Electrochimica Acta*, *55*(22), 6342-6351. https://doi.org/10.1016/j.electacta.2010.05.011
- Wang, L., Lu, J., Li, L., Wang, Y., & Huang, Q. (2020). Effects of chloride on electrochemical degradation of perfluorooctanesulfonate by Magneli phase Ti4O7 and boron doped diamond anodes. *Water Res*, 170, 115254. https://doi.org/10.1016/j.watres.2019.115254
- Wang, L., Nickelsen, M., Chiang, S.-Y., Woodard, S., Wang, Y., Liang, S., Mora, R., Fontanez, R., Anderson, H., & Huang, Q. (2021). Treatment of perfluoroalkyl acids in concentrated wastes from regeneration of spent ion exchange resin by electrochemical oxidation using Magnéli phase Ti4O7 anode. *Chemical Engineering Journal Advances*, 5. https://doi.org/10.1016/j.ceja.2020.100078
- Wang, T. T., Ying, G. G., He, L. Y., Liu, Y. S., & Zhao, J. L. (2020). Uptake mechanism, subcellular distribution, and uptake process of perfluorooctanoic acid and perfluorooctane sulfonic acid by wetland plant Alisma orientale. *Sci Total Environ*, 733, 139383. https://doi.org/10.1016/j.scitotenv.2020.139383
- Wang, Y., Kim, J., Huang, C.-H., Hawkins, G. L., Li, K., Chen, Y., & Huang, Q. (2022). Occurrence of per- and polyfluoroalkyl substances in water: a review. *Environmental Science: Water Research & Technology*, 8(6), 1136-1151. https://doi.org/10.1039/d1ew00851j
- Wang, Y., Li, L., Wang, Y., Shi, H., Wang, L., & Huang, Q. (2022). Electrooxidation of perfluorooctanesulfonic acid on porous Magnéli phase titanium suboxide Anodes: Impact of porous structure and composition. *Chemical Engineering Journal*, 431. https://doi.org/10.1016/j.cej.2021.133929
- Wang, Y., Lin, H., Jin, F., Niu, J., Zhao, J., Bi, Y., & Li, Y. (2016). Electrocoagulation mechanism of perfluorooctanoate (PFOA) on a zinc anode: Influence of cathodes and anions. *Sci Total Environ*, 557-558, 542-550. https://doi.org/10.1016/j.scitotenv.2016.03.114
- Wanninayake, D. M. (2021). Comparison of currently available PFAS remediation technologies in water: A review. *J Environ Manage*, 283, 111977. https://doi.org/10.1016/j.jenvman.2021.111977
- Watanabe, N., Takata, M., Takemine, S., & Yamamoto, K. (2018). Thermal mineralization behavior of PFOA, PFHxA, and PFOS during reactivation of granular activated carbon (GAC) in nitrogen atmosphere. *Environmental Science and Pollution Research*, 25(8), 7200-7205. https://doi.org/10.1007/s11356-015-5353-2
- Winchell, L. J., Ross, J. J., Wells, M. J. M., Fonoll, X., Norton, J. W., & Bell, K. Y. (2021). Perand polyfluoroalkyl substances thermal destruction at water resource recovery facilities: A state of the science review. *Water Environment Research*, *93*(6), 826-843. https://doi.org/10.1002/wer.1483
- Woodard, S., Berry, J., & Newman, B. (2017). Ion exchange resin for PFAS removal and pilot test comparison to GAC. *Remediation Journal*, 27(3), 19-27. https://doi.org/10.1002/rem.21515

- Wu, W., Huang, Z.-H., & Lim, T.-T. (2014). Recent development of mixed metal oxide anodes for electrochemical oxidation of organic pollutants in water. *Applied Catalysis A: General*, 480, 58-78. https://doi.org/10.1016/j.apcata.2014.04.035
- Xu, B., Ahmed, M. B., Zhou, J. L., Altaee, A., Wu, M., & Xu, G. (2017). Photocatalytic removal of perfluoroalkyl substances from water and wastewater: Mechanism, kinetics and controlling factors. *Chemosphere*, *189*, 717-729. https://doi.org/10.1016/j.chemosphere.2017.09.110
- Xu, J., Liu, Z., Zhao, D., Gao, N., & Fu, X. (2020). Enhanced adsorption of perfluorooctanoic acid (PFOA) from water by granular activated carbon supported magnetite nanoparticles. *Sci Total Environ*, 723, 137757. https://doi.org/10.1016/j.scitotenv.2020.137757
- Yang, B., Han, Y., Yu, G., Zhuo, Q., Deng, S., Wu, J., & Zhang, P. (2016). Efficient removal of perfluoroalkyl acids (PFAAs) from aqueous solution by electrocoagulation using iron electrode. *Chemical Engineering Journal*, *303*, 384-390. https://doi.org/10.1016/j.cej.2016.06.011
- Yang, B., Jiang, C., Yu, G., Zhuo, Q., Deng, S., Wu, J., & Zhang, H. (2015). Highly efficient electrochemical degradation of perfluorooctanoic acid (PFOA) by F-doped Ti/SnO2 electrode. *J Hazard Mater*, 299, 417-424. https://doi.org/10.1016/j.jhazmat.2015.06.033
- Yi, L. B., Chai, L. Y., Xie, Y., Peng, Q. J., & Peng, Q. Z. (2016). Isolation, identification, and degradation performance of a PFOA-degrading strain. *Genetics and Molecular Research*, 15(2). https://doi.org/ARTN 1502804310.4238/gmr.15028043
- Yu, J., Nickerson, A., Li, Y. L., Fang, Y. D., & Strathmann, T. J. (2020). Fate of per- and polyfluoroalkyl substances (PFAS) during hydrothermal liquefaction of municipal wastewater treatment sludge. *Environmental Science-Water Research & Technology*, 6(5), 1388-1399. https://doi.org/10.1039/c9ew01139k
- Zeng, C., Atkinson, A., Sharma, N., Ashani, H., Hjelmstad, A., Venkatesh, K., & Westerhoff, P. (2020). Removing per- and polyfluoroalkyl substances from groundwaters using activated carbon and ion exchange resin packed columns. *AWWA Water Science*, 2(1). https://doi.org/10.1002/aws2.1172
- Zhang, W. L., & Liang, Y. N. (2022). Hydrothermal liquefaction of sewage sludge effect of four reagents on relevant parameters related to biocrude and PFAS. *Journal of Environmental Chemical Engineering*, *10*(1). https://doi.org/ARTN 10709210.1016/j.jece.2021.107092
- Zhang, Z. M., Sarkar, D., Biswas, J. K., & Datta, R. (2022). Biodegradation of per- and polyfluoroalkyl substances (PFAS): A review. *Bioresource Technology*, *344*. https://doi.org/ARTN 12622310.1016/j.biortech.2021.126223
- Zhuo, Q., Deng, S., Yang, B., Huang, J., Wang, B., Zhang, T., & Yu, G. (2012). Degradation of perfluorinated compounds on a boron-doped diamond electrode. *Electrochimica Acta*, 77, 17-22. https://doi.org/10.1016/j.electacta.2012.04.145
- Zhuo, Q., Han, J., Niu, J., & Zhang, J. (2020). Degradation of a persistent organic pollutant perfluorooctane sulphonate with Ti/SnO2–Sb2O5/PbO2-PTFE anode. *Emerging Contaminants*, 6, 44-52. https://doi.org/10.1016/j.emcon.2019.11.002
- Zhuo, Q., Xiang, Q., Yi, H., Zhang, Z., Yang, B., Cui, K., Bing, X., Xu, Z., Liang, X., Guo, Q., & Yang, R. (2017). Electrochemical oxidation of PFOA in aqueous solution using highly hydrophobic modified PbO 2 electrodes. *Journal of Electroanalytical Chemistry*, 801, 235-243. https://doi.org/10.1016/j.jelechem.2017.07.018

CHAPTER 3

A REVIEW ON THE RECENT MECHANISMS INVESTIGATION OF PFAS ELECTROCHEMICAL OXIDATION DEGRADATION: MECHANISMS, DFT CALCULATION, AND PATHWAYS

Li, G., Peng, M., Huang, Q., Huang, C. H., Chen, Y., Hawkins, G., & Li, K. (2025). A review on the recent mechanism investigation of PFAS electrochemical oxidation degradation: mechanisms, DFT calculation, and pathways. Frontiers in Environmental Engineering, 4, 1568542.

Reprinted here with permission of the publisher.

Abstract

Per- and polyfluoroalkyl substances (PFAS) have drawn public concern recently due to their toxic properties and persistence in the environment, making it urgent to eliminate PFAS from contaminated water. Electrochemical oxidation (EO) has shown great promise for the destructive treatment of PFAS with direct electron transfer and hydroxyl radical (•OH)-mediated indirect reactions. One of the most popular electrodes is Magnéli phase titanium suboxides. However, the degradation mechanisms of PFAS are still unsure and are under investigation now. The main methodology is the first-principal density functional theory (DFT) computation, which is recently used to explore the degradation mechanisms and interpret by-product formation during PFAS mineralization. From the literature review, the main applications of DFT computation for studying PFAS degradation mechanisms by EO include bond dissociation energy, absorption energy, activation energy, and overpotential η for oxygen evolution reactions. The main degradation mechanisms and pathways of PFAS in the EO process include mass transfer, direct electron transfer, decarboxylation, peroxyl radical generation, hydroxylation, intramolecular rearrangement, and hydrolysis. In the recent four years, 11 papers performed DFT computation to explore the possible PFAS degradation mechanisms and pathways in the EO process. This paper's objectives are to: 1) summarize the main degradation mechanisms of PFAS degradation in EO; 2) review the application of DFT computation for studying PFAS degradation mechanisms during EO; process; 3) review the possible degradation pathways of perfluorooctane sulfonoic acid (PFOS) and per-fluorooctanoic acid (PFOA) during EO process.

3.1 Introduction

Many studies have recently shown the promise of EO for the destructive treatment of PFAS (Schaefer et al., 2017; Z. Wang et al., 2025; Zhao et al., 2025). It is increasingly recognized favorably as a next-generation water treatment technology for a few advantages, such as easy operation under ambient conditions, high degradation efficiency of the contaminants, and ease of manipulation and automation. Electrochemical treatments utilize electrolytic cell composed of at least one anode, one cathode, and a source of electrons (Figure 1) (Ryan et al., 2021). Oxidation reactions occur on the anode and reduction reactions occur on the cathode, with the type of electrode materials determining the specific reactions occurring. Sufficient thermodynamic energy (e.g., working electrode potential) must be available for these reactions to occur (Ryan et al., 2021). Some important parameters in EO influence the degradation efficiency of PFAS, such as the anode material, current density, solution pH, initial PFAS concentration, electrolyte, plate distance and electrical connectors in the EO system (Mirabediny et al., 2023; Y. Wang et al., 2025).

The first principal DFT calculations are useful computational tools for exploring the degradation mechanism and interpreting certain by-product formation during PFAS mineralization (Yamijala et al., 2022). From 2013 to 2025, a decade, there are around twenty papers investigating the mechanism and pathway of PFAS degradation by the EO process. Most focus on PFOA, PFOS, and Perfluorobutanesulfonic acid (PFBS). Among these studies, 11 papers performed density functional theory (DFT) calculations to explore the possible chemical reactions and pathways of PFASs in the aqueous and on anodes (Chen et al., 2021; Cheng et al., 2021; C. Wang et al., 2022).

DFT is recently used to calculate parameters such as, the bond dissociation energy (BDE) of PFAS chains, the adsorption energy of PFAS ion on anodes, the activation energy of PFAS radical, hydroxyl radical, and C-S breaking, as well oxygen evolution reactions (OER) for water splitting (Eslamibidgoli & Eikerling, 2015). Therefore, these DFT calculation parameters can be used as indicators to explore the degradation mechanism and interpret the formation of certain by-products during PFAS mineralization.

Several review papers on removing PFAS with electrochemical techniques have recently been published (Ryan et al., 2021; Zhou et al., 2024). Specifically, some reviews discussed the recent advancements in EO, the PFAS degradation mechanisms, and the key factors that influence PFAS removal efficiency, such as anode material, current density, electrolyte, pH, initial PFAS concentration, and other coexisting pollutants (Alalm & Boffito, 2022; Zhou et al., 2024). However, to the best of our knowledge, no existing review has comprehensively examined how density functional theory (DFT) calculations contribute to understanding PFAS degradation mechanisms.

This review aims to bridge that gap by synthesizing insights from both experimental studies and DFT calculations to provide a more mechanistic understanding of PFAS degradation. By integrating theoretical modeling with empirical findings, this work offers a deeper perspective on degradation pathways and reaction mechanisms, particularly for PFOA and PFOS in the EO process. This approach not only complements existing studies but also enhances predictive capabilities for optimizing PFAS removal strategies.

3.2 PFASs Degradation Mechanisms by EO

The underlying PFAS destruction mechanism for EO is proposed as a combination of the direct electron transfer (DET) and hydroxyl radical (•OH)-mediated indirect reactions (Yaye Wang et al., 2022). In the direct path, the direct electron withdrawal from the organics to the electrode is also the same as the oxidation of organics by holes (h+) on the electrode surface.

Some research has supported this mechanism by comparing experimentally measured kinetics to activation barriers calculated using density functional theory (DFT) (Chen et al., 2022b; H. H. Shi et al., 2019). In the •OH -mediated indirect oxidation process, the •OH is also initiated by the DET of H₂O oxidation on the electrode surface. During EO, the •OH is produced at the anode surface that can only diffuse in a thin layer (<1µm) near the anode surface due to its short lifespan. In contrast, the DET reaction occurs directly on the electrode surface. Also, many reactions happen during the degradation in the EO process, such as mass transfer of PFAS to anodes, decarboxylation of PFCAs, hydroxylation and hydrolysis of by-products, intramolecular rearrangement, and peroxyl radical participated oxidation.

3.2.1 Mass Transfer

Degradation via the electrochemical advanced oxidation process is constrained by the mass transfer of PFAS from the bulk solution to the anode surface, which occurs only at or near the anode surface (Trellu et al., 2018). The mass transfer coefficients can be affected by electricity current, the reactive surface area, flow rate at consistent temperature and pressure. To overcome the mass transfer limitation, a reactive electrochemical membrane operation was suggested, which has improved inter-phase mass transfer through the filtration of polluted samples using porous material that functions simultaneously as a membrane and anode (Liu &

Vecitis, 2012). Consequently, even a single run of water through the membrane can enhance the overall electrochemical oxidation proficiency for treating PFAS.

It has been shown that the most promising way to avoid diffusion, overcome mass transfer limitations, and to increase the electroactive surface area is by using porous electrodes in flow-through configurations. (Y. Y. Wang, R. Pierce, et al., 2022) experimented and compared the PFOS adsorption in REM operation with the batch reactor. The results indicated PFOS adsorption in REM operation was stronger than in the batch reactor because the inner pore surfaces were made available for PFOS adsorption during REM operation. Furthermore, the adsorption of PFOS in the micro-Ti₄O₇ (10 MPa) material was much stronger than that in the nano-Ti₄O₇ (10 MPa) material. It was suggested that the pores of 2–4 nm are most favorable for PFOS diffusion and adsorption because the molecular length of PFOS is 1.32 nm. (Deng et al., 2015). The surface area of the pores in the micro-Ti₄O₇ (10 MPa) anode within the range of 2–4 nm is 0.355 m²·g ⁻¹, while pores of this range are absent in the nano-Ti₄O₇ (10 MPa) anode.

3.2.2 Direct Electron Transfer

In the direct path, the direct electron withdrawal from the organics to the electrode is also the same as the oxidation of organics by electron holes (h⁺) on the electrode surface. During the EO process, electron holes destabilize PFCAs (perfluoroalkyl carboxylic acids) and PFSAs (perfluoroalkyl sulfonic acids) into radicals by direct electron transfer Eq. (1) and (2) Some research has supported this mechanism by comparing experimentally measured kinetics to activation barriers calculated using DFT (Chen et al., 2022b; H. H. Shi et al., 2019). The DET that causes the transformation of PFCAs or PFSAs ion to a free radical via losing an electron to the anode surface was proposed to be the rate-limiting step in their degradation.

At the same time, water in the solution can also be also oxidized by electron holes (h⁺) with DEF to form hydroxyl radical (·OH) and hydrogen ion (Eq. 3).

$$PFCAs^- + h^+ \rightarrow PFCAs^-$$
 (1)

$$PFSAs^- + h^+ \rightarrow PFSAs \cdot (2)$$

$$H_2O + h^+ \rightarrow \cdot OH + H^+$$
 (3)

3.2.3 Decarboxylation

For PFCAs, direct defluorination through nucleophilic substitution is very difficult due to the strong C–F bond. Decarboxylation is a main PFCA degradation process, in which removes a carboxyl group and releases carbon dioxide (CO₂). Usually, decarboxylation refers to a reaction of carboxylic acids, removing a carbon atom from a carbon chain. Previous studies indicated that perfluoroalkyl acids (PFAAs), such as the oxidative degradation of PFOA and PFOS, began in the elimination of the end group. The electron transfer process of carboxylic acid occurred on the anode first, which belongs to the electrochemical process and generates carboxylic radical ($C_nF_{2n+1}COO$). Then the decarboxylation reaction generated perfluoroalkyl radical ($C_nF_{2n+1} \bullet$) and CO₂ (Eq. 4) via the transition state (Niu et al., 2013).

$$C_n F_{2n+1} COO^{\cdot} \rightarrow C_n F_{2n+1} + CO_2$$
 (4)

3.2.4 Peroxyl Radical Generation

Apart from ·OH, the C_nF_{2n+1} could also react with other substances in the electrolyte due to its high activity. A large number of O_2 would be generated at the anode in the electrolysis process. The C_nF_{2n+1} could react with O_2 to generate peroxide (Eq. 5). The O-O bond in peroxides and hydroperoxides is often relatively weak. In most organic hydroperoxides, O-O BDE is 201 ± 8.5 kJ/mol (Sonntag's book). The resulting perfluoroalkyl peroxyl radical can react

with another peroxyl radical as shown by Eq. (6). Then $C_n F_{2n+1} O$ decomposes into perfluoro radical and carbonyl fluoride (Eq. 7) (Niu et al., 2013).

$$C_n F_{2n+1} + O_2 \to C_n F_{2n+1} OO$$
 (5)
 $C_n F_{2n+1} OO + RCOO \to C_n F_{2n+1} O + RCO + O_2$ (6)
 $C_n F_{2n+1} O \to C_{n-1} F_{2n-1} + COF_2$ (7)

3.2.5 Hydroxylation

Hydroxyl radical (•OH) is a strong oxidative radical that plays an important role in reacting with PFAS degradation by-products and contribute to PFAS mineralization. Though •OH is not strong enough to break the C-F bond, the attack of •OH is essential to PFAS degradation (radical chain propagation), otherwise PFAS• may react with water to revert to PFAS (H. Shi et al., 2019).

Furthermore, after losing a CF₂ unit, the new perfluoro radical $(C_{n-1}F_{2n-1})$ is subjected to hydroxylation by the hydroxyl radicals on the anode or in the solution (Eq. 8).

$$C_{n-1}F_{2n-1} + \cdot OH \to C_{n-1}F_{2n-1}OH$$
 (8)

The rate-limiting step in the indirect path is assumed to be the electrochemical production of hydroxyl free radicals (•OH) at the electrode surface as an intermediate of water oxidation, which then reacts with organic contaminants in water. Essentially, the •OH -mediated indirect oxidation process is also initiated by the DET of H₂O oxidation on the electrode surface.

3.2.6 Intramolecular Rearrangement

Defluorination can also be caused by intramolecular rearrangement (Eq. 9).

$$C_{n-1}F_{2n-1}OH \to C_{n-1}F_{2n-3}OF + HF$$
 (9)

3.2.7 Hydrolysis

Hydrolysis plays an important role in the degradation of some small molecules in the EO processes (Li et at., 2004). Since H_2O was the dominant species in the solution, hydrolysis might also contribute to the destruction of organic pollutants. For PFCAs, after $C_nF_{2n+1}O$ decomposes into perfluoro radical and carbonyl fluoride (Eq. 7), carbonyl fluoride COF_2 would further be hydrolyzed to carbon dioxide CO_2 and hydrofluoric acid HF (Eq. 10). Also, after $C_{n-1}F_{2n-3}OF$ was formed, it would undergo hydrolysis reaction to generate $C_{n-1}F_{2n-3}COO^-$, H^+ and HF by hydrolysis (Eq. 11), which also forms a shorter-chain PFCAs with a less CF_2 . $C_{n-1}F_{2n-3}COO^-$ would repeat DET (Eq. 1), decarboxylation (Eq. 4), and form shorter-chain PFCAs until complete mineralization (Chen et al., 2022b).

$$COF_2 + H_2O \rightarrow CO_2 + HF$$
 (10)
 $C_{n-1}F_{2n-3}OF + H_2O \rightarrow C_{n-1}F_{2n-3}COO^- + H^+ + HF$ (11)

3.3 DFT Computation Applications for PFASs Degradation Mechanisms Investigation

DFT computation has gained significant attention in investigating PFAS degradation mechanisms due to its ability to provide detailed insights into molecular structures, energetics, intermediates, and reaction pathways. The electronic structure is assessed using a potential acting on the system electrons in modern DFT techniques. This DFT potential is created by adding the exterior potentials, which are completely governed by the system's structure and elemental makeup representing interelectronic interactions. DFT can accurately predict the molecular structures of PFAS compounds, including their bond lengths, angles, and electronic configurations. This information is crucial for understanding the reactivity and stability of PFAS molecules during degradation processes. DFT calculations can determine the energetics of various degradation reactions involved in PFAS transformation, such as hydrolysis, photolysis,

and oxidative degradation. By calculating reaction energies, activation barriers, and reaction pathways, DFT helps identify the most favorable degradation pathways and mechanisms.

DFT-based simulations have frequently been performed for applications relating to bond dissociation energy (BDE) of PFAS chains, the activation energy of chemical degradation and the adsorption energy for PFAS mass transfer on anodes (Chen et al., 2022a; Jinyu Gao, 2023; Li et al., 2021; Yaye Wang et al., 2022) (Fig 3). The bonds with lower BDE are more likely to be cleaved by ROS than those with higher BDE (Bentel et al., 2019; Chen et al., 2022a). Higher adsorption energy of PFAS ions on anodes is favorable for mass transfer (Li et al., 2021). Lower activation energy of PFAS direct oxidation indicates the PFAS⁻ would be easily oxidized on the surface during the direct electron transfer (Y. Y. Wang, L. Li, et al., 2022). Higher overpotential η for OER means it will be harder to oxide •OH, hence suppressing OER and holding more •OH during the indirectly oxidation for PFAS.

3.3.1 Adsorption Energy

The adsorption energy is one of the most basic parameters for understanding the behavior of a molecule on a surface. It can be defined as the energy changing when a molecule is adsorbed on a solid surface. The formula used to calculate the adsorption energy of PFAS⁻ on an anode supercell during the EO process is described as follows:

$$E_{PFAS-} = E(Anode + PFAS^{-}) - (E(Anode) - E(PFAS^{-}))$$

Where $E(Anode + PFAS^-)$, E(Anode), and $E(PFAS^-)$ are the total energies for anode with a PFAS⁻ adsorbed, anode surface energy, and energy of an isolated PFAS⁻, respectively.

The adsorption energy of a hydroxyl radical (•OH) on anode supercell during the EO process (E_{HO} .) is usually calculated as Equation below:

$$E_{HO} = E(Anode + \bullet OH) - E(Anode) - E(\bullet OH)$$

Where, $E(Anode + \bullet OH)$, E(Anode), and $E(\bullet OH)$ are the total energies of an anode surface with $\bullet OH$, anode surface energy, and energy of an isolated $\bullet OH$, respectively.

Table 3.2 shows some reported DFT adsorption energy calculations for PFOA, PFOS, and PFBS degradation in EO process. Higher adsorption energy indicates stronger adsorption on the anode. (Li et al., 2021) calculated the adsorption energy on the Ti_4O_7 cluster surface with DolM3. The results decrease in the following order: ${}^{\bullet}OH > C_4F_9SO_3^-$ (PFBS $^{-}$) $\sim C_8F_{17}SO_3^-$ (PFOS $^{-}$) $> H_2O$. This suggests that ${}^{\bullet}OH$ formed from water oxidation strongly adsorbs on the Ti_4O_7 cluster surface. The adsorption energies of ${}^{\bullet}OH$ on a Ti_4O_7 surface are much larger than that of H_2O on a Ti_4O_7 surface. This illustrates that hydroxyl radicals, once formed by water oxidation, are more likely bound on a Ti_4O_7 surface rather than diffusing into the bulk solution or reacting with PFOS $^{-}$.

The adsorption energy of different anodes can also be compared. Higher chemical adsorption energies on the anode indicate that the anode drives a much stronger affinity towards the chemical, thus favoring its electrochemical degradation on the anode surface. (Y. Y. Wang, L. Li, et al., 2022) performed and compared the adsorption energies with DolM3 of PFOS on the Ti₄O₇ cluster (~-2.5 eV) and on the Ti₉O₁₇ cluster (-1.5 eV~0.2 eV). The greater adsorption energies of PFOS on the Ti₄O₇ cluster indicate that the Ti₄O₇ cluster drives a much stronger affinity towards PFOS, thus favoring its electrochemical degradation that occurs on the anode surface.

(Wang et al., 2020) also performed molecular simulation based on density functional theory (DFT) using VASP to specifically probe the interactions of Cl atom and OH moieties on Ti₄O₇ (110) and BDD (001), thus providing insights into the formation of Cl• and HO• radicals

on these anodes. (Wang et al., 2020) calculated the adsorption energy of Cl atom and OH moieties adsorbed on Ti₄O₇ (110) and BDD (001) surfaces during PFOS degradation with VASP.

The value of the OH adsorbate on the Ti₄O₇ electrode is -5.13 eV, considerably lower than those on BDD (-7.89 eV) in Table 3.2. Generally, a lower adsorption energy means a higher tendency of desorption to form radicals. Thus, the OH on the Ti₄O₇ electrode has a higher reactivity than those on the BDD. This contributes to the higher PFOS removal rate on Ti₄O₇ than on BDD, since HO⁻ plays an important role on its degradation. The data in Table 3.2 also show that the adsorption energy of Cl and OH adsorbates are close to Ti₄O₇ (110). However, on BDD (001), Cl adsorbate shows significantly lower adsorption energy (-4.16/-3.85 eV) than OH adsorbate (-7.891/-8.80 eV). This suggests that Cl⁻ is more easily released than HO⁻ on BDD (001).

3.3.2 Density of State (DOS)

The density of states (DOS) is one of the most important concepts for understanding the physical properties of materials because it provides a simple way to characterize complex electronic structures. Key aspects that underlie electrical and optical properties of materials are visually apparent from the DOS, including the band gap and effective masses of carriers. Density functional theory is a powerful and effective tool that can be used for predicting the density of state of a material. Density functional theory is widely used to predict and calculate the electronic properties of crystal structures with good accuracy (Bharti et al., 2021). The assumption of DFT that the energy of a system can be calculated using the function of the electronic density rather than solving the complex many-body Schrodinger equations reduces the computational difficulty and time significantly.

The density of states (DOS) plays a crucial role in electron transfer processes. A higher DOS implies more available states for electrons to occupy, facilitating electron transfer by providing a larger pool of states near the Fermi level for electron donation and acceptance. In summary, the density of states directly affects electron transfer by influencing the availability of electronic states, energy level alignment, interface properties, activation energies, and charge carrier transport in materials. Understanding and controlling DOS profiles are essential for optimizing electron transfer rates, designing functional materials, and developing advanced electronic and optoelectronic devices. In semiconductors and metals, the DOS near the conduction band (CB) and valence band (VB) significantly influence electron transfer. A higher DOS near the CB promotes electron conduction and transport, while a higher DOS near the VB facilitates hole conduction and valence band transitions.

Ma et al. first calculated the DOS for Ti₄O₇ and the composite structure of Ti₄O₇/MXene surface in order to compare the electron transport properties of these two electrodes (Ma et al., 2024). Figure 3.2a shows that the Ti₄O₇ conduction band parts are constructed by mainly Ti d states and a small part of O p states (Ma et al., 2024). The Ti₄O₇ valence bonding is constructed by mostly O p states and a small part of Ti d states, in agreement with previous DFT simulations of the electronic construction for a Magnéli phase TiO₂ (Ma et al., 2024). Figure 3.2b shows that both the conduction band position and valence band position of Ti₄O₇/MXene moved down significantly, which narrowed the band gap and thus enhanced electrical conductivity and interfacial electron transfer (Ma et al., 2024). This demonstrates that the charge transfer to the PFAS are more favorable on Ti4O7/MXene (Ma et al., 2024).

3.3.3 Overpotential for Oxygen Evolution Reaction (OER)

In the EO process, the rate-limiting step in the indirect path is assumed to be the electrochemical production of hydroxyl free radicals (•OH) at the electrode surface as an intermediate of water oxidation, which then reacts with organic contaminants in water. Essentially, the •OH mediated indirect oxidation process is also initiated by the DET of H₂O oxidation on the electrode surface.

Overpotential η for OER (•OH \leftrightarrow O• + H⁺ + e⁻) can be an indicator. Higher η means it will be harder to oxidize •OH, hence suppressing OER and holding more •OH during the indirect PFAS oxidation (Man et al., 2011). The descriptor $\Delta G_{\rm O} - \Delta G_{\rm OH}$ has been verified to well describe the trend of OER activities on various metal oxide surfaces (Huang et al., 2019).

DFT calculations are used to estimate the overpotential η for OER for different materials as simulated above. Using the previously validated relationship for a wide range of oxide surfaces, η in V relative to SHE for each material as a function of the descriptor $G_{O^*} - G_{\bullet OH}$:

$$\eta^{OER} = \Delta G/e - 1.23V$$

$$\Delta G = \Delta G_{O*} - \Delta G_{\bullet OH} = E_{O*}^{DFT} - E_{\bullet OH}^{DFT} + \frac{1}{2} E_{H2} + (\Delta ZPE - TS^0)$$

3.2 eV is the average value of ΔG_{HOO^*} - ΔG_{HO^*} of OER on oxide surfaces in university (Man et al., 2011). For the ideal case, ΔG_{HO^*} is 1.23 eV at pH=0 and T=298 K. The descriptor ΔG represents the difference in binding free energies of the critical intermediate species O* and •OH. This is calculated based on total energies of systems consisting of the O* or •OH species bound to each material surface as determined by DFT. The theoretical overpotential is independent of the pH or the potential values. Therefore, the calculations/analysis performed for the free energies is at standard conditions (pH=0, T=298.15 K) and U=0.

The results of DFT calculations were reported to compare Ti₄O₇, TiO₂, and Nb-doped TiO₂ materials for effective •OH production with Quantum Espresso version 6.6 (Ko et al.,

2021). They simulated the Ti₄O₇ (120), TiO₂ (110), and 12.5 at% Nb-doped TiO₂ (110) anode supercell. Ti₄O₇ anode had the highest overpotential η for OER, 2.0V. Overpotential η for OER of 12.5 at% Nb-doped TiO₂ anode (1.4 ±0.49 V) is higher than TiO₂ (1.3 V).

3.3.4 Bond-dissociation Energy (BDE)

The bond-dissociation energy is one measure of the strength of a chemical bond. For PFAS degradation, several studies performed C-F BDE and C-C BDE calculations. Theoretical calculations on the C-F BDE of PFAS structures can reveal relationships among the rate of decay defluorination, the position and number of C-F bonds with low BDE, and fluoroalkyl chain length (Bentel et al., 2019). The bonds with lower BDE are more likely to be cleaved by ROS than those with higher BDE. Therefore, it also can be used to suggest and interpret the formation of certain by-products during PFAS mineralization.

Bentel et al. calculated BDEs for all of the C–F BDEs (kcal mol–1) for PFCAs (C2-C12) using the GAUSSIAN 09 software package with DFT in conjunction with an SDM polarizable continuum model. As expected, BDEs of all primary C–F bonds (i.e., bonds on the terminal –CF₃; 117.8–123.4 kcal mol⁻¹) are higher than all secondary C–F bonds (i.e., bonds on –CF₂–; 106.4–113.6 kcal mol⁻¹) (Table 1). In general, lower BDEs for both primary and secondary C–F bonds are observed in PFAS with longer fluoroalkyl chains. This trend may explain why the rate of parent compound degradation was faster for the longer chain PFCAs and PFSAs, where more –CF₂– functional groups in the middle of the fluoroalkyl chains have low BDEs (typically \leq 107.5 kcal mol⁻¹) (Bentel et al., 2019).

BDE calculations can also help explore the primary pathway. Past studies revealed that $C_7F_{15}COO \bullet$ easily underwent a decarboxylation reaction to form $C_7F_{15} \bullet$. To test whether it was the primary pathway, (Chen et al., 2022b) calculated and compared the C–C BDEs and C–F

BDEs for both C₇F₁₅COO⁻ and C₇F₁₅COO• to get the change for BDEs after C₇F₁₅COO⁻ lost one electron using Gaussian 16 with M06-2X-D3(0)/6-311+G(d,p). Their results showed all C-F bonds (108.7~125.6 kcal mol⁻¹) were much higher than those for C-C bonds (86.3~92.6 kcal mol⁻¹) (Table 1). This indicated that C-F bonds were much harder to break than C-C bonds, and the cleavage of C-F bonds should not be the primary pathway. So, decarboxylation of C₇F₁₅COO• may be the primary pathway. After C₇F₁₅COO⁻ lost one electron to form C₇F₁₅COO•, the BDEs for all of the C-C bonds were lower, and bond 1 (with functional group COO⁻) had the lowest BDE (-25.7 kcal mol⁻¹). This suggested that all of the C-C bonds significantly weakened after C₇F₁₅COO⁻ lost one electron, and the cleavage of bond 1 was most likely to occur. Bond 1 had a BDE of -25.7 kcal mol⁻¹. A negative BDE indicated that bond 1 was remarkably unstable and would easily dissociate to release CO₂ and form C₇F₁₅•.

3.3.5 Activation Energy

In chemistry, activation energy is the minimum amount of energy that must be provided for compounds to result in a chemical reaction. Table 3.2 also shows some reported DFT activation energy calculations for PFOA, PFOS, or PFBS degradation in the EO process. It is found that the activation energies of PFBS degradation by possible hydroxyl radical attacks were prohibitively high (Carter & Farrell, 2008), while those of direct electron transfer (DET) were lower and comparable to experimentally measured values. The density functional simulations were performed to calculate the reaction energies and activation barriers for PFBS oxidation by hydroxyl radicals and by direct electron transfer on BDD anode (Liao & Farrell, 2009). The activation energy determined from the transition state was 1.275 eV by the reaction of hydroxyl radicals at different sites on the PFBS molecule. The activation energy determined was 0.0964 ± 0.0311 eV with the experimental temperature dependence of the PFBS reaction rates method.

The low activation energy of PFAS direct oxidation indicates the PFAS⁻ would be easily oxidized on the surface during direct electron transfer.

Some studies also calculated the activation energy of PFOS by hydroxyl radicals. (H. Shi et al., 2019) contacted DFT simulation of PFOS on an inert anode by calculating its activation energy as a function of anodic potential. It indicates that the DET of PFOS occurs at 3.67 V/SHE without an activation barrier, higher than that for water oxidation (2.74 V/SHE) reported in an earlier study. Therefore, the DET reaction of PFOS would be slower and weaker than water oxidation on an inert anode such as titanium suboxide or BDD. Their calculation revealed that $C_8F_{17}SO_3^*$ may react with water to form $C_8F_{17}SO_3^-$ via an energetically favorable reaction. Therefore, once $C_8F_{17}SO_3^*$ is formed by PFOS oxidation during EO via DET, it can spontaneously transform back to $C_8F_{17}SO_3^-$ in water solution. It is proposed that $C_8F_{17}SO_3^*$ tends to undergo desulfurization, accompanied by a reaction with •OH to form $C_8F_{17}OH$.

3.3.6 Limitations of the DFT Calculation

While DFT calculations provide invaluable insights into PFAS degradation mechanisms in electrochemical oxidation, they are subject to several limitations that must be considered when interpreting results.

One key limitation of DFT is the accuracy of its exchange-correlation functionals. Standard generalized gradient approximation (GGA) functionals, such as PBE or B3LYP, may introduce errors in calculating bond dissociation energies (BDEs) and reaction barriers, particularly for complex reaction systems involving radical intermediates. Hybrid functionals and dispersion-corrected methods can improve accuracy, but their computational cost is significantly higher.

Another major limitation is the treatment of solvation effects. PFAS degradation occurs in aqueous environments, yet many DFT studies employ implicit solvation models (e.g., SMD), which approximate solvent effects rather than explicitly modeling solute-solvent interactions. This can lead to inaccuracies in adsorption energy predictions and reaction barrier calculations. Explicit solvation models, while more accurate, demand significantly higher computational resources.

DFT calculations also struggle with modeling dynamic reaction pathways. Most studies rely on static energy calculations to infer degradation mechanisms, but the actual reaction process involves multiple intermediate steps, solvent interactions, and surface effects that are best captured by molecular dynamics (MD) simulations or hybrid quantum mechanics/molecular mechanics (QM/MM) approaches. For example, the interaction between PFAS radicals and hydroxyl radicals (•OH) on an anode surface is highly dynamic and influenced by local electrochemical conditions, which are difficult to model with standard DFT methods.

Moreover, the choice of computational parameters, such as basis sets and pseudopotentials, can introduce systematic errors. Small basis sets may underestimate binding energies, while large basis sets increase computational demand without always improving accuracy. Similarly, pseudopotential selection can affect the accuracy of adsorption energy calculations on metal-oxide anode surfaces, impacting the predicted reactivity of PFAS species.

Finally, scaling DFT findings to real-world electrochemical conditions presents challenges. Experimental electrochemical oxidation occurs under varying pH, electrode potential, and ionic strength conditions, which influence reaction kinetics and pathways.

However, most DFT studies are conducted at fixed oxidation states and vacuum or simplified solvated conditions, making direct comparison with experimental data difficult.

To address these limitations, future research should incorporate higher-level post-DFT methods, such as coupled-cluster theory for improved energy accuracy, and hybrid approaches integrating molecular dynamics simulations to capture solvent effects and reaction kinetics more realistically. Additionally, experimental validation through spectroscopic techniques, such as in situ Raman spectroscopy or X-ray photoelectron spectroscopy (XPS), can provide critical benchmarks for refining computational predictions (Chen et al., 2024).

By acknowledging these limitations and refining computational approaches, DFT calculations can continue to play a crucial role in elucidating PFAS degradation mechanisms while improving their predictive reliability for practical electrochemical treatment application.

3.4 Degradation Pathways of Some PFAS Species

3.4.1 PFOA Degradation Pathways

Based on the literature review, three possible PFOA degradation pathways in the EO process have been proposed: pathways a), b) and c) in Figure 3.4. These three possible pathways have two common initial steps. The first common step involves the direct oxidation of $C_7F_{15}COO^-$ to generate $C_7F_{15}COO^+$ (Eq. 12) as $C_7F_{15}COO^-$ remains the dominant PFOA species in the solution throughout the electrolysis. The second step is the decarboxylation of $C_7F_{15}COO^+$ to form $C_7F_{15}^+$ (Eq. 13), which is supported by the C-C BDEs DFT calculations by Chen et al. (in 2.1 BDE section).

$$C_7 F_{15} COO^- + h^+ \rightarrow C_7 F_{15} COO^-$$
 (12)

$$C_7 F_{15} COO^{\cdot} \rightarrow C_7 F_{15}^{\cdot} + CO_2$$
 (13)

Pathway a) is widely considered the primary route for PFOA mineralization in the EO process (Chen et al., 2022b). DFT calculations of the reactions' standard Gibbs free energy

change (ΔG_0) and Gibbs free energy of activation (ΔG^{\ddagger}) indicate that the reaction of C_7F_{15} with 'OH to form C_7F_{15} OH (Eq. 14) is highly favorable, with a barrierless reaction and a ΔG_0 of -419.1 kJ/mol. Alternatively, the direct oxidation of C_7F_{15} to C_7F_{15} (Eq. 15) followed by its reaction with OH⁻ to form C_7F_{15} OH (Eq. 16) is also energetically feasible. Given the significantly exergonic nature of both pathways (ΔG_0 of -459.9 kJ/mol for Eq. 16), hydroxylation appears to be the dominant mechanism.

$$C_7F_{15}^{\ \ } + \cdot OH \rightarrow C_7F_{15}OH$$
 (14) $\Delta G_0 = -419.1 \text{ kJ/mol, no barrier}$ $C_7F_{15}^{\ \ } + h^+ \rightarrow C_7F_{15}^{\ \ }$ (15) $\Delta G_0 = -83.1 \text{ kJ/mol, } \Delta G^{\ddagger} = 0.97 \text{ kJ/mol}$ $C_7F_{15}^{\ \ } + \cdot OH \rightarrow C_7F_{15}OH$ (16) $\Delta G_0 = -459.9 \text{kJ/mol, no barrier}$

Once $C_7F_{15}OH$ formed, it dissociates into $C_7F_{15}O^-$ can due to the low pKa (~2) in the solution (Zhang et al., 2019). Accordingly, the majority of $C_7F_{15}OH$ species would become $C_7F_{15}O^-$ in the solution. In the subsequent degradation process, $C_7F_{15}O^-$ can react with h^+ , H_2O , and HO^+ . Chen et al. found that the formation of $C_7F_{15}O^+$ via hole oxidation (Eq. 17) is favorable due to its low activation energy ($\Delta G^{\ddagger} = 5.11 \text{ kJ/mol}$). $C_7F_{15}O^+$ then undergoes cleavage to form $C_6F_{13}^+$ and COF_2 (Eq. 18), a reaction with a ΔG_0 of -90.6 kJ/mol and a low activation energy ($\Delta G^{\ddagger} = 13.3 \text{ kJ/mol}$), making it a highly likely step in the overall degradation process. $C_6F_{13}^+$ subsequently undergoes similar reactions, leading to sequential cleavage until complete mineralization to CO_2 and HF through hydrolysis.

$$C_7 F_{15} O^- + h^+ \to C_7 F_{15} O^-$$
 (17) $\Delta G_0 = -11 \text{ kJ/mol}, \Delta G^{\ddagger} = 5.11 \text{kJ/mol}$
 $C_7 F_{15} O^- \to C_6 F_{13}^- + CO F_2$ (18) $\Delta G_0 = -90.6 \text{ kJ/mol}, \Delta G^{\ddagger} = 13.3 \text{kJ/mol}$

Pathway b), proposed by Niu et al. (2013), suggests that C_7F_{15} reacts with O_2 to form $C_7F_{15}OO^{\bullet}$ (Eq. 19), which then decomposes into $C_7F_{15}O^{\bullet}$ and O_2 (Eq. 20) (Niu et al., 2013). Since electrolysis generates a significant amount of O_2 at the anode, this reaction could occur in

competition with the hydroxylation pathway in pathway a). However, the competition between these two routes is influenced by reaction kinetics and the relative concentrations of reactive oxygen species (ROS) and molecular oxygen. Although the formation of peroxides provides an alternative route for $C_7F_{15}O^{\bullet}$ generation, it is unclear whether this mechanism is dominant under typical electrochemical conditions.

$$C_7F_{15}^{\cdot} + O_2 \rightarrow C_7F_{15}OO$$
 (19)
 $C_7F_{15}OO + C_7F_{15}OO \rightarrow 2C_7F_{15}O + O_2$ (20)

Pathway c), as shown in Figure 3.4, proposes that $C_7F_{15}O^-$ can react with H_3O^+ to form $C_6F_{13}COF$ and release HF (Eq. 21). The relatively low ΔG_0 (-63.6 kJ/mol) suggests that this reaction is thermodynamically feasible and could compete with the hole oxidation pathway (Eq. 17). However, the subsequent hydrolysis of $C_6F_{13}COF$ to $C_6F_{13}COOH$ (Eq. 22) has a high activation energy ($\Delta G^{\ddagger} = 159.8$ kJ/mol), making it less favorable compared to the sequential cleavage mechanism in pathway a). This suggests that while pathway c) may occur in parallel, it is unlikely to be the primary mineralization pathway due to its slower reaction kinetics $C_7F_{15}O^- + H_3O^+ \rightarrow C_6F_{13}COF + HF + H_2O$ (21) $\Delta G_0 = -63.6$ kJ/mol, $\Delta G^{\ddagger} = 14.3$ kJ/mol $C_6F_{13}COF + H_2O \rightarrow C_6F_{13}COOH$ (22) $\Delta G_0 = -41.4$ kJ/mol, $\Delta G^{\ddagger} = 159.8$ kJ/mol

While all three pathways contribute to PFOA degradation, pathway a) is likely the dominant route due to its lower energy barriers and strong exergonic reactions. The direct interaction of C₇F₁₅* with *OH is particularly favorable, given the abundance of hydroxyl radicals in electrochemical oxidation. Pathway b), involving O₂, may become more significant under conditions where hydroxyl radical production is limited or oxygen concentration is high. Pathway c) is less favorable for complete mineralization due to the high activation energy of its hydrolysis step, though it may still contribute to intermediate transformation.

In practical applications, the dominant pathway will depend on operational factors such as anode material, applied potential, pH, and the presence of competing oxidants. Higher anode potentials and catalytic surfaces that enhance hydroxyl radical production will likely favor pathway a), whereas systems with high oxygen evolution may shift the balance toward pathway b). Further experimental validation is needed to quantify the relative contributions of each pathway under real-world conditions.

3.4.2 PFOS Degradation Pathways

There are two proposed possible PFOS degradation pathways on the anode in the EO process by (H. H. Shi et al., 2019) and (Pierpaoli et al., 2021) in Figure 5. However, we found the second pathway proposed by Pierpaoli et al. unreasonable.

(H. H. Shi et al., 2019) 's study explored PFOS degradation with DFT calculations in the EO process and they found the role of hydroxyl free radicals in PFOS. Combining the experiment analysis and DFT theoretical studies they proposed the 1) PFOS degradation pathways in Figure 3.5. By DFT calculations, they also found the role of hydroxyl free radicals in PFOS degradation during EO that C₈F₁₇SO₃• may react with water to form C₈F₁₇SO₃- via an energetically favorable reaction. Therefore, once C₈F₁₇SO₃• is formed by PFOS oxidation during EO via DET, it can transform back to C₈F₁₇SO₃- spontaneously in water solution. It is proposed that C₈F₁₇SO₃• tends to undergo desulfurization, accompanied by a reaction with •OH to form C₈F₁₇OH (Eq. 25). It is proposed that C₈F₁₇OH formed in Eq. 25 decomposes to C₇F₁₅CFO (Eq. 26), and then rapidly hydrolyze to C₇F₁₅COO⁻ (Eq. 27). C₇F₁₅COO⁻ may further go through the decarboxylation cycle stepwise like PFOA degradation pathways (a, b or c pathways in figure 3.4), leading to rip off of a CF₂ unit each step until complete mineralization.

$$C_8F_{17}SO_3^- \to C_8F_{17}SO_3^+ + e^-$$
 (23)

92

$$C_8F_{17}SO_3^- + 2H_2O \rightarrow C_8F_{17}SO_3^- + OH + H_3O^+$$
 (24)

$$C_8 F_{17} SO_3^{\cdot} + \cdot OH \rightarrow C_8 F_{17} OH + SO_3$$
 (25)

$$C_8 F_{17} OH \rightarrow C_7 F_{15} CFO + HF$$
 (26)

$$C_7 F_{15} CFO + H_2 O \rightarrow C_7 F_{15} COO^- + HF + H^+$$
 (27)

However, (Pierpaoli et al., 2021) proposed a free hydrogen radical eliminates a fluoride atom from PFSAs or sulfonated radicals by H-F substitution followed by the transformation to new sulfonated products by hydrogen abstraction, based on the identification of by-product with the UHPLC-ESI-MS technique. They observed the perfluooroheptyl sulphate ion and radical $(C_7F_{15}SO_3^-, \cdot C_7F_{15}SO_3^-)$, as well $C_6F_{13}COO_-$, $C_5F_{11}COO_-$, and $C_4F_9COO_-$. The 2) pathway in Figure 5 includes radical reaction, decarboxylation, hydrolysis, and hydroxylation for PFOS anodic degradation as follows. The elimination of two fluoride ions giving the observed $C_7F_{15}SO_3^-$ may be a result of consecutive radical reactions according to the following reactions:

$$C_8F_{17}SO_3^- + H \cdot \rightarrow C_8HF_{16}SO_3^- + F^- + e^-$$
 (28)

$$C_8 H F_{16} S O_3^- + \cdot O H \rightarrow C_8 F_{16} S O_3^- + H_2 O$$
 (29)

$$.C_8F_{16}SO_3^- + H \cdot \rightarrow C_8HF_{15}SO_3^- + F^-$$
 (30)

$$C_8 H F_{15} S O_3^- + \cdot O H \rightarrow \cdot C_8 F_{15} S O_3^- + H_2 O$$
 (31)

At the same time, the $\cdot C_8 F_{16} S O_3^-$ radical may also react with hydroxyl radical:

$$\cdot C_8 F_{16} S O_3^- + \cdot O H \rightarrow H O C_8 F_{15} S O_3^- + F^-$$
 (32)

$$HOC_8F_{15}SO_3^- + 2F^- \to FOC_8F_{15}SO_3^- + HF$$
 (33)

However, only after hydrolysis of the formed product ($FOC_8F_{15}SO_3^-$) and followed by the Kolbe decarboxylation reaction (Eq. 17) the perfluooroheptyl sulphate radical is observed ($C_7F_{15}SO_3^-$).

$$C_n F_{2n+1} + O_2 \to C_n F_{2n+1} O O$$
 (34)

$$C_n F_{2n+1} OO^{\cdot} + RCOO^{\cdot} \rightarrow C_n F_{2n+1} O^{\cdot} + RCO^{\cdot} + O_2$$
 (35)

$$C_n F_{2n+1} O \to C_{n-1} F_{2n-1} + COF_2$$
 (36)

However, the proposed PFOS degradation pathway by Pierpaoli has been critiqued for issues related to charge balance, as noted in their study. Some of the reactions are not balanced such as there are three negative charges on the right side and only one on the left in reaction Eq. 28. Furthermore, the formation of hydrogen radical is not mentioned in this paper. There may be some wandering hydrogen radicals in the system, but it's doubtful that the hydrogen radicals are reactive enough to eliminate a fluoride atom from PFSA. So, it is not a reasonable possible pathway for PFOS degradation. While the authors did not analyze in depth the rationale behind their pathway proposal or potential directions for its improvement. Further exploration is necessary to refine the mechanistic understanding and address the rationality of the proposed transformations.

3.5 Comparative Analysis of Electrode Materials

A comparative analysis of electrode materials is essential for understanding the effectiveness of electrochemical oxidation (EO) in PFAS degradation. Various anode materials, including boron-doped diamond (BDD), Magnéli phase titanium suboxides (TSO), lead dioxide (PbO₂), and stannous dioxide (SnO₂), have been extensively studied. Each material offers distinct advantages and limitations in terms of degradation efficiency, selectivity, energy consumption, and potential secondary contamination.

BDD electrodes are widely regarded as one of the most effective materials for PFAS degradation due to their high oxygen evolution potential, which minimizes competition from side reactions. This allows for the generation of hydroxyl radicals (•OH) that can efficiently break

94

down PFAS molecules. However, BDD electrodes are expensive to manufacture and have limited scalability for large-scale water treatment applications.

TSO electrodes, particularly Ti₄O₇, have gained attention as a cost-effective alternative to BDD. Studies have shown that Magnéli phase Ti₄O₇ anodes provide a high degree of PFAS mineralization while maintaining good stability. Additionally, the porous structure of TSO electrodes enhances mass transfer, which can improve degradation kinetics. However, their lower oxidation potential compared to BDD can result in partial degradation and the formation of persistent byproducts.

PbO₂ and SnO₂ electrodes have also been investigated for PFAS degradation due to their strong oxidizing properties. PbO₂ anodes demonstrate high degradation efficiency but pose a significant environmental risk due to potential lead leaching, making them unsuitable for drinking water applications. SnO₂ electrodes, particularly when doped with elements like antimony (Sb-SnO₂), have shown promise in PFAS treatment. However, their long-term stability remains a concern, as SnO₂-based electrodes tend to degrade over extended operation times.

Recent advancements in electrode materials include doping strategies and hybrid electrode systems. For example, Nb-doped TiO₂ has been explored as a means to enhance the electrochemical activity of Ti-based electrodes while maintaining stability. Similarly, composite materials, such as Ti₄O₇/MXene hybrids, have been shown to improve electrical conductivity and PFAS adsorption, leading to more efficient degradation pathways.

From an application standpoint, the choice of electrode material depends on the specific treatment objectives. For high-efficiency mineralization with minimal byproduct formation, BDD remains the gold standard, albeit at a higher cost. For scalable and cost-effective alternatives, TSO electrodes provide a balance between efficiency and affordability. PbO₂ and

SnO₂ electrodes, while effective, require careful consideration of stability and potential secondary contamination. Hybrid and doped materials represent promising directions for future research, offering opportunities to optimize both performance and economic feasibility.

Future studies should focus on optimizing electrode surface properties, enhancing longterm stability, and integrating EO with complementary treatment technologies. Additionally, life cycle assessments comparing the environmental and economic impacts of different electrode materials would provide valuable insights for real-world implementation.

3.6 Practical Implications

The insights presented in this study have significant implications for the development of more effective electrochemical oxidation (EO) systems for PFAS remediation. Understanding the mechanistic pathways of PFAS degradation allows for the strategic optimization of electrode materials, operational conditions, and system design to enhance treatment efficiency.

- Optimization of Electrode Materials The findings highlight the critical role of electrode
 composition in PFAS degradation. Electrodes with high overpotential for oxygen evolution,
 should be prioritized to promote direct electron transfer and hydroxyl radical generation.
 Future research should focus on doping strategies and surface modifications to improve
 electrocatalytic performance and stability.
- Operational Condition Enhancement The study suggests that electrolyte composition,
 current density, and applied potential significantly influence PFAS degradation efficiency (Y.
 Wang et al., 2025). Maintaining optimal current densities while avoiding excessive energy
 consumption is crucial. Further research on pH adjustments, electrolyte additives, and pulsed
 voltage application could improve selectivity and degradation rates.

System Design Considerations – The integration of EO with complementary treatment
processes, such as adsorption or photochemical oxidation, could enhance PFAS removal
efficiency (Gomri et al., 2025). Reactor design modifications, including flow cell
optimization and electrode spacing adjustments, may further improve mass transfer and
degradation kinetics. Pilot-scale testing should be prioritized to assess scalability and longterm performance.

By translating these mechanistic insights into practical design and operational strategies, this study provides a foundation for advancing EO systems as a viable technology for PFAS remediation in groundwater and wastewater treatment applications.

3.7 Conclusion and Insights for Future Study

This review elucidates the primary PFAS degradation mechanisms during the EO process, highlighting the critical role of density functional theory (DFT) calculations in understanding reaction pathways. The applications of DFT in mechanism investigation are demonstrated, including bond dissociation energy, adsorption energy of PFAS, activation energy of PFAS and hydroxyl radicals, and the overpotential of oxygen evolution reactions. Furthermore, possible PFOA and PFOS degradation pathways are discussed in detail.

From the literature review, the main PFAS degradation mechanisms in the EO process include mass transfer, direct electron transfer, decarboxylation, peroxyl radical generation, hydroxylation, intramolecular rearrangement, and hydrolysis. While previous studies demonstrate that EO is highly effective for PFAS degradation, significant challenges remain that hinder its large-scale application. These challenges include high energy consumption, the generation of persistent intermediate byproducts, competition between degradation pathways,

and the influence of anode material properties on reaction kinetics. To address these limitations, the following targeted recommendations are proposed:

 Optimizing anode materials to enhance degradation efficiency and reduce energy consumption.

The choice of anode material significantly affects EO efficiency by influencing hydroxyl radical generation, electron transfer rates, and energy demands. Future research should focus on developing high-activity, low-cost anode materials with improved selectivity for PFAS oxidation. Boron-doped diamond (BDD) electrodes have demonstrated high oxidation potential but are costly, while mixed metal oxide (MMO) anodes are more affordable but less efficient. Novel composite anodes, such as doped Ti/IrO₂ or graphene-modified electrodes, could be explored to achieve a balance between efficiency and cost-effectiveness. Additionally, optimizing the anode surface structure to enhance reactive species generation and reduce overpotentials could further improve performance.

- Enhancing electrolyte conditions and reactor design for energy efficiency

 The energy consumption of EO is strongly influenced by electrolyte composition and reactor design. Future studies should investigate the impact of electrolyte pH, ionic strength, and the presence of co-contaminants on PFAS degradation kinetics. Electrolytes with lower resistivity can reduce energy losses, while buffer systems could help maintain optimal reaction conditions. Furthermore, novel reactor designs, such as flow-through electrochemical cells or gas-diffusion electrodes, could enhance mass transfer and improve energy efficiency. The integration of EO with complementary processes, such as adsorption or membrane filtration, could also help reduce overall treatment energy costs by concentrating PFAS before EO treatment.
 - Expanding investigations beyond PFOA and PFOS to other PFAS species

Most research has focused on PFOA and PFOS degradation pathways, but short-chain PFAS and emerging alternatives may exhibit different electrochemical behavior. Future studies should systematically examine the degradation kinetics of a broader range of PFAS compounds and explore whether short-chain PFAS require different operational conditions or anode materials.

 Combining DFT calculations with experimental studies for more accurate mechanistic insights

DFT calculations are valuable for predicting reaction pathways, but experimental validation is essential for practical implementation. Future research should focus on integrating computational models with real-time electrochemical experiments to refine degradation pathway predictions.

This could involve in situ spectroscopic techniques, such as Raman spectroscopy, to track PFAS degradation intermediates and confirm theoretical predictions.

In conclusion, while EO remains a promising approach for PFAS degradation, addressing energy consumption, optimizing electrode materials, and refining mechanistic understanding are critical for its large-scale application. Future research should focus on material innovations, reactor optimization, and hybrid treatment approaches to enhance both efficiency and feasibility.

CRediT authorship contribution statement

Gengyang Li: Conceptualization, Data curation, Formal analysis, Writing - original draft. Mason Peng: Conceptualization, Data curation, Formal analysis. Qingguo Huang: Conceptualization, Supervision - review. Ching-Hua Huang: Conceptualization, Supervision - review. Yongsheng Chen: Conceptualization, Supervision - review. Gary Hawkins: Conceptualization, Supervision - review. Ke Li: Conceptualization, Supervision, Methodology, Formal analysis, Writing-review & finalizing.

Declaration of Competing Interest

The authors declare that they have no known competing financial interests or personal relationships that could have appeared to influence the work reported in this paper.

Acknowledgements

This study was supported in part by U.S. Environmental Protection Agency Grant R840080. It has not been formally reviewed by EPA. The views expressed in this document are solely those of the authors and do not necessarily reflect those of the Agency. EPA does not endorse any products or commercial services mentioned in this publication.

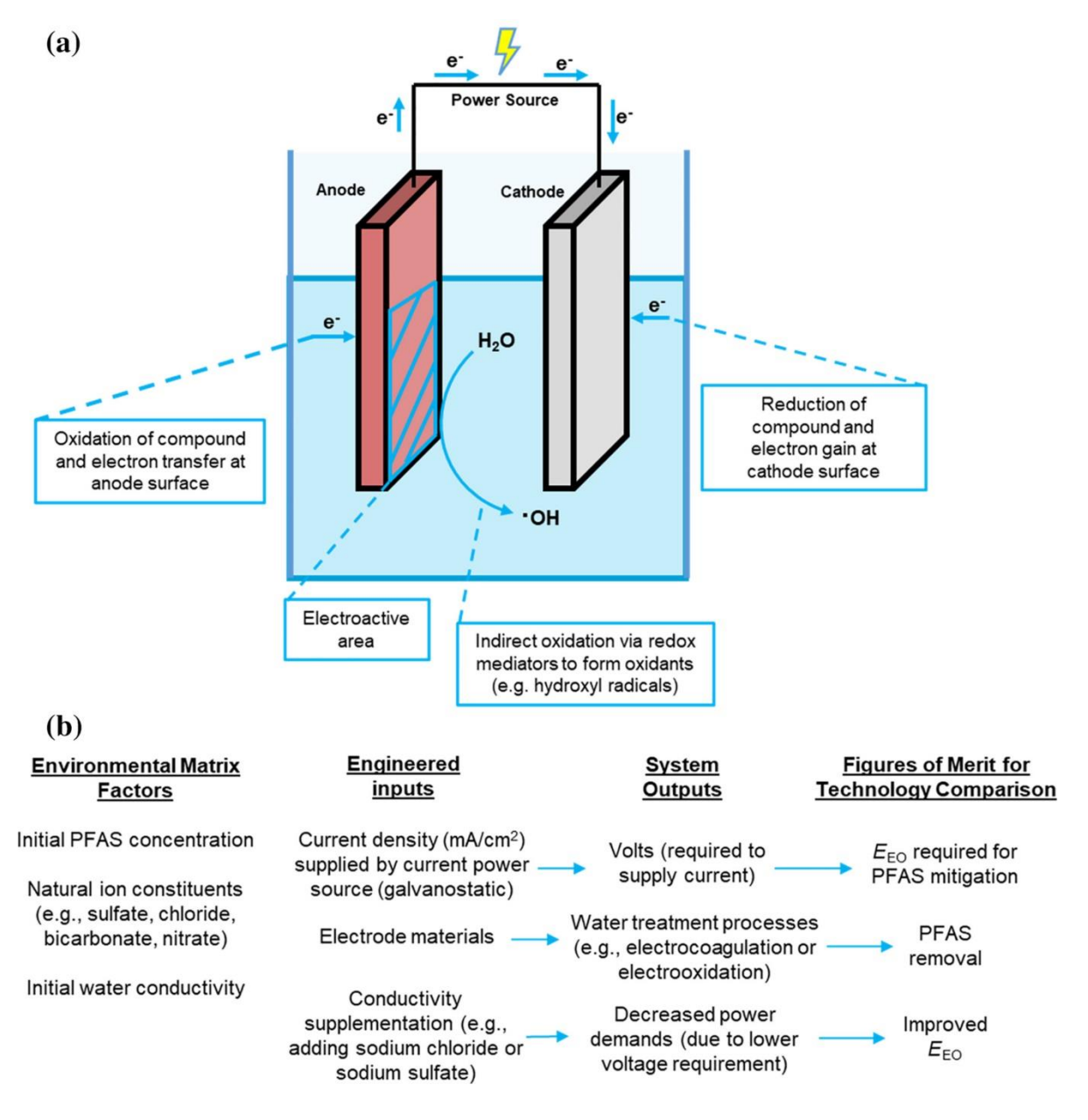


Figure 3.1: (a) Electrolytic cell schematic for electrochemical water treatment reactors. In these cells, oxidation reactions occur at the anode and electrons flow to the cathode, where reduction reactions occur. In these systems, the current density (mA/cm²) is d determined by the amount of current (mA) that passes through the electroactive surface area. (b) Additional information is provided for environmental inputs to the electrolytic cell, in addition to engineered inputs and corresponding system outputs and figures of merit for comparing technology. EEO = electrical energy per order. (Ryan et al., 2021)

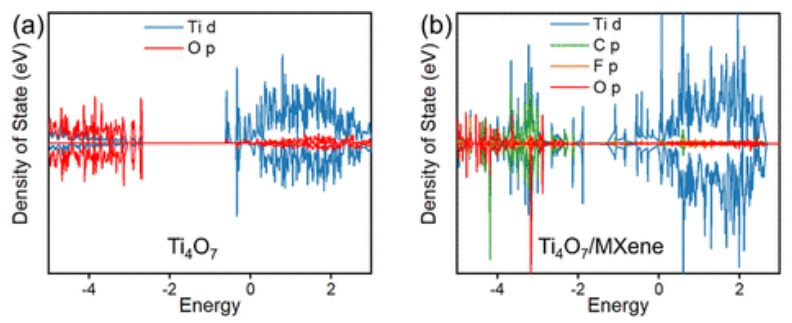


Figure 3.2 Density of states (DOS) of (a) Ti4O7 and (b) Ti4O7/MXene surface (Ma et al., 2024).

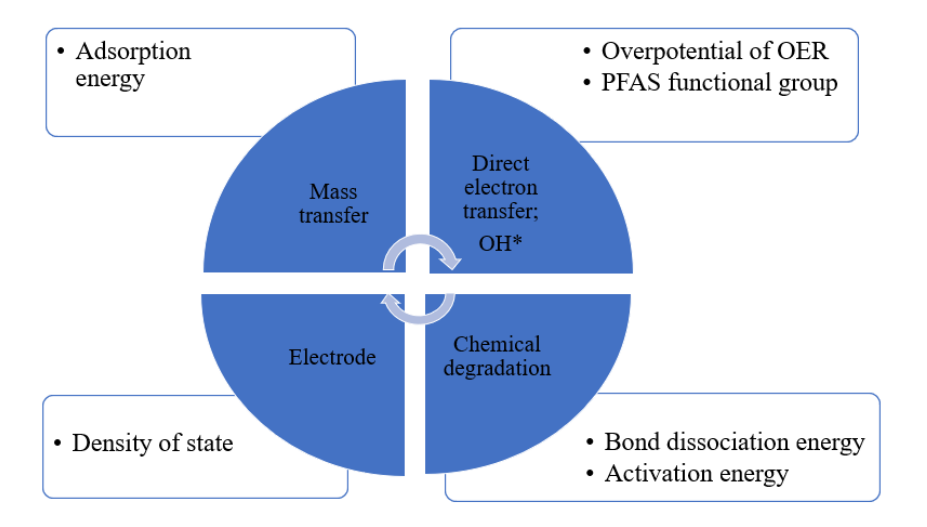


Figure 3.3 DFT quantification descriptors for electrodes and PFAS degradation mechanism

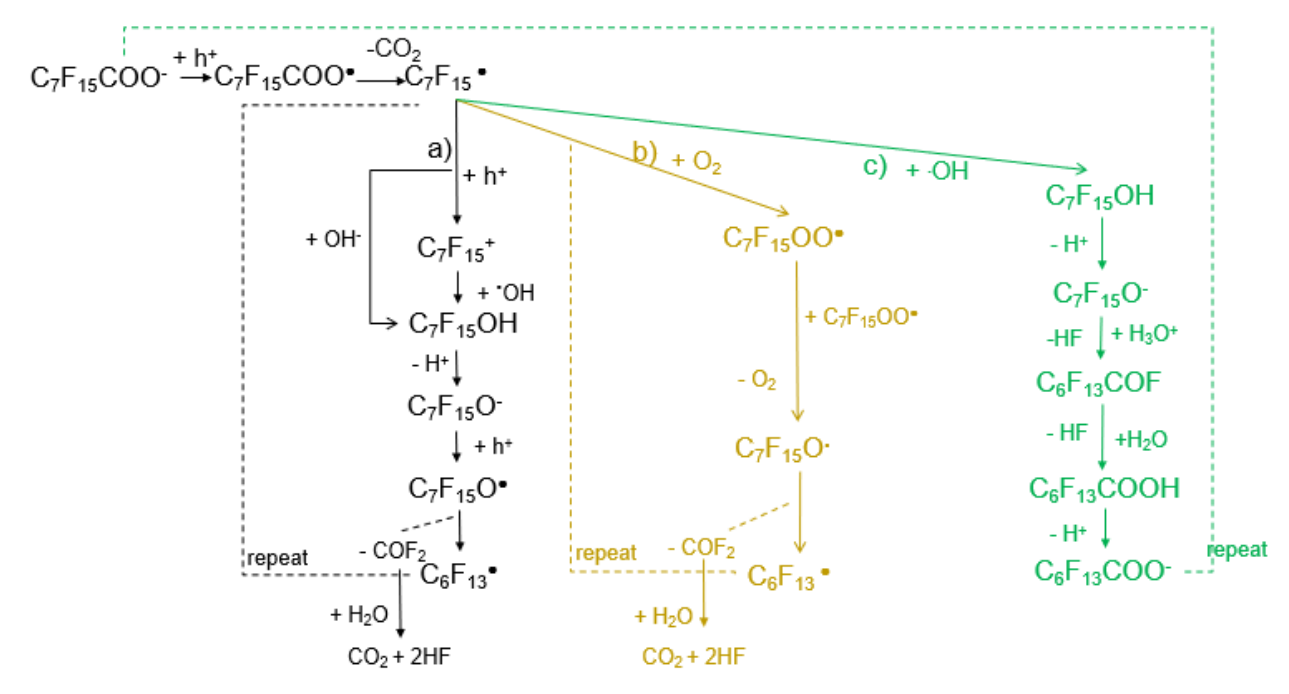


Figure 3.4: The possible PFOA degradation pathways on the anode in the EO process. (a) Direct hydroxylation pathway (black): This involves hydroxyl radical attack, leading to sequential transformations, including the formation of alcohol (C₇F₁₅OH), ketone (C₇F₁₅O*), and further fragmentation to shorter-chain perfluorinated species. (b) Oxygenation pathway (yellow): In the presence of molecular oxygen (O₂), perfluoroalkyl peroxy radicals (C₇F₁₅OO*) form, which subsequently degrade into smaller perfluorinated fragments through oxidative cleavage. (c) Hydroxyl radical-mediated pathway (green): The introduction of hydroxyl radicals promotes successive transformations, leading to the formation of carboxylic acids (C₆F₁₃COOH) and ultimately mineralization into carbon dioxide (CO₂) and fluoride ions (HF).

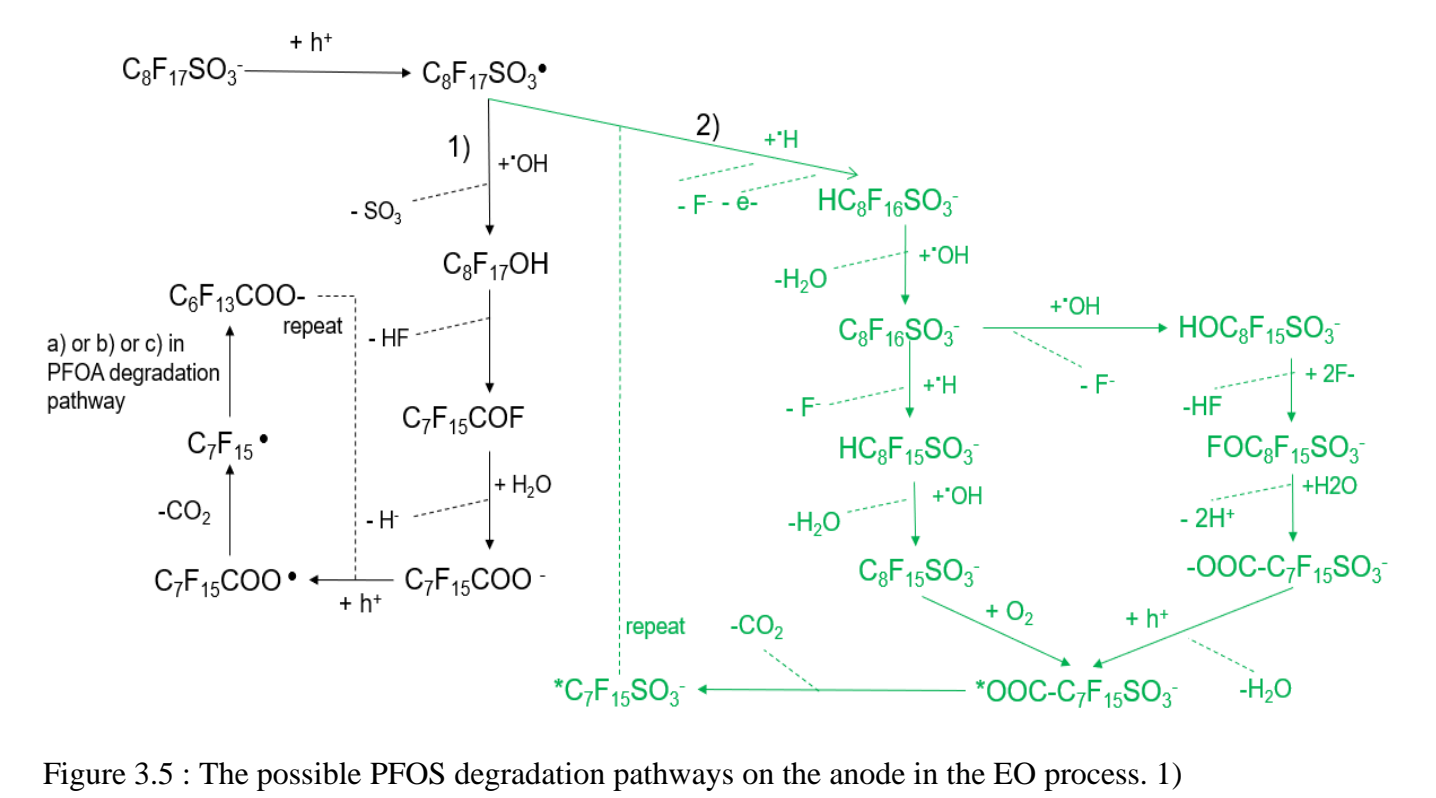


Figure 3.5 : The possible PFOS degradation pathways on the anode in the EO process. 1)

Oxidative Decay Pathway (Black, Left Side): PFOS ion (C₈F₁₇SO₃⁻) undergoes direct electron transfer, forming the perfluorinated sulfonyl radical (C₈F₁₇SO₃⁻); The radical can lose a sulfonate SO₃) group, generating C₈F₁₇OH; Further transformations through dehydrofluorination and hydrolysis produce ketone (C₇F₁₅COF) and shorter perfluorinated carboxylates (C₇F₁₅COO⁻), which follow similar degradation steps as observed in PFOA breakdown; The cycle repeats until the perfluorinated chains are broken down into smaller fragments, eventually forming CO₂ and HF. 2) Reductive and Hydroxylation Pathway (Green, Right Side): PFOS undergoes direct electron transfer and hydrogenation, leading to the formation of partially fluorinated sulfonates (HC₈F₁₆SO₃⁻); Hydrolysis and hydroxyl radical ('OH) attack further drive defluorination, forming species like C₈F₁₆SO₃⁻ and HOC₈F₁₅SO₃⁻; Successive F- and HF eliminations lead to oxidative fragmentation, producing perfluorinated carboxylates (-OOC-C₇F₁₅SO₃⁻) and eventually mineralized products CO₂, HF and H₂O.

Table 3.1: C-F BDEs for C₇F₁₅COO⁻ (Note: The 1st C-F is on the terminal -CF₃.)

C-F BDEs	1.at	2nd	3rd	4th	5th	6th	7th	Software	Basis
$(Kcal mol^{-1})$	lst								set/method
Bentel et al.,	117.7	7 108.3	106.8	107.0	107.3	108.1	107.3	Gaussian 09	B3LYP/6-
2019	11/./								311+G(2d,2p)
Chen et al.,	125.5	1150	114.2	11/2	11/1	116 2	100 7	Gaussian 16	6-311G++(d);
2022	2022	125.5 115.8 114	114.2	114.3	114.1	110.2	100.7	Gaussiali 10	SMD model

Table 3.2: Adsorption energy and activation energy reported for PFOA, PFOS, and PFBS degradation during EO process with DFT computation

References	Anode	Adsorbat e	Software	Basis Set, Functional/Meth od	Anode Simulation	Computation Parameters	Adsorption Energy (eV)	Activation Energy (eV)
Ma et al., 2022	Ti ₄ O ₇ /MXe ne	PFOA	VASP	GGA-PBE	Slab	adsorption energy of PFOA on anode; charge	0.70	
	Ti ₄ O ₇	<u>-</u>				transfer -	0.31	
Ma et al., 2022	Ti ₄ O ₇ /MXe ne	PFBA	VASP	GGA-PBE	Slab	adsorption energy of PFAS on anode; -	0.70	
	Ti_4O_7					11715 on anode,		
Wang et al., 2022	Ti ₄ O ₇	PFOS	DMol3	DNP; VWN-BP	cluster	adsorption energy of PFOS on anode; activation energy of C-S	~2.5	1.38
	Ti ₉ O ₁₇	•				bond break;	-1.5 ~ 0.2	1.47
Li et al., 2021	${ m Ti}_4{ m O}_7$	PFOS	DMol3	DNP; VWN-BP	cluster		-0.27	1.21

		PFBS				adsorption energy of PFAS; activation energy of C-S bond break;	-0.31	1.49
Liao et al., 2009	BDD	PFBS	$DolM_3$ $DNP;$ $VWN-BP$		activation barriers by •OH activation barriers by DET	no	1.275 0.1275	
Wang et al., 2020	Ti ₄ O ₇ (110)	ОН	VASP	PBE	cluster	adsorption energy OH	-5.13	
	BDD (001)		V1151	T D L	cruster	adsorbates on anodes;	-7.89/-8.80	
Wang et al., 2020	Ti ₄ O ₇ (110)	Cl	VASP	PBE	cluster	adsorption energy Cl	-5.07	
	BDD (001)					adsorbates on anodes; –	-4.16/-3.85	
Chen et al., 2022a	BDD	PFOA	Gaussian 16	6-311G++(d); SMD model	no	reactions Gibbs free energy change $\Delta G0$ (kJ/mol); Gibbs free energy of activation ΔG^{\ddagger}_{+} ;	no	0.0665
H. Shi et al., 2019	Ti ₄ O ₇	PFOS	Gaussian 16	6-311G++(d); SMD model	no	activation energy of C-S bond break by •OH		0.76

Table 3.3: Overpotential $\boldsymbol{\eta}$ for OER calculated for anodes in EO process by DFT computation

References	Anodes	PFAS	Software	Basis set	Anode simulation	Calculation parameters	Overpotential η for OER
	Ti ₄ O ₇ (120)		Quantum Espresso version 6.6	PRPBE	supercell	overpotential for OER -	2.0V
Ko et al., 2021 —	TiO ₂ (110)	PFOA					1.3V
	12.5 at% Nb-doped TiO ₂ (110)	- PFOS					1.4 ±0.49 V

3.8 References

- Alalm, M. G., & Boffito, D. C. (2022). Mechanisms and pathways of PFAS degradation by advanced oxidation and reduction processes: A critical review. *Chemical Engineering Journal*, 450. https://doi.org/ARTN 13835210.1016/j.cej.2022.138352
- Bentel, M., Yu, Y. C., Xu, L. H., Li, Z., Wong, B., Men, Y. J., & Liu, J. Y. (2019). Defluorination of per- and polyfluoroalkyl substances (PFASs) with hydrated electrons: Structural dependence and implications to PFAS remediation and management. *Abstracts of Papers of the American Chemical Society*, 258. <Go to ISI>://WOS:000525061500403
- Bharti, Ahmed, G., Kumar, Y., & Sharma, S. (2021). DFT computation of quantum capacitance of pure and doped niobium nitrides for supercapacitor applications. *Ceramics International*, 47(13), 18948-18955. https://doi.org/10.1016/j.ceramint.2021.03.237
- Carter, K. E., & Farrell, J. (2008). Oxidative destruction of perfluorooctane sulfonate using boron-doped diamond film electrodes. *Environmental Science & Technology*, 42(16), 6111-6115. https://doi.org/10.1021/es703273s
- Chen, C., Ma, Q. Q., Liu, F. Z., Gao, J. A., Li, X. Y., Sun, S. B., Yao, H., Liu, C. Q., Young, J., & Zhang, W. (2021). Photocatalytically reductive defluorination of perfluorooctanoic acid (PFOA) using Pt/La2Ti2O7 nanoplates: Experimental and DFT assessment. *Journal of Hazardous Materials*, 419. https://doi.org/ARTN 12645210.1016/j.jhazmat.2021.126452
- Chen, Y., Yang, Y., Cui, J., Zhang, H., & Zhao, Y. (2024). Decoding PFAS contamination via Raman spectroscopy: A combined DFT and machine learning investigation. *Journal of Hazardous Materials*, 465, 133260.
- Chen, Z. F., Wang, X. J., Feng, H. L., Chen, S. H., Niu, J. F., Di, G. L., Kujawski, D., & Crittenden, J. C. (2022a). Electrochemical Advanced Oxidation of Perfluorooctanoic Acid: Mechanisms and Process Optimization with Kinetic Modeling. *Environmental Science & Technology*. https://doi.org/10.1021/acs.est.2c02906
- Chen, Z. F., Wang, X. J., Feng, H. L., Chen, S. H., Niu, J. F., Di, G. L., Kujawski, D., & Crittenden, J. C. (2022b). Electrochemical Advanced Oxidation of Perfluorooctanoic Acid: Mechanisms and Process Optimization with Kinetic Modeling. *Environmental Science & Technology*, 56(20), 14409-14417. https://doi.org/10.1021/acs.est.2c02906
- Cheng, Z. W., Chen, Q. C., Liu, Z. K., Liu, J. Y., Liu, Y. W., Liu, S. Q., Gao, X. P., Tan, Y. J., & Shen, Z. M. (2021). Interpretation of Reductive PFAS Defluorination with Quantum Chemical Parameters. *Environmental Science & Technology Letters*, 8(8), 645-650. https://doi.org/10.1021/acs.estlett.1c00403
- Crone, B. C., Speth, T. F., Wahman, D. G., Smith, S. J., Abulikemu, G., Kleiner, E. J., & Pressman, J. G. (2019). Occurrence of Per- and Polyfluoroalkyl Substances (PFAS) in Source Water and Their Treatment in Drinking Water. *Crit Rev Environ Sci Technol*, 49(24), 2359-2396. https://doi.org/10.1080/10643389.2019.1614848
- Deng, S. B., Nie, Y., Du, Z. W., Huang, Q., Meng, P. P., Wang, B., Huang, J., & Yu, G. (2015). Enhanced adsorption of perfluorooctane sulfonate and perfluorooctanoate by bambooderived granular activated carbon. *Journal of Hazardous Materials*, 282, 150-157. https://doi.org/10.1016/j.jhazmat.2014.03.045
- Eslamibidgoli, M. J., & Eikerling, M. H. (2015). Electrochemical Formation of Reactive Oxygen Species at Pt (111)-A Density Functional Theory Study. *Acs Catalysis*, *5*(10), 6090-6098. https://doi.org/10.1021/acscatal.5b01154

- Gomri, C., Makhoul, E., Koundia, F. N., Petit, E., Raffy, S., Bechelany, M., Semsarilar, M., & Cretin, M. (2025). Electrochemical advanced oxidation combined to electro-Fenton for effective treatment of perfluoroalkyl substances "PFAS" in water using a Magnéli phase-based anode. *Nanoscale Advances*, 7(1), 261-268.
- Hori, H., Hayakawa, E., Einaga, H., Kutsuna, S., Koike, K., Ibusuki, T., Kiatagawa, H., & Arakawa, R. (2004). Decomposition of environmentally persistent perfluorooctanoic acid in water by photochemical approaches. *Environmental Science & Technology*, *38*(22), 6118-6124. https://doi.org/10.1021/es049719n
- Huang, D., Wang, K., Niu, J., Chu, C., Weon, S., Zhu, Q., Lu, J., Stavitski, E., & Kim, J. H. (2020). Amorphous Pd-Loaded Ti4O7 Electrode for Direct Anodic Destruction of Perfluorooctanoic Acid. *Environ Sci Technol*, *54*(17), 10954-10963. https://doi.org/10.1021/acs.est.0c03800
- Huang, X., Wang, J., Tao, H. B., Tian, H., & Xu, H. (2019). An essential descriptor for the oxygen evolution reaction on reducible metal oxide surfaces. *Chemical Science*, 10(11), 3340-3345. https://doi.org/10.1039/c8sc04521f
- Jinyu Gao, Z. L., Zhanghao Chen, Dandan Rao, Shun Che, Cheng Gu, Yujie Men, Jun Huang & Jinyong Liu. (2023). Photochemical degradation pathways and near-complete defluorination of chlorinated polyfluoroalkyl substances. *Nature water*.
- Ko, J. S., Le, N. Q., Schlesinger, D. R., Zhang, D. J., Johnson, J. K., & Xia, Z. Y. (2021). Novel niobium-doped titanium oxide towards electrochemical destruction of forever chemicals (vol 11, 18020, 2021). *Scientific Reports*, 11(1). https://doi.org/ARTN 1901410.1038/s41598-021-98715-0
- Li, L., Wang, Y., & Huang, Q. (2021). First-Principles Study of the Degradation of Perfluorooctanesulfonate and Perfluorobutanesulfonate on a Magnéli Phase Ti4O7 Anode. *ACS ES&T Water*, *I*(8), 1737-1744. https://doi.org/10.1021/acsestwater.1c00086
- Liao, Z. H., & Farrell, J. (2009). Electrochemical oxidation of perfluorobutane sulfonate using boron-doped diamond film electrodes. *Journal of Applied Electrochemistry*, *39*(10), 1993-1999. https://doi.org/10.1007/s10800-009-9909-z
- Lin, H., Niu, J., Liang, S., Wang, C., Wang, Y., Jin, F., Luo, Q., & Huang, Q. (2018).

 Development of macroporous Magnéli phase Ti4O7 ceramic materials: As an efficient anode for mineralization of poly- and perfluoroalkyl substances. *Chemical Engineering Journal*, 354, 1058-1067. https://doi.org/10.1016/j.cej.2018.07.210
- Lin, H., Xiao, R., Xie, R., Yang, L., Tang, C., Wang, R., Chen, J., Lv, S., & Huang, Q. (2021). Defect Engineering on a Ti4O7 Electrode by Ce(3+) Doping for the Efficient Electrooxidation of Perfluorooctanesulfonate. *Environ Sci Technol*, 55(4), 2597-2607. https://doi.org/10.1021/acs.est.0c06881
- Liu, H., & Vecitis, C. D. (2012). Reactive Transport Mechanism for Organic Oxidation during Electrochemical Filtration: Mass-Transfer, Physical Adsorption, and Electron-Transfer. *Journal of Physical Chemistry C*, 116(1), 374-383. https://doi.org/10.1021/jp209390b
- Ma, Q. Q., Gao, J. A., Cheng, K. Y., Young, J., Zhao, M. Q., Ronen, A., & Zhang, W. (2024). Electrooxidation of Perfluorocarboxylic Acids by an Interfacially Engineered Magneli Phase Titanium Oxide (TiO) Electrode with MXene. *ACS ES&T Engineering*. https://doi.org/10.1021/acsestengg.3c00571
- Man, I. C., Su, H. Y., Calle-Vallejo, F., Hansen, H. A., Martinez, J. I., Inoglu, N. G., Kitchin, J., Jaramillo, T. F., Norskov, J. K., & Rossmeisl, J. (2011). Universality in Oxygen

- Evolution Electrocatalysis on Oxide Surfaces. *Chemcatchem*, *3*(7), 1159-1165. https://doi.org/10.1002/cctc.201000397
- Mirabediny, M., Sun, J., Yu, T. T., Akermark, B., Das, B., & Kumar, N. (2023). Effective PFAS degradation by electrochemical oxidation methods-recent progress and requirement. *Chemosphere*, *321*. https://doi.org/ARTN/43810910.1016/j.chemosphere.2023.138109
- Niu, J. F., Lin, H., Gong, C., & Sun, X. M. (2013). Theoretical and Experimental Insights into the Electrochemical Mineralization Mechanism of Perfluorooctanoic Acid. *Environmental Science & Technology*, 47(24), 14341-14349. https://doi.org/10.1021/es402987t
- Pierpaoli, M., Szopinska, M., Wilk, B. K., Sobaszek, M., Luczkiewicz, A., Bogdanowicz, R., & Fudala-Ksiazek, S. (2021). Electrochemical oxidation of PFOA and PFOS in landfill leachates at low and highly boron-doped diamond electrodes. *Journal of Hazardous Materials*, 403. https://doi.org/ARTN 12360610.1016/j.jhazmat.2020.123606
- Rahman, M. F., Peldszus, S., & Anderson, W. B. (2014). Behaviour and fate of perfluoroalkyl and polyfluoroalkyl substances (PFASs) in drinking water treatment: A review. *Water Research*, *50*, 318-340. https://doi.org/10.1016/j.watres.2013.10.045
- Rozen, S., & Filler, R. (1985). Alpha-Fluorocarbonyl Compounds and Related Chemistry. *Tetrahedron*, 41(7), 1111-1153. https://doi.org/Doi 10.1016/S0040-4020(01)96514-7
- Ryan, D. R., Mayer, B. K., Baldus, C. K., Mcbeath, S. T., Wang, Y., & Mcnamara, P. J. (2021). Electrochemical technologies for per- and polyfluoroalkyl substances mitigation in drinking water and water treatment residuals. *AWWA Water Science*, *3*(5). https://doi.org/ARTN e124910.1002/aws2.1249
- Schaefer, C. E., Andaya, C., Burant, A., Condee, C. W., Urtiaga, A., Strathmann, T. J., & Higgins, C. P. (2017). Electrochemical treatment of perfluorooctanoic acid and perfluorooctane sulfonate: Insights into mechanisms and application to groundwater treatment. *Chemical Engineering Journal*, 317, 424-432. https://doi.org/10.1016/j.cej.2017.02.107
- Shi, H., Wang, Y., Li, C., Pierce, R., Gao, S., & Huang, Q. (2019). Degradation of Perfluorooctanesulfonate by Reactive Electrochemical Membrane Composed of Magneli Phase Titanium Suboxide. *Environ Sci Technol*, *53*(24), 14528-14537. https://doi.org/10.1021/acs.est.9b04148
- Shi, H. H., Wang, Y. Y., Li, C. G., Pierce, R., Gao, S. X., & Huang, Q. G. (2019). Degradation of Perfluorooctanesulfonate by Reactive Electrochemical Membrane Composed of Magneli Phase Titanium Suboxide. *Environmental Science & Technology*, *53*(24), 14528-14537. https://doi.org/10.1021/acs.est.9b04148
- Trellu, C., Chaplin, B. P., Coetsier, C., Esmilaire, R., Cerneaux, S., Causserand, C., & Cretin, M. (2018). Electro-oxidation of organic pollutants by reactive electrochemical membranes. *Chemosphere*, 208, 159-175. https://doi.org/10.1016/j.chemosphere.2018.05.026
- Vo, H. N. P., Ngo, H. H., Guo, W. S., Nguyen, T. M. H., Li, J. X., Liang, H., Deng, L. J., Chen, Z., & Nguyen, T. A. H. (2020). Poly?and perfluoroalkyl substances in water and wastewater: A comprehensive review from sources to remediation. *Journal of Water Process Engineering*, 36. https://doi.org/ARTN 10139310.1016/j.jwpe.2020.101393
- Wang, C., Zhang, T. N., Yin, L. F., Ni, C. S., Ni, J. P., & Hou, L. A. (2022). Enhanced perfluorooctane acid mineralization by electrochemical oxidation using Ti3+ self-doping TiO2 nanotube arrays anode. *Chemosphere*, 286. https://doi.org/ARTN13180410.1016/j.chemosphere.2021.131804

- Wang, L., Lu, J., Li, L., Wang, Y., & Huang, Q. (2020). Effects of chloride on electrochemical degradation of perfluorooctanesulfonate by Magneli phase Ti4O7 and boron doped diamond anodes. *Water Res*, 170, 115254. https://doi.org/10.1016/j.watres.2019.115254
- Wang, Y., Kim, J., Huang, C.-H., Hawkins, G. L., Li, K., Chen, Y., & Huang, Q. (2022). Occurrence of per- and polyfluoroalkyl substances in water: a review. *Environmental Science: Water Research & Technology*, 8(6), 1136-1151. https://doi.org/10.1039/d1ew00851j
- Wang, Y., Li, L., Wang, Y., Shi, H., Wang, L., & Huang, Q. (2022). Electrooxidation of perfluorooctanesulfonic acid on porous Magnéli phase titanium suboxide Anodes: Impact of porous structure and composition. *Chemical Engineering Journal*, 431. https://doi.org/10.1016/j.cej.2021.133929
- Wang, Y., Wang, Y., Dong, S., & Huang, Q. (2025). The impact of anions on electrooxidation of perfluoroalkyl acids by porous Magnéli phase titanium suboxide anodes. *Plos One*, 20(1), e0317696.
- Wang, Y. Y., Li, L., Wang, Y. F., Shi, H. H., Wang, L., & Huang, Q. G. (2022). Electrooxidation of perfluorooctanesulfonic acid on porous Magneli phase titanium suboxide Anodes: Impact of porous structure and composition. *Chemical Engineering Journal*, 431. https://doi.org/ARTN 13392910.1016/j.cej.2021.133929
- Wang, Y. Y., Pierce, R., Shi, H. N., Li, C. G., & Huang, Q. G. (2022). Electrochemical degradation of perfluoroalkyl acids by titanium suboxide anodes (vol 6, pg 144, 2020). *Environmental Science-Water Research & Technology*, 8(2), 443-443. https://doi.org/10.1039/d1ew90044g
- Wang, Z., You, X., Lan, L., Huang, G., Zhu, T., Tian, S., Yang, B., & Zhuo, Q. (2025). Electrocatalytic oxidation of hexafluoropropylene oxide homologues in water using a boron-doped diamond electrode. *Environmental Technology*, 46(8), 1280-1291.
- Wanninayake, D. M. (2021). Comparison of currently available PFAS remediation technologies in water: A review. *J Environ Manage*, 283, 111977. https://doi.org/10.1016/j.jenvman.2021.111977
- Yamijala, S. S. R. K. C., Shinde, R., Hanasaki, K., Ali, Z. A., & Wong, B. M. (2022). Photo-induced degradation of PFASs: Excited-state mechanisms from real-time time-dependent density functional theory. *Journal of Hazardous Materials*, 423. https://doi.org/ARTN12702610.1016/j.jhazmat.2021.127026
- Zhang, Y. Y., Moores, A., Liu, J. X., & Ghoshal, S. (2019). New Insights into the Degradation Mechanism of Perfluorooctanoic Acid by Persulfate from Density Functional Theory and Experimental Data. *Environmental Science & Technology*, *53*(15), 8672-8681. https://doi.org/10.1021/acs.est.9b00797
- Zhao, L., Pu, R., Deng, S., Lin, L., Mantzavinos, D., Naidu, R., Fang, C., & Lei, Y. (2025). Enhanced electrochemical degradation of per-and polyfluoroalkyl substances (PFAS) by activating persulfate on boron-doped diamond (BDD) anode. *Separation and Purification Technology*, 359, 130459.
- Zhou, X. D., Zhong, Y. S., Tian, X. C., & Zhao, F. (2024). Electrochemical oxidation of perfluoroalkyl and polyfluoroalkyl substances: Mechanisms, implications, and challenges. *Science China-Technological Sciences*, *67*(10), 2972-2990. https://doi.org/10.1007/s11431-023-2626-7

CHAPTER 4

ENVIRONMENTAL LIFE CYCLE ASSESSMENT (LCA) OF TREATING PFAS WITH ION EXCHANGE AND ELECTROCHEMICAL OXIDATION TECHNOLOGY

Li, G., Dunlap, J., Wang, Y., Huang, Q., & Li, K. (2022). Environmental life cycle assessment (LCA) of treating PFASs with ion exchange and electrochemical oxidation technology. ACS ES&T Water, 2(9), 1555-1564.

Reprinted here with permission of the publisher.

ABSTRACT

Life cycle assessments (LCA) were performed for Per- and Poly-fluoroalkyl substances (PFASs) treatment with ion exchange (IX) followed by electrochemical oxidation (EO). For the studied water quality, the global warming potentials (GWP) for two orders of removal of perfluorooctane sulfonic and perfluorooctanoic acid from 1000 m³ water samples were 72.2 and 84.9 kg CO₂ eq., respectively. The major contributors to the GWP were electricity and resin manufacturing. To understand the environmental impacts of different treatment options, the following scenarios are compared: IX resin single-use followed by incineration (IX+Incin.), IX resin single-use followed by EO (IX/EEO), and regeneration and reuse of the IX resin followed by EO (IX/Re+EO). When the EE/O is less than 192 kWh/m³, the global warming potential of the three are in the order of IX/Re+EO < IX+EO < IX+Incin. When the EE/O is larger than 695 kWh/m³, the order is IX/Re+EO < IX+EO. A greener energy mix favors the EO options and increases these two numbers. An empirical equation was introduced to estimate the overall GWP of PFASs removal based on the EE/O and adsorption isotherms.

4.1 Introduction

Per- and polyfluoroalkyl (PFASs) substances are a broad class of emerging environmental contaminants used heavily by the industrial, commercial, and manufacturing sectors in previous decades. There are various potential health effects that have been attributed to PFASs exposure, particularly perfluorooctane sulfonoic acid (PFOS) and perfluorooctanoic acid (PFOA) which are highly toxic and suspected carcinogens. In the environment, PFASs are highly persistent and bioaccumulate within biota and humans. Because of this, PFASs species have been consistently detected within the environment, in food products, and in humans. 2,3,4

As more is understood regarding the toxicological impacts of PFASs, interest in treating PFASs in drinking water sources is increasing. Due to their high chemical stability, however, traditional water treatment and wastewater remediation methods have not been sufficient in treating PFASs⁵. In general, methods of treating PFASs in drinking water fall into two main categories, including physical technologies that separate and remove PFASs from the wastewater⁶ and chemical technologies that destroy it.⁷ Removal technologies include granular activated carbon (GAC), nano- and microfiltration, reverse osmosis (RO), foam fractionation, and ion exchange (IX). Adsorption on ion exchange resin has been shown to be effective at removing short-chain and long-chain PFASs from wastewater.^{8,9,10} Once saturated, IX resin can be regenerated on-site, allowing for resin reuse. The regenerated solution can then be distilled to recover the solvent used in the regeneration process. The resulting still bottoms contain a highly concentrated solution of PFASs, salt, and organic matters separated from the wastewater stream. Despite their effectiveness, IX only separates the PFASs from the waste stream and does not destroy them.

Ultimately, the concentrated PFASs-containing still bottoms must be either disposed of in a hazardous waste landfill or incinerated. Currently, incineration of PFASs waste streams is one option being considered by the EPA. However, extremely high temperatures between 1000 and 2000 °C are required for destructing PFASs compounds. In addition, incomplete destruction of PFASs can result in the formation of short-chain PFASs and other potentially toxic products of incomplete combustion, which have not yet been researched and could be a potential topic of concern. While research into the disposal and incineration of PFASs is currently ongoing, it is often desirable to have methods capable of destroying PFASs rather than disposing of the still bottoms off-site. Electrochemical oxidation (EO) has been identified as an effective on-site method capable of destroying PFASs at atmospheric pressure and without additional chemical additives. 12,13,14 The fast reaction kinetics, ease of operation, and cost-effectiveness of EO treatment make it an attractive option for the on-site destruction of PFASs. 12,15,16

Despite the advantages of a coupled IX and EO treatment process train, multiple regeneration and reuse options exist for the IX resin. Previous studies have cited the importance of regeneration of IX resin on environmental impacts. Emery et al. performed a life cycle assessment (LCA) of IX and GAC processes for remediation of PFASs that considered recycling of the methanol solution and incineration of the resulting waste stream. To assess the environmental impacts under different regeneration options, Boyer et al. Compared disposal and incineration of the waste stream and recycling the brine and solvent solution. While these studies examined the environmental impacts of different regeneration options for the IX resin, the impacts of a complete process train considering IX coupled with a destructive technology have not been assessed. This study aims to bridge this gap in the literature by analyzing and

comparing the environmental life cycle impacts of a coupled IX and EO treatment process under different scenarios.

4.2 Materials and Methods

4.2.1 Life Cycle Assessment Methodology

Life cycle assessment (LCA) is an environmental impact assessment method that considers the material and energy interactions over the life cycle of a product or process that impacts the environment. The LCA methodology used in this analysis follows international guidelines set by the International Standards Organization (ISO) in ISO 14040-14044. These guidelines set the framework for LCA and consist of four major components: goal and scope definition, life cycle inventory (LCI), life cycle impact assessment (LCIA), and interpretation of results.²⁵

4.2.2 Goal and Scope Definition

The goal of this LCA is to analyze the environmental impacts of coupled IX and EO process trains to treat PFASs-contaminated groundwater. First, an LCA model of the coupled IX and EO treatment process is built to assess the environmental impacts (Figure 4.1, dashed line) of treating different PFASs species. Environmental impacts for two different still bottoms samples with different types and concentrations of PFASs (both long- and short-chain) are calculated and compared. Process contribution analysis is then performed to understand the key operational variables. Afterwards, three scenarios reflecting different regeneration and reuse choices are modeled for both long- and short-chain PFASs. The total global warming potential of the coupled IX and EO treatment process train under different operation modes is compared.

The functional unit chosen in this analysis is two orders of magnitude removal of PFASs from 1000 m³ groundwater. The overall system boundary with each unit process is shown in Figure 4.1. The system diagram includes the ion exchange reactor, regeneration of the resin, distillation to recover methanol, the resulting still bottoms, and ends with the destructive EO treatment cell and resin landfill. Material and energy inputs into the system include the initial contaminated water, the anionic resin, the brine and methanol solutions required for regeneration and elution of the exhausted resin, heat energy for distillation, anode/cathode material, and the DC electricity supply for the treatment cell. General infrastructures are excluded because they are the same for all scenarios in this study. The exclusion of infrastructures eliminates unnecessary complexity and increases the transferability of the results.

4.2.3 Scenario Analysis

Without adequate destruction technology, a common practice for removal of PFASs by IX is to dispose of the resin after a single use. For EO treatment, since the PFASs must first be desorbed from the resin, reuse of the resin becomes a feasible option. Three scenarios are modeled as follows: single use of the IX resin followed by incineration (IX+Incin.), single-use of the IX resin followed by EO treatment (IX+EO), and regeneration and reuse of the IX resin followed by EO treatment (IX/Re+EO). An overview of the unit process, materials, and energy considered in the three scenarios is shown in Figure 4.2, with descriptions of each scenario provided below.

IX+Incin (Figure 4.2a), the IX is used to remove the PFASs contaminants from the contaminated water. After a breakthrough occurs, the PFASs-containing resin is disposed of by incineration.

IX+EO (Figure 4.2b), the IX is used to remove PFASs from the contaminated water, similar to Scenario 1. After the breakthrough, however, the adsorbed PFASs is eluted with a methanol brine solution which is then distilled to recover the methanol, leaving concentrated still bottoms with elevated PFASs concentrations. EO treatment is then used to degrade PFASs, and the spent resin is disposed of at a landfill.

IX/Re+EO (Figure 4.2c) is the same as Scenario 2, except the life span of the resin is accounted for, and the resin is regenerated and reused. Using a typical resin life span of 5 years and a breakthrough time of 5.6 months, as observed in this study, the resin can be regenerated 10 times before having to be replaced. ¹⁹ It is assumed that the resin loses 3% of its total capacity after every use cycle. ¹⁹ After 10 uses, the resin is disposed of in a landfill.

4.2.4 Process Overview and Data Sources

The treatment process modeled in this study is based on data from a series of studies by Huang and co-workers^{13,14,21}. PFASs-containing samples representing contaminated groundwater were pumped through an IXR bed containing 34.6 L of anionic resin for 61,000 bed volumes (BV) (4% breakthrough). The PFASs was then eluted from the resin in a bench column with 2 BV of 2% wt. brine solution of NaCl, followed by 5 BV of a solution containing 80% by volume methanol (MeOH) in a 2% wt. brine solution.¹³ Methanol from the regenerant solution was distilled with heat energy (natural gas) and recovered. It is assumed that all methanol can be recovered to be reused for regeneration.

The resulting still bottoms contained the remaining salt and concentrated PFASs solution. Two still bottoms samples, still bottoms 1 and 2, with different total organic carbon (TOC) concentrations were analyzed in this study. Once collected, the still bottoms were then treated in an EO treatment cell with a Ti₄O₇ anode and stainless-steel cathode. 13,14 Values of the electrical

energy per log order mineralization (EE/O) of several PFASs species in still bottoms samples were obtained from experimental data (Table S4.3). Secondary data sources for the unit emission and environmental impact factors were obtained from environmental databases such as Ecoinvent, ELCD, and USLCI (Table 4.1).²⁰ The PhD version of SimaPro 7.0 was used for access to all environmental databases used in this analysis.

Inventory data for a total of 10 PFASs species were modeled and compared. Based on the availability of EE/O data, 5 species were modeled for still bottoms 1 (PFOS, PFOA, PFHxS, PFHpS, and PFHpA) and 10 species for still bottoms 2 (PFOS, PFOA, PFHxS, PFHpA, PFHpS, PFBA, PFBS, PFPeA, PFHxA, and PFPeS). Tables S4.5 and S4.6 summarize the inventory data for the IX and destructive treatment process for the different PFASs species and still bottoms samples. Water quality data for both still bottoms samples can be found in Table S4.1 in the supporting information.

4.2.5 Life Cycle Impact Assessment (LCIA)

LCIA is a qualitative and quantitative assessment of the environmental impact of a process based on the resource, energy consumption data, and various emission data. In this study, SimaPro 7.0 software was used to build the LCA model and perform the environmental impact assessment using EPA's Tool for Reduction and Assessment of Chemicals and Other Environmental Impacts (TRACI) methodology. A total of 7 environmental impact categories were considered in this study. Impact categories were divided into two general groups: environmental impacts and human impacts. Environmental impact categories include ozone depletion (OD, CFC-11 eq), global warming potential (GWP, kg CO₂ eq), acidification (AD, mol H⁺ eq), marine eutrophication (ME, kg N eq), smog formation (SF, kg O₃ eq) and ecotoxicity

(ET, CTUe). Human impact categories include carcinogens (C, CTUh), non-carcinogens (NC, CTUh), and respiratory effects (RE, kg PM₁₀ eq).

4.3 Results and Discussion

In this section, the impact assessment results of IX coupling EO Treatment process are analyzed following the methodology described in Section 4.2.4. Since the still bottoms varied in water qualities, the following results for both still bottoms samples are presented separately.

Unless otherwise stated, all impact assessment results are presented per functional unit, which is to degrade PFASs two orders of magnitude from 1000 m³ groundwater.

4.3.1 Impact Assessment Results: Still Bottoms 1

The absolute impact assessment results for degrading PFASs in still bottoms 1 are presented in Table 4.2. These results suggest that PFHpA removal had the most significant GWP (180 kg CO₂ eq.) among the 5 long-chain PFASs species, while PFOS had the lowest (72.2 kg CO₂ eq.). Figure 4.3 presents the EE/O of PFASs removal and GWP of PFASs removal, which shows that they have the same trend. GWP impacts in decreasing order are PFHpA> PFOA> PFHxS> PFHpS> PFOS., For the studied baseline water quality, the GWP values for the removal of PFHpA PFOA PFHxS PFHpS, and PFOS are 180, 84.9, 84.4, 79.4, and 72.2 kg CO₂ eq, respectively. Compared with conventional groundwater treatment, which has a GWP of ~50 kg CO₂ eq per 1000 m ^{3 22,23}, adding the removal and destruction of PFOS, PFOA, PFHpS, and PFHxS with IXR and EO does not significantly increase the total global warming potential. An exception is that of PFHpA, which is approximately 2 times higher. These values correspond to the water quality in Table S4.1 only. Using these values to compare with other research

outcomes needs to consider the water quality since TOC concentration significantly impacts the EE/O and the global warming potential.

For the two most common long-chain species, PFOS and PFOA, Figure 4 shows the relative contributions of unit processes, including salt-solution (NaCl), DI-water, electricity, heat energy, resin and anode manufacturing, and resin landfilling. The salt-solution, DI water, and anode manufacturing account for less than 1% of impacts across all categories. For ozone depletion, carcinogens, and non-carcinogens categories, resin manufacturing accounted for the majority of total impacts. For smog formation, acidification, and respiratory effects categories, electricity accounted for the majority of impacts. Landfilling of the resin accounted for over 60% of impacts in marine eutrophication. Resin manufacturing and electricity contributed 63% and 34% for PFOS removal for the GWP category, respectively. By comparison, resin manufacturing and electricity contributed 53% and 44% for PFOA removal, respectively. Across all the impact categories, electricity in EO treatment for PFOA removal contributed more than PFOS removal. The reason is that the EE/O of PFOA removal (531kWh/m³) was higher than that of PFOS removal (350 kWh/m³).

4.3.2 Impact Assessment Results: Still Bottoms 2

The absolute impact assessment results for degrading PFASs in still bottoms 2 are presented in Table 4.3. Still bottoms 2 contained a total of 10 PFASs species, including 5 long-chain PFASs and 5 short-chain PFASs. The 5 long-chain PFASs were the same as still bottoms 1, while the 5 short-chain PFASs included PFBA, PFBS, PFPeA, PFHxA, and PFPeS. Figure 4.5 displays the comparison of EE/O and GWP of PFASs removal for the 10 PFASs species. As we can see, PFBA removal had the most significant GWP (254 kg CO₂ eq.) among the 10 PFASs species, while the GWP impact of PFPeS removal was the lowest (82.1 kg CO₂ eq.). GWP

impacts in decreasing order are PFBA> PFHxA> PFOA> PFHxS > PFBS> PFOS> PFPeA> PFHpA> PFHpS> PFPeS, which follows the same trend as EE/O (Figure 5). The GWP values for the removal of PFBA, PFHxA, PFOA, PFHxS, PFBS, PFOS, PFPeA, PFHpA, PFHpS, PFPeS are 254, 202, 179, 157, 146, 120, 99.3, 98.9, 84.5, and 82.1 kg CO₂ eq. respectively.

For selected common long-chain and short-chain species (PFOS, PFOA, and PFBA), Figure 4.6 displays the relative contributions of each process to the total environmental impacts, including salt-solution (NaCl), DI-water, electricity, heat energy, resin and anode manufacturing, and resin landfilling. Similar to still bottoms 1, salt-solution, DI water, heat energy, and anode manufacturing accounted for less than 1% of impacts across all categories.

For all three species, electricity for EO treatment accounted for the majority (>60%) of impacts in the categories of global warming potential, smog formation, acidification, and respiratory effects. Resin manufacturing accounted for the majority (>90%) of ozone depletion, while resin landfilling accounts for >60% of marine eutrophication. Across all impact categories, electricity accounted for a greater contribution to total impacts for PFBA than PFOS and PFOA because the EE/O of PFBA removal (2,941 kWh/m³) was higher than that of PFOS (1,031 kWh/m³) and PFOA (1,877 kWh/m³) in still bottoms 2 (Figure 4.5).

4.3.3 Discussion and Comparison of Still Bottoms Samples

Though the environmental impacts of individual PFASs species were compared, key differences between the two still bottoms samples were present. Since the still bottoms samples were different, the initial PFASs concentrations between the two samples varied significantly. Still bottoms 2 contained higher initial concentrations of PFOS, PFOA, PFBS, and PFBA compared to still bottoms 1. Still bottoms 2 also contained significantly higher TOC (201,529 mg L⁻¹) compared to still bottoms 1 (13,280 mg L⁻¹). Due to these differences, EE/O values were

larger for still bottoms 2, indicating that more electricity was required to achieve the same level of mineralization for the same species. As a result, the total environmental impacts across all categories were larger in still bottoms 2 compared with still bottoms 1.

4.4 Scenario Analysis Results

The global warming potentials of the three scenarios were compared to gain insight into the impact of technology choices on different PFASs. To illustrate differences between long- and short-chain PFASs under different treatment scenarios, PFOS and PFBA were selected as benchmark species for comparison. A description of the modeling process and GWP calculation results for each scenario can be found in Tables S8 in the supplemental information.

4.4.1 Scenario Analysis: PFOS

PFOS is a long-chain species with an EE/O of 350 kWh/m³ in still bottoms 1. Results of the GWP of different IX scenarios to degrade long-chain PFOS are shown in Figure 4.7. The total GWP impacts for the three scenarios are 61.0, 72.2, and 36.7 kg CO₂ eq., respectively. These results suggest that coupling IX with EO can reduce GWP by approximately ~35.4 kg CO₂ eq. (~49%) when the resin is regenerated and reused (IX/Re + EO). Even without reusing the resin, the overall GWP of IX + EO is only marginally larger (~11 kg CO₂ eq. or ~15%) than IX + Incin.

In scenario 1 (IX + Incin.), the PFASs remains in the exhausted resin. Therefore, it can be disposed of either as hazardous waste or incineration. Process contribution analysis indicates that resin manufacturing and disposal by incineration (IX + Incin.) make up 74% and 26% of the total impact, respectively. For the second scenario (IX + EO), PFASs was flushed out to be treated by the EO process. Therefore, the wasted resin can be sent to a municipal landfill. In this scenario,

resin manufacturing, disposal, regeneration, and EO treatment contribute 63%, 1%, 2% and 34% to the total GWP, respectively. IX/Re + EO has the lowest GWP (\sim 36.7 kg CO₂ eq.), with resin manufacturing and EO treatment making up 29% and 67% of the total impacts, respectively. In this scenario, the resin is landfilled after 10 uses, resulting in resin disposal accounting for less than 1% of the total impact.

Boyer's¹⁵ also conducted a comparative LCA of an anion exchange resin -based PFASs remediation system with different regeneration scenarios, including disposing of waste regeneration solution via incineration, reusing the organic cosolvent, and brine fractions of the waste regeneration solution. The functional unit was 1 m³ of AER-treated groundwater with combined PFOA and PFOS concentration equal to 70 μg/L in untreated water. In his incineration scenario, the GWP result is 0.059 kg CO₂ eq per unit. To treat the same volume groundwater with our study for PFOA (1000 m³), the GWP is 59 kg CO₂ eq, which is close to the GWP (61 kg CO₂ eq.) of PFOS removal in scenario IX + Incin. According to Boyer's research, the incineration of the waste containing PFOA/PFOS had larger environmental impact than recycling solvent therefore there is a need for PFASs destruction technologies to avoid incineration, which is validated with our analysis.

4.4.2 Scenario Analysis: PFBA at High TOC

As a short-chain species, destruction of PFBA is more challenging than PFOS due to its lower adsorption capacity. ⁸ Also, high TOC (201,529 mg C·L⁻¹, Table S2) in still bottoms 2 results in a high EE/O of 2,941 kWh/m³ for PFBA (Table S3). ¹³ GWP results under different scenarios for PFBA are displayed in Figure 8. The large EE/O required by EO to degrade PFBA results in IX + Incin. being most favorable with the lowest GWP (~61.0kg CO₂ eq.) overall. The scenario with the largest GWP is IX+EO (~254kg CO₂ eq.) with resin manufacturing, and EO

treatment making up 18% and 81% of the total impact, respectively. The total GWP of IX/Re+EO (\sim 219 kg CO₂ eq.) is 14% lower than IX+EO. In both scenarios with EO treatment, the impact of disposal and regeneration account for less than 1% of the total.

4.4.3 Scenarios Analysis Discussion

Since the overall environmental impact is largely due to the resin manufacturing, disposal, and electricity required for EO, based on the LCA of the unit processes, the GWP for three scenarios can be calculated by the equations below. The first term on the right side of the equation is the global warming potential of resin manufacturing, which is the quantity of fresh resin times the unit global warming potential of resin. The quantity of resin is calculated using the adsorption model we recently published²⁶. In case of resin regeneration, consumed resin needs to be added each year.

$$GWP1 = \frac{\frac{q_{PFAS} \times V_{gw} \times 10^3}{C_{PFAS}}}{\sum_{k=1}^{k=n} (\alpha_k^i c_k)} \times 4.894$$
 (1)

$$GWP2 = \frac{q_{PFAS} \times V_{gw} \times 10^3}{\frac{C_{PFAS}}{\sum_{k=1}^{k=n} (\alpha_i^k c_k)}} \times 3.715 + \text{ EE/O} \times OM \times V_{st} \times 0.714$$
(2)

$$GWP3 = \frac{q_{PFAS} \times V_{gw} \times 10^{3}}{\frac{C_{PFAS}}{\sum_{k=1}^{k=1} (\alpha_{k}^{i} C_{k})}} \times \left(1 + \sum_{i=1}^{i=(Y/_{T})-1} i \times x\%\right) \times 3.715 \times \frac{1}{Y/_{T}} + \text{EE/O} \times V_{st} \times 0.714 \quad (3)$$

where x% is the capacity loss of resin in each regeneration; Y (year) is the resin life span; T (year) is the time of resin breakthrough. $V_{gw}(m^3)$ is the volume of water; V_{st} (m^3) is the volume of still bottoms and EE/O(kWh/ m^3) is the electricity per order of magnitude of PFASs removed; OM is the order of removal; 4.984 (kg CO₂ eq./kg) is the sum of unit GWP of resin manufacturing and incineration; 3.715 (kg CO₂ eq./kg) is the sum of unit GWP of resin manufacturing and non-hazardous landfill; 0.714 (kg CO₂ eq./kWh) is the unit GWP of electricity based on the energy mix of southeast U.S.; q_{PFAS} (eq/L resin) is resin-phase

concentration of PFASs ion; C_{PFAS} (eq./L resin) is aqueous concentration of PFASs ion; C_k (eq./L resin) is aqueous-phase concentration of exchange ion k; α_i^k : separation factor for ion i with respect to exchange ion k; K (eq./L resin) is the total exchange capacity of resin; ρ (kg/L) is the density of the resin.

Though the environmental impacts of degrading short-chain PFASs are larger than that of long-chain PFASs, our results indicate that the option to regenerate and reuse the IX coupled with EO treatment depends on the EE/O of the PFASs which is determined both by the type of PFASs and the water quality, especially the TOC concentration. A break-even study is attempted to give a rule of thumb for engineering application. The break-even point is the EE/O value where the impacts of scenario 1, 2, and 3 become equal. The lower point is 192 kWh/m³. When EE/O is smaller than this number, EO exerts smaller global warming potential than incineration regardless of whether resin is regenerated and reused. The upper point is calculated to be 695 kWh/m³. When EE/O is larger than this point, incineration is a better option. When EE/O is between these two break-even points, regeneration is the key to make EO option better than incineration.

4.4.4 Impact of Different Energy Mix

Electricity use accounts for a majority of the global warming impacts of destructive treatment. Therefore, the energy source may significantly change the impact results for PFASs degradation. The average energy mix of the southeast United States has a GWP of 0.71 kg CO₂ eq/kWh and consists of 37% of natural gas, 34% of coal, 24% of nuclear, and 7% of renewable energy, including hydro, wind, biomass, and solar energy.²⁴ As indicated in Figure 4.9, this number is relatively high compared to other geographic regions. Therefore, if the energy mix used to supply the power for EO process were derived from more renewable resources, the

overall GWP of the above scenarios will shift in favor of the coupled IX and EO processes. To apply equations above to cases with different energy mix, appropriate values for the GWP for each kWh energy consumption need to be used to replace the 0.71 kg CO₂ eq/kWh. If a smaller number is used, the EE/O value for the break-even points will increase.

4.5 Uncertainty Analysis

Uncertainty is intrinsic to LCA's due to both data quality and LCA methodologies. Correct interpretation of a life cycle analysis requires quantifying uncertainties. A Monte-Carlo simulation tool built in the SimaPro software was applied to calculate the uncertainty of the analysis for the scenario comparison above. The Monte-Carlo simulation calculates the distribution of analysis results by randomly sampling each input data within the given range or distribution. The details of the uncertainty results are included in the Supplemental Materials (Table S4.9, Figure S4.1 and S4.2). The standard deviations are in the range of 1.47% to 7.9% (Table S4.9), which do not change the comparison discussed above.

4.6 Conclusion

A sustainable solution to manage PFASs contamination requires an understanding of the environmental impacts of treatment options for a variety of PFASs under different water quality. The life cycle impacts of PFASs treatment of coupled IX and EO were investigated. For most long-chain PFASs studied (except PFHpA), the global warming potential for the removal is in the same order as that of the conventional groundwater treatment. For short chain PFASs, global warming potential is much larger. Resin manufacturing and energy use for EO are the two main contributors to the global warming potential.

Depending on the EE/O of the PFASs treatment, the comparison of incineration and EO may change. Using southeast energy mix in the U.S., when the EE/O is less than 192 kWh/m³, EO has less global warming potential than incineration, irrespective of whether the resin is regenerated. When the EE/O is larger than 695 kWh/m³, IX with incineration will have the least impact. Between these two numbers, regeneration and reuse of the IX resin with EO has the lowest global warming potential. These numbers could increase if the power network comprises more renewable energies, favoring the EO process. Empirical equations were developed to calculate the global warming potential for the three scenarios. They can be used in different cases after modifying the parameters and constants according to site-specific conditions.

ASSOCIATED CONTENT

Supporting Information: Water quality parameters; Still bottoms Properties; EE/O of PFASs removal for still bottoms 1 and 2; Concentrations of PFASs in still bottoms samples before and after EO treatment (mg/L); Normalized life cycle reference flow table for the treatment and destruction of two orders of magnitude of PFASs species in still bottoms 1 and still bottoms 2 from 1000 m³ groundwater; Environmental impact categories analyzed in this study; GWP results for treating PFOS and PFBA in three different treatment scenarios; Standard deviation of uncertainty analysis for treating PFOS and PFBA in three different treatment scenarios; and GWP uncertainty analysis result for treating PFOS in IX+Incin. and PFBA in IX/Re+EO. This material is available free of charge via the Internet at http://pubs.acs.org

AUTHOR INFORMATION

Corresponding Author

Ke Li - College of Engineering, University of Georgia, Athens, GA 30602, United States;

Telephone: 1-706-542-2201; Email: lukeli@uga.edu

Authors:

Gengyang Li - College of Engineering, University of Georgia, Athens, GA 30602, United States;

Josh Dunlap - College of Engineering, University of Georgia, Athens, GA 30602, United States;

Yifei Wang - College of Agricultural and Environmental Sciences, Griffin, GA 30223, United

States:

Qingguo Huang - College of Agricultural and Environmental Sciences, Griffin, GA 30223,

United States;

Notes

The authors declare no competing financial interest.

ACKNOWLEDGMENT

This study was supported in part by U.S. Environmental Protection Agency Grant

R840080. It has not been formally reviewed by EPA. The views expressed in this document are

solely those of the authors and do not necessarily reflect those of the Agency. EPA does not

endorse any products or commercial services mentioned in this publication.

128

4.7 References

- Wanninayake, D. M. (2021). Comparison of currently available PFAS remediation technologies in water: A review. *J Environ Manage*, 283, 111977.
 https://doi.org/10.1016/j.jenvman.2021.111977
- 2) Conder, J. M., Hoke, R. A., Wolf, W. d., Russell, M. H., & Buck, R. C. (2008). Are PFCAs bioaccumulative? A critical review and comparison with regulatory criteria and persistent lipophilic compounds. *Environmental Science & Technology*, 42(4), 995-1003.
- 3) De Witte, J., Piessens, G., & Dams, R. (1995). Fluorochemical intermediates, surfactants and their use in coatings. *Surface coatings international*, 78(2), 58-64.
- 4) Prevedouros, K., Cousins, I. T., Buck, R. C., & Korzeniowski, S. H. (2006). Sources, fate and transport of perfluorocarboxylates. *Environmental Science & Technology*, 40(1), 32-44.
- 5) Appleman, T. D., Higgins, C. P., Quiñones, O., Vanderford, B. J., Kolstad, C., Zeigler-Holady, J. C., & Dickenson, E. R. (2014). Treatment of poly-and perfluoroalkyl substances in US full-scale water treatment systems. *Water Research*, *51*, 246-255.
- 6) Kucharzyk, K. H., Darlington, R., Benotti, M., Deeb, R., & Hawley, E. (2017). Novel treatment technologies for PFAS compounds: A critical review. *Journal of environmental management*, 204, 757-764.
- 7) Merino, N., Qu, Y., Deeb, R. A., Hawley, E. L., Hoffmann, M. R., & Mahendra, S. (2016). Degradation and removal methods for perfluoroalkyl and polyfluoroalkyl substances in water. *Environmental Engineering Science*, *33*(9), 615-649.

- 8) Dixit, F., Dutta, R., Barbeau, B., Berube, P., & Mohseni, M. (2021). PFAS removal by ion exchange resins: A review. *Chemosphere*, 129777.
- 9) Liu, Y.-L., & Sun, M. (2021). Ion exchange removal and resin regeneration to treat perand polyfluoroalkyl ether acids and other emerging PFAS in drinking water. *Water Research*, 207, 117781. https://doi.org/https://doi.org/10.1016/j.watres.2021.117781
- 10) Woodard, S., Berry, J., & Newman, B. (2017). Ion exchange resin for PFAS removal and pilot test comparison to GAC. *Remediation-the Journal of Environmental Cleanup Costs Technologies & Techniques*, 27(3), 19-27. https://doi.org/10.1002/rem.21515
- 11) USEPA. (2019). Per- and Polyfluoroalkyl Substances (PFAS): Incineration to Manage PFAS Waste Streams. (0010-22021563-521X).
- 12) Liang, S., Pierce Jr, R. D., Lin, H., Chiang, S. Y., & Huang, Q. J. (2018).

 Electrochemical oxidation of PFOA and PFOS in concentrated waste streams.

 Remediation Journal, 28(2), 127-134.
- 13) Wang, L., Nickelsen, M., Chiang, S.-Y., Woodard, S., Wang, Y., Liang, S., Mora, R., Fontanez, R., Anderson, H., & Huang, Q. (2021). Treatment of perfluoroalkyl acids in concentrated wastes from regeneration of spent ion exchange resin by electrochemical oxidation using Magnéli phase Ti4O7 anode. *Chemical Engineering Journal Advances*, 5, 100078. https://doi.org/https://doi.org/10.1016/j.ceja.2020.100078
- 14) Wang, Y. Y., Pierce, R., Shi, H. H., Li, C. G., & Huang, Q. G. (2020). Electrochemical degradation of perfluoroalkyl acids by titanium suboxide anodes. Environmental Science-Water Research & Technology, 6(1),144-152.

 https://doi.org/10.1039/c9ew00759h

- 15) Boyer, T. H., Ellis, A., Fang, Y., Schaefer, C. E., Higgins, C. P., & Strathmann, T. J. (2021). Life cycle environmental impacts of regeneration options for anion exchange resin remediation of PFAS impacted water. *Water Research*, 207, 117798.
 https://doi.org/https://doi.org/10.1016/j.watres.2021.117798
- 16) Liang, S., Mora, R., Huang, Q., Casson, R., Wang, Y., Woodard, S., & Anderson, H. (2022). Field demonstration of coupling ion-exchange resin with electrochemical oxidation for enhanced treatment of per- and polyfluoroalkyl substances (PFAS) in groundwater. *Chemical Engineering Journal Advances*, 9.
 https://doi.org/10.1016/j.ceja.2021.100216
- 17) Emery, I., Kempisty, D., Fain, B., & Mbonimpa, E. (2019). Evaluation of treatment options for well water contaminated with perfluorinated alkyl substances using life cycle assessment. *International Journal of Life Cycle Assessment*, 24(1), 117-128. https://doi.org/10.1007/s11367-018-1499-8
- 18) Maul, G. A., Kim, Y., Amini, A., Zhang, Q., & Boyer, T. H. (2014). Efficiency and life cycle environmental impacts of ion-exchange regeneration using sodium, potassium, chloride, and bicarbonate salts. *Chemical Engineering Journal*, 254, 198-209. https://doi.org/https://doi.org/10.1016/j.cej.2014.05.086
- 19) DuPontTech. (2020). Ion Exchange Resins Resin wear-out guidelines. DuPont Ion Exchange Resins Resin wear-out guidelines Tech Fact
- 20) Althaus, H., Chudacoff, M., Hischier, R., Jungbluth, N., Osses, M., & Primas, A. (2007). Life cycle inventories of chemicals. *Ecoinvent report*, 8.
- 21) Lin, H., Niu, J., Liang, S., Wang, C., Wang, Y., Jin, F., Luo, Q., & Huang, Q. (2018).

 Development of macroporous Magnéli phase Ti4O7 ceramic materials: As an efficient

- anode for mineralization of poly- and perfluoroalkyl substances. *Chemical Engineering Journal*, *354*, 1058-1067. https://doi.org/10.1016/j.cej.2018.07.210
- 22) Biswas, W. K., & Yek, P. (2016). Improving the carbon footprint of water treatment with renewable energy: a Western Australian case study. Renewables: Wind, Water, and Solar. https://doi.org/10.1186/s40807-016-0036-2
- 23) Mo, W., Wang, R., & Zimmerman, J. B. (2014). Energy-water nexus analysis of enhanced water supply scenarios: a regional comparison of Tampa Bay, Florida, and San Diego, California. Environ Sci Technol, 48(10), 5883-5891. https://doi.org/10.1021/es405648x
- 24) DOE. (2015). Climate Change and the U.S. Energy Sector: Regional vulnerabilities and resilience solutions.
- 25) Finkbeiner, M., Inaba, A., Tan, R., Christiansen, K., & Klüppel, H.-J. (2006). The new international standards for life cycle assessment: ISO 14040 and ISO 14044. *The international journal of life cycle assessment*, 11(2), 80-85.
- 26) Wang, Y., Warner, M., Li, K., Hawkins, G. L., & Huang, Q. (2022). Assessing explicit models of per-and polyfluoroalkyl substances adsorption on anion exchange resins by rapid small-scale column tests. Chemosphere, 300, 134547.

Table 4.1: Environmental databases used for the unit emission and environmental impact factors

Inventory Item	Database	Item Name
Sodium	Ecoinvent Unit	Sodium chloride, brine solution, at plant/RER U
chloride	Processes	
De-ionised	ELCD	De-ionised water, reverse osmosis, production mix, at
water		plant, from surface water RER S
Electricity	USLCI	Electricity, at Grid, SERC, 2008/RNA U
Heat,	Ecoinvent Unit	Heat,
natural gas	Processes	natural gas, at boiler modulating <100kW/RER U
Anionic resin	Ecoinvent Unit	Anionic resin, at plant/CH U
	Processes	
Resin	USLCI	Disposal, anion exchange resin f. to municipal
incineration		incineration/CH U
Resin disposal	ELCD	Disposal, polypropylene, to sanitary landfill/CH U
by landfill		
Anode	USLCI	Anode, at plant/RNA

Table 4.2. Impact assessment results to degrade PFASs of two log orders of magnitude in still bottoms 1 (using NaCl as salt-solution)

Impact Category	PFHpA	PFOA	PFHxS	PFHpS	PFOS	Units
OD	0.00215	0.00215	0.00215	0.00215	0.00215	kg CFC-11 eq.
GWP	180	84.9	84.4	79.4	72.2	kg CO ₂ eq.
SF	9.96	3.69	3.66	3.33	2.85	kg O ₃ eq.
AD	65.0	21.9	21.7	19.4	16.2	mol H ⁺ eq.
ME	0.247	0.235	0.235	0.235	0.234	kg N eq.
C	1.16E-6	1.04E-6	1.04E-6	1.03E-6	1.03E-6	CTUh
NC	7.79E-06	5.26E-6	5.24E-6	5.11E-6	4.92E-6	CTUh
RE	0.178	0.0629	0.0623	0.0563	0.0475	kg PM ₁₀ eq.
ET	65.2	40.2	40.1	38.8	36.9	CTUe

(Note: OD-ozone depletion, GWP-global warming potential, SF-smog formation, AD-acidification, ME-marine eutrophication, C-carcinogens, NC-non-carcinogens, RE-respiratory, ET-ecotoxicity)

Table 4.3. Impact assessment results to degrade PFASs in still bottom 2 (using NaI as salt-solution)

Impact Category	PFBA	PFHxA	PFOA	PFHxS	PFBS	PFOS	PFPeA	PFHpA	PFHpS	PFPeS
OD	2.15E-3	3 2.15E-3	3 2.15E-3	3 2.15E-3	3 2.15E-3	2.15E-3	3 2.15E-3	2.15E-3	2.15E-3	2.15E-3
GWP	254	202	179	157	146	120	99.3	98.9	84.5	82.1
SF	14.9	11.4	9.93	8.42	7.70	6.01	4.65	4.61	3.67	3.51
AD	98.6	74.8	64.8	54.4	49.4	37.8	28.5	28.3	21.8	20.7
ME	0.256	0.250	0.247	0.244	0.243	0.240	0.237	0.237	0.235	0.235
C	1.26E-6	51.19E-6	51.16E-6	51.13E-6	51.12E-6	51.09E-6	51.06E-6	51.06E-6	1.04E-6	1.04E-6
NC	9.77E-6	68.37E-6	57.78E-6	57.17E-6	6.88E-6	6.19E-6	5.64E-6	5.63E-6	5.25E-6	5.18E-6
RE	0.269	0.205	0.178	0.150	0.137	0.106	0.0805	0.0799	0.0625	0.0596
ET	84.8	71.0	65.1	59.1	56.2	49.5	44.0	43.9	40.1	39.5

(Note: OD-ozone depletion, unit: kg CFC-11 eq.; GWP-global warming potential, unit: kg CO₂ eq.; SF-smog formation, unit: kg O₃ eq.; AD-acidification, unit: mol H⁺ eq.; ME-marine eutrophication, unit: kg N eq.; C-carcinogens, unit: CTUh; NC-non-carcinogens, unit: CTUh; RE-respiratory, unit: kg PM₁₀ eq.; ET-ecotoxicity, unit: CTUe)

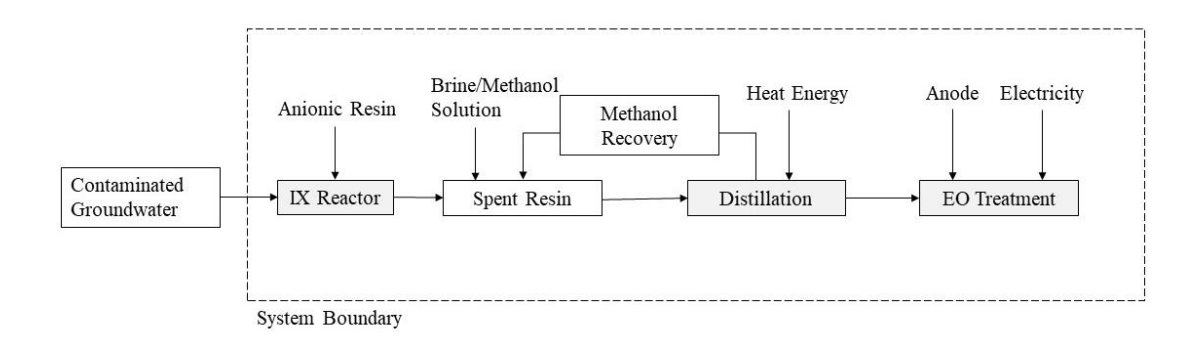


Figure 4.1. Overview of the system boundary for PFASs treatment from spent IX resin. The dashed line represents the system boundary for the coupled IX with EO destructive treatment process.

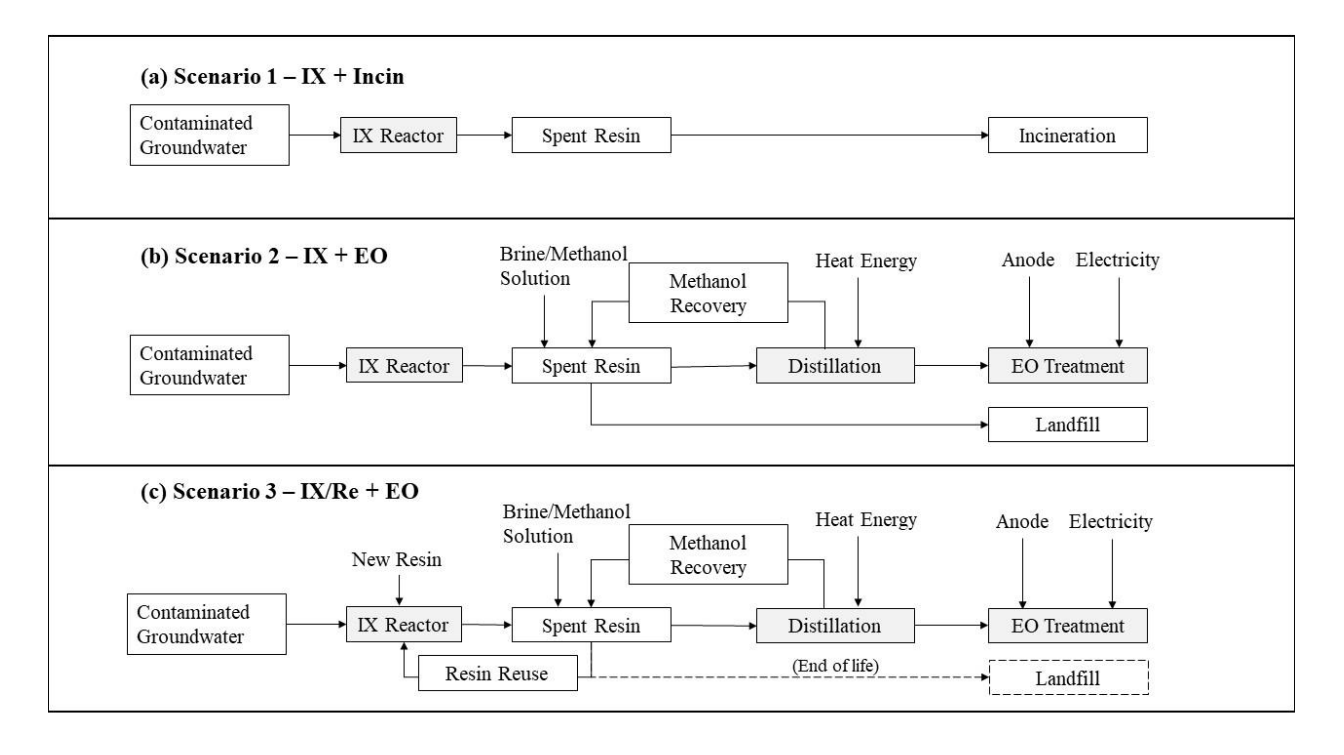


Figure 4.2. Overview of the unit processes and inventory items considered for three different IX and EO operation scenarios

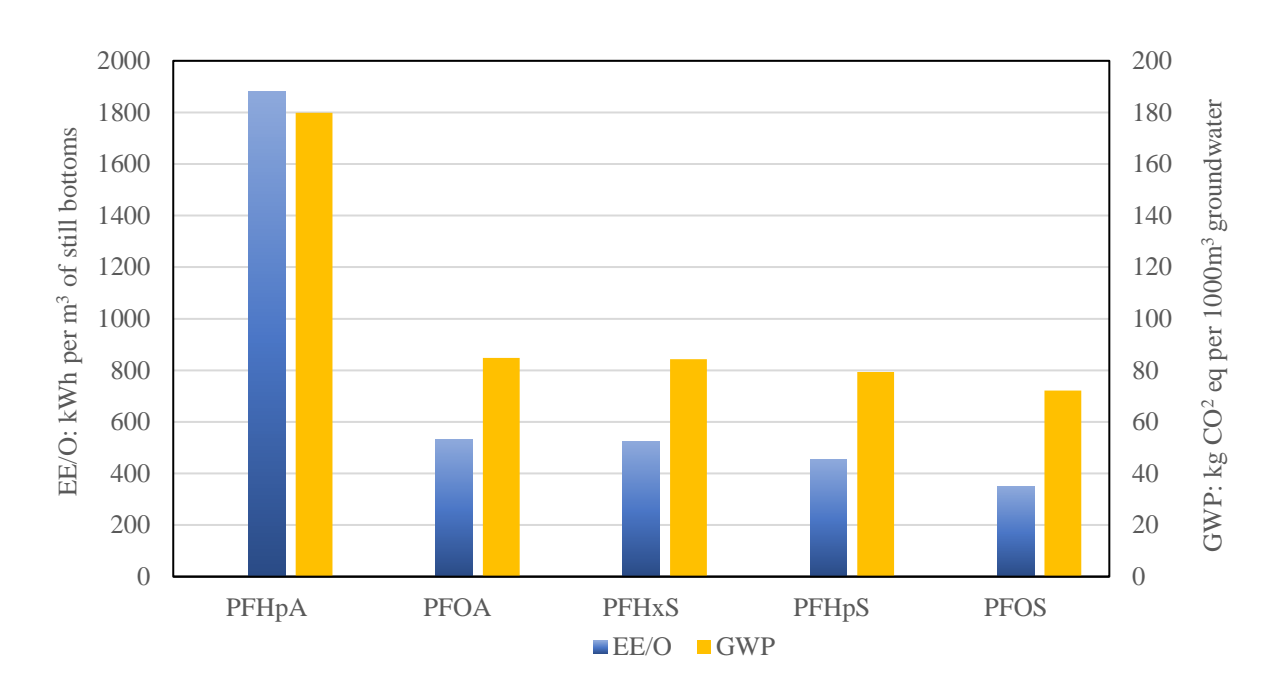


Figure 4.3. EE/O and GWP of PFASs removal per functional unit in still bottoms 1

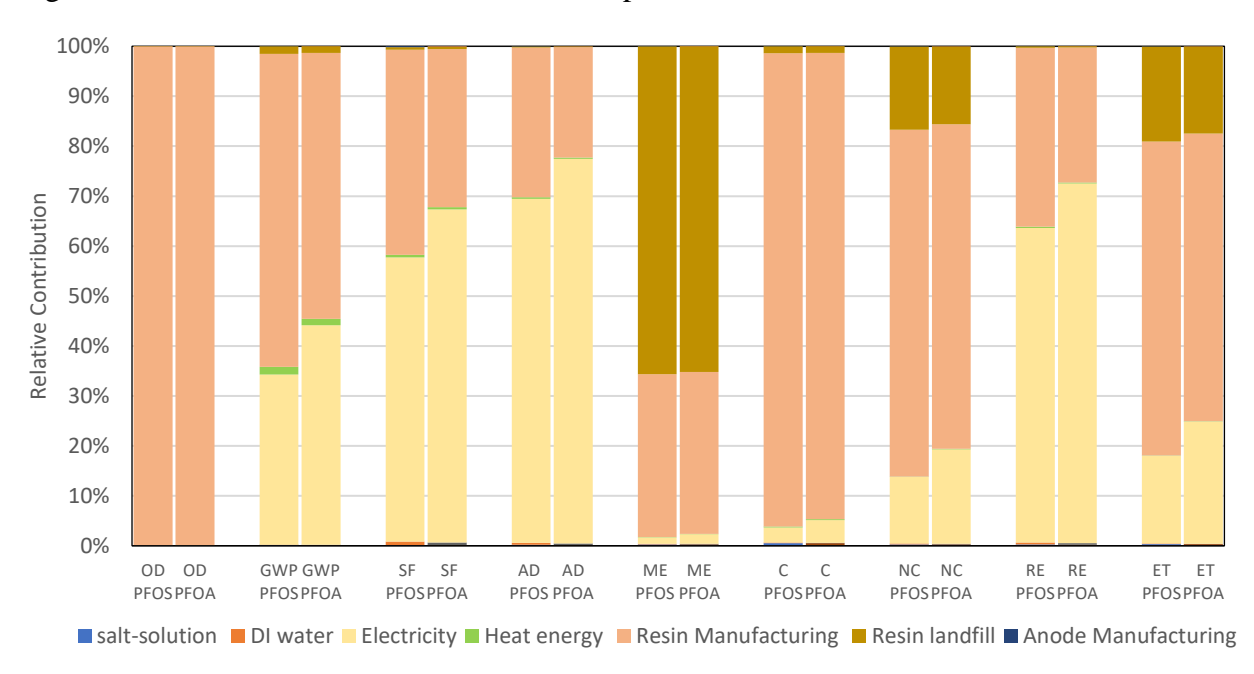


Figure 4.4. Relative contributions of each process to the total environmental impacts of PFOS and PFOA in still bottoms 1. (Note: impacts of salt-solution, DI water, and anode manufacturing account for less than 1% of total impacts across each category)

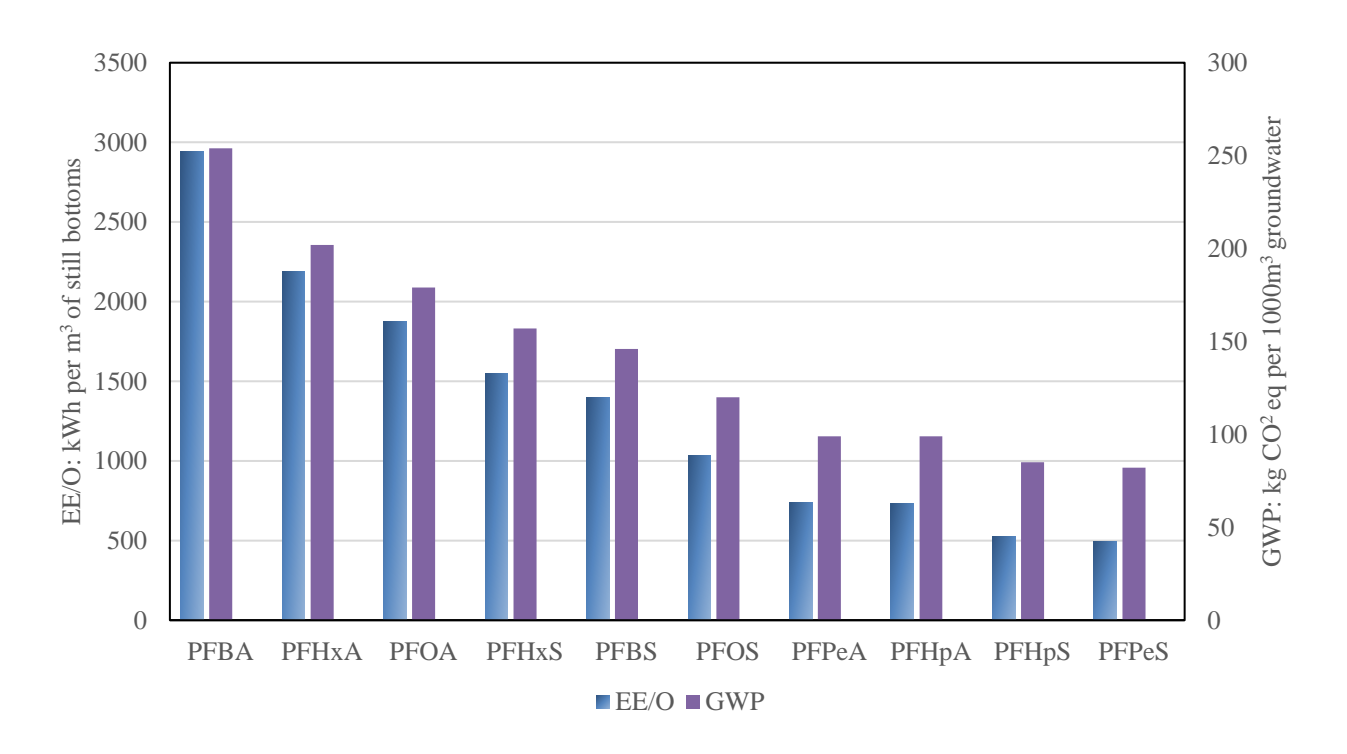


Figure 4.5. EE/O and GWP of PFASs removal per functional unit in still bottoms 2

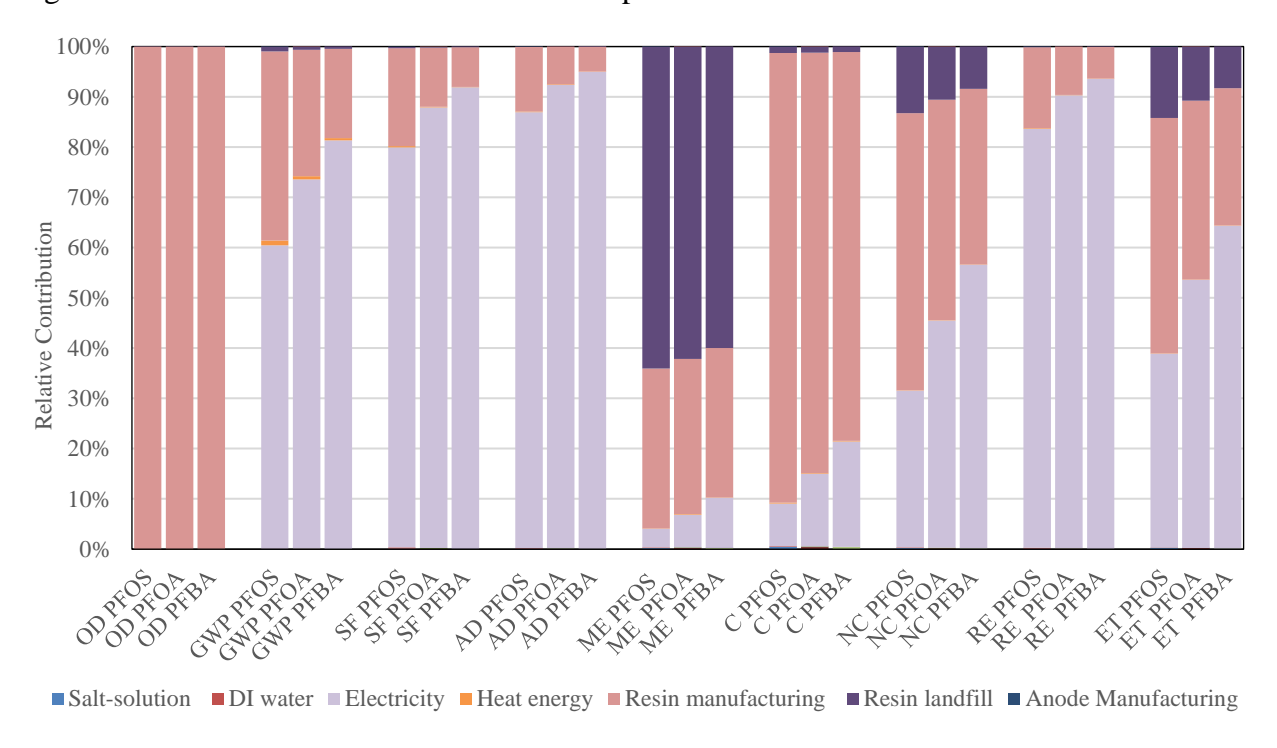


Figure 4.6. Relative contributions of unit processes to the total environmental impacts of PFOS, PFOA, and PFBA in still bottoms 2

(Note: Impacts of salt-solution, DI water, heat energy, and anode manufacturing account for less than 1% of total impacts across each category)

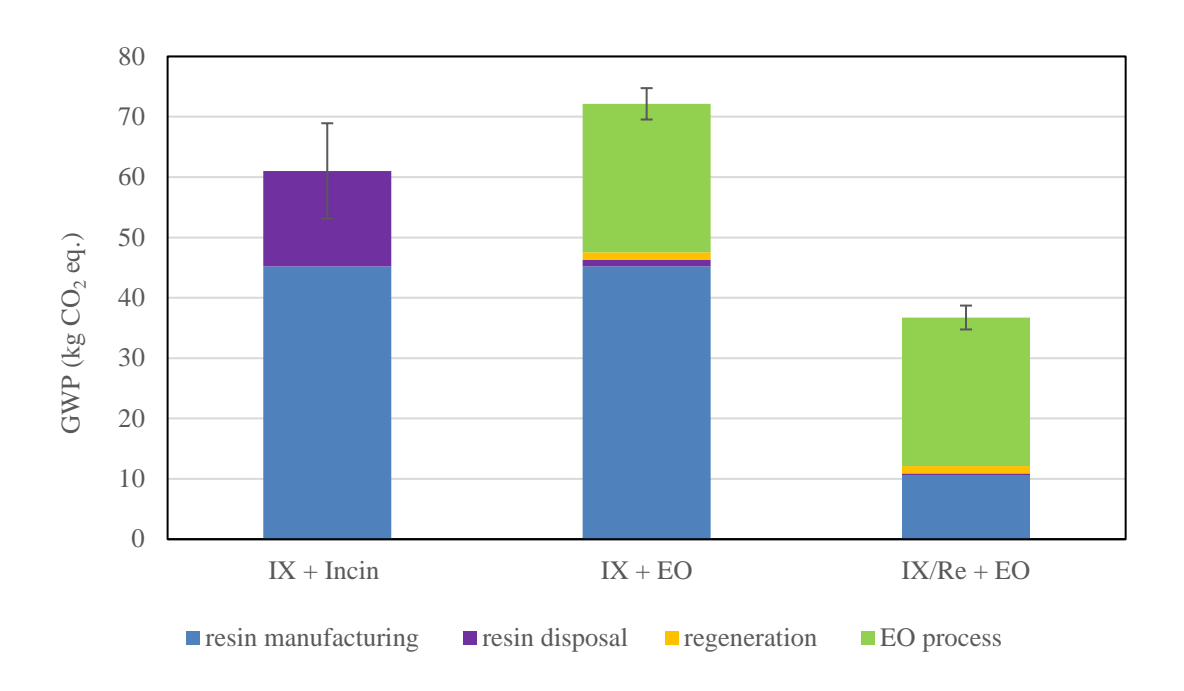


Figure 4.7. Scenario analysis results comparing total GWP for the treatment of PFOS.

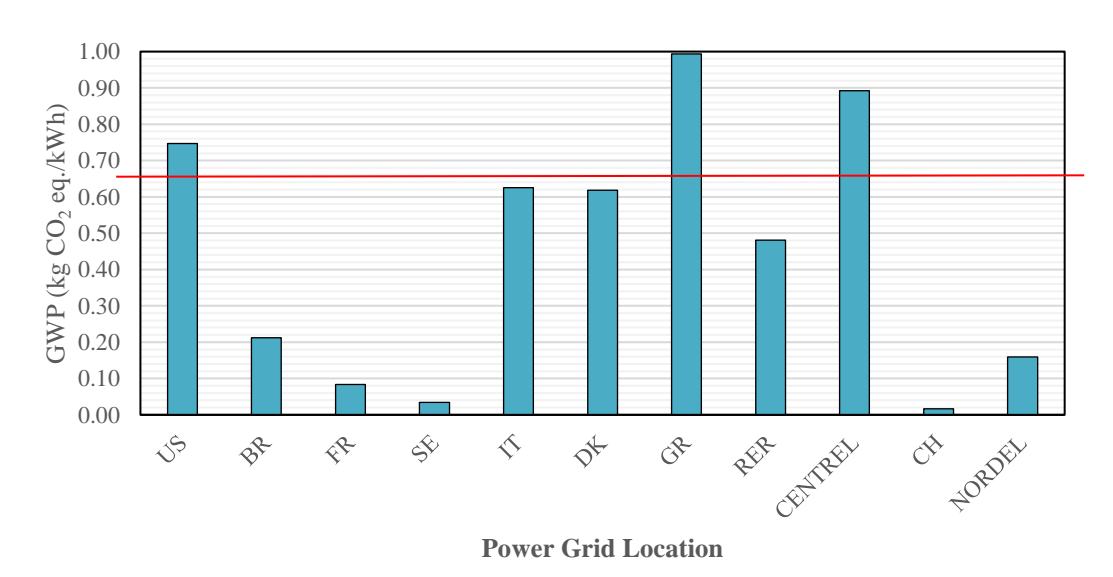


Figure 4.8. Variation in GWP values from different energy mix. Abbreviations include: United States (US), Brazil (BR), France (FR), Sweden (SE), Italy (IT), Denmark (DK), Greece (GR), Average European (RER), Average Central American (CENTREL), Switzerland (CH), Nordic Countries, excluding Iceland (NORDEL). Red line represents the number used in the equations, which uses the southeast energy mix in the US.

CHAPTER 5

LIFE CYCLE ASSESSMENT AND LIFE CYCLE COSTING ANALYSIS FOR REMOVING
PFAS FROM LANDFILL LEACHATE WITH FOAM FRACTIONATION TECHNOLOGY

Li, G., Wang, Y., Huang, Q., Peng, M., & Li, K.

Submitted to ES&T Water, under revision, 4/1/2025

ABSTRACT

Understanding the environmental impacts and economic costs of treatment technologies is essential for developing sustainable strategies for managing per- and polyfluoroalkyl substances (PFASs). This study focuses on the treatment of PFAS-contaminated landfill leachate using foam fractionation (FF) technology. A parameterized life cycle assessment (LCA) and life cycle costing analysis (LCCA) were conducted to evaluate the performance of one-stage and three-stage FF systems. Full-scale operational data and EPA design models were used to assess environmental and economic impacts based on a functional unit of treating 1000 m³ of PFAS-contaminated landfill leachate. The global warming potential (GWP) was estimated at 818 kg CO₂ eq. for the one-stage system and 402 kg CO₂ eq. for the three-stage system. Life cycle costs were estimated at \$77.4 and \$110.6 per functional unit for the one-stage and three-stage systems, respectively, using the Net Present Value method. Sensitivity and scale-up analyses were also performed to evaluate the influence of operational parameters and system configurations on both environmental and economic outcomes.

5.1 Introduction

Per- and polyfluoroalkyl substances (PFASs) have drawn public concern recently due to their toxic properties and environmental persistence. PFAS substances are a broad class of emerging environmental contaminants used heavily by the industrial, commercial, and manufacturing sectors in previous decades; some products include surface coating, lubricants, and firefighting foams. PFASs are highly persistent and bioaccumulated in the environment within biota and humans. Because of this, PFAS species have been consistently detected within the environment, in food products, and in humans. Various potential health effects have been attributed to PFASs exposure due to their high toxicity.

Landfill leachate is a complex matrix containing high ammonia concentrations, chemical oxygen demand, salts, and chemicals. Discharged leachate water from landfills are an important contributor to the origin of PFASs in the environment, with total aqueous concentrations ranging from 100 to 100 000 ng/L.⁶ PFASs in landfills originate from discarded consumer and industrial waste or PFASs-contaminated biosolids.⁷ Moreover, landfilled bottom ash from waste incinerators may still contain incompletely combusted PFASs. Biological leaching and physicochemical desorption of these PFASs result in their release to the landfill leachate, leading to high aqueous PFASs concentrations. Although the production and use of some PFASs are banned or restricted, historically stored wastes in landfills are expected to last for a long time and remain a problem in the foreseeable future.

Foam fractionation (FF) has been proven to effectively remove PFASs from PFASs-contaminated landfill leachate.⁸ Using fine air bubbles, foam fractionation concentrates PFASs from a water phase into a more minor volume foam phase. The foam phase contains highly concentrated PFASs that can be disposed of or further treated.⁹ The advantage of FF technology

is that it can be implemented using a standard aeration process in wastewater treatment facilities. Converting an existing aeration process to foam fractionation for PFAS removal only requires installation of an appropriate foam collection system. PFASs removal depends on several operational parameters such as contact time, air ratio, air flow rate, and foam fraction. Removal efficiencies for long-chain PFASs are typically greater than 90% and removal of short-chain PFASs is typically 50% or less. FF as a potent remediation technology for landfill leachate has been reported at the lab-scale, pilot-scale, and commercial-scale (Table 1). 11,12

A review of the FF operation parameters for lab, pilot, and full scales from literature in recent years is presented in Table 5.1. The air-water ratio, air flowrate, and aeration time are the major parameters that affect the PFASs treatment efficiency. All these studies found that PFASs of longer chain lengths were prone to higher removal and more significant enrichment than the short-chain. Also, the PFASs removal efficiency and the enrichment in the three-stage treatment were higher than in the one-stage FF treatment.

Wang et al. performed the batch experiments to treat PFASs-contaminated LL with the multi-stage FF treatment in the lab. 13 The experiments were operated in an acrylic plastic column of 0.2 L with 5L/min air flow for 2 min in each batch. The removal efficiency of PFASs with chain lengths > C6 in the landfill leachate sample by the three-stage treatment is over 85%. Their results also found that PFASs of longer chain lengths were prone to higher removal and more significant enrichment than the short-chain, partly because interfacial partitioning intensifies as the chain length of PFASs increases.

Buckley et al. experimented the PFASs removal from water using foam fractionation.¹⁴ They concluded that the removal of PFASs by directly exploiting surface-active properties was possible for PFASs with a fluorocarbon tail length of 6 or greater, within the batch experiment

time of 60 min. However, the removal of PFBA was not possible through foam fractionation process. This may be ascribed to the short fluorocarbon tail not imparting enough hydrophobicity, hence the affinity with the surface. McCleaf et al. performed lab-scale FF in batch and continuous modes for PFASs removal from the landfill leachate and found stable removal efficiency of greater than 90% for PFOA (C7), PFOS (C8), PFHxS (C6), and PFHpA (C6) and 6:2 FTSA (C6). The parameters for bath mode tests were air flow rate, water column height, iron chloride coagulant addition, and salinity. In the batch mode, the average removal efficiency was reported to increase 6% with air flowrate increasing from 3500 L min⁻¹ m⁻² to 7500 L min⁻¹ m⁻². The mode of operation was reported to have negligible impacts on PFAS removal, as the reported average removal for the batch mode and continuous mode were reported to be 76% and 81%, respectively.

Smith et al. investigated the applicability of a pilot-scale foam fractionation setup for the removal of PFASs from natural landfill leachate in a novel continuous operating mode. They also systematically evaluated the effect of different operating parameters on this continuous pilot scale process with various air flowrates (5~20 L/min), air-water ratios (2.2~13), and aeration times (10, 15, 20 and 30 mins). Their results indicated that treatment efficiency is associated with contact time, air flow rate, and collected foam fraction. Long-chain compounds were removed better than short-chain PFASs, and perfluoro sulfonic acids (PFSA) were removed more efficiently than perfluoroalkyl carboxylic acids (PFCA). PFOS and PFOA had average removal efficiencies of 95% and 92%, but no removal of PFBA and only 10% removal of PFBS were found.

In the study of Robey et al., the effectiveness of the foaming technique for concentrating PFASs in landfill leachate varied by compound, with a mean removal percentage of 69% and a median removal percentage of 92% among the 10 replicate foaming experiments.¹¹

Burns and his coworkers demonstrated a commercial-scale three-stage semi-batch foam fractionation process, Surface-Active Foam Fractionation (SAFF), for the removal of PFASs from a landfill leachate catchment in Sweden. There have been 23 sampling events for PFASs influent and effluent concentrations over 10 months, during which approximately 80,000m³ of leachate feed has been successfully treated without the need for complex pretreatment. The contracted throughout was 330 m³ per day (120,000m³/year), but, in practice, it varied between 200 m³ and 500m³ per day depending upon the inventory of the upstream leachate catchment. Over the trial period, SAFF was successful in removing ≥98.7% PFOS (C8), ≥99.7% PFOA (C8), and ≥98.8% PFHxS(C6) from the feed stream without using absorbent media or chemical amendment consumables. However, the removal efficiency was relatively low for short-chain PFASs.

Life cycle assessment (LCA) and life cycle costing analysis (LCCA) are methodologies for quantifying and comparing the systems-level environmental impacts and associated economic costs, respectively, of a product or process over a defined life cycle. Recent LCA studies have reported the toxicity of PFASs plumes, alternative surfactants to PFASs, membrane bioreactor treatment of PFASs in landfill leachate, and a hybrid ion exchange-electrochemical oxidation treatment trains. While these studies performed the environmental impacts in the lab scale, this study shows the LCA and LCCA results of the one-stage and three-stage foam fractionation system treating PFASs-contaminated landfill leachate in full scale. Sensitivity analyses were then conducted to identify the system parameters and design decisions that are expected to have

significant effects on the life cycle impact. Moreover, the scale-up analysis section discussed the life cycle impact on the functional unit at various system scales.

5.2 Methods

5.2.1 Goal and Scope Definition

This LCA and LCCA study aims to analyze the environmental impacts and economic costs of remediation of PFAS-containing landfill leachate with one-stage and three-stage FF systems. First, LCA models of one-stage and three-stage FF systems are built to assess the environmental impacts (Fig. 5.1, dashed lines) of treating PFAS-contaminated landfill leachate. The environmental impacts of the two systems are calculated and compared. Process contribution analysis is then performed to understand the key operational variables. Afterward, the economic costs for the two systems are calculated and compared in the life cycle of 30 years. There is only one vessel in the one-stage FF system (Fig. 5.1). Compressed air flows from the bottom, and the high-concentration PFAS foam is generated during this aeration process. Then the foam (20% volume of the input LL) will be extracted by the vacuum from above and sent to the disposal unit, which is hazardous waste incineration. The 80% volume effluent comes out to be the clear treated LL. In the three-stage FF system, there are three vessels. The flow mode is designed to be a semi-batch multi-stage, optimizing separation and concentration steps within a single system.¹⁷ After the FF treatment in the 1st stage, the foam extracted by the vacuum from above (around 20% volume of the input LL) goes to the vessel in the 2nd stage (green line in Fig. 5.2). ¹⁷ Then, the foam (0.0154% volume of the input LL) produced in the 2nd stage goes to the 3rd stage for further treatment. 17 At the same time, the LL bottom solutions of 2nd stage and the 3rd stage goes back to the vessel in the 1st stage (orange lines in Fig. 5.2). Finally, a highly

concentrated PFASs aqueous liquid waste forms and will be treated as hazardous waste by incineration, whose volume is around 0.00006% volume of the initial input LL.¹⁷

The functional unit chosen for the analysis is treating 1000 m³ PFASs-contaminated landfill leachate. The design flow of the FF treatment plant is determined to be 1 MGD (million gallon per day). The overall system boundaries are shown in the Figure 1. The diagram includes the one-stage and three-stage FF treatment systems.

5.2.2 Life Cycle Assessment Methodology

Life cycle assessment (LCA) is an environmental impact assessment method that considers the material and energy interactions over the life cycle of a product or process that impacts the environment. The LCA methodology in this analysis follows international guidelines set by the International Standards Organization (ISO) in ISO 14040-14044. These guidelines set the framework for LCA and consist of four major components: goal and scope definition, life cycle inventory (LCI), life cycle impact assessment (LCIA), and interpretation of results.

In this study, SimaPro 7.0 software was used to build the LCA model with the Eco-invent and USA INPUT OUTPUT 2002 database to perform the environmental impact assessment using EPA's Tool for Reduction and Assessment of Chemicals and Other Environmental Impacts (TRACI) methodology.

LCIA is a qualitative and quantitative assessment of the environmental impact of a process based on the resource, energy consumption data, and various emission data. A total of 7 environmental impact categories were considered in this study, including ozone depletion (OD, CFC-11 eq), global warming potential (GWP, kg CO₂ eq), acidification (AD, mol H⁺ eq), marine eutrophication (ME, kg N eq), smog formation (SF, kg O₃ eq) and ecotoxicity (ET, CTUe),

carcinogens (C, CTUh), non-carcinogens (NC, CTUh), and respiratory effects (RE, kg PM₁₀ eq) (Table S1).

5.2.3 Life Cycle Cost Analysis (LCCA)Methodology

The life cycle inventory for the FF remediation system was also used to estimate costs for treatment, both in actual dollars and on a per-unit-volume basis (\$ per 1000 m³ treated). Unit costs include capital construction costs, operation costs (electricity used for vacuuming foam and generating compressed air), and maintenance costs. The costs for capital construction and maintenance (labor) were estimated using the EPA-derived work breakdown structure (WBS) for multi-stage bubble aeration treatment.²² The operation cost (electricity) was estimated based on a previous energy report for a wastewater treatment plant.²³

In a 30-year life cycle, the inflation-adjusted initial costs, maintenance and rehabilitation costs, and salvage value being used can be indicated with the Net Present Value (NPV). The NPV Eq. (1) can be applied to the FF treatment system case,

$$NPV = Initial\ Construction\ Cost + \sum_{K=1}^{N} (Operation\ Cost + Maintenance\ Cost) [rac{1}{(1+i)^{k}}] - Salvage\ Vaue\ [rac{1}{(1+i)^{N}}] (1)$$

where: Initial construction cost and maintenance cost derive from the EPA WBS model; operation cost is calculated based on the electricity used for compressed air and vacuum; N = analysis period in years (N=30 in this study); i = discount rate in percent (i=9.8% in this study); $k = \text{number of years from the initial construction to the } K^{th} \text{ expenditure}$;

5.2.4 Inventory Data Collection

The LCA inventory data collection includes capital construction, vacuum electricity, compressed air generation, and hazardous waste disposal (Table 5.2). The LCCA inventory data collection includes all of the LCA inventory items and maintenance costs.

The capital construction cost used in the inventory is built from the EPA-derived Work Breakdown Structure (WBS) for multi-stage bubble aeration treatment, seeing details in the Appendix section 1 for one-stage and section 5.2 for three-stage.²² Also, as for the scale-up analysis, the total construction cost is determined by Eq. (2).²³ Costs are correlated in terms of a base cost multiplied by a ratio of sizes raised to the power n. The Qis flowrate or capacity. In this study, n is determined to be 0.8 for foam fractionation (Woods, 2007).

$$Cost_{scales} = Cost_{ref} \times \left(\frac{Q_{scaled}}{Q_{ref}}\right)^n (2)$$

The operation parameters are referenced in Smith et al.'s pilot study and Burns et al.'s full-scale field study.¹⁷ The operational input for FF is mainly from blowing the compressed air, which can be calculated using the Air-Water Ratio (AWR). The AWR was assumed to be 4.3, according to Smith's pilot study.¹⁰ The foam flow in the three-stage FF system was determined by the commercial filed FF study of Burns et al., which as described in the section 2.1.¹⁰ The electricity input was estimated based on a previous municipal wastewater treatment plant energy evaluation report for Tonawanda town.²³ According to the EPA-WBS model, the average electricity price for water treatment was estimated to be \$0.11.²² The maintenance cost was estimated using the EPA-derived work breakdown structure (WBS) for multi-stage bubble aeration treatment.²²

5.3 Results and Discussion

This section analyzes the environmental impact and economic cost assessment results of the one-stage and three-stage FF treatment systems following the methodology described in Section 5.2. All impact assessment results are presented per functional unit, treating 1000 m³ PFASs-contaminated landfill leachate.

5.3.1 Environmental Impact Assessment Analysis

5.3.1.1 Environmental Impact Assessment Results and Comparison

The LCA results show that the one-stage FF system causes a more significant total environmental impact than the three-stage FF system in all impact categories (Table 5.3). Table S2 and Table S3 also show the breakdown impact values from the inventory items for the one-stage and the three-stage FF system, respectively. For the one-stage FF system, treating 1000 m³ PFASs-contaminated landfill leachate causes the most significant environmental impact regarding ecotoxicity (1380 CTUe) and the second highest impact of global warming potential, 818 kg CO₂ eq. As for the three-stage FF system, the treatment system causes the highest ecotoxicity impact (700 CTUe) and the second highest global warming potential impact (402 kg CO₂ eq.) (Table S3). The results indicate that the environmental impact caused by hazardous waste disposal of the one-stage system is much higher than the three-stage system, which is shown in the volume of the hazardous waste in the one-stage system (200 m³) compared to the three-stage system (0.0006 m³).

5.3.1.2 Contributions to Impacts

Figure 5.3 shows the relative contributions to the environmental impact of each inventory item, including capital construction, electricity for vacuum, compressed air, and hazardous waste disposal. Hazardous waste disposal and compressed air contribute significantly to the one-stage FF system. The hazardous waste also contributes the most regarding ozone depletion, global warming potential, carcinogens, and ecotoxicity impact. The compressed air contributes most to smog formation, acidification, marine eutrophication, non-carcinogens, and respiratory. However, the disposal has little environmental impact on three-stage FF system because there is

little hazardous waste foam at the end. In contrast, compressed air contributes most in all impact categories (>90% except for the ozone depletion category).

5.3.1.3 Impact Normalization and Interpretation

Unit normalization is employed to facilitate direct comparison among environmental impact categories of varying magnitudes. This standardization utilizes 'impact per person per year' data aggregated for the average American citizen in a given year (2008); the analysis uses this to divide the raw impact quantity in each category thereby yielding units presented in "person-years". This method enables comparison across all categories.

Table 5.4 presents impact data of all four remediation systems for all impact categories normalized in terms of these person-year units.²⁵ Presenting the data in this way reveals that acidification is the most impactful category relative to the average US emissions.

Among all categories, acidification exhibits the highest relative impact when normalized against average U.S. emissions. This suggests that acidification may serve as a critical indicator for identifying and optimizing environmentally sensitive parameters in system design and operation. Furthermore, the normalized comparison shown in Figure S1 highlights that the three-stage FF system consistently results in lower environmental impacts across all categories compared to the one-stage system. These results further support the environmental advantages of the three-stage configuration, particularly when considering long-term sustainability goals.

5.3.1.4 Sensitivity Analysis for Environmental Impact

The life cycle assessment presented above compared the environmental impacts of two full-scale foam fractionation (FF) systems. However, operational parameters, particularly those related to energy inputs, can significantly influence environmental performance. To identify the most impactful design and operational factors, a sensitivity analysis was conducted.

Among all inputs, compressed air generation emerged as a key contributor to environmental impacts in both the one-stage and three-stage FF systems. Due to its central role in the aeration process, variations in the power requirements and operating pressure of air compressors can substantially affect emissions across multiple impact categories.

To explore this sensitivity, we analyzed the unit environmental impacts of compressed air generation under various power and pressure conditions, referencing data for systems operating at >30 kW and 6 bar gauge as the baseline. The impacts were then normalized using "person-year" metrics for comparability. Figure S4 illustrates the normalized environmental impact across scenarios, while raw data are provided in Table S4.

The analysis showed that increasing compressor power and pressure correlates with a notable rise in impact, especially in the categories of carcinogens, non-carcinogens, and ecotoxicity. These categories exhibited the greatest sensitivity to changes in compressed air generation parameters, highlighting the importance of optimizing aeration efficiency in system design and operation. Overall, the results emphasize that minimizing energy intensity in compressed air production is critical for reducing the environmental footprint of FF-based PFAS treatment systems.

5.3.2 Life Cycle Costing Assessment Analysis

5.3.2.1 Life Cycle Costing Assessment Results and Comparison

The LCCA results for the one-stage and three-stage FF systems are in Table S4. The unit costs were calculated using NPV equation in a 30-year life cycle according to the methodology described in section 5.2.3. The economic cost assessment included capital construction cost, operation cost (electricity), and maintenance cost (labor).

The comparison of the life cycle costing between the one-stage FF system and the three-stage FF treatment system is shown in Figure 5.4. The maintenance cost for the three-stage FF system is 66% more than the one-stage FF system with the functional unit. However, the operation cost for the three-stage FF system has a smaller difference, which cost 25% more than the one-stage FF system. The capital construction cost for the three-stage FF system is around 32% more than the one-stage FF system with the functional unit. These results indicate that while the three-stage system offers notable environmental benefits, it incurs a higher total life cycle cost. This trade-off should be considered when evaluating full-scale implementation scenarios.

5.3.2.2 Sensitivity Analysis for Economic Cost

In addition to environmental impacts, variations in system design can significantly affect the overall economic cost of foam fractionation (FF) treatment systems. To evaluate these influences, a sensitivity analysis was conducted focusing on capital construction costs, which represent a substantial portion of the life cycle cost.

The capital cost is determined by several design choices, including the number and size of vessels, pumps, blowers, piping, and control systems. To assess how different design references affect cost estimation, we compared values from four sources for treating 1000 m³ of PFAS-contaminated landfill leachate using a one-stage FF system: EPA WBS model (2022): \$37.31, Woods (2007): \$18.31, Westech (2016): \$21.90, and Minnesota Pollution Control Agency (2023): \$161.6. These results, summarized in Table S6, highlight a variation of nearly 50% depending on the design reference used. Such a spread demonstrates the sensitivity of capital cost estimates to assumed equipment specifications and data sources.

The analysis suggests that capital cost is a major driver of total system cost, and careful selection of design assumptions is essential for accurate life cycle costing. For real-world applications, site-specific design data should be incorporated whenever possible to improve cost accuracy²⁶.

5.3.3 Scale-up Analysis

To evaluate the scalability of foam fractionation (FF) systems for PFAS remediation, we analyzed how the system size affects the global warming potential (GWP) per functional unit (1000 m³ treated). This section presents scale-up results for both one-stage and three-stage FF systems, based on operational and economic data from full-scale case studies.

According to the analysis above in section 3.1, the overall environmental impact is largely due to the capital construction cost, vacuum and compressed air electricity, and hazardous waste disposal. The capital construction impact was scaled using the power law equation for cost estimation in the Equation 2:

$$Cost_{scales} = Cost_{ref} \times \left(\frac{Q_{scaled}}{Q_{ref}}\right)^n (2)$$

Where: Q is the flowrate (scale), n=0.8 (scaling exponent), and Cost_{ref} is the capital cost at 1 MGD (baseline). The GWP contribution from capital construction is then:

$$GWP_{captial} = Cost_{scaled} \times 0.61 (kg CO2 eq/\$) (3)$$

The total GWP for each system includes vacuum energy, compressed air, and incineration for one-stage and three-stage FF system as follow:

$$GWP_{1-stage} = 0.61 \times C_1 \times S^n + 12.12 + (0.715 \times AWR \times 1000) + \left(2.42 \times \frac{1000}{x}\right) (4)$$

$$GWP_{3-stage} = 0.61 \times C_3 \times S^n + 14.55 + (0.715 \times AWR \times 1000) \times \left(1 + \frac{1}{x} + \frac{1}{y}\right) + \left(2.42 \times \frac{1000}{z}\right) (5)$$

Where: $C_1 = 22.12$ and $C_3 = 29.30$ (capital costs at baseline); S is the scale factor (e.g., 2 for 2 MGD); AWR = air-water ratio (unitless); V_{waste} = hazardous waste volume (m³); 0.715 kg CO₂ eq./m³ is the emission factor for compressed air; 2.42 kg CO₂ eq./m³ is the emission factor for incineration; x, y, z are enrichment factors for foam volume reduction per stage.

5.3.4 Disposal Methods Alternative

In addition to incineration, electrochemical oxidation (EO) has recently emerged as a promising method for destroying PFASs in the concentrated foam solution generated by foam fractionation.²⁷When EO is used following the FF process, the global warming potential (GWP) per 1000 m³ of treated landfill leachate can be estimated for both the one-stage and three-stage systems as a function of system scale and air-water ratio (AWR). The equations below estimate GWP (in kg CO₂ eq.) for each system:

$$GWP_{1-stage+EO} = 0.61 \times C_1 \times S^n + 12.12 + 0.715 \times AWR \times 1000 + EE/O \times OM \times \left(\frac{1000}{x}\right) \times 0.714$$
 (6)

$$GWP_{1-stage+EO} = 0.61 \times C_3 \times S^n + 14.55 + 0.715 \times AWR \times 1000 \times (1 + \frac{1}{x} + \frac{1}{y}) + EE/O \times OM \times \left(\frac{1000}{Z}\right) \times 0.714 \quad (7)$$

EE/O (kWh/m³) is the electric energy required to degrade PFASs by one order of magnitude in a unit volume; *OM* is the order of removal; 0.714 (kg CO₂ eq./kWh) is the GWP of unit electricity (1 kWh) based on the energy mix of southeast U.S.

For both FF systems, the primary difference between GWP calculations lies in the disposal method. To assess the conditions under which EO becomes more sustainable than incineration, we analyzed the threshold at which the EO-related GWP exceeds that of incineration. It was determined that incineration is more favorable when EE/O >3.39 kWh/m³ for

one log-order removal. Since many EO processes currently exceed this energy intensity, incineration remains the lower-GWP option in most practical scenarios. However, advances in EO energy efficiency or renewable electricity sourcing could shift this balance in the future.

5.4 Conclusion

A sustainable solution to managing PFASs contamination requires understanding of the environmental impacts and costs. The life cycle environmental impact and life cycle costing of PFASs-contaminated landfill leachate treatment with foam fractionation were investigated based on reported one-stage and three-stage systems on a full scale.

- One-stage FF system has more significant environmental impacts than the three-stage FF system because the much larger volume of the hazardous waste formed in the one-stage system (200 m³) than the three-stage system (0.0006 m³) for treating 1000 m³ PFASs-contaminated landfill leachate.
- Hazardous waste disposal and compressed air contribute the most to the one-stage system. However, compressed air takes up the majority of the three-stage system's environmental impact categories.
- Comparing the LCA results, the three-stage FF system has around 82%~42% lower environmental impact than the one-stage FF system in all categories.
- Comparing the total cost of the one-stage FF system, the three-stage FF system
 costs 43% more than the functional unit. For details, the maintenance, operation,
 and capital construction costs for three-stage FF systems are 66%, 25%, and 32%
 more than the one-stage FF system, respectively.

The generation conditions of compressed air influence the environmental impacts,

especially on carcinogens, non-carcinogens, and ecotoxicity categories.

At various system scales, the life cycle GWP impact is determined by the air-water

ratio, enrichment factors, and the treatment capacity of the FF system.

ASSOCIATED CONTENT

Supporting Information: Environmental impact categories analyzed in this study; The unit

environmental impact of 1m³ compressed air generated under various power and pressure

conditions; The capital construction costs to treat 1000m³ PFAS-contaminated landfill leachate

in the one-stage FF system from various system design sources; The normalized environmental

impact between one-stage FF system and three-stage FF system; Normalized unit environmental

impacts of compressed air under different generation conditions (compressed air generated under

>30kW and 6 bar gauge is as the reference); Appendix: Input/output parameters and economic

cost data obtained using the Work Breakdown Structure-Based Cost Model for Multi-Stage

Bubble Aeration Drinking Water Treatment from the U.S. EPA website.

AUTHOR INFORMATION

Corresponding Author

Ke Li - College of Engineering, University of Georgia, Athens, GA 30602, United States;

Telephone: 1-706-542-2201; Email: lukeli@uga.edu

Authors:

Gengyang Li - College of Engineering, University of Georgia, Athens, GA 30602, United States;

Yifei Wang - College of Agricultural and Environmental Sciences, Griffin, GA 30223, United

States;

156

Qingguo Huang - College of Agricultural and Environmental Sciences, Griffin, GA 30223, United States;

Notes: The authors declare no competing financial interest.

ACKNOWLEDGMENT

This study was supported in part by U.S. Environmental Protection Agency Grant R840080. It has not been formally reviewed by EPA. The views expressed in this document are solely those of the authors and do not necessarily reflect those of the Agency. EPA does not endorse any products or commercial services mentioned in this publication.

Table 5.1: Summary of Foam Fractionation Operational Parameters for PFAS Removal from Landfill Leachate: Laboratory, Pilot, and Full-Scale Studies

References	Flow mode	Scale	Vessel volume (L)	Air flowrate (L/min)	Air- water- ratio	Aeration time (min)
Wang et al., 2023	batch	lab	0.20	5	50	2
Mcleaf et al.,	batch	lab	1.2 and 2.4	3.6, 7.1, 15	15~180	5, 10, 20, 40, and 60
	continuous	· -	2.4	15	31~124	5,10, and 20
Robey et al., 2020	batch	lab	1	2.6	N	N
Smith et al., 2022	continuous	pilot	300	5~20	2.2~13	10, 15, 20 and 30
Burns et al., 2022	semi- continuous	full	2500	N	N	21

Table 5.2. Inventory data and environmental database used for one-stage FF system and three-stage FF system.

Inventory Item	One-stage FF	Three- stage FF	Units	Item Name in SimaPro	Database
Capital construction	22.12*	29.30*	\$	Other nonresidential structures	USA INPUT OUTPUT 2002
Electricity for vacuum	15.72	18.87	kWh	Electricity, medium voltage, at grid, US/U	Eco-invent
Compressed	4300	5161	m ³	Compressed air, optimized generation, >30kW, 6 bar gauge, at compressor/RER	Eco-invent
Hazardous waste disposal	200	0.0006	m ³	Disposal, hazardous waste, 25% water, to hazardous waste incineration/kg/CH	Eco-invent

^{*} The capital construction cost was converted to the currency value in 2002 to perform LCA analysis with SimaPro software.

Table 5.3. The total environmental impact results for one-stage and three-stage FF system with the functional unit.

Impact	One-stage FF	Three-stage FF	Unit
category	system	system	Omt
OD	5.60E-05	3.56E-05	kg CFC-11 eq
GWP	8.18E+02	4.02E+02	kg CO ₂ eq.
SF	2.15E+01	1.62E+01	kg O ₃ eq
AD	1.11E+02	9.60E+01	mol H ⁺ eq
ME	3.84E+00	2.97E+00	kg N eq
C	1.09E-04	4.01E-05	CTUh
NC	1.24E-04	9.66E-05	CTUh
RE	4.89E-01	4.37E-01	$kg \ PM_{10} \ eq$
ET	1.38E+03	7.00E+02	CTUe

Table 5.4. The environmental impact normalized values for the one-stage and three-stage FF treatment systems (person-years per1000m³ treated)

Impact category	One-stage	Three-stage	Unit
OD	0.00035	0.00022	person-years
GWP	0.034	0.017	person-years
SF	0.015	0.012	person-years
AD	12.20	10.54	person-years
ME	1.74	1.35	person-years
C	2.15	0.79	person-years
NC	0.12	0.093	person-years
RE	0.20	0.18	person-years
ET	0.13	0.064	person-years

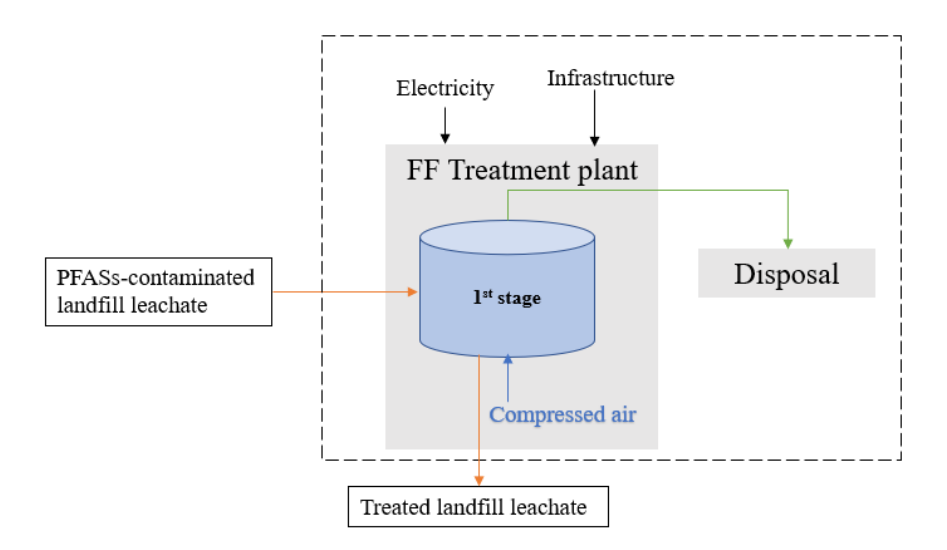


Figure 5.1. The system boundary of the one-stage FF system for PFASs treatment; the orange line is the landfill leachate flow; the green line is the foam flow; the blue line is the compressed air flow.

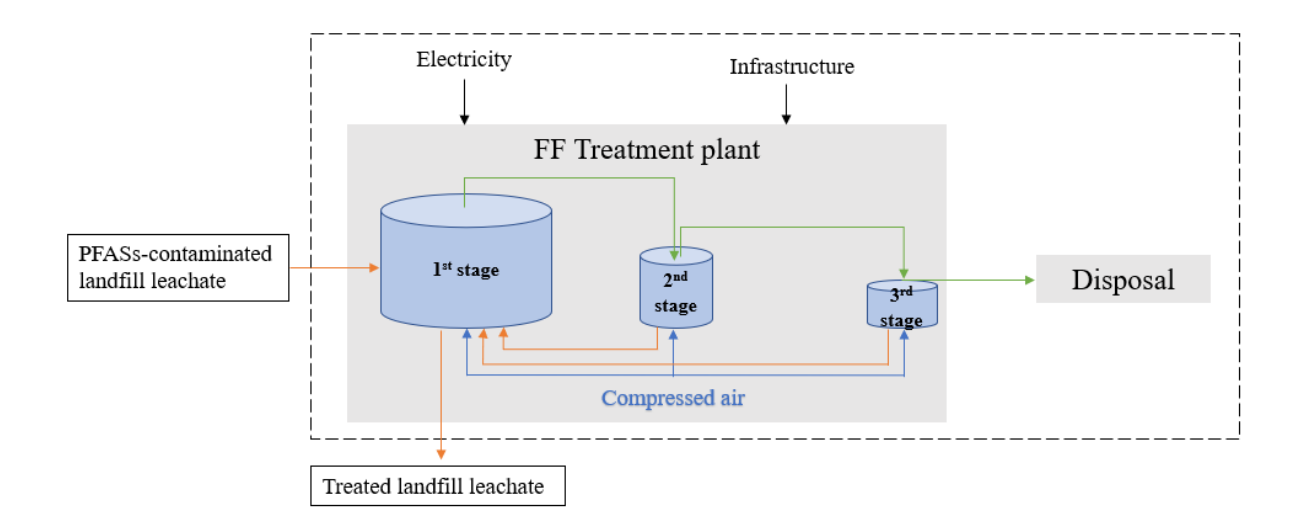


Figure 5.2. The system boundary of the three-stage FF system for PFASs treatment; the orange line is the landfill leachate flow; the green line is the foam flow; the blue line is the compressed air flow.

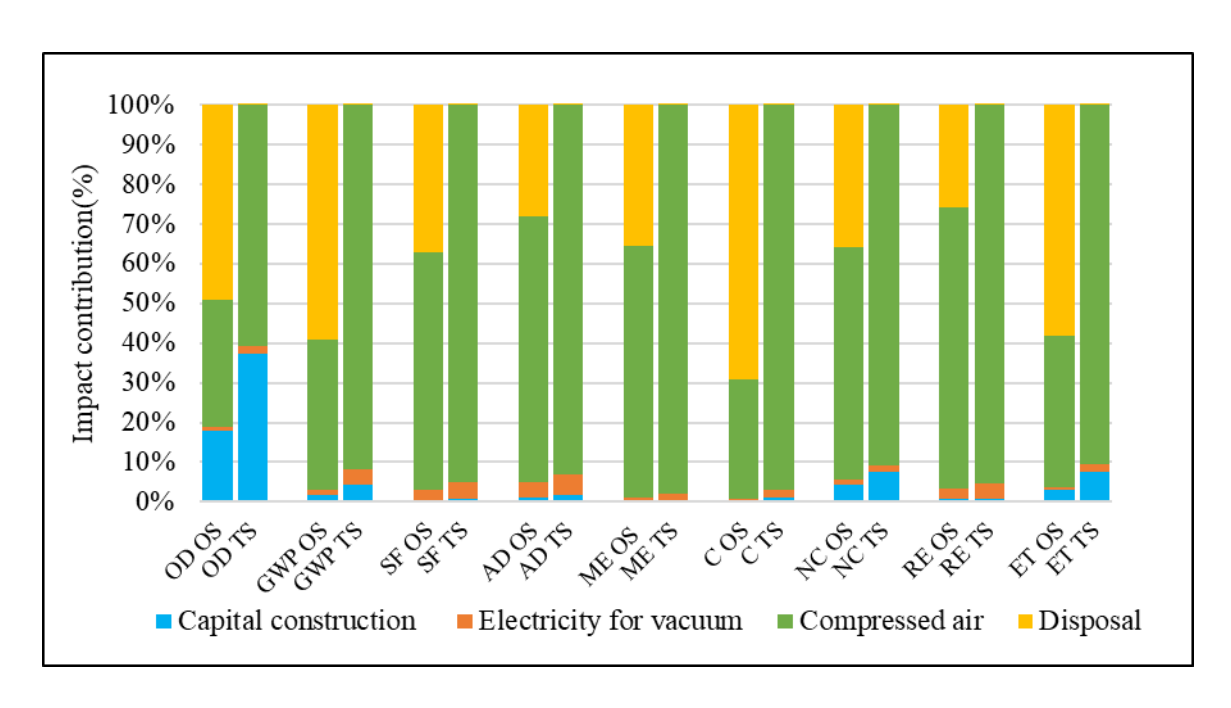


Figure 5.3. Relative contributions of each inventory item to the total environmental impacts in the one-stage (OS) and three-stage (TS) FF treatment system (Note: OD-ozone depletion, GWP-global warming potential, SF-smog formation, AD-acidification, ME-marine eutrophication, C-carcinogens, NC-non-carcinogens, RE-respiratory, ET-ecotoxicity)

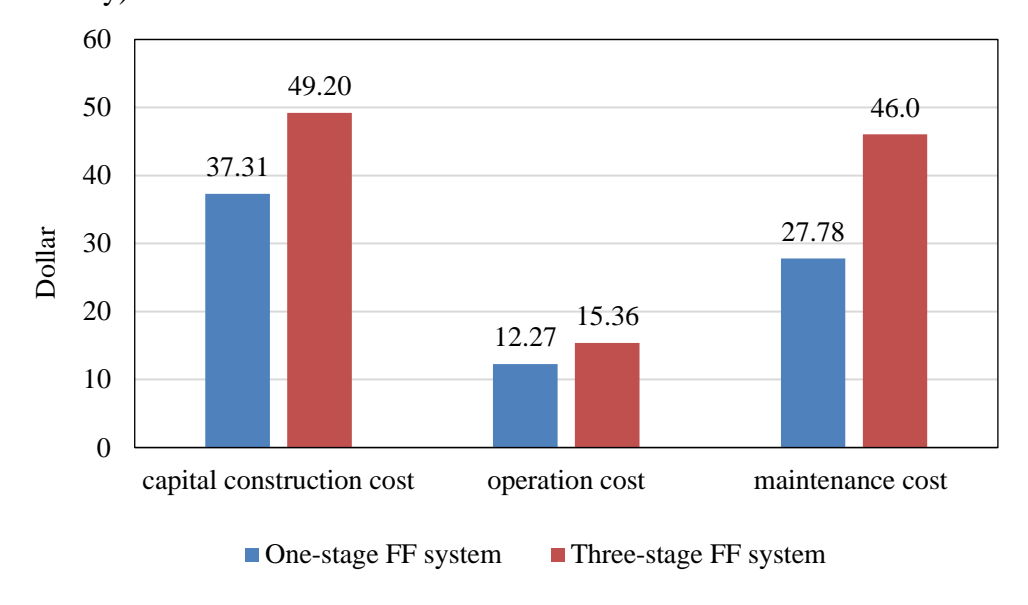


Figure 5.4. The life cycle costing comparison of one-stage FF system and three-stage FF treatment system

5.5 References

- Rozen, S., & Filler, R. (1985). Alpha-Fluorocarbonyl Compounds and Related Chemistry. *Tetrahedron*, 41(7), 1111-1153. https://doi.org/Doi 10.1016/S0040-4020(01)96514-7
- 2) Crone, B. C., Speth, T. F., Wahman, D. G., Smith, S. J., Abulikemu, G., Kleiner, E. J., & Pressman, J. G. (2019). Occurrence of Per- and Polyfluoroalkyl Substances (PFAS) in Source Water and Their Treatment in Drinking Water. *Crit Rev Environ Sci Technol*, 49(24), 2359-2396. https://doi.org/10.1080/10643389.2019.1614848 DOE. (2015). *Climate Change and the U.S. Energy Sector: Regional vulnerabilities and resilience solutions*.
- 3) Rahman, M. F., Peldszus, S., & Anderson, W. B. (2014). Behaviour and fate of perfluoroalkyl and polyfluoroalkyl substances (PFASs) in drinking water treatment: A review. *Water Research*, *50*, 318-340. https://doi.org/10.1016/j.watres.2013.10.045
- 4) Hori, H., Hayakawa, E., Einaga, H., Kutsuna, S., Koike, K., Ibusuki, T., Kiatagawa, H., & Arakawa, R. (2004). Decomposition of environmentally persistent perfluorooctanoic acid in water by photochemical approaches. *Environmental Science & Technology*, 38(22), 6118-6124. https://doi.org/10.1021/es049719n
- 5) Wanninayake, D. M. (2021). Comparison of currently available PFAS remediation technologies in water: A review. *J Environ Manage*, 283, 111977. https://doi.org/10.1016/j.jenvman.2021.111977
- 6) Wang, Y., Kim, J., Huang, C.-H., Hawkins, G. L., Li, K., Chen, Y., & Huang, Q. (2022). Occurrence of per- and polyfluoroalkyl substances in water: a review. *Environmental Science: Water Research & Technology*, 8(6), 1136-1151. https://doi.org/10.1039/d1ew00851j
- 7) Ahrens, L. (2011). Polyfluoroalkyl compounds in the aquatic environment: a review of their occurrence and fate. *Journal of Environmental Monitoring*, *13*(1), 20-31. https://doi.org/10.1039/c0em00373e
- 8) Lee, Y. C., Wang, P. Y., Lo, S. L., & Huang, C. P. (2017). Recovery of perfluorooctane sulfonate (PFOS) and perfluorooctanoate (PFOA) from dilute water solution by foam flotation. *Separation and Purification Technology*, *173*, 280-285. https://doi.org/10.1016/j.seppur.2016.09.012
- 9) Wong, C. H., Hossain, M. M., & Davies, C. E. (2001). Performance of a continuous foam separation column as a function of process variables. *Bioprocess and Biosystems Engineering*, 24(2), 73-81. https://doi.org/10.1007/s004490100225
- 10) Smith, S. J., Wiberg, K., McCleaf, P., & Ahrens, L. (2022). Pilot-Scale Continuous Foam Fractionation for the Removal of Per- and Polyfluoroalkyl Substances (PFAS) from Landfill Leachate. *ACS ES&T Water*, 2(5), 841-851.
- 11) Robey, N. M., da Silva, B. F., Annable, M. D., Townsend, T. G., & Bowden, J. A. (2020). Concentrating Per- and Polyfluoroalkyl Substances (PFAS) in Municipal Solid Waste Landfill Leachate Using Foam Separation. *Environmental Science & Technology*, 54(19), 12550-12559. https://doi.org/10.1021/acs.est.0c01266
- 12) Vo, P. H. N., Buckley, T., Xu, X. Y., Nguyen, T. M. H., Rudolph, V., & Shukla, P. (2023). Foam fractionation of per- and polyfluoroalkyl substances (PFASs) in landfill leachate using different cosurfactants. *Chemosphere*, 310. https://doi.org/ARTN13686910.1016/j.chemosphere.2022.136869

- 13) Wang Y. F., Y. J., Ke Li, Qingguo Huang (2023). Foam Fractionation and Electrochemical Oxidation for the Treatment of Per- and Polyfluoroalkyl Substances (PFAS) in Environmental Water Samples. *Chemosphere*.
- 14) Buckley, T., Karanam, K., Xu, X. Y., Shukla, P., Firouzi, M., & Rudolph, V. (2022). Effect of mono- and di-valent cations on PFAS removal from water using foam fractionation A modelling and experimental study. *Separation and Purification Technology*, 286. https://doi.org/ARTN 12050810.1016/j.seppur.2022.120508
- 15) McCleaf, P., Kjellgren, Y., & Ahrens, L. (2021). Foam fractionation removal of multiple per- and polyfluoroalkyl substances from landfill leachate. *AWWA Water Science*, *3*(5). https://doi.org/10.1002/aws2.1238
- 16) Burns, D. J., Stevenson, P., & Murphy, P. J. C. (2021). PFAS removal from groundwaters using Surface-Active Foam Fractionation. *Remediation-the Journal of Environmental Cleanup Costs Technologies & Techniques*, *31*(4), 19-33. https://doi.org/10.1002/rem.21694
- 17) Burns, D. J., Hinrichsen, H. M., Stevenson, P., & Murphy, P. J. C. (2022). Commercial-scale remediation of per- and polyfluoroalkyl substances from a landfill leachate catchment using Surface-Active Foam Fractionation (SAFF (R)). *Remediation-the Journal of Environmental Cleanup Costs Technologies & Techniques*, 32(3), 139-150. https://doi.org/10.1002/rem.21720
- 18) Peyman Babashamsi, N. I. M. Y., Halil Ceylan. (2016). Evaluation of pavement life cycle cost analysis: Review and analysis. *International Journal of Pavement Research and Technology*.
- 19) Holmquist, H., Roos, S., Schellenberger, S., Jonsson, C., & Peters, G. (2021). What difference can drop-in substitution actually make? A life cycle assessment of alternative water repellent chemicals. *Journal of Cleaner Production*, 329. https://doi.org/ARTN12966110.1016/j.jclepro.2021.129661
- 20) Feng, D., Song, C., & Mo, W. (2021). Environmental, human health, and economic implications of landfill leachate treatment for per-and polyfluoroalkyl substance removal. Journal of environmental management, 289, 112558.
- 21) Li, G. Y., Dunlap, J., Wang, Y. F., Huang, Q. G., & Li, K. (2022). Environmental Life Cycle Assessment (LCA) of Treating PFASs with Ion Exchange and Electrochemical Oxidation Technology. *ACS ES&T Water*, 2(9), 1555-1564. https://doi.org/10.1021/acsestwater.2c00196
- 22) EPA, 2022 https://www.epa.gov/sdwa/drinking-water-treatment-technology-unit-cost-models
- 23) Malcolom Pirnie, I. (2005). https://doi.org/10.1021/acsestwater.2c00032 The New York State Energy Research
- 24) Woods. (2007). Rules of Thumb in Engineering Practice.
- 25) Ryberg, M., Vieira, M. D. M., Zgola, M., Bare, J., & Rosenbaum, R. K. (2014). Updated US and Canadian normalization factors for TRACI 2.1. *Clean Technologies and Environmental Policy*, *16*(2), 329-339. https://doi.org/10.1007/s10098-013-0629-z
- 26) Barr Engineering Co., H. a. S. (2023). Evaluation of Current Alternatives and Estimated Cost Curves for PFAS Removal and Destruction from Municipal Wastewater, Biosolids, Landfill Leachate, and Compost Contact Water. *Minnesota Pollution Control Agency*.

27) Wang, Y. F., Ji, Y. Q., Tishchenko, V., & Huang, Q. G. (2023). Removing per- and polyfluoroalkyl substances (PFAS) in water by foam fractionation. *Chemosphere*, 311. https://doi.org/ARTN 13700410.1016/j.chemosphere.2022.137004

CHAPTER 6

FIRST PRINCIPLES CALCULATION AIDED ELECTRODE MATERIALS DEVELOPMENT FOR PFAS DEGRADATION

6.1 Introduction

In recent years, first-principles density functional theory (DFT) calculations have been increasingly applied to investigate critical parameters related to the degradation of PFAS compounds. These include bond dissociation energy (BDE) of PFAS chains, adsorption energies of PFAS ions on anode surfaces, activation energies for PFAS and hydroxyl radicals, C–S bond cleavage, and the overpotential of the oxygen evolution reaction (OER) during water splitting (Eslamibidgoli & Eikerling, 2015). DFT is also a valuable tool for evaluating key electronic properties of electrode materials, such as the density of states (DOS), adsorption energies of molecules, and the formation energy of oxygen vacancies (Yamijala et al., 2022).

Adsorption energy is a basic yet crucial parameter that reflects the strength of interaction between a molecule and the electrode surface. A more negative adsorption energy suggests stronger chemical bonding, which promotes the adsorption and subsequent degradation of PFAS on the anode surface.

Oxygen vacancies are positively charged point defects formed by the removal of oxygen atoms, often compensated by local electron redistribution. The presence of oxygen vacancies can increase the density of active sites, enhance catalytic performance, and improve adsorption of organic molecules (Chen, 2019; Liu et al., 2022). The surface oxygen vacancy formation energy

(Eovac) is commonly used as a descriptor for the catalytic activity of metal oxides (Hinuma et al., 2021).

In the EO process, the rate-limiting step in the indirect path is assumed to be the electrochemical production of hydroxyl free radicals (*OH) at the electrode surface as an intermediate of water oxidation, which then reacts with organic contaminants in water. Essentially, the *OH mediated indirect oxidation process is also initiated by the DET of H₂O oxidation on the electrode surface. Overpotential η for OER (*OH \leftrightarrow O* + H*+ e*) can be an indicator. Higher η means it will be harder to oxidize *OH, hence suppressing OER and holding more *OH during the indirect PFAS oxidation (Man et al., 2011). The descriptor $\Delta G_{\rm O}$ – $\Delta G_{\rm OH}$ has been verified to well describe the trend of OER activities on various metal oxide surfaces (Huang et al., 2019).

Density of State (DOS) is a property in condensed matter physics that describes the number of states that are allowed per unit of energy range. It is represented by a function of energy called g(E), which is the number of states per unit volume in the energy range (E, E+dE). A higher DOS near the Fermi level implies more accessible states for electron transfer, which is essential for facilitating electrochemical reactions.

In this study, we calculate four key DFT-based descriptors—adsorption energy, oxygen vacancy formation energy (Eovac), OER overpotential, and DOS—for a series of titanium suboxide (TSO) electrodes using the VASP software. These properties serve as theoretical indicators of electrode performance in PFAS degradation. Specifically, stronger PFAS adsorption on the anode supports effective mass transfer, lower PFAS oxidation activation energy implies faster direct electron transfer, and higher OER overpotential suggests suppressed

radical consumption, thereby improving indirect oxidation efficiency (Li et al., 2021; Wang et al., 2022).

Despite the potential of DFT in elucidating degradation mechanisms and by-product formation, there remains a significant knowledge gap regarding the interaction between various PFAS species and anode materials during electrochemical oxidation. This work aims to address that gap and contribute to a more comprehensive understanding of PFAS degradation at the molecular level.

6.2 Methodology

6.2.1 Surface Models

The investigation of the Ti_4O_7 surface involved the initial construction of a $2 \times 2 \times 2$ supercell based on the Ti_4O_7 primitive cell (with lattice parameters: a = 5.34 Å, b = 6.99 Å, c = 7.21 Å). Subsequently, slabs of Ti_4O_7 were created on these supercells, specifically on the (110) facets. To separate the surface slab from its periodic duplicates, the z direction is added a vacuum layer in the depth of 20 Å.

The Nb, Ce, and Pd doping atomic percentage is determined by 5% according to the experiment information from Dr. Huang. So, 4 Ti atoms get changed to the doping element.

6.2.2 Geometry Optimization

The Vienna Ab initio Simulation Package (VASP) was utilized for all computations with the projector-augmented wave (PAW) potential (Hafner, 2007). Exchange—correlation effects is incorporated within the generalized gradient approximation (GGA), using the exchange-correlation functional by Perdew-Burke-Ernzerhof (PBE) (Hammer et al., 1999; Perdew et al., 1996). The Kohn—Sham one-electron wave functions is expanded in a plane wave basis set up to

an energy cutoff of 520 eV. Geometry optimization studies are terminated when all forces on ions are less than 0.05 eV Å-1. A global break condition of 10⁻⁴ eV per slab was adopted for achieving electronic self-consistency.

6.2.3 Absorption Energy Calculation

The adsorption sites for PFOS molecule were identified by evaluating the adsorption energy with one, two, or three O ions binding to Ti ions on the Ti₄O₇ (110) terrace surface. The configuration with the lowest adsorption energy was determined to be the most stable, involving two O ions of a PFOS molecule bridging two outermost Ti ions at the peak site. This configuration was designated as the reference, named PFOS-Ti₄O₇(110). To explore the impact of a doped metal element, a metal atom was placed adjacent to the aforementioned outermost Ti ions on the Ti₄O₇(110) surface. Subsequently, a PFOS molecule was adsorbed, with its two O ions connecting the two outermost Ti ions at the peak sites. This configuration was denoted as PFOS-Ti₄O₇(110)@M, where "M" represents the dopant metal element.

The adsorption energy is one of the most basic parameters for understanding the behavior of a molecule on a surface. It can be defined as the energy changing when a molecule is adsorbed on a solid surface. The formulas used to calculate the adsorption energy of a molecule on anode are described as follow:

$$E_a = E(Anode + molecule) - E(Anode) - E(molecule)$$
 (1)

Where, E(Anode + molecule) are the total energies for anode with the molecule adsorbed; E(Anode) and E(molecule) are anode system energy, and energy of a molecule isolated, respectively.

6.2.4 Oxygen Vacancy Formation Energy Calculation

For the oxygen vacancy formation energy (Eovac) calculation, Monkhorst–Pack grid of $1\times1\times1$ k-point is used to sample the Brillouin zone at Gamma point for geometry optimization.

$$E_{ovac} = E_{removed} - E_{slab} + \mu_o/2 \tag{2}$$

 $E_{removed}$: the energy of the slab with 1 O atom defect; E_{slab} : the energy of the original slab without O defect; μ_o : the chemical potential of O₂ gas.

6.2.5 Overpotential Modeling

In electrochemistry, the overall OER in solution involves four electron transfer steps. The corresponding anodic reaction mechanism has been described in detail by Rossmeisl, which can be sequentially written as follows:

$$2H_{2}O(l) + * \rightarrow H_{2}O + HO* + H^{+} + e^{-}(3)$$

$$\Delta G_{1} = \Delta G_{HO} - \Delta G_{H2O} - eU$$

$$H_{2}O(l) + HO* + e^{-} + H^{+} \rightarrow H_{2}O + O* + 2(H^{+} + e^{-})(4)$$

$$\Delta G_{2} = \Delta G_{O} - \Delta G_{HO} - eU$$

$$H_{2}O(l) + O* + 2(H^{+} + e^{-}) \rightarrow HOO* + 3(H^{+} + e^{-})(5)$$

$$\Delta G_{3} = \Delta G_{HOO} - \Delta G_{O} - eU$$

$$HOO* + 3(H^{+} + e^{-}) \rightarrow * + O2(g) + 4(H^{+} + e^{-})(6)$$

$$\Delta G_{4} = \Delta G_{O2} - \Delta G_{HOO} - eU$$

 ΔG_1 , ΔG_2 , ΔG_3 , ΔG_4 were the free energy changes of the four reaction steps in OER. The symbol "*" represented the active sites on the exposed surface of the catalyst. In addition, the key intermediates (HO, O, HOO) adsorbed at active sites were written as "HO*", "O*" and "HOO*". The free energy change ΔG was calculated by a method proposed by Nørskov, which can be expressed by formula (7):

$$\Delta Gi = \Delta E + \Delta ZPE - T\Delta S + \Delta G_U + \Delta G_{pH}$$
 (7)

When PH = 0, T = 298 K, P = 1 bar, and the electrode potential (U) was zero, the chemical potential for (H⁺ + e⁻) was equal to that of $1/2H_2$ gas phase. ΔE was the adsorption energies of adsorbed intermediates obtained from DFT computations. The changes of zero-point energy (ΔZPE) were calculated by the formula (8), which reflected the relationship between zero-point energy and vibration frequency.

$$ZPE = 1/2 \sum hv$$
 (8)

The changes in entropy ΔS were calculated from the standard entropy table of gas-phase molecules. In addition, $\Delta G_U = -eU$, where U was the potential of the electrode relative to the standard hydrogen electrode. In this work, the calculation condition was set to pH = 0, thus the correction value ΔG_{pH} can be ignored. Moreover, the thermodynamic overpotential η^{OER} of the electrocatalyst was determined by Eq.

$$G^{OER} = max \{ \Delta G1, \Delta G2, \Delta G3, \Delta G4 \}$$
 (9)
$$\eta^{OER} = G^{OER} / e - 1.23 V$$
 (10)

The zero-point energy (ZPE) corrections and entropic energy contributions calculated for gaseous molecules and reactive species on Ti₄O₇ (110) surface were listed in Table 6.1. For the adsorbed solid surface, the entropic energy contributions are usually small and they were neglected here. According to the chemical reaction equations of OER, the corrected values of the formation energies for the adsorbed HO*, O*, HOO* were calculated to be 0.375, 0.04, and 0.43, respectively.

6.2.6 Density of State

The first step involved the full structural relaxation of the electrode material to obtain a stable geometry. This was achieved by allowing both the atomic positions and cell parameters to

relax until the forces on all atoms were less than 0.02 eV/Å. The Perdew–Burke–Ernzerhof (PBE) generalized gradient approximation (GGA) was used for the exchange-correlation functional, and a plane-wave energy cutoff of 500 eV was applied. A Monkhorst–Pack k-point mesh was selected based on the size of the unit cell to ensure accurate Brillouin zone sampling.

Following optimization, a static Self-Consistent Field (SCF) calculation was performed to compute the converged charge density. In this step, all atomic positions were fixed and no further ionic relaxation was allowed, which was specified by setting NSW = 0 in the INCAR file. This ensures that the charge density and potential are fully self-consistent with the optimized atomic structure, providing a reliable basis for subsequent electronic structure analysis.

Finally, the electronic density of states was calculated using a denser k-point grid with a high number of energy points to achieve fine energy resolution. The number of DOS points was set to NEDOS = 3000 to generate a smooth and detailed DOS profile. The total and partial DOS were extracted from the DOSCAR and PROCAR files, respectively, and plotted to analyze the electronic properties of the electrode material. The Fermi level was set as the energy reference (E = 0 eV).

6.3 Results and Discussion

6.3.1 Absorption Energy Results

Table 6.2 presents the calculated adsorption energies (Ea) of H₂O, PFOA, and PFOS molecules on pristine Ti₄O₇ and doped Ti₄O₇ electrodes, including Nb-, Ce-, and Pd-substituted structures. Adsorption energy is a key indicator of the interaction strength between the adsorbate and electrode surface, with more negative values signifying stronger binding affinity.

For H₂O adsorption, all doped electrodes showed stronger interaction compared to pristine Ti₄O₇ (-0.54 eV). Among the doped electrodes, Ce-Ti₄O₇ exhibited the strongest H₂O adsorption (-1.23 eV), followed by Pd-Ti₄O₇ (-0.93 eV) and Nb-Ti₄O₇ (-0.90 eV), suggesting enhanced hydrophilicity and potential for improved interfacial reactivity.

Regarding PFOA, the adsorption energies were consistently high across all electrodes (ranging from -5.35 to -5.81 eV), indicating strong chemisorption of PFOA to the surface. Nb-Ti₄O₇ showed the highest adsorption energy for PFOA (-5.81 eV), slightly higher than the pristine (-5.73 eV) and Ce-doped surfaces (-5.73 eV), while Pd-Ti₄O₇ exhibited the weakest interaction (-5.35 eV).

For PFOS, the Ce-doped Ti₄O₇ electrode demonstrated the strongest adsorption (–9.36 eV), significantly greater than both the pristine (–7.72 eV) and the other doped structures. This suggests Ce doping may provide a superior active site for PFOS adsorption and subsequent degradation. Pd-Ti₄O₇ and Nb-Ti₄O₇ had slightly stronger and weaker PFOS adsorption compared to the pristine, respectively.

In summary, Ce-doping considerably enhances both water and PFOS adsorption on the Ti₄O₇ surface, which may improve electrochemical degradation performance. These results indicate the promising potential of Ce-Ti₄O₇ as an electrode material for PFAS treatment applications.

6.3.2 Oxygen Vacancy Formation Energy Results

Table 6.2 also summarizes the calculated oxygen vacancy formation energies (Eovac) for pristine Ti₄O₇ and Ti₄O₇ surfaces doped with Nb, Ce, and Pd. These values reflect the energy required to remove a surface oxygen atom, which directly relates to the material's ability to form

oxygen vacancies—an important factor in enhancing catalytic activity during electrochemical oxidation processes.

The pristine Ti₄O₇ surface shows the highest Eovac at 6.31 eV, indicating strong oxygen binding and limited natural formation of oxygen vacancies. Upon doping, all three transition metals reduce the vacancy formation energy, suggesting improved catalytic potential. Nb doping slightly lowers Eovac to 6.11 eV, indicating modest enhancement in oxygen vacancy formation. Ce doping further reduces Eovac to 5.91 eV, showing greater potential for boosting catalytic reactivity. Pd doping results in the most significant reduction, with Eovac dropping to 3.23 eV, suggesting a much more favorable formation of oxygen vacancies and, therefore, a higher density of reactive sites.

These results suggest that Pd-doped Ti₄O₇ may offer the best catalytic performance among the tested materials due to its enhanced ability to generate oxygen vacancies, which can support greater production of reactive oxygen species (e.g., •OH) for PFAS degradation. Ce and Nb dopants also show promise by moderately improving vacancy formation compared to the pristine surface.

6.3.3 Overpotential of OER Results

Figure 6.1 presents the calculated overpotentials for the oxygen evolution reaction on pristine Ti₄O₇ and doped Ti₄O₇ surfaces with Nb, Ce, and Pd. The OER overpotential η^{OER} is a critical descriptor for assessing a material's ability to resist unwanted oxidation side reactions, especially the oxidation of hydroxyl radicals (•OH) that are vital for indirect PFAS degradation.

The results reveal that pristine Ti₄O₇ exhibits the lowest η^{OER} of 1.01 V, indicating a relatively low energy barrier for OER, which may lead to the undesired consumption of •OH and lower oxidative efficiency for PFAS. Nb-doped Ti₄O₇ increases the overpotential to 1.46 V,

suggesting moderate suppression of OER and improved •OH retention. Ce-doped Ti₄O₇ shows a significantly higher η^{OER} of 3.77 V, indicating strong resistance to OER and, therefore, the highest potential to preserve reactive •OH species during PFAS degradation. Pd-doped Ti₄O₇ also shows elevated suppression of OER with an η^{OER} of 2.61 V, ranking second after Ce doping.

Overall, Ce and Pd dopants substantially suppress the OER process, thereby favoring the accumulation of hydroxyl radicals needed for efficient indirect PFAS oxidation. In contrast, the pristine and Nb-doped Ti₄O₇ surfaces are more susceptible to OER, which could compete with PFAS degradation pathways. These findings highlight Ce_Ti₄O₇ as the most promising candidate for electrochemical PFAS destruction, due to its high resistance to OER and enhanced retention of reactive species.

6.3.4 Density of State Results

Figure 6.2 presents the total density of states (DOS) of pristine Ti₄O₇ and Ti₄O₇ doped with Nb, Ce, and Pd. These DOS plots offer critical insights into the electronic structure modifications induced by doping, which directly impact the material's electrochemical activity and its potential for PFAS degradation.

Pristine Ti_4O_7 exhibits a semiconducting character with a narrow band gap around the Fermi level (E = 0 eV). The conduction and valence bands are separated by a relatively low density of states at the Fermi level, suggesting moderate electrical conductivity. Nb-doped Ti_4O_7 shows a substantial increase in DOS near the Fermi level, effectively closing the band gap. This metallization effect indicates improved electrical conductivity and enhanced charge transfer capability. Ce-doped Ti_4O_7 maintains a similar band structure to pristine Ti_4O_7 but introduces localized states just above the Fermi level. The DOS near the Fermi level is moderately increased, suggesting an improvement in electrical conductivity. Pd-doped Ti_4O_7 demonstrates

the most significant alteration in electronic structure, with a very high DOS centered directly at the Fermi level. This confirms a transition to strong metallic behavior. The broad distribution states across the Fermi level implies superior electron mobility, which can enhance electrochemical reactivity and facilitate direct electron transfer to PFAS molecules during degradation.

In summary, doping Ti₄O₇ with transition metals modifies its electronic properties in distinct ways. These changes suggest that Pd-doped Ti₄O₇ holds the highest promise as an advanced anode material for electrochemical PFAS degradation due to its superior electronic conductivity and favorable charge transport characteristics.

6.4 Conclusion

This chapter presented a comprehensive investigation into the application of first-principles density functional theory (DFT) calculations to guide the development of advanced electrode materials for electrochemical oxidation (EO) of per- and polyfluoroalkyl substances (PFAS). By integrating computational modeling with mechanistic insights, the study elucidated how key parameters—such as adsorption energy, oxygen vacancy formation energies (Eovac), oxygen evolution reaction (OER) overpotential, and density of states—inform the design of electrode materials that enhance PFAS degradation performance.

The results demonstrate that Magnéli phase titanium suboxide (Ti₄O₇) and its doped or composite variants exhibit strong potential as cost-effective, efficient, and durable anodes for EO processes. These materials not only provide favorable electron transfer properties and adsorption capacities but also suppress competitive OER pathways, thereby preserving hydroxyl radicals critical for indirect PFAS degradation.

Despite the promise of DFT-guided electrode development, several challenges remain, including the scalability of high-performance materials, the need for improved modeling of real-world electrochemical environments, and the limitations of current DFT functionals in accurately simulating radical-mediated reactions. Nevertheless, the synergy between theoretical modeling and material synthesis offers a powerful platform for accelerating innovation in PFAS remediation technologies.

Table 6.1: ZPE corrections ($T=298\ K$) and entropy energy contributions for gaseous molecules and reactants

	H ₂ O(l)	$H_2(g)$	НО*	O*	HOO*
ZPE (eV)	0.57	0.27	0.34	0.07	0.425
TS (eV)	0.67	0.40	0	0	0
$\Delta G (eV)$	-0.10	-0.13	0.34	0.07	0.425

Table 6.2: Adsorption energy of H_2O , PFOA, PFOS, and Eovac on the pristine, Nb-TSO, and Ce-TSO electrode

Electrode	H ₂ O_Ea (eV)	PFOA_Ea (eV)	PFOS_Ea (eV)	Eovac (eV)
Ti ₄ O ₇	-0.54	-5.73	-7.72	6.31
Nb_Ti ₄ O ₇	-0.90	-5.81	-7.17	6.11
Ce_ Ti ₄ O ₇	-1.23	-5.73	-9.36	5.91
Pd_ Ti ₄ O ₇	-0.93	-5.35	-7.79	3.23

Table 6.3: η^{OER} of pristine Ti₄O₇ and Nb/Ce/Pd_ Ti₄O₇ surfaces

Electrode	$\eta^{\textit{OER}}(V)$
Ti ₄ O ₇	1.01
Nb_Ti ₄ O ₇	1.46
Ce_Ti ₄ O ₇	3.77
Pd_ Ti ₄ O ₇	2.61

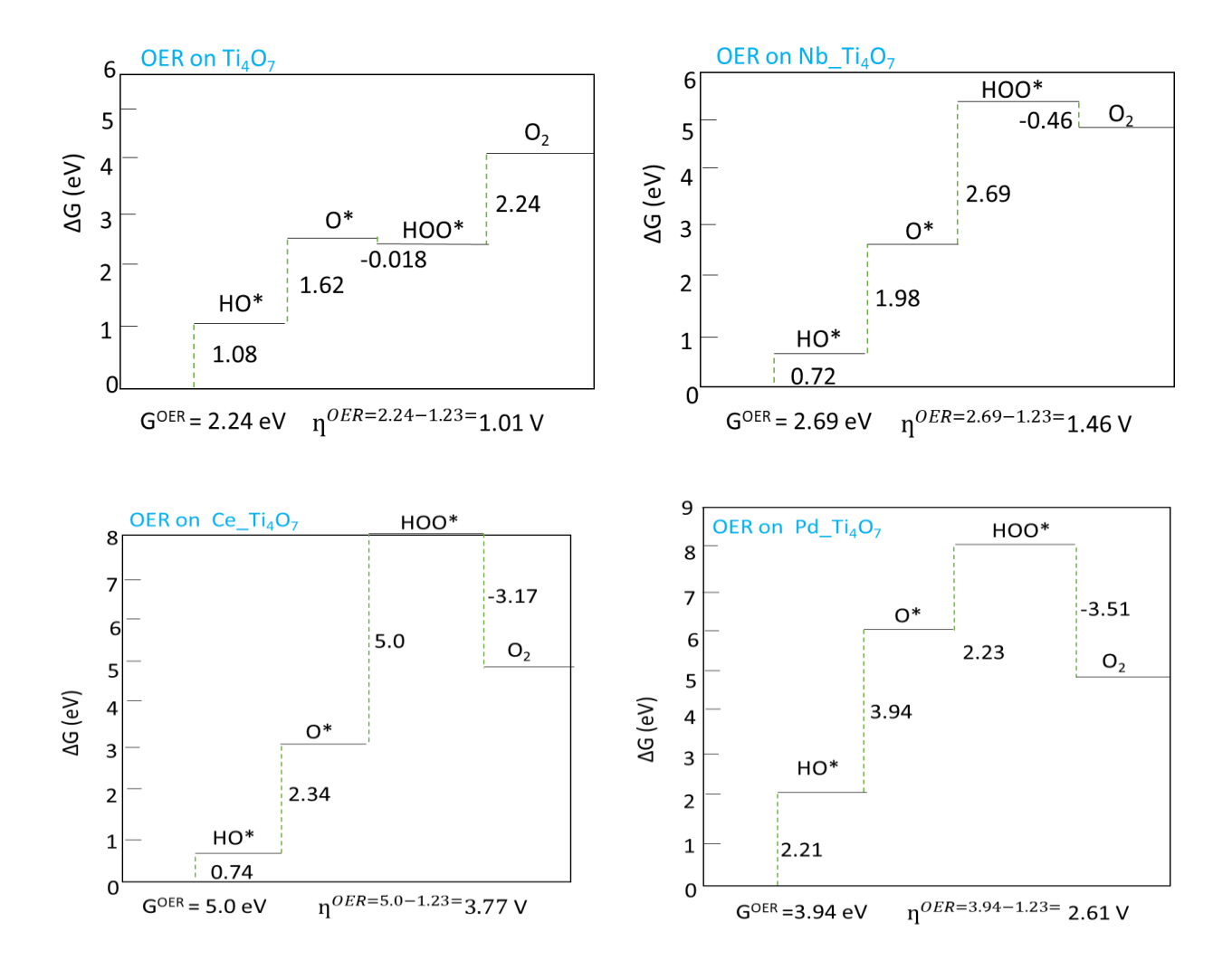


Figure 6.1: Free energy diagram for OER on Ti₄O₇, Nb_Ti₄O₇, Ce_Ti₄O₇, and Pd_Ti₄O₇

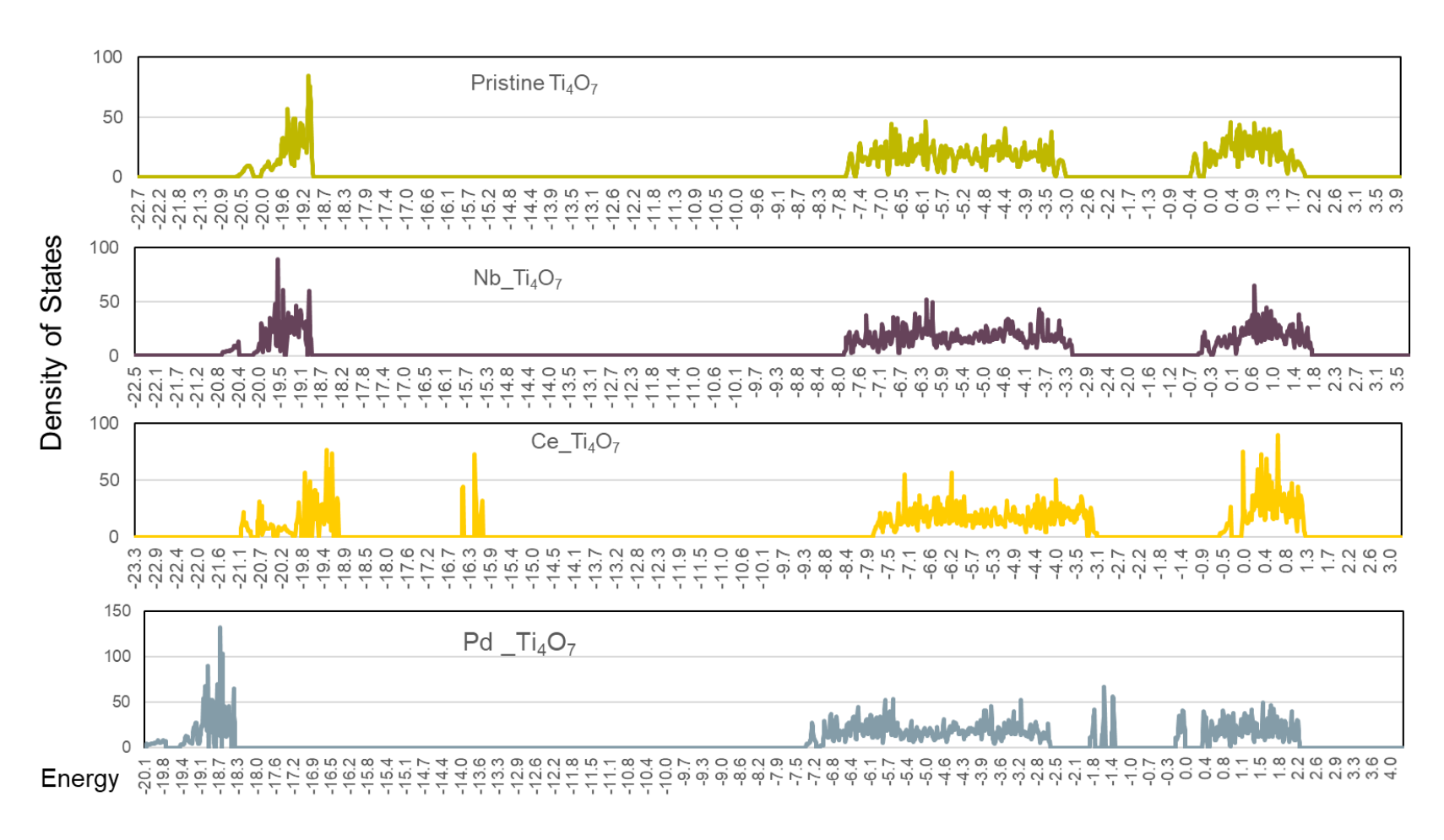


Figure 6.2: DOS of the pristine Ti₄O₇ and Nb/Ce/Pd_ Ti₄O₇

6.5 References

- Chaplin, B. P. (2014). Critical review of electrochemical advanced oxidation processes for water treatment applications. *Environmental Science-Processes & Impacts*, *16*(6), 1182-1203. https://doi.org/10.1039/c3em00679d
- Chen, C., Ma, Q. Q., Liu, F. Z., Gao, J. A., Li, X. Y., Sun, S. B., Yao, H., Liu, C. Q., Young, J., & Zhang, W. (2021). Photocatalytically reductive defluorination of perfluorooctanoic acid (PFOA) using Pt/La2Ti2O7 nanoplates: Experimental and DFT assessment. *Journal of Hazardous Materials*, 419. https://doi.org/ARTN12645210.1016/j.jhazmat.2021.126452
- Chen, S., Wang, H., Kang, Z., Jin, S., Zhang, X., Zheng, X., ... & Xie, Y. (2019). Oxygen vacancy associated single-electron transfer for photofixation of CO2 to long-chain chemicals. *Nature Communications*, 10(1), 788
- Chen, Z. F., Wang, X. J., Feng, H. L., Chen, S. H., Niu, J. F., Di, G. L., Kujawski, D., & Crittenden, J. C. (2022a). Electrochemical Advanced Oxidation of Perfluorooctanoic Acid: Mechanisms and Process Optimization with Kinetic Modeling. *Environmental Science & Technology*. https://doi.org/10.1021/acs.est.2c02906
- Chen, Z. F., Wang, X. J., Feng, H. L., Chen, S. H., Niu, J. F., Di, G. L., Kujawski, D., & Crittenden, J. C. (2022b). Electrochemical Advanced Oxidation of Perfluorooctanoic Acid: Mechanisms and Process Optimization with Kinetic Modeling. *Environmental Science & Technology*, 56(20), 14409-14417. https://doi.org/10.1021/acs.est.2c02906
- Cheng, Z. W., Chen, Q. C., Liu, Z. K., Liu, J. Y., Liu, Y. W., Liu, S. Q., Gao, X. P., Tan, Y. J., & Shen, Z. M. (2021). Interpretation of Reductive PFAS Defluorination with Quantum Chemical Parameters. *Environmental Science & Technology Letters*, 8(8), 645-650. https://doi.org/10.1021/acs.estlett.1c00403
- Ciobica, I. M., Frechard, F., van Santen, R. A., Kleyn, A. W., & Hafner, J. (2000). A DFT study of transition states for C-H activation on the Ru(0001) surface. *Journal of Physical Chemistry B*, 104(14), 3364-3369. https://doi.org/DOI 10.1021/jp9933141
- Eslamibidgoli, M. J., & Eikerling, M. H. (2015). Electrochemical Formation of Reactive Oxygen Species at Pt (111)-A Density Functional Theory Study. *Acs Catalysis*, *5*(10), 6090-6098. https://doi.org/10.1021/acscatal.5b01154
- Fabbri, E., Habereder, A., Waltar, K., Kotz, R., & Schmidt, T. J. (2014). Developments and perspectives of oxide-based catalysts for the oxygen evolution reaction. *Catalysis Science & Technology*, 4(11), 3800-3821. https://doi.org/10.1039/c4cy00669k
- Garg, S., Wang, J. S., Kumar, P., Mishra, V., Arafat, H., Sharma, R. S., & Dumee, L. F. (2021). Remediation of water from per-/poly-fluoroalkyl substances (PFAS) Challenges and perspectives. *Journal of Environmental Chemical Engineering*, *9*(4). https://doi.org/ARTN 10578410.1016/j.jece.2021.105784
- Hafner, J. (2007). Materials simulations using VASP a quantum perspective to materials science. *Computer Physics Communications*, 177(1-2), 6-13. https://doi.org/10.1016/j.cpc.2007.02.045
- Hammer, B., Hansen, L. B., & Norskov, J. K. (1999). Improved adsorption energetics within density-functional theory using revised Perdew-Burke-Ernzerhof functionals. *Physical Review B*, *59*(11), 7413-7421. https://doi.org/DOI 10.1103/PhysRevB.59.7413
- Henkelman, G., Uberuaga, B. P., & Jonsson, H. (2000). A climbing image nudged elastic band method for finding saddle points and minimum energy paths. *Journal of Chemical*

- *Physics*, *113*(22), 9901-9904. https://doi.org/Pii [S0021-9606(00)71246-3]Doi 10.1063/1.1329672
- Hinuma, Y., Mine, S., Toyao, T., Kamachi, T., & Shimizu, K. I. (2021). Factors determining surface oxygen vacancy formation energy in ternary spinel structure oxides with zinc. Physical chemistry chemical physics, 23(41), 23768-23777.
- Huang, D., Wang, K., Niu, J., Chu, C., Weon, S., Zhu, Q., Lu, J., Stavitski, E., & Kim, J. H. (2020). Amorphous Pd-Loaded Ti4O7 Electrode for Direct Anodic Destruction of Perfluorooctanoic Acid. *Environ Sci Technol*, 54(17), 10954-10963. https://doi.org/10.1021/acs.est.0c03800
- Huang, D. H., Wang, K. X., Niu, J. F., Chu, C. H., Weon, S., Zhu, Q. H., Lu, J. J., Stavitski, E., & Kim, J. H. (2020). Amorphous Pd-Loaded Ti4O7 Electrode for Direct Anodic Destruction of Perfluorooctanoic Acid. *Environmental Science & Technology*, 54(17), 10954-10963. https://doi.org/10.1021/acs.est.0c03800
- Huang, X., Wang, J., Tao, H. B., Tian, H., & Xu, H. (2019). An essential descriptor for the oxygen evolution reaction on reducible metal oxide surfaces. *Chemical Science*, 10(11), 3340-3345. https://doi.org/10.1039/c8sc04521f
- Huang, Z. F., Wang, J., Peng, Y. C., Jung, C. Y., Fisher, A., & Wang, X. (2017). Design of Efficient Bifunctional Oxygen Reduction/Evolution Electrocatalyst: Recent Advances and Perspectives. *Advanced Energy Materials*, 7(23). https://doi.org/ARTN170054410.1002/aenm.201700544
- Ko, J. S., Le, N. Q., Schlesinger, D. R., Zhang, D. J., Johnson, J. K., & Xia, Z. Y. (2021). Novel niobium-doped titanium oxide towards electrochemical destruction of forever chemicals (vol 11, 18020, 2021). Scientific Reports, 11(1). https://doi.org/ARTN 1901410.1038/s41598-021-98715-0
- Kishore, R., Cao, X., Zhang, X., & Bieberle-Hütter, A. (2019). Electrochemical water oxidation on WO3 surfaces: A density functional theory study. *Catalysis Today*, *321*, 94-99.
- Li, L., Wang, Y., & Huang, Q. (2021). First-Principles Study of the Degradation of Perfluorooctanesulfonate and Perfluorobutanesulfonate on a Magnéli Phase Ti4O7 Anode. *ACS ES&T Water*, *I*(8), 1737-1744. https://doi.org/10.1021/acsestwater.1c00086
- Lin, H., Niu, J., Liang, S., Wang, C., Wang, Y., Jin, F., Luo, Q., & Huang, Q. (2018). Development of macroporous Magnéli phase Ti4O7 ceramic materials: As an efficient anode for mineralization of poly- and perfluoroalkyl substances. *Chemical Engineering Journal*, 354, 1058-1067. https://doi.org/10.1016/j.cej.2018.07.210
- Lin, H., Xiao, R., Xie, R., Yang, L., Tang, C., Wang, R., Chen, J., Lv, S., & Huang, Q. (2021). Defect Engineering on a Ti4O7 Electrode by Ce(3+) Doping for the Efficient Electrooxidation of Perfluorooctanesulfonate. *Environ Sci Technol*, 55(4), 2597-2607. https://doi.org/10.1021/acs.est.0c06881
- Lin, M. H., Bulman, D. M., Remucal, C. K., & Chaplin, B. P. (2020). Chlorinated Byproduct Formation during the Electrochemical Advanced Oxidation Process at Magneli Phase Ti4O7 Electrodes. *Environmental Science & Technology*, *54*(19), 12673-12683. https://doi.org/10.1021/acs.est.0c03916
- Liu, L. B., Wu, L. L., Liu, B. Y., Hou, J. L., Fang, C., Du, A. J., Tang, Y. H., & Zhang, H. P. (2020). Strain induced variation of PFOS adsorption on pristine and defected phosphorene: A DFT study. *Applied Surface Science*, *532*. https://doi.org/ARTN14745210.1016/j.apsusc.2020.147452

- Malik, H., Sarkar, S., Mohanty, S., & Carlson, K. (2020). Modelling and synthesis of Magneli Phases in ordered titanium oxide nanotubes with preserved morphology. *Scientific Reports*, 10(1). https://doi.org/ARTN 805010.1038/s41598-020-64918-0
- Man, I. C., Su, H. Y., Calle-Vallejo, F., Hansen, H. A., Martinez, J. I., Inoglu, N. G., Kitchin, J., Jaramillo, T. F., Norskov, J. K., & Rossmeisl, J. (2011). Universality in Oxygen Evolution Electrocatalysis on Oxide Surfaces. *Chemcatchem*, *3*(7), 1159-1165. https://doi.org/10.1002/cctc.201000397
- Perdew, J. P., Burke, K., & Ernzerhof, M. (1996). Generalized gradient approximation made simple. *Physical Review Letters*, 77(18), 3865-3868. https://doi.org/DOI 10.1103/PhysRevLett.77.3865
- Schaefer, C. E., Andaya, C., Burant, A., Condee, C. W., Urtiaga, A., Strathmann, T. J., & Higgins, C. P. (2017). Electrochemical treatment of perfluorooctanoic acid and perfluorooctane sulfonate: Insights into mechanisms and application to groundwater treatment. *Chemical Engineering Journal*, *317*, 424-432. https://doi.org/10.1016/j.cej.2017.02.107
- Shi, H. H., Wang, Y. Y., Li, C. G., Pierce, R., Gao, S. X., & Huang, Q. G. (2019). Degradation of Perfluorooctanesulfonate by Reactive Electrochemical Membrane Composed of Magneli Phase Titanium Suboxide. *Environmental Science & Technology*, *53*(24), 14528-14537. https://doi.org/10.1021/acs.est.9b04148
- Vo, H. N. P., Ngo, H. H., Guo, W. S., Nguyen, T. M. H., Li, J. X., Liang, H., Deng, L. J., Chen, Z., & Nguyen, T. A. H. (2020). Poly?and perfluoroalkyl substances in water and wastewater: A comprehensive review from sources to remediation. *Journal of Water Process Engineering*, 36. https://doi.org/ARTN 10139310.1016/j.jwpe.2020.101393
- Wang, C., Zhang, T. N., Yin, L. F., Ni, C. S., Ni, J. P., & Hou, L. A. (2022). Enhanced perfluorooctane acid mineralization by electrochemical oxidation using Ti3+ self-doping TiO2 nanotube arrays anode. *Chemosphere*, 286. https://doi.org/ARTN13180410.1016/j.chemosphere.2021.131804
- Wang, L., Lu, J. H., Li, L., Wang, Y. Y., & Huang, Q. G. (2020). Effects of chloride on electrochemical degradation of perfluorooctanesulfonate by Magneli phase Ti4O7 and boron doped diamond anodes. *Water Research*, *170*. https://doi.org/ARTN11525410.1016/j.watres.2019.115254
- Wang, Y., Kim, J., Huang, C.-H., Hawkins, G. L., Li, K., Chen, Y., & Huang, Q. (2022). Occurrence of per- and polyfluoroalkyl substances in water: a review. *Environmental Science: Water Research & Technology*, 8(6), 1136-1151. https://doi.org/10.1039/d1ew00851j
- Wang, Y., Li, L., Wang, Y., Shi, H., Wang, L., & Huang, Q. (2022). Electrooxidation of perfluorooctanesulfonic acid on porous Magnéli phase titanium suboxide Anodes: Impact of porous structure and composition. *Chemical Engineering Journal*, 431. https://doi.org/10.1016/j.cej.2021.133929
- Wang, Y. Y., Li, L., Wang, Y. F., Shi, H. H., Wang, L., & Huang, Q. G. (2022). Electrooxidation of perfluorooctanesulfonic acid on porous Magneli phase titanium suboxide Anodes: Impact of porous structure and composition. *Chemical Engineering Journal*, 431. https://doi.org/ARTN 13392910.1016/j.cej.2021.133929
- Yamijala, S. S. R. K. C., Shinde, R., Hanasaki, K., Ali, Z. A., & Wong, B. M. (2022). Photo-induced degradation of PFASs: Excited-state mechanisms from real-time time-dependent

- density functional theory. *Journal of Hazardous Materials*, 423. https://doi.org/ARTN12702610.1016/j.jhazmat.2021.127026
- Zhang, L., Luo, Y. J., Huang, H. M., Zhang, H. J., Wang, Y. Y., & Wang, Y. (2022). Ordered Ag@Pd alloy supported on Ti4O7 by ascorbic acid-assisted galvanic replacement for efficient oxygen reduction. *Journal of Alloys and Compounds*, 929. https://doi.org/ARTN16725110.1016/j.jallcom.2022.167251
- Zhao, J., Wang, J. Q., Du, E. D., Ai, Y. J., Liu, J. J., & Guo, H. G. (2022). Water decontamination under high salinity using the TiO2 NT/PbO2-Cu electrochemical oxidation system: kinetics mechanism and DFT studies. *Environmental Science-Water Research & Technology*, 8(10), 2231-2244. https://doi.org/10.1039/d2ew00322h

CHAPTER 7

CONCLUSION

7.1 Conclusion

This dissertation presents a comprehensive and interdisciplinary investigation into the remediation of per- and polyfluoroalkyl substances (PFAS), integrating mechanistic degradation studies, environmental life cycle assessment (LCA), and first-principles computational modeling. Through this multifaceted approach, the work addresses both the technical challenges of PFAS destruction and the broader sustainability implications of deploying treatment technologies at scale.

The research began with a critical review of emerging PFAS remediation technologies, revealing that no single method currently offers a universally effective or sustainable solution. Concentration methods like granular activated carbon (GAC) and ion exchange (IX) remain widely used, but they primarily transfer PFAS from one matrix to another. Destructive methods, particularly electrochemical oxidation (EO), show strong potential for PFAS mineralization, but are limited by high energy consumption, anode degradation, and reduced effectiveness for short-chain PFAS.

To address these limitations, Chapter 3 explored the underlying mechanisms of PFAS degradation during EO. Combining literature synthesis with density functional theory (DFT) results, this chapter clarified the roles of direct electron transfer, decarboxylation, hydroxylation, and hydrolysis in the breakdown of PFAS such as PFOA and PFOS. Understanding these

pathways provides a mechanistic foundation for optimizing electrode performance and treatment conditions.

Chapters 4 and 5 applied life cycle assessment (LCA) and life cycle costing (LCC) to two different PFAS treatment systems: IX combined with EO, and foam fractionation (FF). These analyses revealed that environmental and economic performance is highly dependent on operational scenarios, energy sources, and system configurations. For example, while multi-stage FF systems offer improved removal efficiencies, they also result in higher environmental burdens and costs unless optimized for scale and energy input.

Chapter 6 leveraged DFT-based modeling to guide the rational design of highperformance electrode materials for EO systems. By calculating bond dissociation energies, adsorption energies, activation barriers, and oxygen evolution reaction overpotentials, this work identified Ti₄O₇ and its doped variants as promising anode materials. These insights help bridge the gap between atomic-scale understanding and practical electrode development, offering a scientific basis for improving EO treatment efficiency and longevity.

Collectively, this dissertation demonstrates that integrated treatment trains—combining concentration and destruction technologies—are necessary to achieve comprehensive, cost-effective, and environmentally responsible PFAS remediation. It also illustrates the value of coupling experimental research with theoretical modeling and sustainability assessment to guide technology development from the molecular to the systems level.

This work contributes to the growing body of knowledge supporting the development of next-generation PFAS remediation strategies. It offers not only mechanistic insights and material innovations, but also a decision-support framework for evaluating the trade-offs between treatment performance, environmental impact, and economic feasibility. In doing so, it provides

a foundation for future research and real-world implementation of effective, scalable, and sustainable solutions for one of the most persistent environmental contaminants of our time.

7.2 Future study

While this dissertation has demonstrated the value of density functional theory (DFT) in elucidating PFAS degradation mechanisms and guiding electrode material selection, future research can be significantly accelerated and expanded through the integration of machine learning (ML) with first-principles modeling. The rapidly growing field of materials informatics offers a transformative opportunity to overcome the computational bottlenecks associated with traditional DFT workflows and to enable high-throughput screening of novel electrode materials. Specifically, the development of ML models trained on DFT-computed datasets can allow for the rapid prediction of key material properties such as adsorption energy, oxygen vacancy formation energy, and density of states (DOS). These properties have been identified as critical descriptors for evaluating the catalytic activity, stability, and electronic characteristics of titanium suboxide (TSO) electrodes and their doped variants in electrochemical oxidation (EO) systems. By learning complex relationships between atomic composition, structural features, and electronic behavior, ML models can prioritize candidate materials before conducting resource-intensive DFT calculations.

Recently, machine learning (ML) potentials for estimating atomic forces and energies have shown significant progress on standard benchmarks while being orders of magnitude faster than DFT. Compared with computational simulation, machine learning can identify patterns in large high dimensional data sets effectively, extract useful information quickly and discover hidden laws. Therefore, it is well suited for material discovery and can accelerate the process of

predicting the properties of materials, which typically requires computationally expensive theoretical calculations. (Wei et al., 2019).

For example, recent studies have shown that machine learning potentials can be leveraged to identify low-energy adsorbate-surface configurations more accurately and efficiently. Our algorithm provides a spectrum of trade-offs between accuracy and efficiency, with one balanced option finding the lowest energy configuration 87.36% of the time, while achieving a ~2000× speedup in computation (Lan et al., 2023). To standardize benchmarking, we introduce the Open Catalyst Dense dataset containing nearly 1000 diverse surfaces and ~100,000 unique configurations.

Incorporating such ML frameworks into the electrode discovery pipeline would enable the exploration of a broader chemical design space, including high-dimensional doping strategies and surface modifications. These models can be further refined through transfer learning and active learning techniques, in which initial DFT results inform model training, and new calculations are selectively performed to improve predictive accuracy in underexplored regions of the material space.

By uniting first-principles accuracy with data-driven efficiency, the DFT-ML hybrid framework represents a promising frontier in the rational design of next-generation EO electrodes. This approach aligns with broader efforts to develop smart, sustainable, and scalable PFAS treatment technologies capable of addressing the global contamination crisis.

7.3 References

- Lan, J., Palizhati, A., Shuaibi, M., Wood, B. M., Wander, B., Das, A., Uyttendaele, M., Zitnick, C. L., & Ulissi, Z. W. (2023). AdsorbML: a leap in efficiency for adsorption energy calculations using generalizable machine learning potentials. *Npj Computational Materials*, *9*(1). https://doi.org/ARTN 17210.1038/s41524-023-01121-5
- Wei, J., Chu, X., Sun, X. Y., Xu, K., Deng, H. X., Chen, J., ... & Lei, M. (2019). Machine learning in materials science. *InfoMat*, *1*(3), 338-358.

APPENDICES A Supplemental material for Chapter 4

Table S1. Water quality parameters for baseline groundwater.

Analyses	Units	Concentration
рН	pH unit	6.98
Iron	mg/L	7.92
Chloride	mg/L	37.6
Fluoride	mg/L-N	0.121
Nitrate	mg/L-N	< 0.2
Nitrite	mg/L	< 0.2
Sulfate	mg/L	4.6
Total organic carbon (TOC)	mg/L	6.3
Total dissolved solids (TDS)	mg/L	552.5
Total suspended solids (TSS)	mg/L	22
Alkalinity	as CaCO ₃	50-500
Turbidity	NTU	2.95
Oil and grease	mg/L	< 2.0
Biochemical oxygen demand	mg/L	< 1.0
(BOD)		
Chemical oxygen demand (COD)	mg/L	6.2

Table S2. Still bottoms Properties

Property	Still Bottoms	Still Bottoms
	I	II
рН	9.57 ± 0.3	9.64 ± 0.5
Conductivity	15.89	25.15
$(mS \cdot cm - 1)$		
$TOC (mg C \cdot L-1)$	13280	201529
$[Cl-](mg\cdot L-1)$	62716	3579
Methanol (mg·L-1)	124	216

Table S3. EE/O of PFASs removal for still bottom 1 and 2

PFAS Species	Still Bottom	Still Bottom 2	Unit
	1		
PFBA		2941.06	kWh/m ³
PFPeA		736.75	kWh/m ³
PFHxA		2192.16	kWh/m ³
PFHpA	1882.58	729.93	kWh/m ³
PFOA	530.66	1876.72	kWh/m ³
PFBS		1395.18	kWh/m ³
PFPeS		491.97	kWh/m^3
PFHxS	523.66	1551.39	kWh/m ³
PFHpS	452.89	525.91	kWh/m^3
PFOS	349.79	1031.08	kWh/m ³

Table S4: Concentrations of PFASs in still bottom samples before and after EO treatment (mg/L)

PFAA s		Still bottom I		S	Still bottom II		
	Initial concentratio n	Final concentratio n	Removal percentag e	Initial concentratio n	Final concentratio n	Removal percentag e	
PFBA	1.66	2.48	-49.6	2.32	0.31	86.8	
PFBS	1.45	1.55	-6.8	2.29	0.01	99.7	
PFPeA	10.10	11.13	-10.2	6.95	<loq*< td=""><td>100</td></loq*<>	100	
PFPeS	2.64	2.36	10.8	1.46	<loq< td=""><td>100</td></loq<>	100	
PFHx A	13.16	14.07	-6.9	7.17	0.21	100	
PFHxS	40.94	2.03	95.0	18.71	0.21	100	
PFHp A	3.69	1.60	56.6	2.42	<loq< td=""><td>100</td></loq<>	100	
PFHpS	2.58	0.08	96.8	1.57	<loq< td=""><td>100</td></loq<>	100	
PFOA	7.56	0.39	94.8	11.92	0.15	98.7	
PFOS	8.08	0.09	98.9	12.02	0.42	96.5	

6:2		_	-	9.64	0.38	96.1
FTS*	-					

^{*}Only included in analysis of still bottom sample 2.

Table S5: Normalized life cycle reference flow table for the treatment and destruction of two orders of magnitude of PFAS species in still bottom 1 from 1000 m³ groundwater

Species	PFOS	PFOA	PFHpA	PFHxS	PFHpS	Units
Inputs:						
Groundwater	1000.00	1000.00	1000.00	1000.00	1000.00	m^3
Resin	12.46	12.46	12.46	12.46	12.46	
NaCl	2.03	2.03	2.03	2.03	2.03	kg
DI Water	47.78	47.78	47.78	47.78	47.78	kg
PFASs	397.49	371.48	2013.73	181.73	126.94	mg
Outputs:						
PFASs	3.97	3.71	20.14	1.82	1.27	mg
Energy:						
Heat, natural	5.87	5.87	5.87	5.87	5.87	MJ
gas						
Electrical	34.42	52.21	51.52	185.23	44.56	kWh

Table S6: Normalized reference flow table for the treatment and destruction of two orders of magnitude of PFAS species in still bottom 2 from 1000 m³ groundwater

Species	PFOS	PFOA	PFHxS	PFHpA	PFHpS	PFBS	PFBA	PFPeA	PFHxA	PFPeS
Inputs:										
Groundwater	1000.00	1000.00	1000.00	1000.00	1000.00	1000.00	1000.00	1000.00	1000.00	1000.00
Resin	12.46	12.46	12.46	12.46	12.46	12.46	12.46	12.46	12.46	12.46
Nal	2.03	2.03	2.03	2.03	2.03	2.03	2.03	2.03	2.03	2.03
DI Water	47.78	47.78	47.78	47.78	47.78	47.78	47.78	47.78	47.78	47.78
PFASs	591.15	586.24	920.18	119.02	77.51	112.62	114.10	341.81	352.63	71.80
Outputs:										
PFASs	5.91	5.86	9.20	1.19	0.78	1.13	1.14	3.42	3.53	0.72
Energy:										
Heat, natural	5.87	5.87	5.87	5.87	5.87	5.87	5.87	5.87	5.87	5.87
gas										
Electrical	101.42	184.60	152.60	71.80	51.73	137.23	289.29	72.47	215.63	48.39

^{*}LOQ: limit of quantification.

Table S7: Environmental impact categories analyzed in this study

Impact Category	Units
Global Warming Potential (GWP)	kg CO ₂ eq.
Smog Formation (SF)	$kg O_3 eq.$
Acidification (AD)	mol H ⁺ eq.
Marine Eutrophication (ME)	kg N eq.
Non-Carcinogenics (NC)	CTUh
Respiratory Effects (RE)	$kg PM_{10} eq$
Ecotoxicity (ET)	CTUe

Table S8: GWP results for treating PFOS and PFBA in three different treatment scenarios

GWP (kg CO2 eq.)	Scenario 1	Scenario 2	Scenario 3
PFOS	61.03	71.47	36.06
PFBA	61.03	253.57	218.16

(scenario1: single-use of the IXR followed by disposal by incineration; scenario2: single-use of the IXR followed by EO treatment and disposal of the IXR in a landfill; scenario 3: regeneration and reuse of the IXR followed by EO treatment with disposal of the IXR after 10 uses)

Table S9: Standard deviation of uncertainty analysis for treating PFOS and PFBA in three different treatment scenarios

Standard deviation (%)	Scenario 1	Scenario 2	Scenario 3
PFOS	7.9	2.6	1.98
PFBA	7.9	7.7	1.47

(scenario1: single-use of the IXR followed by disposal by incineration; scenario2: single-use of the IXR followed by EO treatment and disposal of the IXR in a landfill; scenario 3: regeneration and reuse of the IXR followed by EO treatment with disposal of the IXR after 10 uses)

Figure S1: GWP uncertainty analysis result for treating PFOS in scenario 1

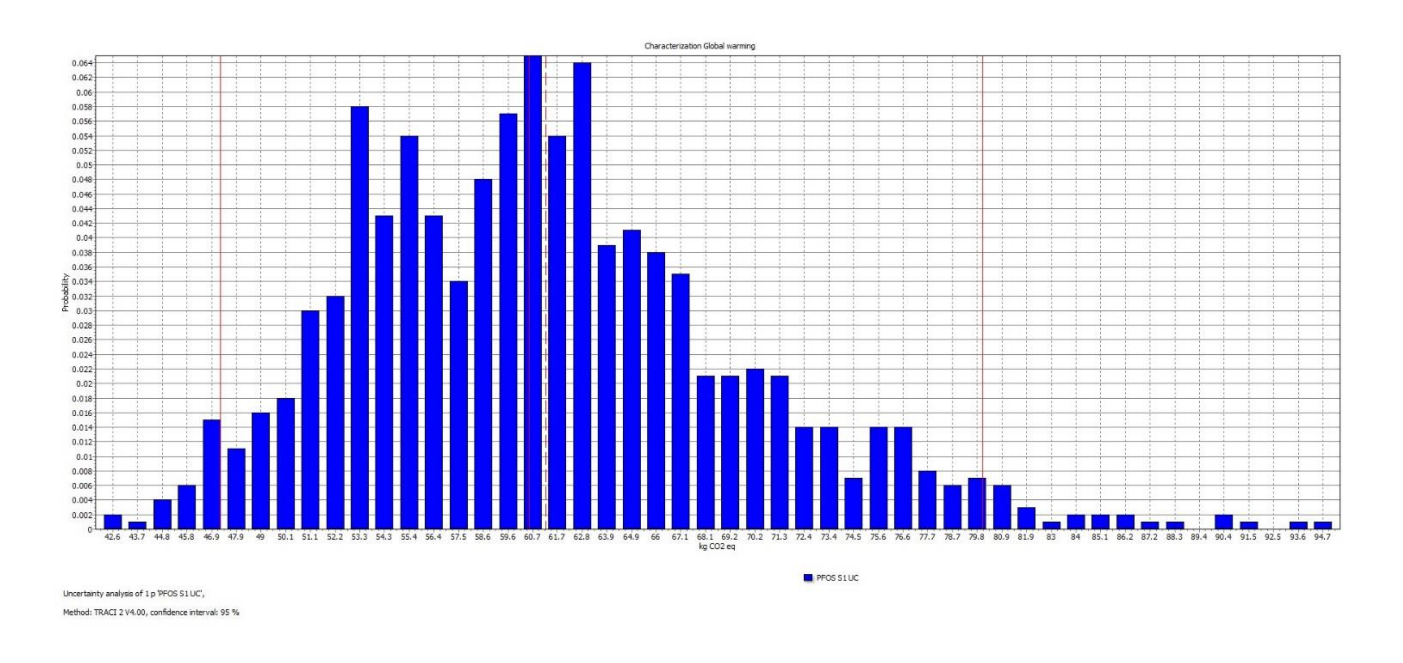
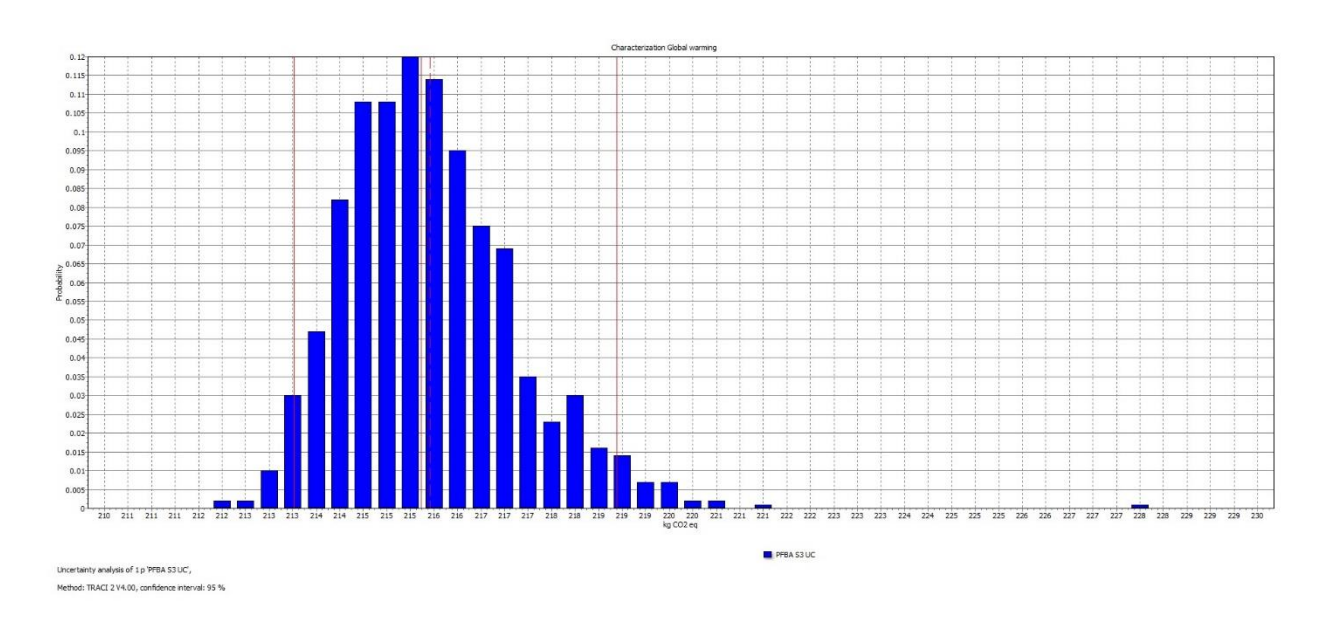


Figure S2: GWP uncertainty analysis result for treating PFBA in scenario 3



APPENDICES B Supporting information for Chapter 5

Table S1: Environmental impact categories analyzed in this study

Impact Category	Units
Ozone Depletion (OD)	kg CFC-11 eq
Global Warming Potential (GWP)	kg CO ₂ eq.
Smog Formation (SF)	kg O ₃ eq.
Acidification (AD)	mol H ⁺ eq.
Marine Eutrophication (ME)	kg N eq.
Non-Carcinogenics (NC)	CTUh
Respiratory Effects (RE)	kg PM ₁₀ eq
Ecotoxicity (ET)	CTUe

Table S2. Environmental impact results for treating 1000 m³ PFASs-contaminated landfill leachate with one-stage FF system

Impact	Capital	Electricity	Compressed	Disposal	Total	Unit
category	construction	for vacuum	air	Disposai	Total	Omt
OD	1.00E-05	5.51E-07	1.80E-05	2.74E-05	5.60E-05	kg CFC-11 eq
GWP	1.35E+01	1.21E+01	3.07E+02	4.85E+02	8.18E+02	kg CO ₂ eq
SF	1.03E-01	5.69E-01	1.28E+01	7.98E+00	2.15E+01	kg O ₃ eq
AD	1.23E+00	4.28E+00	7.43E+01	3.12E+01	1.11E+02	mol H ⁺ eq
ME	1.45E-03	4.65E-02	2.42E+00	1.37E+00	3.84E+00	kg N eq
C	2.87E-07	6.68E-07	3.24E-05	7.54E-05	1.09E-04	CTUh
NC	5.44E-06	1.51E-06	7.30E-05	4.45E-05	1.24E-04	CTUh
RE	3.11E-03	1.31E-02	3.47E-01	1.26E-01	4.89E-01	$kg \ PM_{10} \ eq$
ET	4.04E+01	1.12E+01	5.27E+02	8.00E+02	1.38E+03	CTUe

Table S3. Environmental impact results for treating 1000 m³ PFASs contaminated landfill leachate with three-stage FF system.

Impact category	Capital construction	Electricity for vacuum	Compressed air	d Disposal Total		Unit
OD	1.33E-05	6.61E-07	2.16E-05	8.23E-11	3.56E-05	kg CFC-11 eq
GWP	1.79E+01	1.45E+01	3.69E+02	1.45E-03	4.02E+02	kg CO ₂ eq.
SF	1.36E-01	6.83E-01	1.54E+01	2.39E-05	1.62E+01	kg O ₃ eq
AD	1.62E+00	5.14E+00	8.92E+01	9.35E-05	9.60E+01	mol H ⁺ eq
ME	1.93E-03	5.58E-02	2.91E+00	4.10E-06	2.97E+00	kg N eq
С	3.81E-07	8.02E-07	3.89E-05	2.26E-10	4.01E-05	CTUh
NC	7.21E-06	1.82E-06	8.76E-05	1.34E-10	9.66E-05	CTUh
RE	4.12E-03	1.57E-02	4.17E-01	3.78E-07	4.37E-01	kg PM ₁₀ eq
ET	5.35E+01	1.34E+01	6.33E+02	2.40E-03	7.00E+02	CTUe

Table S4: Life cycling costing assessment results for treating 1000 m³ PFASs contaminated landfill leachate with one-stage and three-stage FF system

Category	One-stage (\$)	Three-stage (\$)
Capital construction cost	37.31	49.20
Operation cost (electricity)	12.27	15.36
Maintenance cost (labor)	27.78	46.0
Total	77.36	110.6

Table S5: The unit environmental impact of 1m³ compressed air generated under various power and pressure conditions

	Compressed air, optimized generation, at compressor/RER U											
Impact	>30kW, 6	>30kW, 7	>30kW, 8	<30kW, 8	<30kW, 12	Units						
category	bar gauge	bar gauge	bar gauge	bar gauge	bar gauge	Omts						
OD	4.19E-09	4.50E-09	4.81E-09	1.26E-08	1.41E-08	kg CFC-11 eq						
GWP	7.15E-02	7.69E-02	8.22E-02	1.74E-01	1.99E-01	kg CO ₂ eq						
SF	2.99E-03	3.21E-03	3.43E-03	9.03E-03	1.01E-02	kg O ₃ eq						
AF	1.73E-02	1.86E-02	1.98E-02	5.91E-02	6.51E-02	mol H ⁺ eq						
ME	5.64E-04	6.05E-04	6.47E-04	2.27E-03	2.47E-03	kg N eq						
C	7.54E-09	8.04E-09	8.54E-09	6.32E-08	6.55E-08	CTUh						
NC	1.70E-08	1.81E-08	1.93E-08	2.17E-07	2.22E-07	CTUh						
RE	8.08E-05	8.66E-05	9.24E-05	4.43E-04	4.70E-04	$kg \ PM_{10} eq$						
ET	1.23E-01	1.31E-01	1.39E-01	1.23E+00	1.26E+00	CTUe						

Table S6: The capital construction costs to treat 1000m³ PFAS-contaminated landfill leachate in the one-stage FF system from various system design sources

Design sources	Capital construction cost for one- stage FF system (\$ in 2023)
EPA model, 2022	37.31
Donald R.Woods, 2003	18.31
Westech, 2018	21.90
Minnesota Pollution Control Agency, 2023	161.6

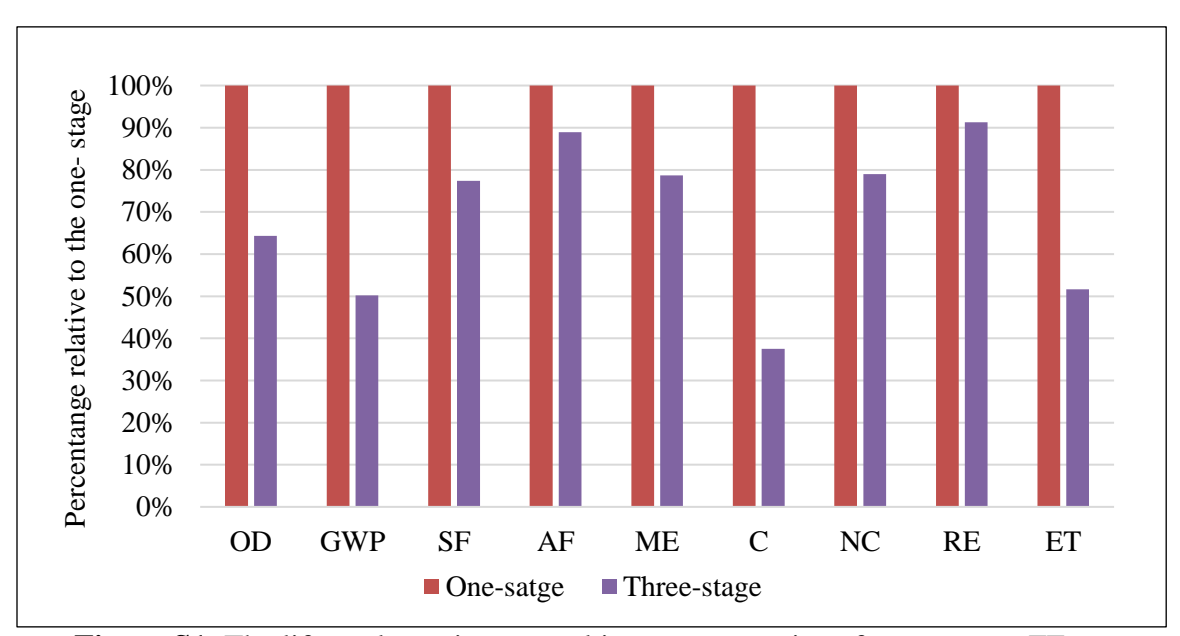


Figure S1: The life cycle environmental impact comparison for one-stage FF system and three-stage FF system. Impacts are normalized to one-stage FF system.

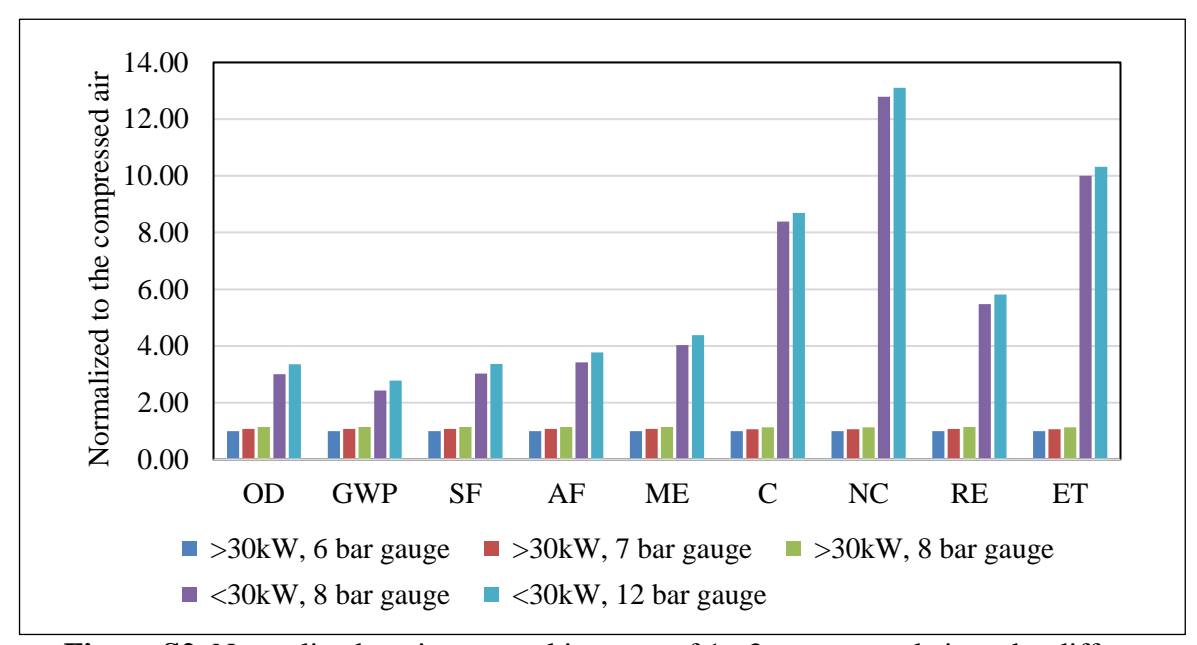


Figure S2. Normalized environmental impacts of 1m3 compressed air under different generation conditions (compressed air generated under >30kW and 6 bar gauge is as the reference)

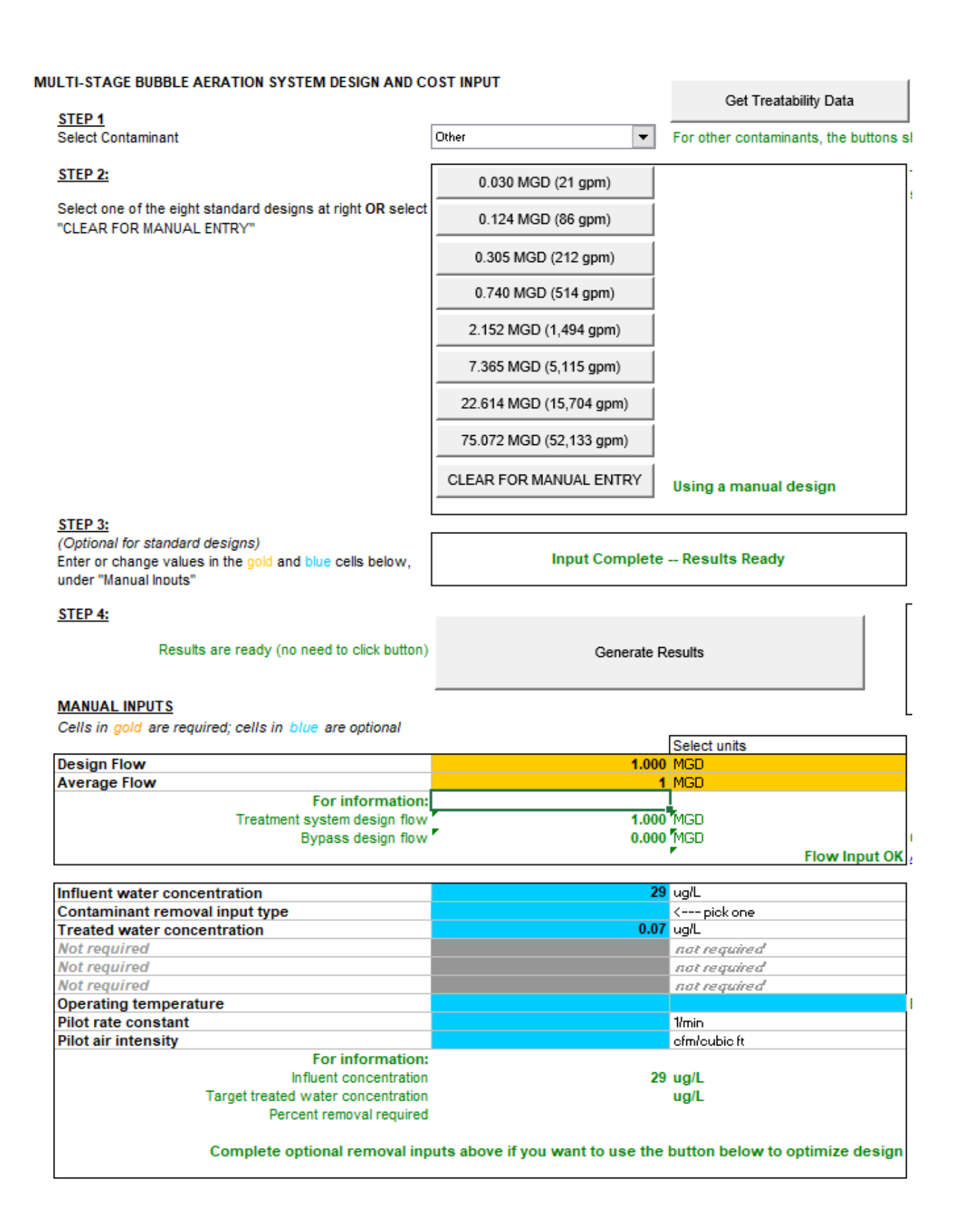
Appendix

Input/output parameters and economic cost data obtained using the Work Breakdown Structure-Based Cost Model for Multi-Stage Bubble Aeration Drinking Water Treatment from the U.S. EPA website.

Section 1 – Single stage FF system

Below include all input parameters for the Multi-Stage Bubble Aeration WBS model derived from the U.S. EPA. Spreadsheets used in this model are available under the "Drinking Water Treatment Technology Unit Cost Models" <u>Drinking Water Treatment Technology Unit Cost Models | US EPA.</u>

While this model was not used for every component of the life cycle cost assessment (e.g., electricity used for vacuum), sample outputs used in the costing model are included below for aeration basins, pumps, blowers, and piping (Figure 1.2), valves (Figure 1.3), instrumentation (Figure 1.4), building structures (Figure 1.5), and labor (Figure 1.6).



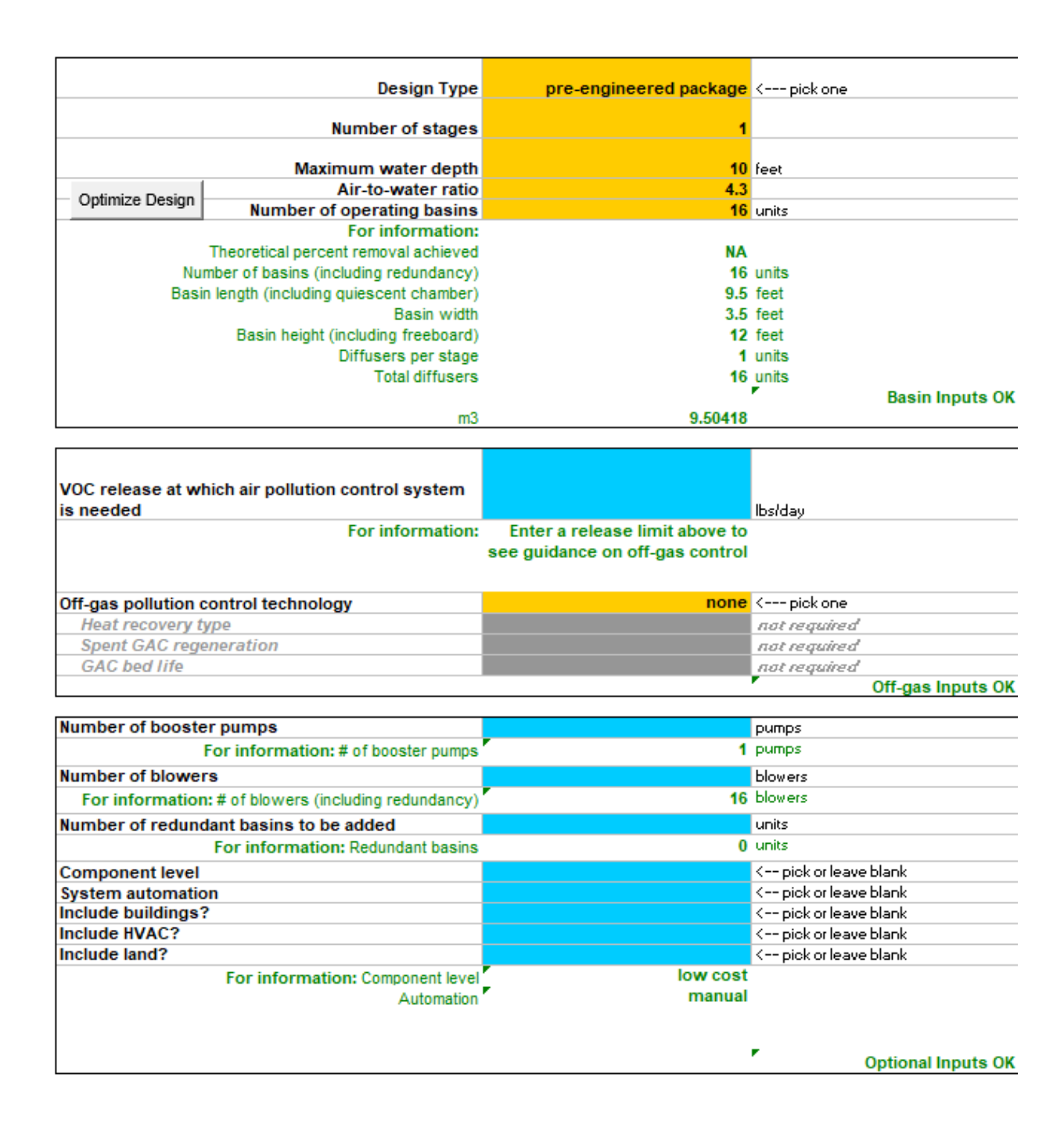


Figure 1.1. All input parameters used in the life cycle costing assessment model for the single stage FF system.

WBS#	Item	Design Quantity	Design Size	Size used in estimate	Unit Cost	Total Cost	Useful Life Use?
1.	Aeration Basins						
1.1	Custom Designed						
1.1.1	Concrete	- units	NA	NA	NA.		NA
1.1.2	Excavation	- cy	NA	NA	NA.	-	NA
1.1.3	Backfill and Compaction	- 09	NA NA	NA	NA.	_	NA
1.1.4	Steel Cover	- st	NA	NA	NA.	_	NA
1.1.5	Membrane Baffles	- units	NA	NA NA	NA.	-	NA
1.2	Prefabricated	•					
1.2.1	Stainless Steel	16 units	421 sf	421 sf	\$ 62,155	\$ 994,474	35 0
1.2.1	Plastic with Stainless Steel Frame	16 units	421 sf	421 sf	contact vendor	-	25 0
1.2.1	Fiberglass	16 units	421 sf	421 sf	\$ 38,226	\$ 611,610	25 1
1.3	Aerators						
1.3.1	Diffusers	16 units	25 cfm	25 cfm	\$ 79	\$ 1,263	10 1
2.	Pumps and Blowers						
2.1	Booster Pumps	1 units	868 gpm	868 gpm	\$ 22,347	\$ 22,347	20 1
2.2	Blowers		-				
2.2.1	Centrifugal	16 units	31 cfm	31 cfm	\$ 14,110	\$ 225,758	25 0
2.2.1	Regenerative	16 units	31 cfm	31 cfm	\$ 901	\$ 14,423	25 1
3.	Piping						
3.1	Process Piping						
3.1.1	Ductile Iron	100 If	2.5 in. diam	2.5 in. diam	contact vendor	-	40 0
3.1.1	CPVC	100 If	2.5 in. diam	2.5 in. diam	\$ 13	\$ 1,298	22 0
3.1.1	PVC	100 lf	2.5 in. diam	2.5 in. diam	\$ 4	\$ 404	22 1
3.1.1	Stainless Steel	100 If	2.5 in. diam	2.5 in. diam	\$ 119	\$ 11,946	45 0
3.1.1	Steel	100 If	2.5 in. diam	2.5 in. diam	\$ 48	\$ 4,842	35 0
3.2	Air Piping						
3.2.1	Ductile Iron	362 If	2.5 in. diam	2.5 in. diam	contact vendor	_	40 0
3.2.1	CPVC	362 If	2.5 in. diam	2.5 in. diam	\$ 13	\$ 4,699	22 0
3.2.1	PVC	362 If	2.5 in. diam	2.5 in. diam	\$ 4	\$ 1,461	22 1
3.2.1	Stainless Steel	362 If	2.5 in. diam	2.5 in. diam	\$ 119	\$ 43,245	45 0
3.2.1	Steel	362 If	2.5 in. diam	2.5 in. diam	\$ 48	\$ 17,529	35 0
3.3	Influent and Treated Water Piping						
3.3.1	Ductile Iron	100 lf	6 in. diam	6 in. diam	\$ 100		40 0
3.3.1	CPVC	100 If	6 in. diam	6 in. diam	\$ 47	\$ 4,661	22 0
3.3.1	PVC	100 If	6 in. diam	6 in. diam	\$ 10		22 1
3.3.1	Stainless Steel	100 If	6 in. diam	6 in. diam	\$ 259	\$ 25,856	45 0
3.3.1	Steel	100 If	6 in. diam	6 in. diam	S 109	\$ 10.872	35 0

Figure 1.2 Output from the EPA WBS model using the above inputs for expenses of aeration basins, pumps, blowers, and piping.

4.	Valves								
4.2	Manual								
4.2.1	Influent and treated water - Polypropylene/PVC	2	units	6 in. diam	6 in. diam	\$ 820	\$ 1,639	25	1
4.2.1	Influent and treated water - Stainless Steel	2	units	6 in. diam	6 in. diam	\$ 1,429	\$ 2,857	25	0
4.2.1	Influent and treated water - Cast Iron	2	units	6 in. diam	6 in. diam	\$ 1,446	\$ 2,892	25	0
4.2.2	Process - Polypropylene/PVC	50	units	2.5 in. diam	2.5 in. diam	\$ 301	\$ 15,069	25	1
4.2.2	Process - Stainless Steel	50	units	2.5 in. diam	2.5 in. diam	\$ 635	\$ 31,763	25	0
4.2.2	Process - Cast Iron	50	units	2.5 in. diam	2.5 in. diam	\$ 579	\$ 28,925	25	0
4.2.3	Air - Polypropylene/PVC	16	units	2.5 in. diam	2.5 in. diam	\$ 301	\$ 4,822	25	1
4.2.3	Air - Stainless Steel	16	units	2.5 in. diam	2.5 in. diam	\$ 635	\$ 10,164	25	0
4.2.3	Air - Cast Iron	16	units	2.5 in. diam	2.5 in. diam	\$ 579	\$ 9,256	25	0
4.2.4	Bypass - Polypropylene/PVC	-	units	NA NA	NA	NA.		NA.	
4.2.4	Bypass - Stainless Steel	-	units	NA NA	NA	NA.		NA.	
4.2.4	Bypass - Cast Iron	-	units	NA NA	NA	NA		NA.	
4.3	Check Valves								
4.3.1	Treated water - Polypropylene/PVC	1	units	6 in. diam	6 in. diam	\$ 1,226	\$ 1,226	25	1
4.3.1	Treated water - Stainless Steel	1	units	6 in. diam	6 in. diam	\$ 2,809	\$ 2,809	25	0
4.3.1	Treated water - Cast Iron	1	units	6 in. diam	6 in. diam	\$ 2,863	\$ 2,863	25	0
4.3.2	Process - Polypropylene/PVC	1	units	2.5 in. diam	2.5 in. diam	\$ 327	\$ 327	25	1
4.3.2	Process - Stainless Steel	1	units	2.5 in. diam	2.5 in. diam	\$ 854	\$ 854	25	0
132	Process - Cast Iron	1	unite	2.5 in diam	2.5 in diam	836	\$ 836	25	0

Figure 1.3 Output from the EPA WBS model using the above inputs for valves expenses.

5.	Instrumentation						
5.1	Flow Meters - Influent and Treated Water						
5.1.1	Orifice Plate	1 units	6 in. diam	6 in. diam	\$ 3,418	\$ 3,418	15 0
5.1.1	Propeller	1 units	6 in. diam	6 in. diam	\$ 4,479	\$ 4,479	15 1
5.1.1	Venturi	1 units	6 in. diam	6 in. diam	\$ 3,069	\$ 3,069	15 0
5.1.1	Magnetic	1 units	6 in. diam	6 in. diam	\$ 6,186	\$ 6,186	15 0
5.2	Flow Meters - Process						
5.2.1	Orifice Plate	16 units	2.5 in. diam	2.5 in. diam	\$ 1,972	\$ 31,550	15 0
5.2.1	Propeller	16 units	2.5 in. diam	2.5 in. diam	\$ 2,873	\$ 45,968	15 1
5.2.1	Venturi	16 units	2.5 in. diam	2.5 in. diam	\$ 2,394	\$ 38,299	15 0
5.2.1	Magnetic	16 units	2.5 in. diam	2.5 in. diam	\$ 4,349	\$ 69,581	15 0
5.3	Air Flow Meters						
5.3.1	Rotameter	16 units	NA	NA	\$ 2,900	\$ 46,401	15 1
5.4	High/low alarms (for contact basins)	16 units	NA	NA	\$ 600	\$ 9,603	15 1
5.5	pH Meters	2 units	NA	NA	\$ 3,047	\$ 6,094	15 1
5.6	Pressure Gauges	32 units	NA	NA	\$ 268	\$ 8,563	15 1

Figure 1.4 Output from the EPA WBS model using the above inputs for instrumentation expenses.

8.	Building Structures and HVAC								
8.1	Building 1								
8.1.1	Small Low Cost Shed	-	units	2460 sf	2460 sf		NA		N/A
8.1.1	Low Quality	1	units	2460 sf	2460 sf	\$	77.85	\$ 191,517	40 1
8.1.1	Medium Quality	1	units	2460 sf	2460 sf	\$	93.40	\$ 229,767	40 0
8.1.1	High Quality	1	units	2460 sf	2460 sf	S	130.13	\$ 320,116	40 0
8.2	Heating System								
8.2.1	Electric resistance	1	zones	50 MBH	50 MBH	\$	23,098	\$ 23,098	25 0
8.2.1	Natural gas non-condensing furnace	1	zones	50 MBH	50 MBH	S	16,597	\$ 16,597	25 0
8.2.1	Natural gas condensing furnace	1	zones	50 MBH	50 MBH	\$	16,597	\$ 16,597	25 1
8.2.1	Standard efficiency oil furnace	1	zones	50 MBH	50 MBH	\$	19,131	\$ 19,131	25 0
8.2.1	Mid-efficiency oil furnace	1	zones	50 MBH	50 MBH	S	19,131	\$ 19,131	25 0

Figure 1.5 Output from the EPA WBS model using the above inputs for expenses of building structures.

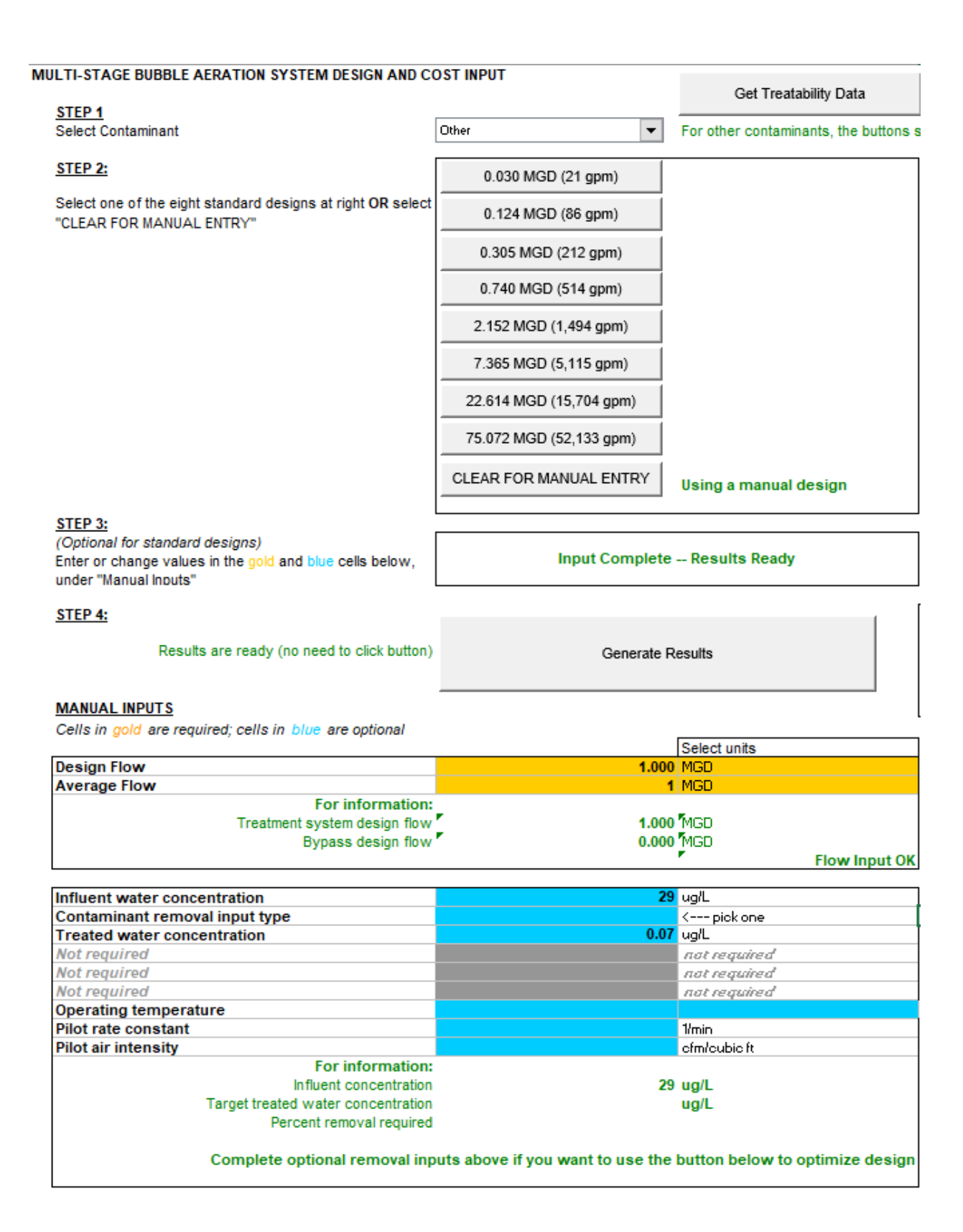
structures.				
Item	Quantity	Unit Cost	Total Cost (\$/yr)	Use?
Labor				
Manager	264 hrs/yr	\$ 57.93	/hr \$ 15,288	1
Administrative	264 hrs/yr	\$ 32.90	/hr \$ 8,683	1
Operator	2.639 hrs/vr	\$ 36.43	/hr \$ 96.145	1

Figure 1.6 Output from the EPA WBS model using the above inputs for labor expenses.

Section 2 – Three-stage FF system

Below include all input parameters for the Multi-Stage Bubble Aeration WBS model derived from the U.S. EPA. Spreadsheets used in this model are available under the "Drinking Water Treatment Technology Unit Cost Models" Drinking Water Treatment Technology Unit Cost Models | US EPA.

While this model was not used for every component of the life cycle cost assessment (e.g., electricity used for vacuum), sample outputs used in the costing model are included below for aeration basins, pumps, blowers, and piping (Figure 2.2), valves (Figure 2.3), instrumentation (Figure 2.4), building structures (Figure 2.5), and labor (Figure 2.6).



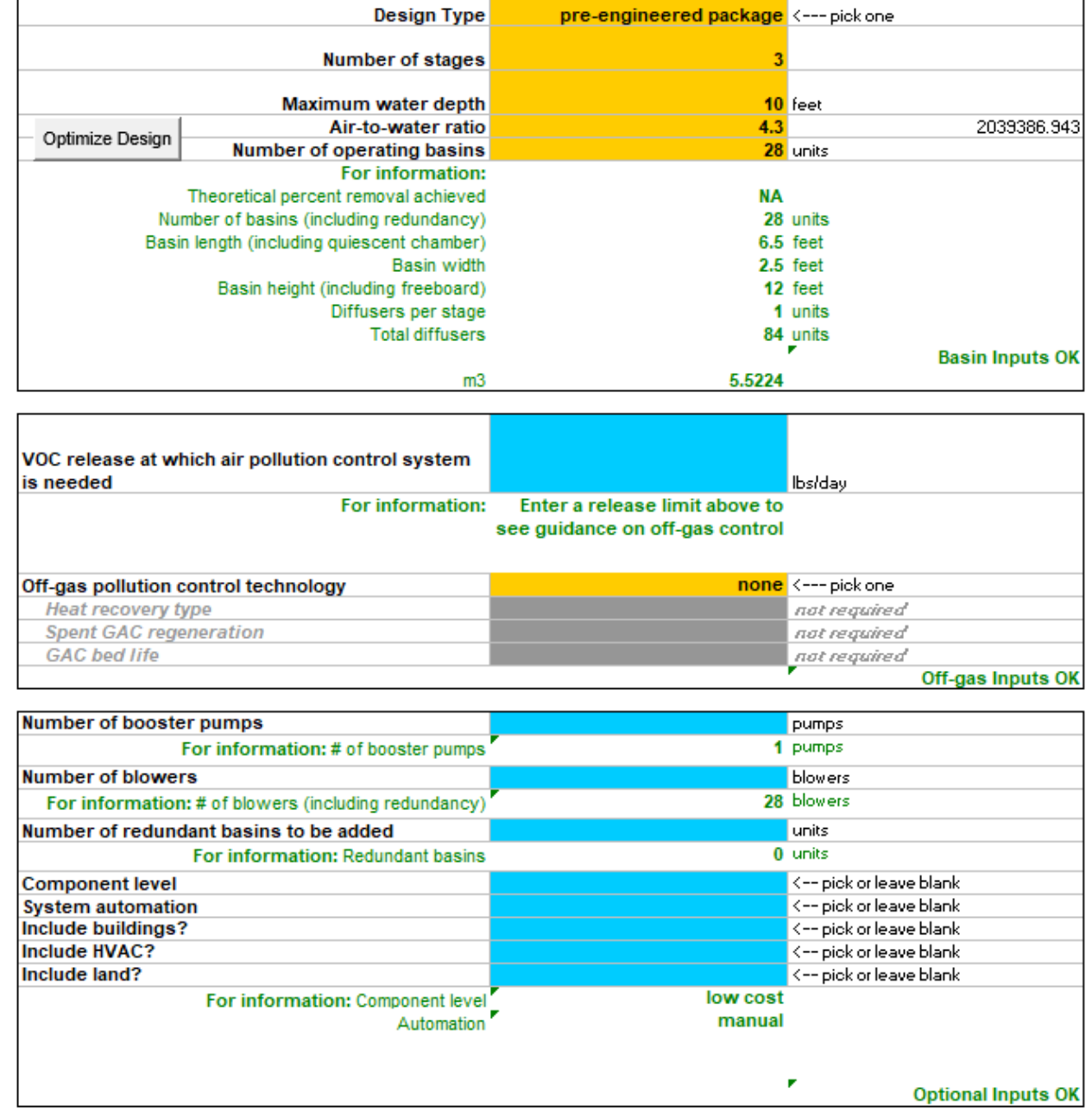


Figure 2.1. All input parameters used in the life cycle costing assessment model for the three-stage FF system.

WBS#	Item	Item Design Quantity Design Size Size		Size used in estimate	Unit Cost		Total Cost	Useful Life	Use?
1.	Aeration Basins								
1.2	Prefabricated								
1.2.1	Stainless Steel	28 units	339 sf	339 sf	\$ 54,10	1 \$	1,514,822	35	0
1.2.1	Plastic with Stainless Steel Frame	28 units	339 sf	339 sf	contact vendor	r	-	25	0
1.2.1	Fiberglass	28 units	339 sf	339 sf	\$ 31,54	4 \$	883,242	25	1
1.3	Aerators								
1.3.1	Diffusers	84 units	5 cfm	5 cfm	\$ 40	6 \$	3,898	10	1
2 .	Pumps and Blowers								
2.1	Booster Pumps	1 units	868 gpm	868 gpm	\$ 22,34	7 \$	22,347	20	1
2.2	Blowers			-					
2.2.1	Centrifugal	28 units	18 cfm	18 cfm	\$ 13,81	7 \$	386,874	25	0
2.2.1	Regenerative	28 units	18 cfm	18 cfm	\$ 629	9 \$	17,620	25	1
3.	Piping								
3.1	Process Piping								
3.1.1	Ductile Iron	100 If	2 in. diam	2 in. diam	contact vendor	\top		40	0
3.1.1	CPVC	100 If	2 in. diam	2 in. diam	\$ 10	0 \$	980	22	0
3.1.1	PVC	100 If	2 in. diam	2 in. diam	\$	3 \$	342	22	1
3.1.1	Stainless Steel	100 If	2 in. diam	2 in. diam	\$ 9:	5 \$	9,544	45	0
3.1.1	Steel Steel	100 If	2 in. diam	2 in. diam	\$ 3:	9 \$	3,940	35	0
3.2	Air Piping								
3.2.1	Ductile Iron	1,072 If	2 in. diam	2 in. diam	contact vendor		-	40	0
3.2.1	CPVC	1,072 If	2 in. diam	2 in, diam	S 1	0 8	10,507	22	0
3.2.1	PVC	1,072 If	2 in, diam	2 in. diam	\$	3 \$		22	1
3.2.1	Stainless Steel	1.072 If	2 in. diam	2 in. diam	\$ 9	5 S	102.313	45	0
3.2.1	Steel Steel	1,072 If	2 in. diam	2 in. diam	\$ 3:	9 \$	42,239	35	0
3.3	Influent and Treated Water Piping								
3.3.1	Ductile Iron	100 If	6 in. diam	6 in. diam	\$ 10	0 \$	9,979	40	0
3.3.1	CPVC	100 If	6 in. diam	6 in, diam	\$ 4	7 \$	4,661	22	0
3.3.1	PVC	100 If	6 in. diam	6 in. diam	\$ 10	9	973	22	1
3.3.1	Stainless Steel	100 If	6 in. diam	6 in. diam	\$ 25	9 \$	25,856	45	0
3.3.1	Steel	100 If	6 in. diam	6 in. diam	\$ 10:	9 \$	10,872	35	0

Figure 2.2 Output from the EPA WBS model using the above inputs for expenses of aeration basins, pumps, blowers, and piping.

4.	Valves								
4.2	Manual								
4.2.1	Influent and treated water - Polypropylene/PVC	2 units	6 in. diam	6 in. diam	\$	820	\$ 1,639	25	1
4.2.1	Influent and treated water - Stainless Steel	2 units	6 in. diam	6 in. diam	\$	1,429	\$ 2,857	25	0
4.2.1	Influent and treated water - Cast Iron	2 units	6 in. diam	6 in. diam	\$	1,446	\$ 2,892	25	0
4.2.2	Process - Polypropylene/PVC	86 units	2 in. diam	2 in. diam	\$	252	\$ 21,636	25	1
4.2.2	Process - Stainless Steel	86 units	2 in. diam	2 in. diam	\$	517	\$ 44,435	25	0
4.2.2	Process - Cast Iron	86 units	2 in. diam	2 in. diam	\$	458	\$ 39,392	25	0
4.2.3	Air - Polypropylene/PVC	28 units	2 in. diam	2 in. diam	\$	252	\$ 7,044	25	1
4.2.3	Air - Stainless Steel	28 units	2 in. diam	2 in. diam	\$	517	\$ 14,467	25	0
4.2.3	Air - Cast Iron	28 units	2 in. diam	2 in. diam	\$	458	\$ 12,825	25	0
4.3	Check Valves								
4.3.1	Treated water - Polypropylene/PVC	1 units	6 in. diam	6 in. diam	\$	1,226	\$ 1,226	25	1
4.3.1	Treated water - Stainless Steel	1 units	6 in. diam	6 in. diam	\$	2,809	\$ 2,809	25	0
4.3.1	Treated water - Cast Iron	1 units	6 in. diam	6 in. diam	\$	2,863	\$ 2,863	25	0
4.3.2	Process - Polypropylene/PVC	1 units	2 in. diam	2 in. diam	\$	247	\$ 247	25	1
4.3.2	Process - Stainless Steel	1 units	2 in. diam	2 in. diam	\$	663	\$ 663	25	0
4.3.2	Process - Cast Iron	1 units	2 in. diam	2 in. diam	S	715	S 715	25	0

Figure 2.3 Output from the EPA WBS model using the above inputs for valves expenses.

5.	Instrumentation									
5.1	Flow Meters - Influent and Treated Water									
5.1.1	Orifice Plate	1	units	6 in. diam	6	in. diam	\$ 3,418	\$ 3,418	15	0
5.1.1	Propeller	1	units	6 in. diam	6	in. diam	\$ 4,479	\$ 4,479		1
5.1.1	Venturi	1	units	6 in. diam	6	in. diam	\$ 3,069	\$ 3,069	15	0
5.1.1	Magnetic	1	units	6 in. diam	6	in. diam	\$ 6,186	\$ 6,186	15	0
5.2	Flow Meters - Process									
5.2.1	Orifice Plate	28	units	2 in. diam	2	in. diam	\$ 1,731	\$ 48,473	15	0
5.2.1	Propeller	28	units	2 in. diam	2	in. diam	\$ 2,615	\$ 73,234	15	1
5.2.1	Venturi	28	units	2 in. diam	2	in. diam	\$ 2,310	\$ 64,682	15	0
5.2.1	Magnetic	28	units	2 in. diam	2	in. diam	\$ 4,096	\$ 114,678	15	0
5.3	Air Flow Meters									
5.3.1	Rotameter	28	units	NA	NA		\$ 2,900	\$ 81,202	15	1
5.4	High/low alarms (for contact basins)	28	units	NA	NA		\$ 600	\$ 16,805	15	1
5.5	pH Meters	2	units	NA	NA		\$ 3,047	\$ 6,094	15	1
5.6	Pressure Gauges	56	units	NA	NA		\$ 268	\$ 14,984		1
5.7	Electrical Enclosure	-	units	NA	NA		NA	_	NA.	

Figure 2.4 Output from the EPA WBS model using the above inputs for instrumentation expenses.

8.	Building Structures and HVAC												
8.1	Building 1												
8.1.1	Small Low Cost Shed	-	units	2330	sf	2330	sf		NA			N/A	
8.1.1	Low Quality	1	units	2330	sf	2330	sf	\$	78.26	\$	182,336	40	
8.1.1	Medium Quality	1	units	2330	sf	2330	sf	\$	93.89	\$	218,765	40	-
8.1.1	High Quality	1	units	2330	sf	2330	sf	\$	131.10	\$	305,458	40	- (
8.2	Heating System												
8.2.1	Electric resistance	1	zones	46	MBH	46	MBH	\$	21,630	\$	21,630	25	- (
8.2.1	Natural gas non-condensing furnace	1	zones	46	MBH	46	MBH	\$	15,567	\$	15,567	25	0
8.2.1	Natural gas condensing furnace	1	zones	46	MBH	46	MBH	\$	15,567	\$	15,567	25	
8.2.1	Standard efficiency oil furnace	1	zones	46	MBH	46	MBH	\$	17,994	\$	17,994	25	-
821	Mid-efficiency oil furnace	1	zones	46	MBH	46	MBH	S	17 994	S	17 994	25	- 0

Figure 2.5 Output from the EPA WBS model using the above inputs for expenses of building structures.

Item	Quant	ity	Unit Cost			Total	Cost (\$/yr)	Use?
Labor								
Manager	437	hrs/yr	\$	57.93	/hr	\$	25,334	1
Administrative	437	hrs/yr	\$	32.90	/hr	\$	14,388	1
Operator	4,373	hrs/yr	\$	36.43	/hr	\$	159,320	1

Figure 2.6 Output from the EPA WBS model using the above inputs for labor expenses.

APPENDIX C Paper copyright permissions

C1 Permission to Use Paper Contents in Chapter 3



Outlook

Re: Copyright release-Dissertation

From EIC <eic@estwater.acs.org>

Date Thu 2025-06-05 9:46

Gengyang Li <Gengyang.Li@uga.edu>

[EXTERNAL SENDER - PROCEED CAUTIOUSLY]

Dear Dr. Li,

Thank you for your patience as I heard back from Dr. Synder. He has responded and says, "Yes, I entirely agree! Thanks"

Therefore, Dr. Snyder approves the use of your published paper in your dissertation.

Best, Elsa Lantz ACS ES&T Water Editorial Office eic@estwater.acs.org

From: Gengyang Li <Gengyang.Li@uga.edu>

Sent: Tuesday, June 3, 2025 1:54 PM To: EIC <eic@estwater.acs.org>

Subject: Copyright release-Dissertation

Hi Editor-in-Chief,

I am Gengyang Li. I have published a paper in ES&T Water "Environmental life cycle assessment (LCA) of treating PFASs with ion exchange and electrochemical oxidation technology"

I plan to add this paper to my Ph.D. dissertation, and the graduate school needs the Copyright Release statement. Could you please provide me with a letter of permission or an email for the Copyright Release about this paper? Thank you so much!

Best regards, Gengyang

C1 Permission to Use Paper Contents in Chapter 4

